Siderophile Element Constraints on the Origin of Components of Unequilibrated Chondrites

Yogita Kadlag

Dissertation submitted to obtain
the academic degree

Doktor der Naturwissenschaften
(Dr. rer. nat.)

Fachbereich Geowissenschaften
Freie Universität Berlin

Freie Universität Berlin

Berlin, 1 April 2015

Referees:

1. First Referee: Prof. Dr. Harry Becker
   Institut für Geologische Wissenschaften,
   Freie Universität Berlin
   Malteserstrasse 74-100, Haus B
   12249 Berlin, Germany

2. Second Referee: Prof. Dr. Maria Schoenbaechler
   Inst. f. Geochemie und Petrologie
   ETH Zürich
   NW D 81.2
   Clausiusstrasse 25
   8092 Zürich, Switzerland

Date of defense: 27 May 2015

Selbständigkeitserklärung

Hiermit versichere ich, die vorliegende Dissertation eigenständig und ausschließlich unter Verwendung der angegebenen Hilfsmittel, angefertigt zu haben. Alle Aussagen innerhalb der vorliegenden Arbeit, welche dem Wortlaut oder dem Sinne nach aus anderen Quellen entnommen wurden, einschließlich solcher aus elektronischer Medien, sind im Text kenntlich gemacht und befinden sich in einem vollständigen Verzeichnis.

Die vorliegende Arbeit ist in dieser oder anderer Form zuvor nicht als Prüfungsarbeit zur Begutachtung vorgelegt worden.

Unterschrift Berlin, 1 April 2015

CONTENTS

Summary

Abundances of highly siderophile elements (HSE: Re, Os, Ir, Ru, Pt, Rh, Pd and Au), chalcogen elements (S, Se and Te) and Os isotopic composition in components of chondrites are important to constrain the element fractionation processes in the early solar nebula, alteration processes on the meteorite parent bodies and later element fractionation processes during terrestrial weathering in case of meteorite finds.

All components of the EH chondrites show higher Au/HSE compared to CI and other chondrites. The history of the components of EH chondrites is complex and involves early fractional condensation and loss of refractory element rich phases, subsequent condensation of moderately volatile elements in a highly reduced environment with partly chalcophile behavior of Au during this stage and melting, evaporation and recondensation of metal grains in sulfur rich environments.

Primary variations of the HSE abundances and ratios in the components of carbonaceous chondrites were overprinted by the parent body alteration processes. Fractional condensation and isolation of refractory metal alloys was a major early process, responsible for the element variation in carbonaceous chondrites. Some refractory metal alloys were trapped in silicates and occur in nonmagnetic fractions. A Pd depleted component occurs in the major HSE carrier phases present in the Allende and Murchison. This component is either the product of fractional condensation (the complementary Pd rich component is missing) or resulted from the evaporation of Pd during high temperature processing of metal. Gold is heterogeneously distributed in different splits of the Allende and Murchison bulk rocks. Components of Murchison show similar heterogeneous distribution of Au, which was likely caused by aqueous alteration. In case of Allende linear correlations of siderophile and chalcophile elements (Te-Se, S-Se, Ni/Fe-Co/Fe and Au-Pd) in the components suggest that the chemical variations reflect mixing of components with compositions affected by preaccretionary processes (e.g. inherited from chondrule formation). The complementary behavior of some concentrations and element ratios, and CI chondrite like compositions in the bulk rock of Allende (such as, Cr-Fe, refractory HSE-Ir, S-Se and Te-Se) suggest closed system behavior during alteration and chondrule formation. Higher refractory element/volatile element ratios in Allende compared to Murchison may reflect differences in heliocentric distances in which the dust assemblages of Allende and Murchison were processed.

Ordinary chondrites are depleted in refractory HSE in the order H < L < LL, consistent with the decreasing Fe-Ni metal content, which is also the main host phase of the HSE. An important difference among these ordinary chondrite groups are the higher HSE abundances of metal rich fractions of LL chondrites compared to metal rich fractions of H chondrites. This behavior of metal suggests that the proportion of HSE relative to Fe and Ni was not homogenous in the

formation regions of the different ordinary chondrite groups. Despite of these differences, all groups of ordinary chondrites contain a common component in silicate rich fractions that is depleted in Pd compared to other HSE.

The chalcogen element systematics in enstatite chondrites were influenced by volatility-controlled fractionation and partly by terrestrial weathering. This study suggests that enstatite chondrite finds from hot desert show significant disturbance in the chalcogen element systematics due to S loss, compared to minor or almost no disturbance in ordinary chondrite finds from cold deserts. Thus, sulfur mobilization and loss during weathering in different chondrite compositions is highly dependent on the processes in these different terrestrial environments. Loss of Te during terrestrial weathering is very unlikely. Nearly similar Te depletion in H, L and LL chondrites compared to CI chondrites suggests that Te loss is independent of the removal of Fe-Ni metal from L and LL chondrites. Tellurium shows different geochemical behavior in the components of different chondrites classes. Variation diagrams of Te with Se, S and the HSE indicate that Te is chalcophile in components of carbonaceous chondrites, whereas it is predominantly siderophile in the components of ordinary and enstatite chondrites. The depletion of Te compared to S and Se in components of ordinary and EH chondrites are due to its siderophile nature during condensation and subsequent evaporation during melting of metal grains. The possible role of thermal metamorphism on meteorite parent bodies on the S-Se-Te abundance systematics is difficult to evaluate. The well preserved correlations between HSE (Ir or Pd) and Te in almost all components of ordinary and enstatite chondrites favour the hypothesis that the Te loss is inherited from high temperature processes in the solar nebula.

Rhenium is the most refractory element under solar conditions, but highly mobile in oxidizing environments compared to other elements analyzed in this study. Many of the chondrite components analyzed in this study show non-isochronous behavior in the Re-Os isochron diagram which was likely caused by the redistribution of Re among the components. Particularly in samples of small size (less than 10 mg) from meteorite finds, the ^{187}Re-^{187}Os systematics is highly susceptible to terrestrial weathering and hydrothermal/aqueous alteration.

Relative and absolute abundances of HSE and chalcogen elements in separated components of unequilibrated chondrites from different classes show resolvable differences indicating that the chondrite precursors are heavily influenced by non-equilibrium condensation/evaporation processes and heterogeneous sampling of primitive and already processed dust. The HSE abundance patterns of separated components of unequilibrated chondrites from different classes indicate the existence of at least two types of HSE carrier phases in chondrite components. Refractory HSE carrier phases in some components were never completely equilibrated with the Fe-Ni metal in the same rocks. Compositions of unequilibrated solar system objects were affected by the local or regional heterogeneity in the solar nebula before the accretion of the chondrite components. Collision and fragmentation processes were prominent in the early solar system and even some of most unequilibrated enstatite and ordinary chondrites contain fragments of material

which likely formed from collision, melting and evaporation of primitive and differentiated precursors. Thus, it is very likely that the building materials of planetary bodies were influenced by similar local or regional differences in elemental abundances in the nebula. Therefore, the initial elemental composition of the terrestrial planets may not reflect the average solar system composition. In order to better understand and construct the bridge between the early solar system processes and evolution of planetary bodies, mass balance of different components which were accreted into planetesimals need to be identified in further studies.

Zusammenfassung

Häufigkeiten von hoch siderophilen Elementen (HSE: Re, Os, Ir, Ru, Pt, Rh, Pd and Au), chalkogenen Elementen (S, Se und Te) und die Osmium-Isotopenverhältnisse in Chondritkomponenten liefern wichtige Hinweise um Element- Fraktionierungsprozesse im solaren Nebel, Alterationsprozesse auf den Meteoritmutterkörpern und, im Falle von gefundenen Meteoriten, terrestrische Alterationsprozesse zu identifizieren.

Alle Komponenten der EH- Chondrite zeigen größere Au/HSE-Verhältnisse als CI- und andere Chondrite. Die Evolution der Komponenten der Enstatitchondrite ist komplex und beinhaltet frühe fraktionierte Kondensation und Verlust von an refraktären Elementen angereicherten Phasen, die nachfolgende Kondensation von mäßig volatilen Elementen in stark reduzierter Umgebung, Gold verhält sich während dieser Phase wahrscheinlich teilweise chalkophil und Aufschmelzen, Evaporation und Rekondensation von Metallkörnern in schwefelreicher Umgebung.

Primäre Variationen der HSE- Häufigkeiten und Verhältnisse in den Komponenten der kohligen Chondrite sind von späteren Alterationsprozessen auf den Mutterkörpern überprägt worden. Fraktionierte Kondensation und Isolierung von refraktären Metalllegierungen war ein früher Hauptprozess, welcher für die Elementverteilung in kohligen Chondriten verantwortlich ist. Einige refraktäre Metalllegierungen wurden in Silikaten gefangen und treten in den nicht-magnetischen Fraktionen auf. Eine Pd- verarmte Komponente tritt in der wichtigsten HSE-tragenden Phase auf, die in Allende und Murchison vorhanden ist. Diese Komponente ist entweder das Produkt fraktionierter Kondensation (die komplementäre Pd- reiche Komponente fehlt) oder resultiert aus der Evaporation von Pd während eines Hochtemperaturprozesses. Au ist ungleichmäßig auf die verschiedenen Teile vom Allende- und Murchison- Gesamtgestein verteilt. Gold ist in verschiedenen Teilen der Allende und Murchison Gesamtgesteine heterogen verteilt. Komponenten von Murchison zeigen eine ähnlich heterogene Verteilung von Gold, welche wahrscheinlich durch wässrige Alteration verursacht wurde. Im Fall von Allende deuten lineare Korrelationen von siderophilen und chalkophilen Elementen (T-Se, S-Se, Ni/Fe-Co/Fe und Au-Pd) in den Komponenten auf chemische Variationen hin, welche die Mischung von Komponenten wiederspiegeln, die durch vor- akkretionäre Prozesse beeinflusst wurden (z.B. von der Bildung der Chondren ererbt). Das komplementäre Verhalten einiger Konzentrationen und Elementverhältnisse und CI- ähnliche Zusammensetzungen des Allende Gesamtgesteins (wie: Cr-Fe, refraktäre HSE-Ir, S-Se und Te-Se) deuten auf ein „geschlossenes-System-Verhalten“ während der Alteration und Bildung der Chondren hin. Größere Verhältnisse zwischen refraktären zu volatilen Elementen in Allende als in Murchison können eventuell von Unterschieden in den heliozentrischen Distanzen zwischen Murchison und Allende herrühren, in denen die Staubansammlungen von Allende und Murchison prozessiert wurden.

Gewöhnliche Chondrite zeigen eine Verarmung an refraktären HSE in der Reihenfolge H < L < LL. Die Verarmung ist gegenläufig zum Fe-Ni- Metallgehalt in den Chondriten, welche die Hauptträgerphase der HSE in diesen Chondriten ist. Ein wichtiger Unterschied unter diesen gewöhnlichen Chondritgruppen sind die größeren HSE- Häufigkeiten der metallreichen Fraktionen der LL Chondrite verglichen mit den metallreichen Fraktionen der H- Chondrite. Dieses Verhalten der Metalle lässt darauf schließen, dass die Verteilung der HSE relativ zu Fe und Ni in den Bildungsregionen der verschiedenen gewöhnlichen Chondritgruppen nicht homogen war. Trotz dieser Unterschiede beinhalten alle Gruppen von gewöhnlichen Chondriten eine häufige Komponente in den silikatreichen Fraktionen, die verglichen mit den anderen HSE an Pd verarmt ist.

Die Systematik der chalkogenen Elemente in Enstatitchondriten ist von Evaporation und terrestrischer Verwitterung beeinflusst. Diese Studie legt nahe, dass in heißen Wüsten gefundene Enstatitchondrite aufgrund von Schwefelverlust eine stark gestörte Systematik der chalkogenen Elemente zeigen. Im Vergleich dazu zeigen in kalten Wüsten gefundene gewöhnliche Chondrite diese Störung nicht. Somit sind die Mobilisierung von Schwefel und der Verlust durch Verwitterung in verschiedenen Chondritzusammensetzungen stark von den Prozessen der jeweiligen terrestrischen Umgebung abhängig. Verlust von Te während terrestrischer Verwitterung ist sehr unwahrscheinlich. Die in H-, L- und LL- Chondriten ähnlich ausgeprägte Verarmung von Te im Vergleich zu CI- Chondriten lässt darauf schließen, dass der Verlust von Te unabhängig vom Verlust des Fe-Ni- Metalls in L- und LL- Chondriten ist. Tellurium zeigt unterschiedliches geochemisches Verhalten in den Komponenten der verschiedenen Chondritklassen. Variationsdiagramme von Te mit Se, S und den HSE deuten ein chalkophiles Verhalten in Komponenten kohliger Chondrite an, wogegen es sich in den Komponenten gewöhnlicher und von Enstatit- Chondriten vorwiegend siderophil verhält. Die Verarmung von Te verglichen mit S und Se in Komponenten von gewöhnlichen und EH- Chondriten ist seinem siderophilen Verhalten während der Kondensation und nachfolgender Evaporation während dem Schmelzen von Metallkörnern geschuldet. Der mögliche Einfluss von thermalen Metamorphismus auf den Mutterkörpern der Meteorite auf die S-Se-Te Häufigkeitsverteilungen ist schwierig zu bewerten. Die gut erhaltenen Korrelationen zwischen HSE (Ir oder Pd) und Te in beinahe allen Komponenten der gewöhnlichen und der Enstatit- Chondrite unterstützen die Annahme, dass der Verlust von Te von Hochtemperaturprozessen des solaren Nebels ererbt ist.

Rhenium ist unter solaren Bedingungen das refraktärste Element, aber in oxidierenden Umgebungen hoch mobil im Vergleich zu allen anderen in dieser Studie analysierten Elementen. Die meisten der hier analysierten Chondritkomponenten zeigen kein isochrones Verhalten, was wahrscheinlich der Umverteilung von Re innerhalb der Komponenten verursacht wurde. Speziell bei kleine Probenmengen (weniger als 10 mg) und gefundenen Meteoriten, ist die ^{187}Re- ^{187}Os Systematik hoch anfällig für terrestrische Verwitterung und hydrothermale/wässrige Alteration.

Die relativen und absoluten Häufigkeiten der HSE und chalkogenen Elemente in separierten Komponenten unequilibrierter Chondrite unterschiedlicher Klassen zeigen auflösbare Unterschiede. Diese deuten darauf hin, dass Vorgängermaterialien der Chondrite stark durch die Ungleichgewichts- Kondensation und heterogene Beprobung von primitivem und schon verändertem Staub beeinflusst sind. Die HSE Häufigkeitsmuster der separierten Komponenten unequilibrierter Chondrite verschiedener Klassen weisen auf die Existenz von mindestens zwei verschiedenen Typen von HSE- enthaltenden Phasen in Chondritkomponenten hin. In einigen Komponenten waren die refraktären HSE- tragenden Phasen nie vollständig mit dem Fe-Ni-Metall der selben Gesteine equilibriert. Zusammensetzungen von unequillibrierten Objekten das Sonnensystems wurden von den lokalen oder regionalen Heterogenitäten im solaren Nebel bevor der Akkretion der Chondritkomponenten beeinflusst. Kollisionen und Fragmentierungsprozesse waren bedeutend im frühen Sonnensystem und sogar einige der am stärksten unequillibrierten Enstatit- und gewöhnlichen Chondriten beinhalten Material, das wahrscheinlich durch Kollisionen, Aufschmelzen und Evaporation von primitiven und differenzierten Vorläufermaterialien gebildet wurden. Somit ist es sehr wahrscheinlich, dass die Baumaterialien der planetaren Körper von ähnlichen lokalen oder regionalen Unterschieden in den Elementhäufigkeiten im Nebel beeinflusst wurden. Dadurch spiegelt die initiale Elementzusammensetzung der terrestrischen Planeten vielleicht nicht die durchschnittliche Sonnensystemzusammensetzung wieder. Um ein besseres Verständnis zu erlangen und eine Brücke zwischen den Prozessen im frühen Sonnensystem und der Evolution der planetaren Körper zu spannen, bedarf es der Identifizierung von Massenbilanzen verschiedener Komponenten, die in Planetesimalen akkreiert wurden.

Chapter 1

Introduction

1.1 Evolution of the solar system and meteorites

4.57 Ga ago, the journey of our solar system began as a consequence of collapse of a giant molecular cloud (Blitz, 1993; Shu et al., 1993; Tscharnuter and Boss, 1993). The disrupted cloud mass was accumulated in small fragments. Almost 99% of the mass (dust and gas) of one such fragment was accumulated to form the Sun at the center and the remaining small fraction of mass was rotating around the Sun in the form of a disk called 'the solar nebula'. Eventually, due to accretion and change in temperature the gaseous material in the solar nebula condensed into small dust particles which accumulated together by dynamics and various processes in the solar nebula and accumulated into bigger planetesimals (Fig.1.1.)

Initially, the solar nebula was made up of the same initial chemical reservoir, but soon physical and chemical differences were established in different regions. All solar system objects like asteroids, planetary satellites, dwarf planets, major planets and comets were formed from the nebular dust and gas within the first 10-100 million years after the formation of the first solar system solids (Cameron, 1993; Lissauer and Stewart, 1993; Strom et al., 1993; Swindle, 1993; Cameron, 1995).

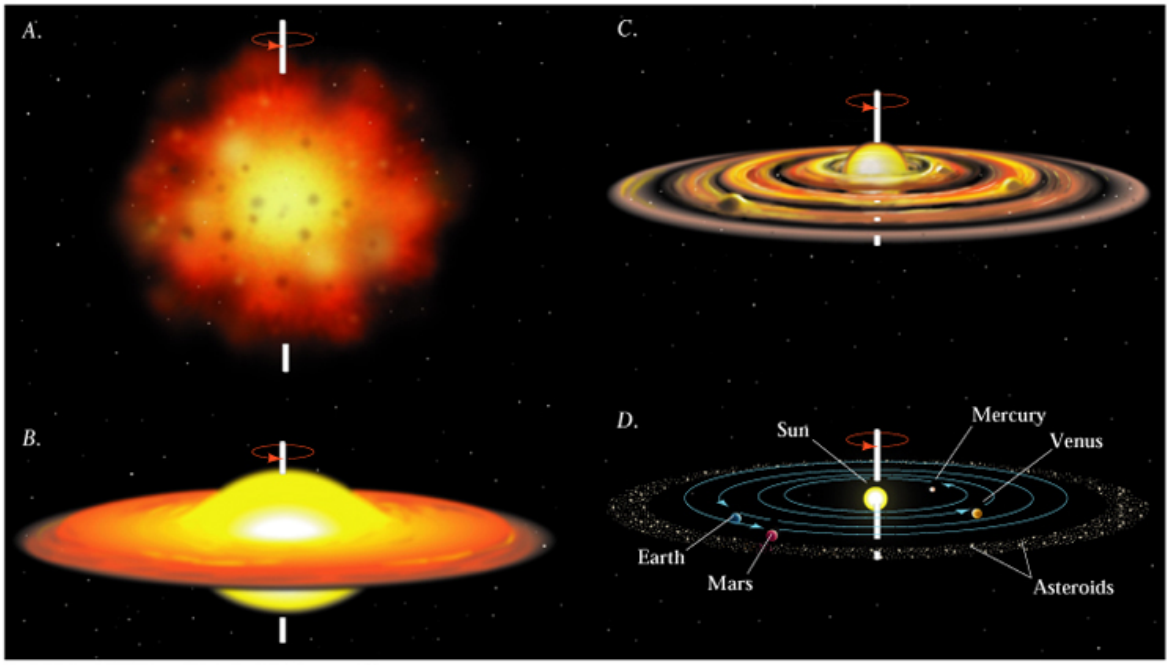

Fig.1.1. The widely accepted theory of the formation and evolution of the solar system. A) Gravitational collapse of a giant molecular cloud which mostly comprised gas and little presolar dust. B) Formation of the Sun and the solar nebula (4.57 Ga ago). C) Accretion and separation of nebular mass in orbits around the Sun and, D) Current status and partial view of the solar system objects until asteroidal belt.

Solar system bodies evolved into different paths due to the disk dynamics and therefore variability in orbit, size, chemical and isotopic composition of matter can be observed among solar system objects. To trace back the history of the solar system to 4.57 Ga, objects which did not change with time and preserve their primitive chemical composition without large-scale elemental and isotopic fractionation on their parent bodies are needed. The most promising candidates for this objective that can be studied in the laboratory are primitive meteorites. By definition meteorites are the solid rock pieces which originated from solar system bodies and had escaped into the space from their parent body. When these rock pieces come under the influence of the gravitational force of a large solar system object, then, they collide with or fall on the surface of that object. Every year nearly 18,000-84,000 meteorites hit the Earth, although, most of them are too small to be analyzed or recovered (Bland et al., 1996).

Meteorites originated from different solar system bodies, thus they vary in elemental and isotopic composition. Planetesimals larger than 20 km in diameter (Moskovitz and Gaidos, 2011) often underwent processes like differentiation and chemical fractionation and therefore, the information regarding the early solar system processes were erased from differentiated objects. Depending on the chemical composition, meteorites are broadly classified into three categories, stony (nearly 95% meteorites we have in collections are from this category, they are mainly composed of silicates and commonly little metal), stony iron (1% meteorites are from this category, made up of 50% metal and 50% silicates) and iron meteorites (5%, mainly made up of iron metal alloys; McSween, 1999). Among all these meteorite classes, most stony meteorites are undifferentiated.

About 75-90% volume of stony meteorites are composed of silicate minerals and about 10-25% are of iron-nickel metal alloys and sulfides (McSween, 1999). Most of the stony meteorites are derived from undifferentiated bodies and very few of them may have a cometary origin (McSween, 1999).

Stony meteorites are classified into two categories, chondrites (undifferentiated meteorites) and achondrites (differentiated meteorites) depending on the mineral composition and presence of silicate-rich spherules called ‘chondrules’ which are only present in chondrites, with the exception of CI chondrites. Out of all the meteorites known so far, chondrites are the most primitive rocks in our solar system.

1.1.1 Chondrites and their components

Chondrites are further classified into four groups, ordinary, enstatite, carbonaceous and two other small groups, K and R chondrites based on differences in chemical composition, oxygen isotopic composition and proportion of the chondrite components. A further subdivision of these groups is shown in Fig. 1.2.

All chondrite classes have distinct chemical compositions. Al/Mg, Al/Si, Ca/Si, HSE/Ni ratios of chondrites show that carbonaceous chondrites are enriched in refractory lithophile and siderophile elements, whereas enstatite chondrites are enriched in moderately volatile elements compared to CI chondrites (Kallemeyn and Wasson, 1981, 1982, 1985, 1986; Wasson and Kallemeyn, 1988; Palme and Boynton, 1993).

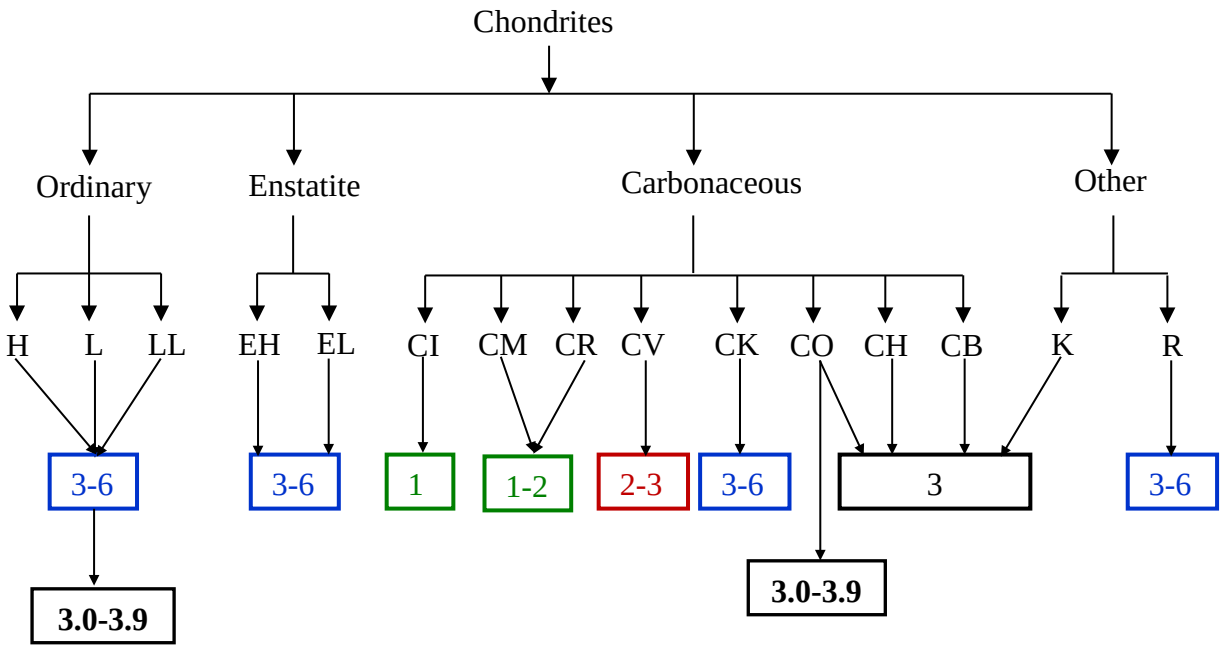

Fig.1.2. Classification of chondrites based on the chemical composition, variation in oxygen isotopic composition and proportion of chondritic components. Further classification of each group is broadly depending on the chemical variation and total Fe content. Number classification is based on the degree of thermal metamorphism and aqueous alteration (Van Schmus and Wood, 1967; Sears et al., 1980; Scott and Jones, 1990; Sears et al., 1991; Krot et al., 2003).

Chondrites are also classified on the basis of the degree of aqueous alteration and thermal metamorphism into type 1 to 6 (Van Schmus and Wood, 1967). Type 1 and 2 are the most aqueously altered, type 3 are the least altered chondrites, whereas type 4-6 chondrites had experienced thermal metamorphism in increasing order (Van Schmus and Wood, 1967; Krot et al., 2003). Therefore, type 3 meteorites are the most ideal candidates to study early solar system processes.

This study is mainly focused on the elemental and osmium isotopic differences in the components of type 3 chondrites. Note that though type 3 chondrites represent the most primitive and unequilibrated meteorites; based on the slight influence of thermal metamorphism, type 3 ordinary and CO chondrites are classified into 10 different sub-types from 3.0 to 3.9, 3.0 representing the most unequilibrated rock type compared to all known meteorites so far (Sears et al., 1980; Scott and Jones, 1990; Sears et al., 1991; Krot et al., 2003).

Chondrite components

Chondrites are mainly composed of four easily distinguishable components, which are briefly introduced in the following sections. All chondrite classes have variable proportions of these components.

I) Refractory Inclusions: Refractory inclusions are sub mm to few cm sized irregular to spheroidal shaped high temperature nebular condensates. Some inclusions are fine grained and some were melted several times after their formation (MacPherson, 2003; Scott and Krot, 2003; Krot et al., 2004). Refractory inclusions are abundant in some carbonaceous chondrite groups, but rare or absent in other chondrite groups (Scott and Krot, 2003).

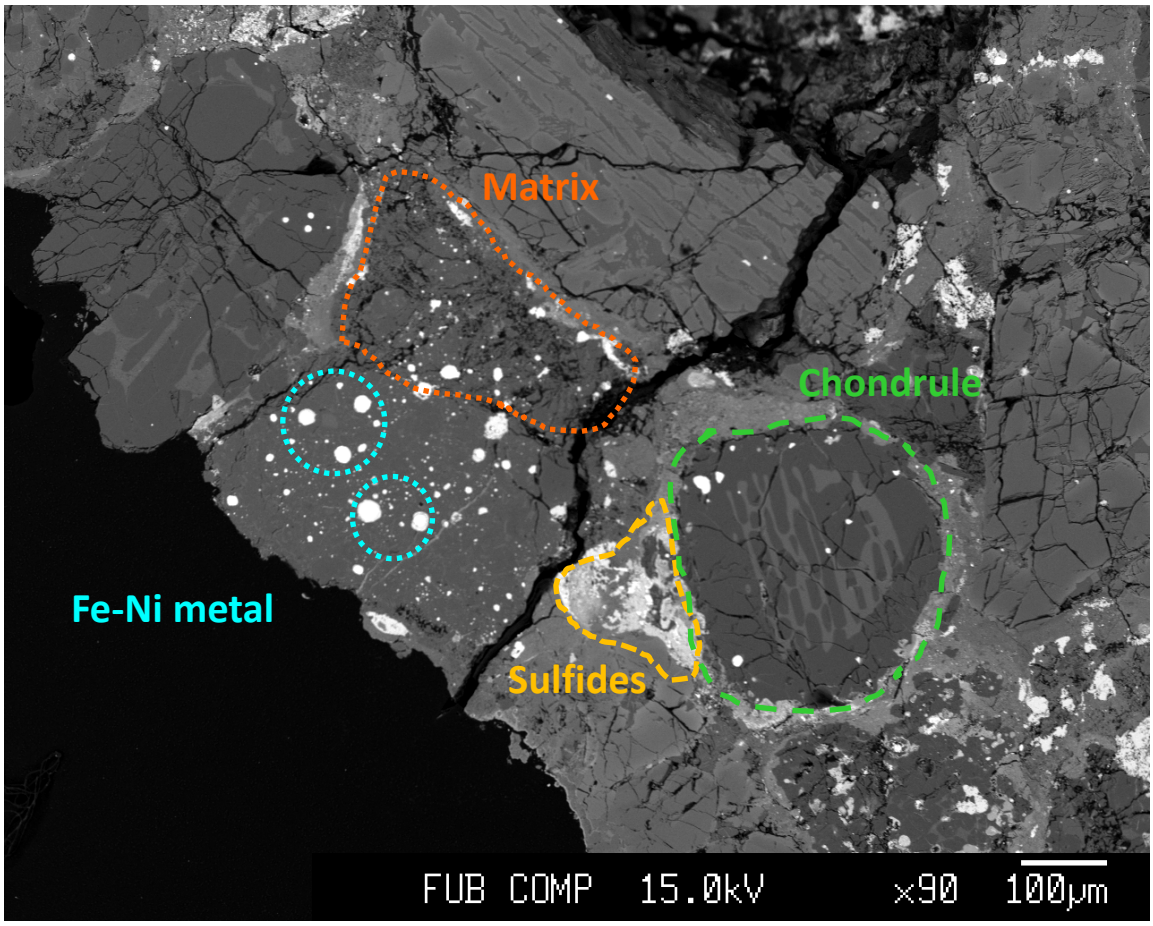

Fig.1.3. A backscattered electron image of a thick section of the unequilibrated ordinary chondrite QUE 97008 (L3.05). Silicates are dark gray, sulfides are light gray and metal grains are white in color. Image shows different chondrite components, except refractory inclusions, because these are very rare in ordinary chondrite groups (Scott and Krot, 2003)

Two types of refractory inclusions are found in chondrites: i) Calcium-Aluminum rich Inclusions (CAIs) and ii) Amoeboid Olivine Aggregates (AOAs).

CAIs are made up from the most refractory mineral phases. Mainly refractory oxides and silicates like perovskite ($CaTiO_3$), hibonite ($CaAl_{11-x}(Mg, Ti)_xO_{19}$), melilite ($Ca_2Al_2SiO_7$-$Ca_2MgSi_2O_7$), spinel ($MgAl_2O_4$), pyroxene ($(Ca, Na)(Al, Mg, Ti, Fe)(Al, Si)_2O_6$), olivine

(Mg_2SiO_4-Fe_2SiO_4) and anorthite ($CaAl_2Si_2O_8$) are some common mineral phases found in CAIs that condense at high temperatures at pressure of~10^{-3}-10^{-4} bar from gas of solar composition (Grossman 1972, 1980; Lodders, 2003; Davis and Richter, 2003; Krot et al., 2004). Physical conditions for the formation and transportation of CAI minerals in the solar nebula were likely achieved near to the proto-Sun (Fig.1.4). Some CAIs contain tiny refractory metal nuggets, which are highly enriched in refractory HSE (Palme and Wlotzka, 1976; Grossman 1972, 1980; Blander et al., 1980; Blum et al., 1989; Sylvester et al., 1990; Palme et al., 1994; Campbell et al., 2003; Davis and Richter, 2003). The mineralogy and age data of CAIs suggest that they are the most refractory and oldest known objects in our solar system (Grossman 1972, 1980; Lodders, 2003; Davis and Richter, 2003; Bouvier and Wadhwa, 2010). CAIs are classified into different groups depending on their textures, mineralogy and rare earth element abundance patterns (Mason and Taylor, 1982; Scott and Krot, 2003 and references therein). AOAs are mainly irregular-shaped aggregates of forsterite, aluminum-diopside, spinel, anorthite and Fe-Ni metal (Scott and Krot, 2003).

II) Chondrules: Chondrules are silicate-rich spherules, mainly composed of olivine and low-Ca pyroxene. In addition, chondrules also contain small and variable proportions of Fe-Ni metal and troilite (FeS). Chondrules are present in all chondrite groups, except CI chondrites (Scott and Krot, 2003). Condensation temperatures of chondrule minerals at the solar conditions are 1500-1200 K and FeS condensation occurs at about ~ 650 K (Lodders, 2003). Chondrules are also

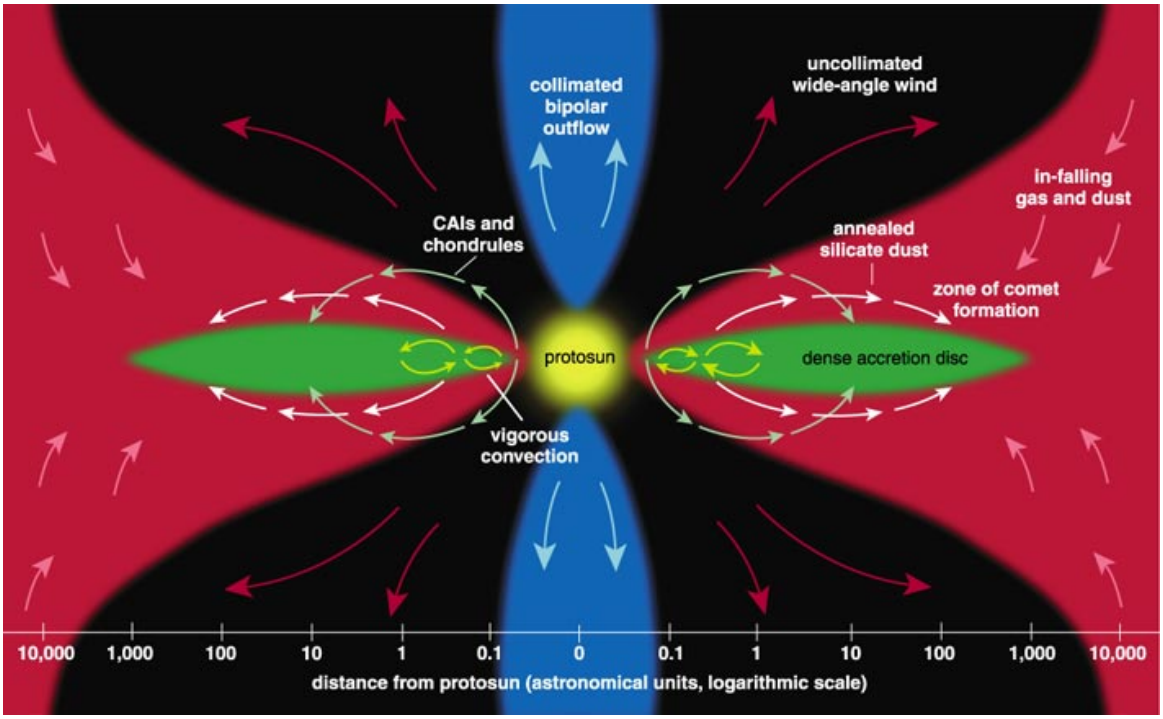

Fig.1.4. Demonstration of the physical conditions of the inner solar nebula and formation and circulation of the refractory mineral phases (Image: Nuth, 2001). CAIs and chondrules are made up from refractory mineral phases, more likely formed near to the Sun and transported to the other parts of the solar nebula (Shu et al., 1997).

classified into different types, depending on variations in their textures and mineral composition (Scott and Krot, 2003).

III) Fe-Ni metal: Fe-Ni metal in chondritic meteorites may have formed from condensation in the solar nebula, from desulfurization of FeS or other sulfides (Hewins et al., 1997) and reduction of FeO (Connolly et al., 2001). Condensation of Fe-Ni metal took place at 1300-1400 K in the solar nebula, overlapping with the condensation temperature of chondrule silicates (Grossman, 1972; Lodders, 2003). Some tiny metal grains exist in the chondrules and most of them were more likely expelled from the silicate rich chondrule liquid during the chondrule formation process, whereas some were either lost into the space or later incorporated into the matrix (Campbell et al., 2005 and references therein).

IV) Matrix: Matrix is the most volatile-rich and fine grained component (size ranging from 10 nm to 5 µm) of chondrites (Scott and Krot, 2003). It mainly fills the interstitial space between coarser objects such as refractory inclusions, chondrules and Fe-Ni metal grains. Matrix is the least thermally processed component compared to all other chondrite components; hence some of the earliest dust particles such as presolar grains are preserved in the matrix.

1.1.2 Siderophile element abundances in the chondrite components

Chondrite components were formed in the solar nebula and underwent different elemental fractionation processes before and after the accretion into the chondrite parent bodies (Scott and Krot, 2003). To understand the origin and evolution of the chondrite components, it is necessary to distinguish the effect of earlier nebular and later parent body processes on elemental fractionation. One promising tool to evaluate the influence of primary and secondary element fractionation processes is the abundances of siderophile elements in chondrites and their

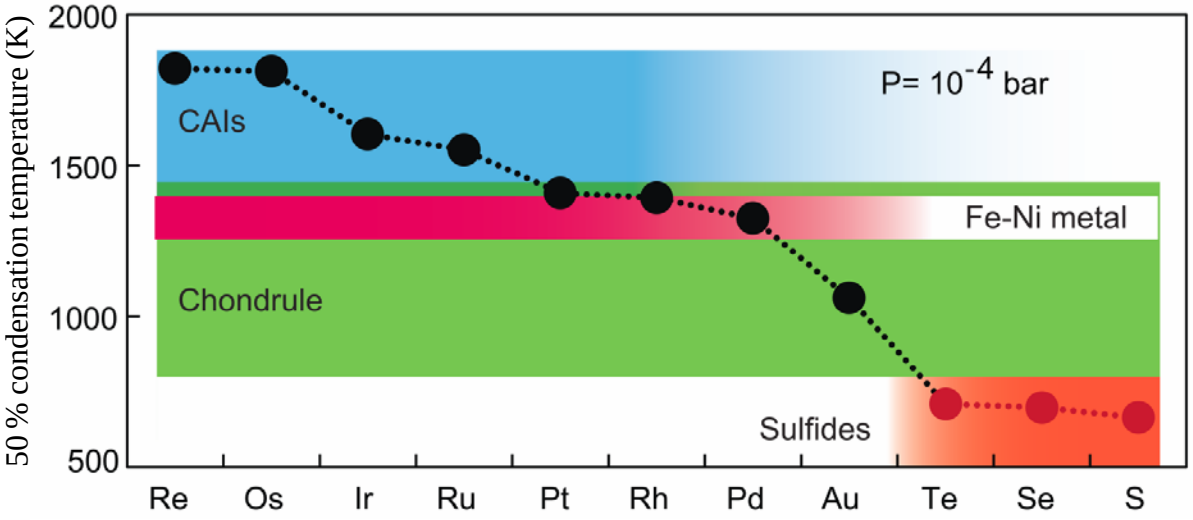

Fig.1.5. Condensation sequence of siderophile elements and chondrite components in the gas of solar composition at P= 10^{-4} bar (Lodders, 2003). Color variation for each component over the fixed temperature range indicates the presence of (dark area) or absence of (light area) siderophile elements in the major mineral phases of corresponding components.

components (Wasson and Kallemeyn, 1988; Lorand, 1990; Dreibus et al., 1995; Walker et al., 2002b; Campbell et al., 2002; Chabot and Jones, 2003; Chabot et al., 2003; Horan et al., 2003; Brandon et al., 2005a; Brandon et al., 2005b; Chabot et al., 2006; Huber et al., 2006; van Niekerk et al., 2009; Fischer-Gödde et al., 2010; Horstmann et al., 2014). Siderophile elements analyzed in this study are divided into two groups: Highly siderophile elements (HSE: here this term is exclusively used for the elements Re, Os, Ir, Ru, Pt, Rh, Pd and Au) and chalcogen elements (Te, Se and S). The HSE are strongly partitioning into metal with $D^{metal/silicate} > 10^4$ under low pressure conditions (O'Neill et al., 1995), whereas the chalcogens are moderately to highly siderophile under relevant conditions (Rose-Weston et al., 2009). These elements condensed over a wide range of temperatures in the solar nebula (Fig.1.5) and cover almost the entire temperature range during which all major chondrite mineral phases condensed (Lodders, 2003). Whole rock and component data of unequilibrated chondrites from different chondrite classes show resolvable differences in the absolute abundances of HSE and significant differences in the Re/Os, Re/Ir, Rh/Ir, Pd/Ir and Au/Ir ratios (Rambaldi, 1977b; Rambaldi et al., 1978; Wasson and Kallemeyn, 1988; Jochum, 1996; Chen et al., 1998; Walker et al., 2002b; Horan et al., 2003; Brandon et al., 2005a; Brandon et al., 2005b; Campbell et al., 2005; Horan et al., 2009; Fischer-Gödde et al., 2010; Archer et al., 2014). Previous studies suggest that the processes that may have affected the HSE abundance patterns included fractional condensation and isolation of earlier formed refractory condensates, metal-silicate-sulfide partitioning, solid metal-liquid metal partitioning, exsolution of metal and sulfide phases, melting and evaporation of volatiles, hydrothermal/aqueous alteration processes on chondrite parent bodies as well as redistribution or/and loss of mobile and volatile elements during terrestrial weathering (Rasmussen et al., 1988; Wasson and Kallemeyn 1988; Hsu et al., 1998; Campbell et al., 2002; Campbell and Humayun, 2003; Chabot and Jones, 2003; Chabot et al., 2003; Horan et al., 2003; Chabot et al., 2006; Ash et al., 2007; van Niekerk et al., 2009; Fischer-Gödde et al., 2010; Horstmann et al., 2014).

All chondrite classes are depleted in chalcogen elements compared to CI chondrites (Kallemeyn and Wasson, 1986; Dreibus et al., 1995). Chalcogen element abundance patterns also show substantial variation in chondrites and chondritic components from different classes. The variable compositions may reflect nebular heterogeneity, melting and evaporation, metal-silicate partitioning, parent body metamorphism and terrestrial weathering (Rose-Weston et al., 2009; Lorand, 1990; Dreibus et al., 1995; Huber et al., 2006; Schaefer and Fegley, 2009). Different in volatilities under nonsolar conditions was proposed as a model to account for the depletion of some volatile chalcogen elements in some chondrite groups (Wai and Wasson, 1977).

A combined systematic study of HSE and chalcogen elements in different chondrite components is important to understand the origin and evolution of those and to obtain information about the local nebular environment and processes during the formation of the precursors of chondrites and their components as well as to resolve the influence of later parent body and weathering processes.

1.1.3 ^{187}Re-^{187}Os systematics of the chondrite components

^{187}Re is the most abundant naturally occurring radioactive isotope of Re which decays to ^{187}Os by negative beta decay,

$$^{187}\text{Re} \xrightarrow{t_{1/2} \sim 4.16 \times 10^{10}} {}^{187}\text{Os} + \beta^- + \bar{V}_e \quad \text{..... (1)}$$

Rhenium and Os both have similar volatility and were condensed into the same phases at high temperatures in the solar nebula (Lodders, 2003). However, bulk chondrites and chondrite components show significant differences in ^{187}Re-^{187}Os systematics (Chen et al., 1998; Becker et al., 2001; Archer et al., 2014). Most bulk chondrites plot close to or on the 4.56 Ga ^{187}Re-^{187}Os reference isochron and chondrite classes show differences in the primordial Re/Os which is reflected in the difference of the ^{187}Os/^{188}Os between the chondrite classes (Walker et al., 2002b; Brandon et al., 2005a; Chen et al., 1998; Fischer-Gödde et al., 2010). Some chondrite components display significant scatter from the isochron and some components plot on or close to the 4.56 Ga isochron but show resolvable variations in the ^{187}Re/^{188}Os and ^{187}Os/^{188}Os (Chen et al., 1998; Becker et al., 2001; Archer et al., 2014). Previous studies suggested that late redistribution of Re and/or Os among the components is the most likely process for the disturbance in the ^{187}Re-^{187}Os systematics of the chondrite components (Chen et al., 1998; Becker et al., 2001; Walker et al., 2002b; Brandon et al., 2005a; Rankenburg et al., 2007; Horan et al., 2009; Fischer-Gödde et al. 2010; Archer et al., 2014). The details and timing of such a process can be variable for different chondrites and difficult to constrain due to large and random scatter from the reference isochron.

Most bulk rocks of primitive chondrites are undeviated from isochron but show correlated differences in ^{187}Re/^{188}Os and ^{187}Os/^{188}Os (Walker et al., 2002b; Fischer-Gödde et al., 2010). These differences in chondrite components could have been achieved by either fractional condensation followed by the isolation of earlier condensed phases or other processes such as oxidation, volatilization and mobilization processes that occurred at 4.56 Ga (Chen et al., 1998; Becker et al., 2001; Walker et al., 2002b; Brandon et al., 2005a; Rankenburg et al., 2007; Horan et al., 2009; Fischer-Gödde et al. 2010; Archer et al., 2014). However, the detailed processes that fractionated Re/Os remain obscure. This study also aims to better constrain processes that may have fractionated Re/Os in components from different chondrite classes.

1.2 Scope of the thesis

The main objective of the present thesis is to constrain the fractionation processes related to the formation and evolution of chondrite components. The foundation of the dissertation is

constructed on the processes that may affect the abundances of HSE, chalcogen, major and minor elements and the ^{187}Re-^{187}Os systematics in the separated components of unequilibrated chondrites from carbonaceous, ordinary and enstatite chondrite groups.

The core of the dissertation are four scientific manuscripts. The first manuscript (Chapter 2) was resubmitted after review and is designated to be published in Geochimica et Cosmochimica Acta soon. The second manuscript (Chapter 3) has been submitted to Meteoritics & Planetary Science and is currently under review. The third has been submitted to Geochimica et Cosmochimica Acta and is currently under review. The fourth manuscripts will be submitted soon to Meteoritics & Planetary Science.

All four manuscripts were written by Yogita Kadlag and Harry Becker affiliated with the Freie Universität Berlin, Germany. The present work is based on research proposals written by Harry Becker and Yogita Kadlag and funded by the Deutsche Forschungsgemeinschaft (DFG) under the special priority program 'The First 10 Million Years of the Solar System - a Planetary Material approach'.

1.2.1 Chapter 2: Fractionation of highly siderophile and chalcogen elements in components of EH3 chondrites.

Harry Becker designed the project and obtained the required funding for the project from DFG SPP 1385. Yogita Kadlag carried out the sample preparation, chemistry and performed the analyses data reduction and interpretation. Yogita Kadlag and Harry Becker wrote the manuscript. Christiane Behr, Ralf Milke and Franziska Mangels helped in the thick section preparation and electron microprobe analysis which were used for the petrological description of the bulk rock sections in the appendix. This manuscript is submitted to Geochimica et Cosmochimica Acta.

Chapter 2 discusses the variation in the abundances of HSE, chalcogen elements, ^{187}Re-^{187}Os systematics, major and minor elements in separated components of enstatite chondrites. One of the enigmas associated with these highly reduced primitive rocks in our solar system, is the enrichment of Au (Baedecker and Wasson, 1975; Hertogen et al., 1983; Kallemeyn and Wasson, 1986; Kong et al., 1997; Fischer-Gödde et al., 2010). The important questions I want to address in this chapter concern the possible processes for the enrichment of Au and fractionation of chalcogen elements in enstatite chondrites.

1.2.2 Chapter 3: Highly siderophile and chalcogen element constraints on the origin of components of the Allende and Murchison meteorites

Harry Becker was responsible for obtaining samples from the Field Museum, Chicago. Yogita Kadlag was responsible for the component separation, chemistry and analysis, data

reduction and interpretation Yogita Kadlag and Harry Becker wrote the manuscript. This manuscript is submitted to Meteoritics & Planetary Science.

Chapter 3 focusses on the variation in the ^{187}Re-^{187}Os systematics, HSE and chalcogen element abundances in the separated components of carbonaceous chondrites. Previous work on the HSE abundances in carbonaceous chondrites was mainly focused on the refractory metal nuggets and chondrite components from random sample material (Palme and Wlotzka, 1976; Blander et al., 1980; Blum et al., 1989; Sylvester et al., 1990; Palme et al., 1994; Becker et al., 2001; Campbell et al., 2003; Berg et al., 2009; Archer et al., 2014). This chapter shows results of a systematic mass balance study of HSE and chalcogen elements in all separated components of aliquots of the Allende and Murchison meteorites.

1.2.3 Chapter 4: ^{187}Re-^{187}Os systematics, highly siderophile and chalcogen element abundances in the components of unequilibrated L chondrites

Project proposal, funding and samples were organised by Harry Becker. Yogita Kadlag was responsible for the component separation, chemistry, instrumental analysis and data reduction. B.Sc. students Franziska Schubring and Tanja Giebner worked on some components of QUE 97008 for their bachelor thesis. Christiane Behr, Ralf Milke and Franziska Mangels helped in the thick section preparation and electron microprobe analysis of the bulk rock section of QUE 97008.Yogita Kadlag and Harry Becker wrote the manuscript. This manuscript is submitted to Geochimica et Cosmochimica Acta.

Chapter 4 discusses the processes responsible for the fractionation of HSE and chalcogens in the separated components of L chondrites.

1.2.4 Chapter 5: Origin of highly siderophile and chalcogen element fractionations in the components of unequilibrated H and LL chondrites

Harry Becker and Yogita Kadlag were responsible for writing and planning the project proposal, obtaining the funding from DFG and samples from the Smithsonian National Museum of Natural History, Washington D.C. Yogita Kadlag was responsible for the component separation, chemistry, instrumental analysis and data reduction. Yogita Kadlag and Harry Becker wrote the manuscript. This manuscript will be submitted to Meteoritics & Planetary Science.

Chapter 5 is focused on HSE and chalcogen element fractionations in components of H and LL chondrites. Previous studies suggested that components with different HSE ratios are present in the magnetic portion of ordinary chondrites (Chou et al., 1973; Rambaldi, 1976, 1977a and b; Rambaldi et al., 1978; Grossman and Wasson, 1985; Kong and Ebihara, 1997; Humayun and Campbell, 2002). Two different carriers were also observed in the magnetic and nonmagnetic components of H chondrites (Horan et al., 2009), with resolvable Pd/Ir ratios. Wheather similar components also exist in L and LL group chondrites as well as alternative possibilities for the

origin of these components exists will be discussed in chapter 4 and 5. The most important secondary process in case of meteorite “finds” is alteration during terrestrial weathering. These chapters also discuss effects of metamorphism and terrestrial weathering in cold desserts on the abundances of HSE and chalcogen elements.

Chapter 2

Fractionation of highly siderophile and chalcogen elements in components of EH3 chondrites

2.1 Abstract

Abundances of highly siderophile elements (HSE: Re, platinum group elements and Au), chalcogens (Te, Se and S), $^{187}Os/^{188}Os$ and the major and minor elements Mg, Ca, Mn, Fe, Ni and Co were determined in the components of Sahara 97072 (EH3, find) and Kota Kota (EH3, find) in order to understand the element fractionation processes. In a ^{187}Re-^{187}Os isochron diagram, most magnetic components lie close to the 4.56 Ga IIIA iron meteorite isochron, whereas most other components show deviations from the isochron caused by late redistribution of Re, presumably during terrestrial weathering. Metal- and sulfide rich magnetic fractions and metal-sulfide nodules are responsible for the higher $^{187}Os/^{188}Os$ in bulk rocks of EH chondrites compared to CI chondrites. The HSE and chalcogens are enriched in magnetic fractions relative to slightly magnetic and nonmagnetic fractions and bulk compositions, indicating that Fe-Ni metal is the main host phase of the HSE in enstatite chondrites. HSE abundance patterns indicate mixing of two components, a CI chondrite like end member and an Au-enriched end member. Because of the decoupled variations of Au from those of Pd or the chalcogens, the enrichment of Au in EH metal cannot be due to metal-sulfide-silicate partitioning processes. Metal and sulfide rich nodules may have formed by melting and reaction of pre-existing refractory element rich material with volatile rich gas. A complex condensation and evaporation history is required to account for the depletion of elements having very different volatility than Au in EH chondrites. The depletions of Te relative to HSE, Se and S in bulk EH chondrites are mainly caused by the depletion of Te in metal. S/Se and S/Mn are lower than in CI chondrites in almost all components and predominantly reflect volatility-controlled loss of sulfur. The latter most likely occurred during thermal processing of dust in the solar nebula (e. g., during chondrule formation), followed by the non-systematic loss of S during terrestrial weathering.

2.2 Introduction

^{187}Re-^{187}Os systematics, concentrations of highly siderophile elements (HSE) and chalcogen elements display resolvable differences between different chondrite classes (Dreibus et al., 1995; Walker et al., 2002b; Horan et al., 2003; Brandon et al., 2005a; Brandon et al., 2005b; Fischer-Gödde et al., 2010). The most obvious differences occur in the form of depletions or enrichments of the moderately volatile elements Pd and Au relative to refractory HSE in some carbonaceous, enstatite and ordinary chondrites, which are approximately mirrored by lithophile volatile elements (Wasson and Kallemeyn, 1988). Fractionations of some refractory HSE of up to 20% between different chondrite groups also have been noted. They are most obvious for Re (or its time-integrated proxy ^{187}Os/^{188}Os) and Rh and their ratios with other refractory HSE (e. g., Ir). Such fractionations either reflect incorporation of differentiated precursor material in chondrules (Libourel and Krot, 2007), or fractional condensation, evaporation or volatility control at variable fo_2, or several of these processes (Palme et al., 1998; Becker et al., 2001; Walker et al., 2002b; Horan et al., 2003; Horan et al., 2009; Fischer-Gödde et al., 2010).

Additional processes which might be responsible for the fractionation of HSE in ordinary and in enstatite chondrites include metal-silicate partitioning, sulfide-silicate partitioning and solid metal-liquid metal partitioning during chondrule formation or during impacts on the parent bodies (Rambaldi and Cendales, 1980; Kallemeyn and Wasson, 1986; Kong et al., 1997; Chabot and Jones, 2003; Chabot et al., 2003; Horan et al., 2003; Chabot et al., 2006; van Niekerk et al., 2009; Fischer-Gödde et al., 2010; Horstmann et al., 2014). Hints for impact induced redistribution of some HSE by solid metal-liquid metal partitioning have been reported for brecciated enstatite and R chondrites (Kallemeyn et al., 1996; van Niekerk et al., 2009; Fischer-Gödde et al., 2010). In contrast recent *in situ* data on the E chondrite metal (Horstmann et al., 2014) suggests that melt objects were formed prior to the accretion of primitive E chondrites. What fraction of the bulk rock HSE pattern of enstatite chondrites can be explained by such processes is uncertain. The relative importance of these processes for the HSE fractionations in chondrites and at which stage of their evolution they occurred, predominantly in the nebular environment or during impact-induced melting on the parent bodies, remains unclear.

HSE abundance variations in unequilibrated chondrites (except EL chondrites, which show nearly CI chondritic patterns) indicate that the bulk rocks are composites of two or more unequilibrated components (Horan et al., 2003; Fischer-Gödde et al., 2010 and references therein, Horstmann et al., 2014). Because chondrites are mixtures of different components, which were formed at different physicochemical conditions in the early solar nebula (e. g., Scott and Krot, 2003), bulk rock data alone cannot provide clear answers regarding the origin of the fractionated HSE abundance patterns of chondrites.

Some early studies carried out on chondrite components have identified differences in abundances of Os, Re, Ru and Pt and HSE/Ni of different size fractions of metal from H, L and LL chondrites (Rambaldi, 1977a, 1977b and Rambaldi et al., 1978). These workers have argued for volatility-controlled fractionation of the HSE and Ni in metal from unequilibrated ordinary chondrites. Kong et al. (1995) and Kong and Ebihara (1996, 1997) have studied siderophile elements in metals from H, L and LL chondrites and concluded that the abundances of moderately siderophile elements in metal from unequilibrated ordinary chondrites are consistent with metal-silicate partitioning. Horan et al. (2009) have obtained very distinct patterns and abundances of the HSE in 'magnetic' and 'nonmagnetic' fractions of Dhajala (H3.8) and Ochansk (H4). The data require two distinct HSE carrier phases in the components of these chondrites. The presence of two metal carriers with variable Re/Os and Pd/Ir reflect fractionation at different temperatures or exposure of metal carriers to different fo_2 conditions after their formation. Physically separated components of carbonaceous chondrites including CAIs, chondrules and matrix also show fractionated Re/Os compared to bulk rocks and CI chondrites (Becker et al., 2001; Walker et al., 2002b; Archer et al., 2014).

Previous work on metal-silicate and sulfide-silicate intergrowths, textures, metal nodules and trace element abundances in enstatite chondrites have been interpreted to reflect i) pre-accretionary events like nebular condensation or pre-accretionary melting on earlier parent bodies (Weisberg et al. (1997, 2013); Lehner et al., 2010; El Goresy et al., 2012; Horstmann et al., 2014) or ii) post-accretionary impact melting (van Niekerk et al., 2009; Rubin and Wasson, 2011; van Niekerk and Keil, 2011). Systematic study of the components of EH3 chondrites will help in distinguishing between these different models.

Enstatite chondrites are special in that they are the most reduced primitive rocks known from our solar system (Hertogen et al., 1983; Kallemeyn and Wasson, 1986). Their unique mineralogy include various types of primary and secondary sulfides (troilite FeS, niningerite (Mg, Fe, Mn)S, oldhamite CaS, daubreelite $FeCr_2S_4$, caswellsilverite $NaCrS_2$, djerfisherite K_6Na [Fe, Cu, $Ni]_{25}S_{26}Cl$, sphalerite (Zn, Fe, Mn)S) are the host phases of S and Se in EH chondrites (Lin and El Goresy, 2002 and references therein). Their oxygen isotopic composition is very similar to the Earth and Moon (Clayton et al., 1984) and they are believed to have formed at shorter heliocentric distances compared to other chondrite classes (Wasson, 1988; Shukolyukov and Lugmair, 2000). EH chondrites show the highest Au abundances of all chondrite classes (Baedecker and Wasson, 1975; Hertogen et al., 1983; Kallemeyn and Wasson, 1986; Kong et al., 1997; Fischer-Gödde et al., 2010), the origin of which is still not clear. Hence, study of components of enstatite chondrites provides a unique opportunity to understand fractionation processes, which might also have been operating in or close to the terrestrial planet formation region of the solar system.

Because very little work was performed on the trace element abundances in components of unequilibrated enstatite chondrites (Kong et al., 1997; Barrat et al., 2014; Horstmann et al., 2014), the present study is focusing on the components of the EH3 chondrites Sahara 97072 and Kota Kota. Both meteorites are finds. Kota Kota was classified with shock stage S3 (Rubin et al., 1997), Sahara 97072 may have experienced shock stage S2, like its paired meteorite Sahara 97096 (Grossman, 1998). Sahara 97072 represents a highly unequilibrated breccia and its mineralogy and composition suggest that S-rich areas mainly have formed from the reaction of enstatite and Fe-Ni metal with S_2 and CO rich gas at 1000-1100 K (Lehner and Buseck, 2009; Lehner et al., 2010, 2013). Matrix of this meteorite shows a unique trace element abundance pattern and was interpreted to have formed in a different nebular location compared to other components (Lehner and Buseck, 2011). Presolar grains found in the matrix of Sahara 97072 supports the presence of a highly unequilibrated matrix component (Ebata et al., 2006, 2008). A textural and compositional study of Kota Kota (Leitch and Smith, 1981) suggests that enstatite chondrites are comprised of material from at least two different sources. These different sources may also have different HSE carriers.

Recently, we have developed techniques that permit simultaneous determination of the abundances of all HSE, $^{187}Os/^{188}Os$, and the chalcogens S, Se and Te in the same sample digestion aliquot of chondrites by using isotope dilution, internal standardization, ICP-MS and negative thermal ionization mass spectrometry (Fischer-Gödde et al., 2010; Wang et al., 2013). In the present contribution, we have applied these techniques to obtain precise data on physically and magnetically separated components from Sahara 97072 and Kota Kota. We have expanded these methods to include abundances of the major and minor elements Mg, Ca, Mn, Fe, Co and Ni in digested components. Major element data will help to distinguish the affinity of trace elements for different phases because most of these analyzed elements have overlapping condensation temperatures in the solar nebula (Fig.2.1). The goal of present study is to provide a comprehensive data set for the HSE, chalcogens, major and minor elements in components of EH3 chondrites to better understand the element fractionation processes in these primitive objects and in their formation region in the solar nebula. Another goal is to resolve the chemical effects of terrestrial weathering from the nebular and planetary processes on enstatite chondrites. Terrestrial weathering may affect specific

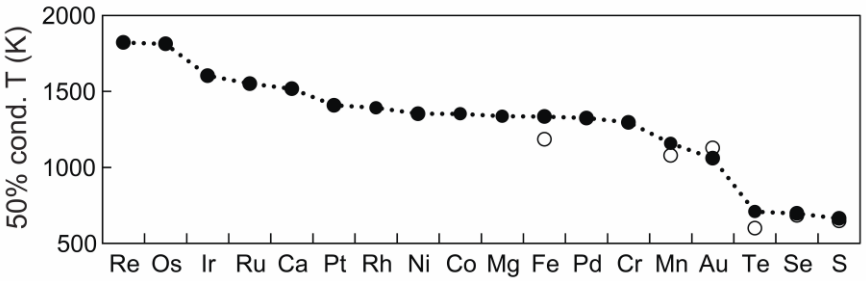

Fig.2.1. Closed circles show the condensation sequence of the analyzed elements in a gas of solar composition, at 10^{-4} bar (50% condensation temperatures are from Lodders, 2003). Open circles represents change in the 50% condensation temperature at 10-6 bar (Wai and Wasson, 1977) for some elements.

siderophile elements, notably S, Se and Re (Lorand, 1990; Dreibus et al., 1995; Walker et al., 2002b; Huber et al., 2006; Rankenburg et al., 2007).

2.3 Experimental

2.3.1 Sample Preparation

Specimens of Kota Kota (BM.1905, 355, Natural History Museum London) and Sahara 97072 of about one gram weight were broken into pieces. The larger part was separated into components and digested for the analysis of HSE, chalcogen and major elements in this study. Remaining bulk rock fragments were embedded into epoxy resin and used for petrologic study (see Fig.2.A1 and 2.A2 of the appendix). Components like large chondrules, metal-sulfide nodules and fine grained matrix, which were easy to identify by naked eye and under the binocular microscope, were separated from broken pieces. Fine grained bright white colored mineral phases found in matrix. These phases were separated from matrix named as white mineral phases (WMPs). A dark, big (~9-10 mm) enstatite rich clast (DC) occurred in our aliquot of Sahara 97072, containing the large enstatite crystals and small grains of pure silica (<50 µm) enclosed in the enstatite crystals. A part of the clast was digested for the trace element study and another part was preserved for petrological study on the electron microprobe. A petrological description of the dark clast is given in Fig.2.A3. Plastic tweezers have been used to pick up different components and to mechanically separate matrix material in order to avoid sample contamination.

Pieces were gently crushed in an agate mortar in order to remove small chondrules and fragments thereof. Matrix attached to chondrules, metal-sulfide nodules (MSN), WMPs and DC was removed as much as possible using tweezers. As both meteorites are ‘finds’, any weathered or rusty material was removed mechanically as much as possible. After separation of WMPs, DC, chondrules, MSN and fragments of these components, remaining material was separated into different size fractions using nylon sieves. Samples with increasing order of grain coarseness are named as: less than 80 µm (<80), 80-150 µm (80-150), 150-200 µm (150-200), 200-250 µm (200-250) and the coarsest fraction is greater than 250 µm (>250). Each size fraction was further separated into three types magnetic (M), slightly magnetic (SM) and nonmagnetic (NM) using a hand magnet (Becker et al., 2001; Walker et al., 2002b; Horan et al., 2009). Amounts of nonmagnetic fractions were very small; therefore NM fractions of all sizes were finally combined together and digested as a single sample. Weights of digested samples ranged from 0.9 mg to 29.6 mg (Table 2.1). The low weights of WMPs reflect their low abundances.

2.3.2 Sample dissolution and chemical separation

The isotope dilution method has been used to obtain precise concentration and isotopic data for HSE and chalcogens, except for the monoisotopic elements Au and Rh concentrations, which were obtained by internal standardization with respect to Ir and Ru intensities, respectively. Samples were weighed into quartz vessels and a ^{185}Re-^{190}Os mixed spike, a ^{191}Ir-^{99}Ru-^{194}Pt-^{105}Pd mixed spike, a ^{77}Se-^{125}Te mixed spike and a ^{34}S spike were added to samples. Reverse aqua regia (1ml HCl: 2 ml HNO_3) was added to the sample-spike mixture and vessel lids were sealed by using teflon tape. Samples and total chemistry blanks were digested in sealed quartz vessels under a nitrogen gas pressure of 100 bars for 16 hours at 320°C in the Anton Paar^{TM} HPAS (High Pressure Asher System). After opening the HPAS, Os was separated from other HSE and matrix by solvent extraction in CCl_4 and back extraction in HBr (Cohen and Waters, 1996; Walker et al., 2002a), this process was carried out in an ice bath to avoid the escape of volatile Os. Osmium was further purified by micro distillation into distilled HBr (Roy-Barman, 1993).

After Os separation, part of the reverse aqua regia aliquot (~1/3) was evaporated and converted into chloride form by adding HCl three times (two times 9M and once 1.25M). Re, Ir, Ru, Pt, Rh, Pd and Au were separated on Biorad^{TM} Econo-column filled with 10 ml cation exchange resin (Eichrom^{TM}AG50 W-X8, 100-200 mesh). A detailed description of the HSE separation procedure is given by Fischer-Gödde et al. (2010). About 1/5 of the digestion solution (0.5-0.6 ml) was taken to dryness and converted into chloride form using 9M HCl. Te was separated on a Bio-Rad column filled with 3ml of pre-cleaned anion exchange resin (Eichrom^{TM} AG1-X8, 100-200 mesh) and eluted with 1M HNO_3. Se and S were separated from Fe and collected with remaining matrix during Te separation and further separated from other matrix elements on another Bio-Rad column filled with 3ml cation exchange resin (Eichrom^{TM}AG50 W-X8, 100-200 mesh) and collected in 0.1M HNO_3 (for details see Wang et al., 2013).

A small aliquot (0.1 ml) of reverse aqua regia was dried down at 85°C and then converted into nitric acid form by adding two times 0.1 ml 14M HNO_3. After evaporation, this fraction was diluted in 0.28M HNO_3 and analyzed on the Element XR ICP-MS at Freie Universität Berlin. Concentrations of major and minor elements were determined by an external calibration against dilutions of a solution made from about 10 mg of the Smithsonian Allende meteorite standard reference powder (USNM 3529, Split 18, position 1). The standard was digested in reverse aqua regia and processed the same way as the samples. Experience shows that the aqua regia digestion method can efficiently dissolve metal, sulfide, labile silicates (including olivine) and oxide phases but pyroxenes may not dissolve completely if the sample/acid ratio is too large. No visible undigested residue or precipitate was observed in the reverse aqua regia digestion solution, which may reflect the low sample/acid ratio during digestion. Ratios of Ca/Mg, Fe/Ni and Ni/Co of all dilutions of the Allende standard powder analyzed in this study are within 5% of the data by Jarosewich et al. (1987). Thus ratios and abundances of all relevant elements should give internally consistent results. The dilution factor ranging from $4.5*10^5$ to $1.2*10^7$ was chosen

depending on the concentrations of the elements in the aliquot and the required signal intensity to obtain precise enough data. A 10 ppb Sc solution was added to the samples and to the different dilutions of the calibration standard as an internal standard for drift correction. Signal intensities of all elements were normalized to ^{45}Sc intensities. Major and minor element abundances were calibrated using Sc-normalized intensities of dilutions of the digested Allende standard.

2.3.3 Mass spectrometry

Osmium was loaded on ESPN Pt filaments outgassed in air and Os isotopes were measured as OsO_3^- on the Thermo Finnigan™ Triton at Freie Universität Berlin. Isotopic ratios are corrected for isobaric interferences from other O isotopes, spike contribution and linear mass fractionation relative to $^{192}Os/^{188}Os = 3.0827$ (Luck and Allégre, 1983). Osmium isotopic measurements of all magnetic and slightly magnetic components and Sahara 97072 MSN fraction were carried out on faraday cups, whereas other components were measured on the electron multiplier. $^{187}Os/^{188}Os$ values of the University of Maryland Os standard solution (Shirey and Walker, 1998; Fischer-Gödde et al., 2010) over the period of analysis were 0.11381 ± 0.00005 (2σ, n=8) for faraday cup measurements and 0.1139 ± 0.0006 (2σ, n=11) for electron multiplier measurements. ^{185}Re was also measured to monitor interferences on ^{187}Os.

Other elements were analyzed on an Element XR sector field ICP-MS at Freie Universität Berlin. Analyses of Re, Ir, Pt and Au were carried out in the low resolution mode using a Scott-type glass spray chamber. Ir, Ru, Pt, Rh and Pd were measured in the low-resolution mode by using an Aridus membrane desolvator sample introduction system, which enhances signal intensity and limits oxide formation. Oxide formation rates were monitored by the ratio of $^{156}CeO^{2+}/^{140}Ce$ which was < 0.5% in case of all measurements with the Aridus. Te and Se were measured in the low resolution mode by using hydride generation and a modified cyclone double pass Scott-type spray chamber setup.

Sulfur isotopic measurements were carried out at medium resolution to exclude minor interferences from oxides and doubly charged ions as well as to avoid major hydride interferences on ^{33}S and ^{34}S from $^{32}S^{1}H$ and $^{33}S^{1}H$, respectively. Details of the measurement protocols of the HSE and chalcogens were given by Fischer-Gödde et al. (2010) and Wang et al. (2013).

Concentrations of Mg, Ca, Mn, Fe, Co and Ni were measured with a normal Scott-type glass spray chamber at medium resolution (R = 4500-5000) in order to avoid isobaric and molecular interferences. ^{25}Mg, ^{42}Ca, ^{44}Ca, ^{45}Sc (internal standard), ^{55}Mn, ^{57}Fe, ^{59}Co, ^{60}Ni and ^{61}Ni were chosen for analysis because these masses are less affected by interferences than other masses. All isotopes were measured with a counting time of 0.1sec/scan (total number of scans n = 150).

2.3.4 Precision, accuracy and analytical blanks

Total procedure blanks have been determined with each set of digestion. Average values of total procedure blanks over a period of time were (n = 15): Re = 8 ± 3 pg, Os = 0.5 ± 0.3 pg, Ir = 0.9 ± 0.8 pg, Ru = 1 ± 1 pg, Pt = 9 ± 4 pg, Rh = 3 ± 1 pg, Pd = 41 ± 19 pg, Au = 5 ± 3 pg, Te = 50 ± 20 pg, Se = 2.4 ± 0.5 ng and S = 9 ± 1 μg. Total procedure blanks have negligible effects (<5%) on most components because of the high concentrations of analyzed elements, whereas blank corrections are critical for the nonmagnetic fractions because of the low concentration of the HSE in these fractions and the small sample weight (Table 2.1). The resulting corrections are as much as 50% for Re and Rh and less than 20% for all other elements.

The typical precision of HSE and chalcogen data is < 0.2% relative standard error (RSE) and accuracy is < 3% in case of all measurements (mostly spike calibration uncertainties for specific elements). For major elements, uncertainties of most samples are less than 5%, except for Ca (9-20%). In few cases like WMPs and NM fractions uncertainties are also relatively high for other major elements such as for Mg ~ 6%, Mn ~ 6%, Fe ~ 8%, Co ~ 20% and Ni ~ 10%. These uncertainties were calculated from the standard deviation of measured intensities and the error associated with the slope of the linear regression calibration curves of the different dilutions of digested Allende standard reference powder.

2.4 Results

2.4.1 Major element distribution in components

The methods used to separate different components are imperfect. Therefore, separated components in this study are a mixture of phases with some dominating the mixture. To verify the quality of separation of different phases in components, we analyzed lithophile, chalcophile and siderophile major and minor elements (Table 2.2). The variation of some of these elements in components is shown in Fig.2.2 and Fig.2.3. The components show well resolved differences in the ratios of lithophile (e. g., Mg and Ca, Fig.2.3d) and siderophile (Fe, Ni, Fig.2.2) elements, indicating a good separation of metals and silicates (Fig.2.3), although sulfides tend to be intergrown with both metals and silicates (Fig.2.3a and e). Approximate estimates of silicates, sulfides and metal phases in each separate are shown in Table 2.3. The sulfide content was calculated by assuming that S is contained exclusively in sulfide phases. The metal content was determined by assuming that most Fe is present in metal and sulfides (Campbell et al., 2005). Silicates were calculated by subtracting metal and sulfide content from total. Metal rich (M) fractions have higher Mn/S, Fe/Mn, Fe/S, Fe/Mg and Mn/Mg (Fig.2.3) than other components and CI chondrites (Fig.2.3). M components have very similar sulfide content (Table 2.3), but show large variations in Mn, Mg and Fe abundances and a linear correlation between Mn and Mg

(Fig.2.3f). Nonmagnetic and slightly magnetic components show weak inverse correlations between Mn and Mg, presumably because of a higher proportion of Mn-Mg rich niningerite in magnetic components. Nonmagnetic components are mainly consisting of enstatite (Fig.2.3f). The lower metal and sulfide content of WMPs, chondrules and nonmagnetic fractions indicate that these components are predominantly comprised of silicates rich in Mg and Ca (Fig.2.3).

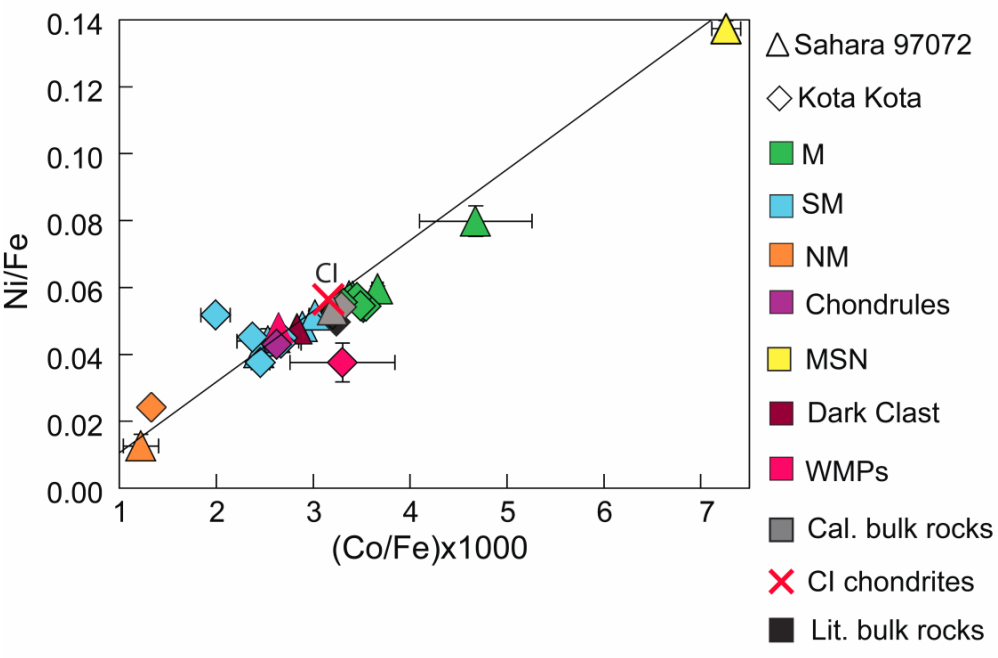

Fig.2.2. Ratios of siderophile elements Ni/Fe and Co/Fe. Triangles: Sahara 97072, diamonds: Kota Kota. Black reference line indicates the Ni/Co ratio in CI chondrites. Error bars represent 2σ uncertainty on concentration. M, SM, NM are magnetic, slightly magnetic and nonmagnetic fractions, respectively. Gray symbol shows corresponding bulk rock values calculated from a mass balance of all components. Black symbols show literature bulk rock data. Red cross represents CI chondritic values. Bulk rock data for Kota Kota and CI chondrites from Easton and Elliott (1977), Easton (1985) and Lodders (2003), respectively.

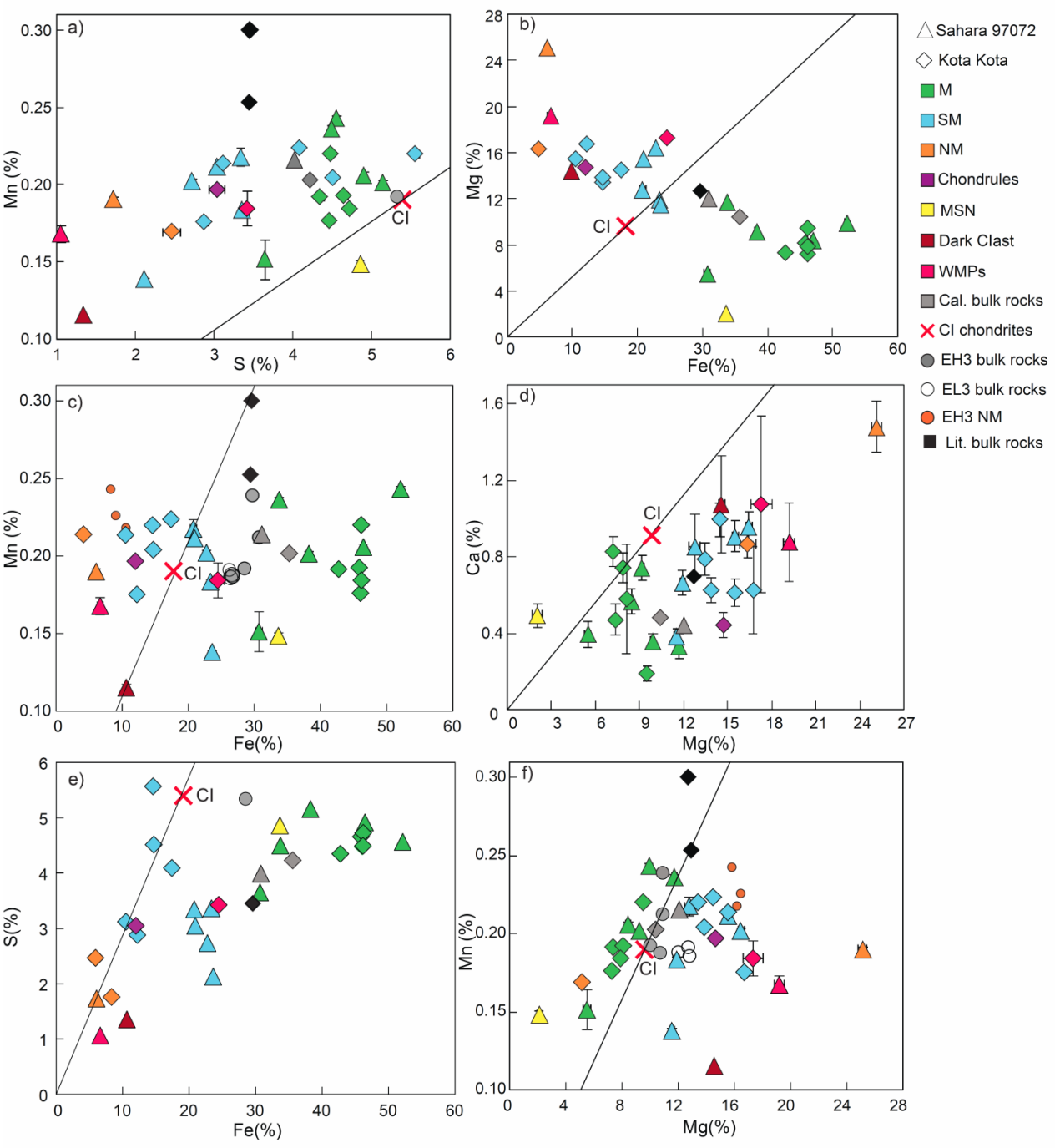

Fig.2.3. Variation of trace, minor and major elements of different geochemical affinities in components of Sahara 97072 and Kota Kota. a) Mn-S, b) Mg-Fe, c) Mn-Fe, d) Ca-Mg, e) S-Fe and f) Mn-Mg. Circles represent literature data for nonmagnetic fractions and bulk rocks of EH3 and EL3 chondrites (Easton and Elliott, 1977; Easton, 1985; Kong et al., 1997 and references therein). CI chondrite data from Lodders, (2003).

2.4.2 ^{187}Re-^{187}Os isotopic systematics

Data for $^{187}Os/^{188}Os$, $^{187}Re/^{188}Os$ and Δ_{Os} of the components are listed in Table 2.1. A ^{187}Re-^{187}Os isochron diagram and the variation of Δ_{Os} with $^{187}Re/^{188}Os$ among components is shown in Fig.2.4. Rhenium, the most refractory HSE during condensation in solar gas (Fig.2.1), can be easily mobilized in oxidizing environments (Palme et al., 1998; Rankenburg et al., 2007; Horan et al., 2009). It shows variable CI chondrite-normalized abundances in different components (Fig.2.5). The Re/Os ratios vary from 0.03 to 0.19 and are mostly controlled by variations in Re abundances. In most components, except some M and SM components, variation in Re/Os does

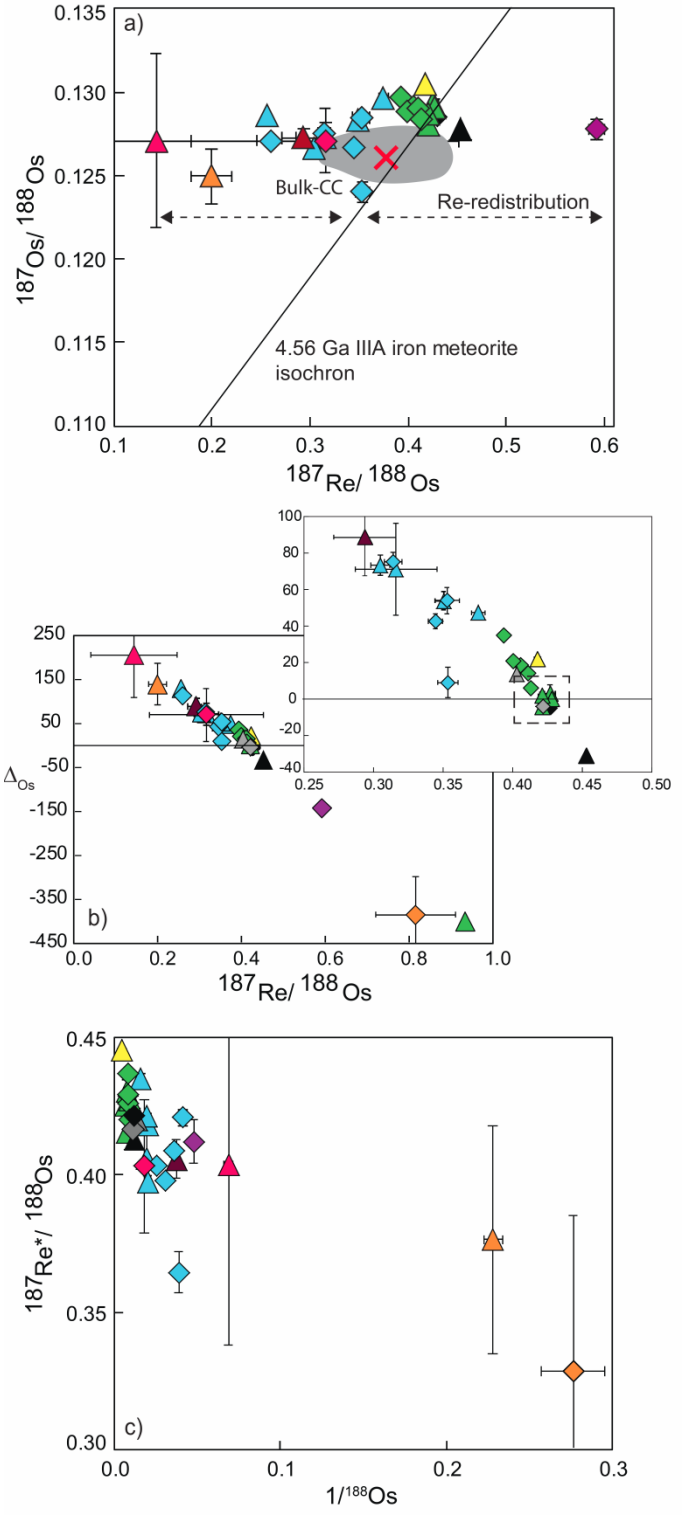

Fig.2.4. a) Variation of $^{187}Os/^{188}Os$ and $^{187}Re/^{188}Os$ in components of Sahara 97072 and Kota Kota. The black line is the IIIA iron meteorite isochron reflecting an age of 4.56 Ga (Smoliar et al., 1996). b) Δ_{Os} - $^{187}Re/^{188}Os$ variation in the components of Sahara 97072 and Kota Kota. Δ_{Os} represent the deviation of $^{187}Os/^{188}Os$ of components from the $^{187}Os/^{188}Os$ at 4.56 Ga. Definition of the Δ_{Os} is given in the caption of Table 2.1. c) $^{187}Re^*/^{188}Os$-$1/^{188}Os$ plot. The dashed square in the enlarged version of b) shows the magnetic components that plot on or very close to the isochron. The higher Re-Os in these components, likely reflect nebular fractionation processes, whereas all components that show deviations from the isochron were affected by recent open system behavior of Re. Bulk rock values shown (black symbols) from Walker et al. (2002b) and Fischer-Gödde et al., (2010). Symbols are as in other figures. Gray field in a) represents the data for bulk rocks of carbonaceous chondrites (Walker et al., 2002b; Brandon et al., 2005a and Fischer-Gödde et al., 2010).

not correlate with the Os isotopic composition, implying that the isotopic systematics have been reset recently. Re/Os ratios in magnetic components are higher than in CI chondrites and most of the SM and NM fractions. The Re/Os ratios in magnetic separates are closest to the bulk rock values because they host most of the Re and Os of the bulk rock. Most of the magnetic components lie near the 4.56 Ga IIIA iron meteorite reference isochron (Fig.2.4a) of Smoliar et al. (1996). In SM and NM fractions (except one NM fraction of Kota Kota), Re/Os ratios are often lower than in the bulk rock. Re* is the Re abundance calculated from the measured $^{187}Os/^{188}Os$ ratio and an age of the sample of 4.56 Ga, assuming that the Os isotopic composition was not affected by later processes (Fig.2.4c). In NM fractions the blank contribution to Re is high so it is hard to say if the variation of $^{187}Re^*/^{188}Os$ compared to the bulk rock is indigenous or not. In case of SM fractions differences in $^{187}Re^*/^{188}Os$ of up to 50% exist compared to the bulk rocks (Fig.2.4). The M 80-150 fraction from Sahara 97072 and a NM and chondrule fraction from Kota Kota show suprachondritic $^{187}Re/^{188}Os$ (0.934 ± 0.001, 0.82 ± 0.09 and 0.593 ± 0.008, respectively).

2.4.3 HSE abundances

Abundances of the HSE for components of Sahara 97072 and Kota Kota are listed in Table 2.1. Bulk rock data of both meteorites from the literature are also given (Horan et al., 2003; Fischer-Gödde et al., 2010). HSE abundances normalized to CI chondrites are shown in Fig.2.5. Important features of the abundance pattern are: (1) Large variations in Re/Os ratios among the components, magnetic components from both meteorites show slightly higher measured Re/Os and Os/Ir than CI chondrites (Fig.2.6). (2) Most components (except WMPs and NM fractions from Kota Kota) show almost unfractionated abundance patterns of Os, Ir, Ru, Pt and Rh with respect to the bulk rock as well as CI chondrites (Fig.2.5, 2.6). (3) Enrichment of moderately volatile elements (Pd, Au) in most components (Fig.2.5 and 2.7). The enrichment of Pd compared to refractory HSE in M and SM components is similar to bulk rocks of EH chondrites (Figs.2.5 and 2.7a). Au/Ir in M components is higher than bulk rocks and in other components (Fig.2.7b). The high Au/Ir in M components are the cause of the high Au/Ir ratio in bulk rocks of EH chondrites.

Re and Os abundances do not show systematic variations with grain size (Table 2.1). In case of Sahara 97072, Ir, Ru, Pt, Rh and Pd abundances are inversely correlated with grain size of magnetic separates (except for the M 150-200 fraction, which shows higher concentrations of all HSE than the M 80-150 fraction, Table 2.1). Abundances of refractory HSE are higher in the fine grained magnetic fractions and may represent matrix metal. In contrast to Sahara 97072, components of Kota Kota do not show a relationship between grain sizes and HSE abundances.

WMPs show low abundances (~ 0.3-0.7*CI) of HSE. WMPs and the DC from Sahara 97072 show CI chondrite-like HSE ratios. Spherical MSN from Sahara 97072 show unfractionated HSE abundance patterns relative to CI chondrites and show the highest abundances of refractory HSE of all components (Fig.2.4-2.7). The Kota Kota chondrule fraction is composed of metal poor silicate chondrules and thus shows depleted abundances of refractory HSE compared to CI chondrites, yet unfractionated HSE abundance patterns (Fig.2.5). Variations of Ca, Mg and siderophile elements in the chondrule fraction of Kota Kota are similar to the slightly magnetic material of *both* Kota Kota and Sahara 97072 (Figs. 2.2, 2.3 and 2.5- 2.7). Thus, slightly magnetic fractions probably represent mostly silicate rich chondrule material, which, besides metal and sulfides, comprises the main constituent of EH3 chondrites.

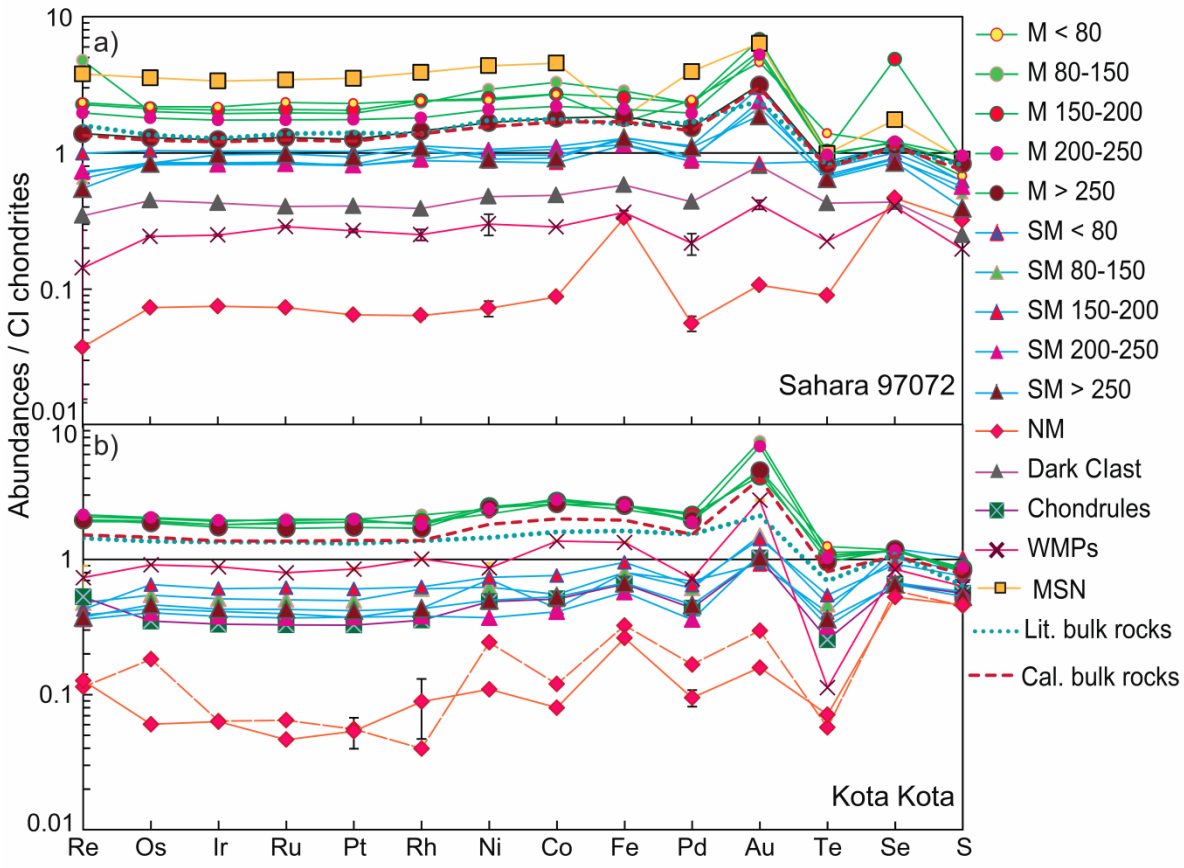

Fig.2.5. Element abundances in components of Sahara 97072 and Kota Kota normalized to CI chondrites. Elements are ordered from left to right on the basis of decreasing 50% condensation temperatures in the solar nebula (Lodders, 2003). Literature bulk rock data of CI chondrites, Kota Kota, Sahara 97072 and EH3 chondrites from the sources mentioned in the captions of Table 2.1 and 2.2 and Fig.2.3.

HSE abundances of the NM fraction of Sahara 97072 are nearly unfractionated (except Re and Au) relative to CI chondrites, but depleted compared to Fe concentrations (Fig.2.5). The NM fraction of Kota Kota has a strongly fractionated HSE abundance pattern with higher abundances of Re, Os, Pd and Au compared to other HSE, indicating more complex HSE fractionation

processes compared to other fractions (Fig.2.5). Another nonmagnetic fraction of Kota Kota shows higher CI normalized abundances of Re, Pd and Au compared to other HSE.

2.4.4 Chalcogen element abundances

Chalcogen element abundances are listed in Table 2.1 and CI normalized concentrations are shown in Fig.2.5. In case of Sahara 97072, average EH3 chondrite values (Binz et al., 1974; Bhandari et al., 1980; Easton, 1985; Kallemeyn and Wasson, 1986; Kaczaral et al., 1988; Yanai et al., 1995; Zhang et al., 1995; Kong et al., 1997) are given for bulk rock chalcogen abundances, because of the lack of published bulk rock data. In comparison to the HSE, CI normalized S, Se and Te abundances are depleted in all magnetic components except Sahara 97072 M 150-200, which is anomalously enriched in Se (Fig.2.5). The Se/Te ratio is variable in all components (Fig.2.8c). In the Te-Se diagram, metal-rich components and the DC from Sahara 97072 scatter near the CI line and display considerable variations, whereas chondrules, MSN, SM, NM and others have much higher Se/Te, without clear systematics (Fig.2.8c). Tellurium correlates with Ir and Au in most components (Fig.2.8d and e) except M fractions and WMPs of Kota Kota. For most components, Se correlates with S (Fig.2.8a) in both meteorites. Exceptions are MSN and M 150-200 from Sahara 97072, which show very high Se and the highest abundance of Au among all components of Sahara 97072. Nearly all components (except MSN of Sahara 97072 which show CI chondritic S/Mn) show lower S/Se and S/Mn than CI chondrites (Figs.2.3a and 2.8a).

2.5 Discussion

2.5.1 Re-Os systematics

The ^{187}Re-^{187}Os systematics indicates that the major processes that may have been responsible for the fractionation of Re/Os are either fractional condensation or slight variations in metal-sulfide-silicate partition coefficients of Re and Os and, in some cases, terrestrial weathering.

Variable fractionation of Re/Os in metal within the first few Ma of solar system history, which gave rise to variable radiogenic ^{187}Os/^{188}Os in different chondrite classes, e.g. magnetic fractions that deviate least from the isochron (Fig.2.4). The variation of ^{187}Re*/^{188}Os with 1/^{188}Os in different components indicate that components with low HSE abundances have low Re*/Os, whereas the opposite is true for magnetic fractions with high HSE abundances (Fig.2.4c). The relationship in Fig.2.4c is similar to the mixing relations between magnetic and non-magnetic components observed for other siderophile elements (Fig.2.7-2.8).Most magnetic components of both meteorites lie on or close to the 4.56 Ga reference isochron (Fig.2.4). Magnetic components show slightly higher ^{187}Os/^{188}Os than other components and the corresponding measured EH bulk

rocks (which have higher $^{187}Os/^{188}Os$ than bulk carbonaceous chondrites). The difference of $^{187}Os/^{188}Os$ in bulk rocks of Kota Kota (Walker et al., 2002b) compared to carbonaceous chondrites is caused by the higher $^{187}Os/^{188}Os$ in magnetic components. The variations in $^{187}Re^*/^{188}Os$ were inherited from partitioning processes at 4.56 Ga. These differences may either reflect fractionation during fractional condensation or slight variations in concentrations of Re and Os during metal-sulfide-silicate partitioning processes (Hertogen et al., 1983; Walker et al., 2002b; Horan et al., 2003, 2009; Fischer-Gödde et al., 2010; Archer et al., 2014; Horstmann et al., 2014).

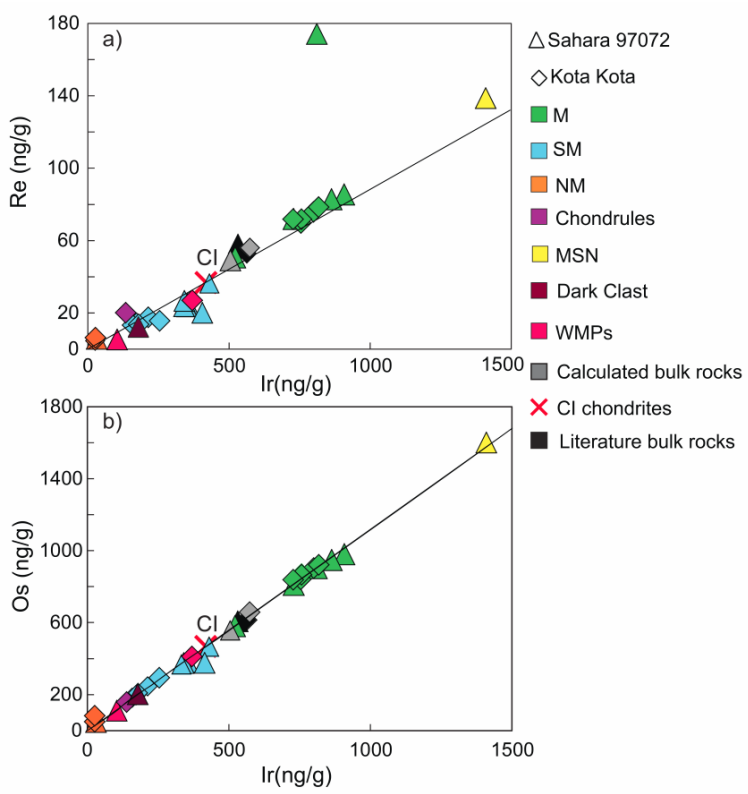

Fig.2.6. a) Re-Ir and b) Os-Ir variation among the separated components of Sahara 97072 and Kota Kota. Bulk rock data from Horan et al. (2003) and Fischer-Gödde et al. (2010). Almost all components preserve CI chondritic Os/Ir. Large variations are observed in Re/Ir for most components compared to CI chondrites indicating that the disturbance in the Re-Os isotopic systematics (Fig.2.4) is mainly caused by redistribution of Re.

Another process which may have been responsible for the Re/Os fractionation in components is late stage open system behavior of Re which is indicated by components which significantly deviate from the reference isochron (Fig.2.4a and b). Bulk rocks of Sahara 97072 and Kota Kota also display small deviations from the reference isochron (Walker et al., 2002b; Fischer-Gödde et al., 2010). As in bulk rocks of some chondrites and in other Re-Os studies of chondrite components, variations of $^{187}Re/^{188}Os$ are not always supported by their $^{187}Os/^{188}Os$, which likely reflects redistribution of Re, because of late stage open system behavior and its high mobility under oxidizing conditions (Chen et al., 1998; Becker et al., 2001; Walker et al., 2002b; Brandon et al., 2005a; Rankenburg et al., 2007; Horan et al., 2009; Fischer-Gödde et al. 2010; Archer et al., 2014).

We note that the variability of $^{187}Re/^{188}Os$ is likely not due to analytical reasons, because in many cases the blank contribution is small or deviations from the isochron are outside analytical uncertainties. Mass balance calculations show that components like the M 80-150 metal fraction of Sahara 97072, which has very high Re/Os, contribute significantly to the Re/Os of the bulk

rock. The NM, WMPs and DC fractions plot to the left of the reference isochron towards low $^{187}Re/^{188}Os$, similar to type II CAIs from CV chondrites (Becker et al., 2001). These components may have been affected more easily by late-stage Re mobilization, because the total amount of Re is much lower than in magnetic components.

All components have ~ CI chondritic Os/Ir (Fig.2.6), suggesting that the Re/Os ratio during condensation and putative early partitioning processes should also be chondritic (Lodders, 2003; Chabot et al., 2003, 2006). In contrast, large variations are observed in Re/Ir (0.031-0.216) among components which deviate significantly from the CI chondrite value (0.088). Therefore, redistribution of Re is the most likely explanation for resetting of the Re-Os systematics for the components which deviate from the 4.56 Ga isochron.

Experimental work (Xiong and Wood, 2002) suggests that in sulfur-bearing reducing environments, the solubility of ReS_2 in reducing aqueous fluids is much less compared to solubility of ReO_2 in oxidizing fluids. Differences in $^{187}Os/^{188}Os$ among the components and the fact that enstatite chondrites formed at highly reducing conditions indicate that Re-mobilization must have taken place recently. Interaction of HSE carriers with oxidizing terrestrial fluids could have provided the conditions for Re mobilization and resetting of the ^{187}Re-^{187}Os systematics. Mobilization of Re during terrestrial weathering was also suggested for bulk rocks and components of chondrites in other studies (Walker et al., 2002b; Rankenburg et al., 2007; Horan et al., 2009; Fischer-Gödde et al. 2010).

2.5.2 HSE abundances and ratios in the components

According to the S-Fe diagram (Fig.2.3e), magnetic fractions are predominantly comprised of Fe-Ni metal and variable proportions of sulfides and silicates. Non-magnetic or slightly magnetic fractions are predominantly comprised of silicates and variable amounts of sulfides, but little metal (Fig.2.3e and Table 2.3). With the exception of a few components that display enrichments in Au and Re, (Fig.2.5) most components display good correlations of the HSE with Fe, Ni and Co, (Table 2.1 and 2.2, Figs.2.2 and 2.5), indicating that the HSE are predominantly hosted by Fe-Ni metal (e. g., Rambaldi and Cendales, 1980; Kallemeyn and Wasson, 1986; Kong et al., 1997; Horstmann et al., 2014). Co/Fe and Ni/Fe are correlated with each other in most of the components and display CI chondrite-like Ni/Co (Fig.2.2). Higher Ni/Co in the SM <80 and NM fractions from Kota Kota reflects the significant presence of Ni in minerals such as schreibersite, perryite and djerfisherite, as previously observed in EH3 chondrites (Kong et al., 1997).

CI chondrite normalized abundance patterns (Fig.2.5) and element variation systematics indicate that HSE abundances in the components and in the bulk rocks to a first approximation can be explained by two mixing end members and additional dilution by HSE-free silicates. Variation diagrams of abundances of Fe with refractory HSE (Fig.2.7c) display linear trends, which suggest that in the magnetic components; HSE bearing metal + sulfides (see Fe-S

variations in Fig.2.3e) are diluted by HSE–free silicates. In addition, variations between moderately volatile and refractory HSE (e.g. Pd and Au vs. Ir, Fig.2.7) among the components are caused by two-component mixing between a Pd-Au enriched component hosted by the magnetic fraction and NM, WMPs and DC fractions, which are closer to CI chondrite like ratios (Fig.2.7). Nonlinear variations and scatter in magnetic fractions (e. g., Au vs Ir) seem to reflect mixing of two or more components with different HSE ratios, and dilution by HSE poor silicates (e. g., Fig.2.7b). In the following sections, we will discuss the processes that may be responsible for the origin of the Pd and Au-enriched metal and the CI chondrite-like component in EH chondrites.

2.5.2.1 *Enrichment and the variability of Au*

Because of the strong enrichment of Au in magnetic fractions of Sahara 97072 and Kota Kota (Figs.2.5 and 2.7), magnetic components control the abundances of Au in bulk enstatite chondrites. No component displays a complementary depletion in Au compared to the HSE, Fe and S (Fig.2.5).

Intermediate size magnetic fractions show the strongest enrichment of Au (Table 2.1). The enrichment of Au in the magnetic components is not correlated with other HSE or with the chalcogen elements (Figs.2.5, 2.7b and 2.8e). As no components show Au depletions relative to the HSE and Fe, processes such as fractional condensation or metal-sulfide-silicate partitioning in the nebula must have enriched Au selectively compared to other siderophile elements. These processes either occurred during chondrule formation, or the precursor dust of EH chondrules and metal must have been affected by such processes.

Horstmann et al. (2014) explained the grain-scale composition and textures of metals in E chondrites by three different processes i) crystallization of solid metal from metal melt where the liquid metal fraction is depleted in compatible siderophile elements (such as Re, Os, Ir). However, the complementary residual melt fraction which must be enriched in compatible siderophile elements is not observed in any of these samples. ii) Metamorphic equilibration, most prominently in case of equilibrated and EL3/4 type chondrites. And iii) perryite-schreibersite-sulfide exsolution from metal in case of EH3 chondrites. In the present study, bulk analysis of components was employed. Therefore the depletion of Re, Os, Ir and Pt relative to Au and Pd in metal of EH3 chondrites due to the perryite-schreibersite exsolution (Horstmann et al., 2014) is not observed. Fractionations of HSE due to the exsolution are small-scale processes that occurred during melting and cooling of the chondrite components. These processes cannot be responsible for the overall Au enrichment and variation in EH chondrite bulk rocks.

Fe/Ir, Au/Ir and Au/Pd in all components analyzed in this study are higher than in CI chondrites (Fig.2.5), which indicates that the depletion of refractory HSE and the enrichment of Au reflect pre-accretionary high temperature events that must have occurred prior to the formation of major phases such as Fe-Ni metal and FeS and also prior to the presumed sulfidation

of silicate minerals and metal proposed for the late history of enstatite chondrites (Lehner et al., 2010, 2013).

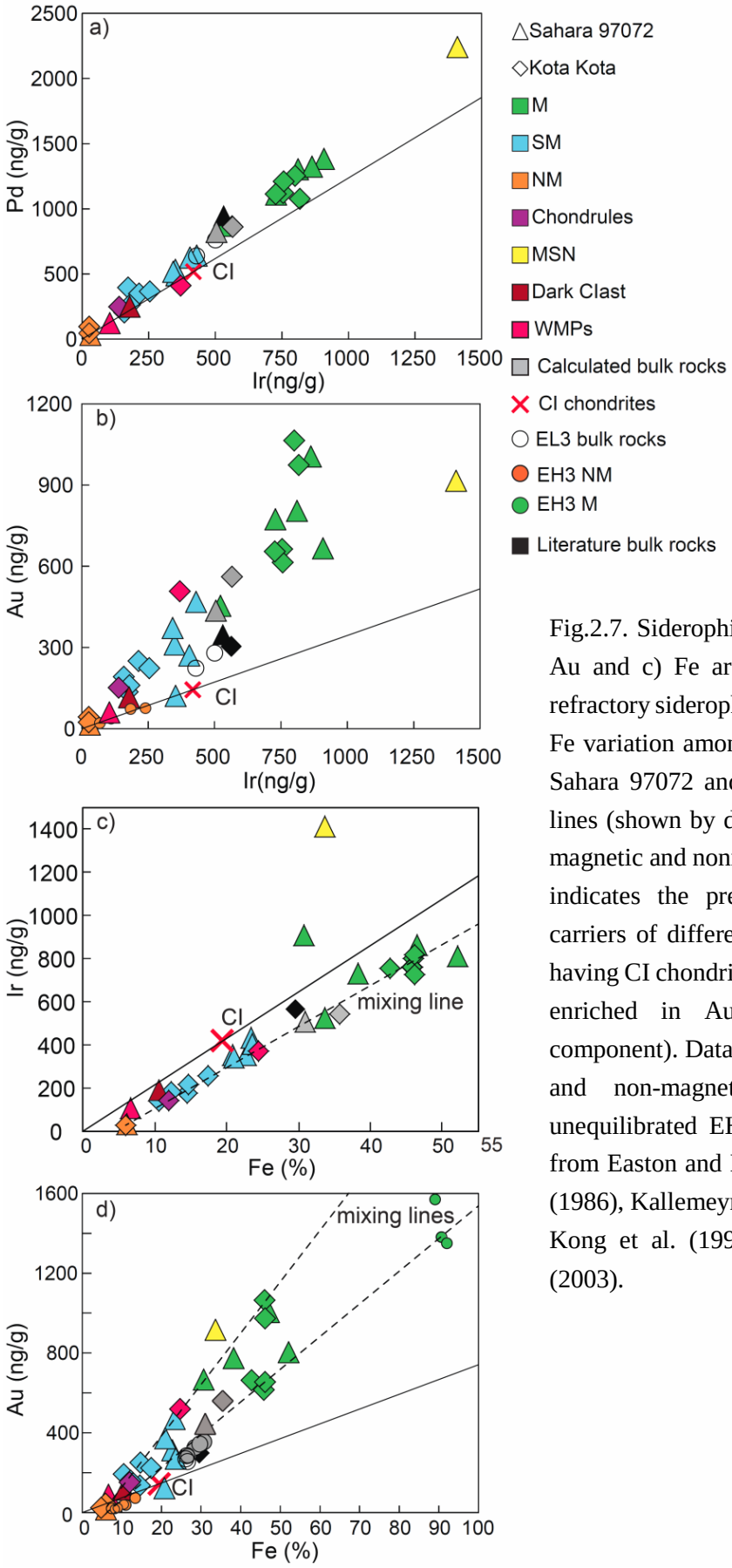

Fig.2.7. Siderophile elements a) Pd, b) Au and c) Fe are plotted against the refractory siderophile element Ir, d) Au-Fe variation among the components of Sahara 97072 and Kota Kota. Mixing lines (shown by dashed lines) between magnetic and nonmagnetic components indicates the presence of two HSE carriers of different compositions, one having CI chondritic Au/Fe and another enriched in Au (the main metal component). Data for bulk rocks, metal and non-magnetic components of unequilibrated EH and EL chondrites from Easton and Elliott (1977), Easton (1986), Kallemeyn and Wasson (1986), Kong et al. (1997) and Horan et al. (2003).

Another prominent feature of the element spectrum in this study is the variability of Au. Heterogeneity of Au abundances is common in chondrites and has been also observed even for different splits of bulk rocks, in particular for carbonaceous chondrites (e. g., Fischer-Gödde et al., 2010). In carbonaceous chondrites these variations were linked to the hydrothermal alteration on the parent body (Ebihara et al., 1982; Fischer-Gödde et al., 2010). There is no evidence of aqueous alteration in case of the enstatite chondrite parent body (Weisberg et al., 2014). We cannot exclude that such alteration may have occurred during terrestrial weathering because both meteorites were finds. Our data shows that Re, Au and S, which are easily affected by terrestrial weathering, do not show a correlated behavior (See Fig.2.5). Most of the magnetic components lie on or very close to the ^{187}Re-^{187}Os isochron (Fig.2.4). Even if we consider that the disturbance in Re-Os might not be visible in magnetic components due to their higher Re abundances then the same should also be true for S due to its high abundances in magnetic fractions. In contrast, magnetic components show higher apparent S loss compared to Se and CI compositions (Fig.2.8a) but show random variations in Au (Fig.2.7). These contradicting observations do not support that terrestrial weathering was the only process as a cause of Re mobilization, Au enrichment and S loss from the components. The primary petrographic features preserved in the components of EH3 chondrite finds also suggest that Au enrichment and variability more likely represents an early process related to the condensation of moderately volatile elements in S-rich environments (Lehner et al., 2013; Weisberg et al., 2014, Horstmann et al., 2014). Terrestrial weathering may cause Au variation only if Re, S and Au behave completely different during weathering, as no coupled behavior is evident.

In the following sections we will discuss in detail the role and feasibility of high-temperature processes to explain HSE variations and in particular the enrichment and variation of Au.

2.5.2.2 Evaluation of the role of solid metal-liquid metal partitioning

The possible influence of solid metal-liquid metal partitioning during impact induced melting on the HSE abundances in enstatite chondrites was discussed by van Niekerk et al. (2009); Fischer-Gödde et al. (2010) and Horstmann et al. (2014). In these partitioning processes, Au, Pd (and Ni) become more enriched in liquid metal coexisting with solid metal, compared to other HSE (Scott, 1972; Chabot et al., 2006). Chondrule fractions, MSN and magnetic components of both chondrites and the nonmagnetic fraction of Kota Kota are indeed enriched in Pd and Au with respect to refractory HSE (Fig.2.7), and thus may reflect liquid metal compositions, separated from solid metal during chondrule formation processes. Experimentally determined solid metal-liquid metal partition coefficients of Pd and Au in the Fe-Ni-S and Fe-Ni-C systems are not much different. $D^{\text{sol met/liq met}}$ values are dependent on the amount of nonmetals like S and C in metallic liquid, e.g. in case of 2% C in metallic liquid, $D^{\text{sol met/liq met}}$ are 0.8 and 0.56 for Pd and Au, respectively (Chabot and Jones, 2003; Chabot et al., 2006). Therefore similar variation of Au and Pd with S concentration should be observed in components, if solid metal–liquid metal partitioning played a major role for the observed abundance patterns. The hint of

abundance patterns of some components are influenced by solid metal- liquid metal partitioning cannot explain the high Au abundances in all components. Furthermore, components with complementary patterns that are depleted in Au and Pd compared to the HSE were not observed in this study. Recent modeling of solid metal-liquid metal partitioning of HSE in enstatite chondrite metal in S and C-rich systems by Horstmann et al. (2014) also show poor agreement of this partitioning process with the abundances of siderophile volatile elements in the range of Au and As. We conclude that even if solid metal-liquid metal partitioning played a role in some components (or in some other E chondrites), abundances of Au in components and bulk rocks must have increased subsequently to the partitioning process in all EH chondrites by some other processes. For instance, melting and recondensation in S rich environments and volatility related processes.

2.5.2.3 Volatility

The enrichment of siderophile and lithophile moderately volatile elements with 50% condensation temperatures near 1000 K (Au, As, Ag, K, Na) relative to more refractory elements such as Fe, Pd, Ca, Mg, Mn is indicative of volatility control of these elements in EH3 chondrites (e. g. Hertogen et al., 1983; Kallemeyn and Wasson, 1986 and references therein). There are two clear observations from all bulk rock studies on enstatite chondrites, i) the enrichment of elements having condensation temperature near 1000 K and ii) the enrichment of siderophile elements over lithophile and chalcophile elements in this temperature range. The details of processes and why the abundance peak occurs in this particular temperature range have remained obscure.

It is conceivable that activities of volatile elements in condensates of the EH chondrite formation region are different compared to solar conditions. The behavior of refractory and volatile siderophile elements in EH chondrites suggests a complicated condensation-evaporation history (Fig.2.5 and 2.7). Fractional condensation and partial loss of refractory metal nuggets and refractory oxides may have left the gas depleted in the HSE and enriched in volatile elements (Baedecker and Wasson, 1975). Depletion of refractory HSE and enrichment of Fe, Si and the moderately volatile elements Pd and Au could be the effect of differences in volatility, fractional condensation and loss of earlier condensed solids at high temperatures. The major and minor element data indicate that most components have lower Ca/Mg than CI chondrites (Fig.2.3d); which is consistent with the depletion of refractory lithophile elements compared to less refractory lithophile elements in enstatite chondrites (Kallemeyn and Wasson, 1986).

2.5.3 Chalcogen element fractionations in EH3 chondrites

Sulfur and Te abundances in most bulk EH3 chondrites are depleted compared to CI chondrites, whereas Se abundances are higher than in CI chondrites and therefore, EH3 chondrites have higher Se/Te and lower S/Se than CI chondrites (Hertogen et al., 1983; Easton and Elliott, 1977, Easton, 1985; Kallemeyn and Wasson 1986; Kong et al., 1997). The data on

components of Sahara 97072 and Kota Kota show the same behavior as S/Se and Se/Te in bulk EH3 chondrites, with the exception of fine grained magnetic components, which display Se/Te close to the value of CI chondrites (Fig.2.8a).

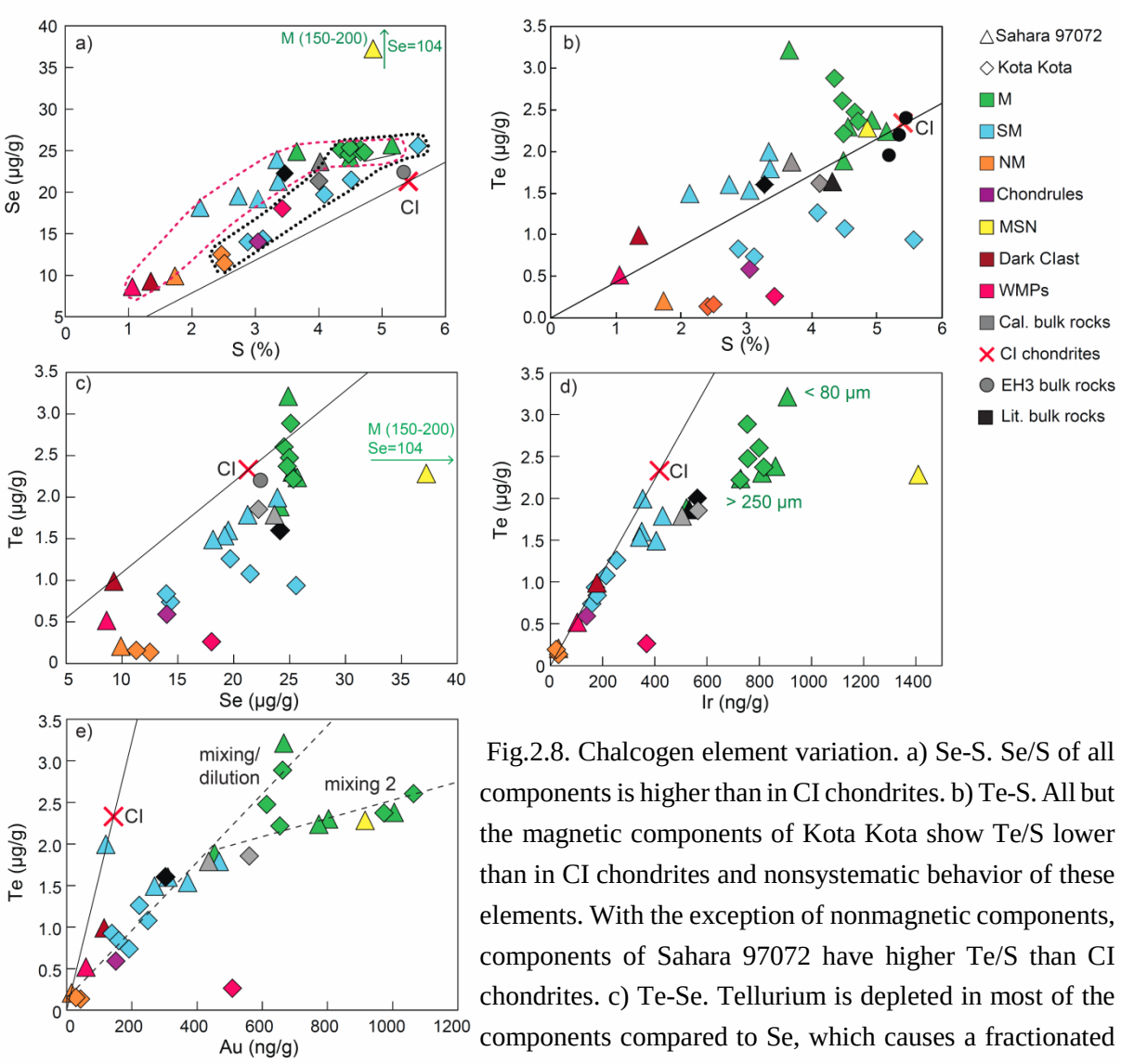

Fig.2.8. Chalcogen element variation. a) Se-S. Se/S of all components is higher than in CI chondrites. b) Te-S. All but the magnetic components of Kota Kota show Te/S lower than in CI chondrites and nonsystematic behavior of these elements. With the exception of nonmagnetic components, components of Sahara 97072 have higher Te/S than CI chondrites. c) Te-Se. Tellurium is depleted in most of the components compared to Se, which causes a fractionated Se/Te compared to the CI chondrite value (c). MSN and a metal component (M150-200) from Sahara 97072 show a strong enrichment in Se with respect to Te. d) Te-Ir. Te/Ir is similar to CI chondritic values in non- and slightly magnetic fractions. Te is depleted in magnetic fractions. e) Te-Au shows two different mixing trends between metal rich fractions and slightly magnetic material. Bulk rock data for Kota Kota and EH3 chondrites is from Easton and Elliott (1977), Easton (1985), Kallemeyn and Wasson (1986) and Horan et al. (2003).

The variation of Te abundances in the components is decoupled from Se and S (Fig.2.8a and b). For instance, despite of an almost 2 fold variation in Te concentrations there is no significant variation in Se abundances in magnetic components (Fig.2.8c). If both Se and Te have similar geochemical affinity in enstatite chondrites (Hertogen et al., 1983) and considering the experimental observations that they show similar behavior during metal-sulfide-silicate partitioning processes (Rose-Weston et al., 2009), some form of correlation would be expected

between these elements if the depletion of these elements in the magnetic fractions were caused by melting of metal-sulfide-silicate systems. This is not observed (see Fig.2.8c), especially not in magnetic components. The decoupled behavior of Se and Te, particularly in the metal rich fractions, is consistent with the notion that both elements have condensed into different phases.

Because of the decoupling of Te from S, Se, we discuss the nature of fractionation processes of these elements separately in sections 2.5.3.1 and 2.5.3.2.

2.5.3.1 Origin of the variable depletion of Te in components of EH chondrites

Nearly all components display systematically lower Te abundances compared to Se, with Se/Te in most components higher than in CI chondrites (Figs.2.5, 2.8c). This observation reflects loss of Te compared to HSE and Se at some time in the history of the components. We note that the CI chondrite like Te/Ir ratio (Fig.2.8d) in WMPs, DC, SM and NM components require a very different history of Te in these components. It is important to realize that these components mostly comprise material from enstatite rich and metal poor chondrules, indicating that their tiny metal and sulfide inclusions have their own high-temperature fractionation histories that may be different to that of the main metal- sulfide fraction in EH3 chondrites. Evaporation may account for the variable Te depletion in the magnetic components because CI normalized Te abundances are more depleted than CI normalized abundances of Au, Pd and Ir, if we assume the volatility sequence from Lodders (2003). However, because the element systematics does not easily fit a simple model, we must consider several explanations:

(1) Loss of volatile elements by evaporation or loss of fractional condensates may be a plausible mechanism for elements more volatile than Au, if they display smooth depletion patterns. This model was discussed in detail for ordinary chondrites by Wai and Wasson (1977). To explain the Te depletion in ordinary chondrites these authors proposed that such a process requires conditions where Te is more volatile than Se, consistent with the observed high Se/Te in most components of the present work (Fig.2.8c). For Te to become more volatile than Se and S, these authors concluded that the local nebular pressure likely was $< 10^{-6}$ bars (Fig.2.1). The high chondrule fraction (60-80 volume %) in EH chondrites and some previous studies on EH chondrites suggest a high dust to gas ratio and thus a high nebular pressure (Blander, 1971; Hertogen et al., 1983; Blander et al., 2009). However, these inferences were not supported by the abundances of primordial noble gases in enstatite chondrites (Crabb and Anders, 1981, 1982, Hertogen et al., 1983). Consequently, if the model by Wai and Wasson (1977) can be applied to EH3 chondrites, the Te depletion relative to Se and S from the precursors of EH chondrites should have taken place *before* the chondrule formation process. The problem with this model is that it is inadequate to explain the nearly CI chondritic ratio of Te and Ir (with very different volatilities) in components such as NM, SM, DC and WMPs (Fig.2.8d).

(2) In another model that may explain the Te depletion in the magnetic fractions, HSE carriers condensed at higher temperature than the 50% condensation temperature of Te (e. g. with

Fe-Ni metal). These metal grains formed with very low Te/Ir, were transported to or mixed with the gas in the EH-chondrite formation region where most of the gas has a CI chondrite like Te/Ir ratio. It is conceivable that during cooling of the metal grains, Te and other volatile siderophiles condensed around these metal grains. Size dependent variations of Te abundances in magnetic components and CI chondritic ratios of Te/Ir in some components support this argument, because in magnetic components, the magnitude of the depletion of Te shows an inverse relationship with grain size (Table 2.1, Fig.2.8d). A variation of this model would be that the metal grains have a CI chondritic Te/Ir ratio initially, but later melting, partial evaporation and recondensation gave rise to size dependent variations of Te abundances and lower Te/Ir. We note that the small fraction of metal components with CI like Te/Ir which is present in nonmagnetic components (mostly chondrule material) may be sourced from a different compartment of the nebula and may not have been present during the melting processes that affected the main metal phase of the matrix (see section 2.5.4). Alternatively, if the metal with CI like Te/Ir was present during the melting processes, it must have escaped significant evaporative loss of Te because the metal grains were trapped in silicates.

(3) As both meteorites are of petrologic type 3 and finds, it is necessary to consider that the Te loss might have occurred during thermal metamorphism or terrestrial weathering (Ikramuddin et al., 1976; Hertogen et al., 1983). Heating experiments conducted on enstatite chondrites have shown that Te is more mobile and volatile compared to Se when temperatures exceed 500 °C (Ikramuddin et al., 1976; Biswas et al., 1980). Both meteorites were likely heated to about 500 °C. Comparison of Se/Te ratios and Te concentrations in equilibrated and unequilibrated enstatite chondrites and results of heating experiments of the Abee (EH4) meteorite under simulated metamorphic conditions show no evidence of loss of these elements during post-accretionary heating on unequilibrated enstatite chondrites (Kaczaral et al., 1988). Although Te is more depleted than Se and S in most components, the evidence that is not so easy to reconcile with the metamorphic heating hypothesis is the correlation between Te and Ir, and the CI chondritic Te/Ir in some components. Selective mobilization of Te by metamorphic processes would not preserve the Te-Ir correlation, unless their carrier phases were inclusions shielded by enstatite. Weathering is also less likely to affect Te because, similar to Se, reaction of Te with O_2 forms solid TeO_2, which is insoluble in water.

2.5.3.2 Origin of S/Se variations in EH chondrites

Previous studies suggested that S is depleted in bulk EH chondrites compared to CI chondrites (Easton and Elliott, 1977; Easton, 1985). The present work confirms these early data, in particular since we have applied high-precision isotope dilution method and have looked into variations of components. The components of Kota Kota show higher S/Se than the bulk rock data (Figs.2.8a) from previous studies (Easton and Elliott, 1977; Easton, 1985). We observe similar Se abundances in calculated bulk rocks (22.6 μg/g) compared to literature bulk rock data (22.3 μg/g) which indicates that either the data for bulk Kota Kota (Easton and Elliott, 1977;

Easton, 1985) have underestimated the S concentration, that the distribution of S in Kota Kota is not homogeneous, or the random S loss is an effect of terrestrial weathering. Indeed, S/Se and S/Mn ratios of almost all components in this study are subchondritic (Fig.2.8a). Several explanations may account for this observation.

Systematically low S/Se can be explained in a straightforward way by evaporative loss of S, which is also supported by higher Mn/S than in CI chondrites in almost all components (Fig.2.3a). Sulfur may have evaporated during local partial melting during impacts on the parent body. Both meteorites experienced shock stage S2/S3 and therefore post-shock temperatures experienced by them should be similar and much lower than the condensation temperature of S. Though they experienced similar shock stages, the S/Se systematics of these meteorites are different from each other (Fig.2.8a). Therefore S loss and S/Se fractionation during impact or shock event seems unlikely.

A linear S-Se correlation can be observed for Kota Kota components and less clearly for components of Sahara 97072 (fields outlined by dashed line in Fig.2.8a). Both correlations are similar to correlations found for the HSE and Fe (e. g., Pd-Ir, Fig. 2.6, 2.7) as they are defined by M and NM components as end members, with most slightly magnetic fractions in-between. The preservation of the loose linear S-Se variation of the components of Kota Kota and of most components of Sahara 97072 (Fig.2.8a) requires a rather systematic S depletion regardless of the concentrations of S and Se. The systematic behavior of S and Se concentrations and the limited variations in S/Se (with the exception of MSN and M 150-200 from Sahara 97072) in most NM, SM and magnetic components in both meteorites provide arguments for the notion that the main S loss event occurred prior to the accretion of the components.

Effects of terrestrial weathering on S loss were reported for terrestrial samples and meteorite find (Lorand, 1990; Dreibus et al., 1995; Huber et al., 2006) of some bulk chondrites. Oxidation of sulfides during weathering may have affect S/Se in the different components because of the high mobility of S compared to Se under oxidizing surface conditions (Dreibus et al., 1995). In Fig.2.8a, scatter parallel to the S concentration axis affects the correlations of the components of each meteorite and may be a direct consequence of random weathering. Because of their particularly low S/Se compared to CI chondrites (S/Se = 2540), the M 150-200 (S/Se = 473) and MSN (S/Se = 1306) fractions of Sahara 97072 deserve special attention (Fig.2.5 and 2.8a). These low values may have resulted from weathering.

We conclude that incomplete condensation or partial evaporation of S can explain the depletion of S and Se relative to the HSE and the linear correlation between S and Se in components of Kota Kota and Sahara 97072. Random scatter and extreme fractionations of S/Se in a few components are likely the result of terrestrial weathering.

2.5.4 Origin of components with CI chondrite-like compositions

With the exception of Re, some of the components show nearly CI chondritic relative abundances of refractory HSE (Fig.2.5). The NM fraction and WMPs of Sahara 97072 display nearly CI chondritic Au/Ir, Te/Ir and Au/Te (Fig.2.7b, 2.8d and e) indicating that the HSE signature carried by the host phases in NM components is different from the signature of magnetic components, which show higher Re*/Os, Pd/Ir, Au/Ir and lower Te/Ir than CI chondrites (Figs.2.5, 2.6 and 2.7). Because of the nearly CI chondritic ratios of the refractory HSE, the host phase(s) of siderophile elements in the NM fractions has formed at different conditions than the HSE carriers in magnetic fractions. It is likely that these host phases condensed in a different location of the nebula and later mixed with the EH chondrite precursors of the magnetic fractions. Barrat et al. (2014) analyzed lithophile trace element abundances in leachates and residues of EH3 chondrites and also concluded that they preserve pre-accretionary, nebular signatures and display very minor deviation from chondritic element patterns. Out data confirm these conclusions.

The history of MSN in EH3 chondrites may be more complex and different from that of silicate rich chondrules and sulfides, silicates and metal in the matrix. The textural position of MSN in Sahara 97072 and the differences in grain sizes compared with other components in the meteorite (Fig.2.A1) suggest that melting and crystallization of these objects occurred before the accretion of the parent body (Weisberg et al., 1997, 2013; Lehner et al., 2010; Horstmann et al., 2014). Ca/Mg, Ir/Fe and Re/Os in these MSN are higher than in CI chondrites (Figs.2.3d, 2.4 and 2.7c), indicating that these objects may have formed from refractory condensates. Greater losses of the volatile elements Te, Se and S compared to HSE may have occurred during melting and sulfidation processes (Lehner et al., 2013).

2.5.5 Siderophile elements and EH chondrite formation models

CI chondrite normalized abundances of siderophile, chalcophile and lithophile volatile elements in bulk rocks of EH chondrites show a maximum near Au and lower abundances of elements more volatile and refractory than Au or K (e. g., Kallemeyn and Wasson 1986; Kong et al., 1997 and the calculated bulk rock values in the present study). The depletion of refractory and volatile to highly volatile elements compared to Au and the alkalies, regardless of geochemical behavior, indicates that either metal grains and silicates underwent melting and evaporation before their incorporation into the EH chondrite parent body, or that refractory and major elements such as the HSE, Ca, Al and Mg were removed as a result of early fractional condensation.

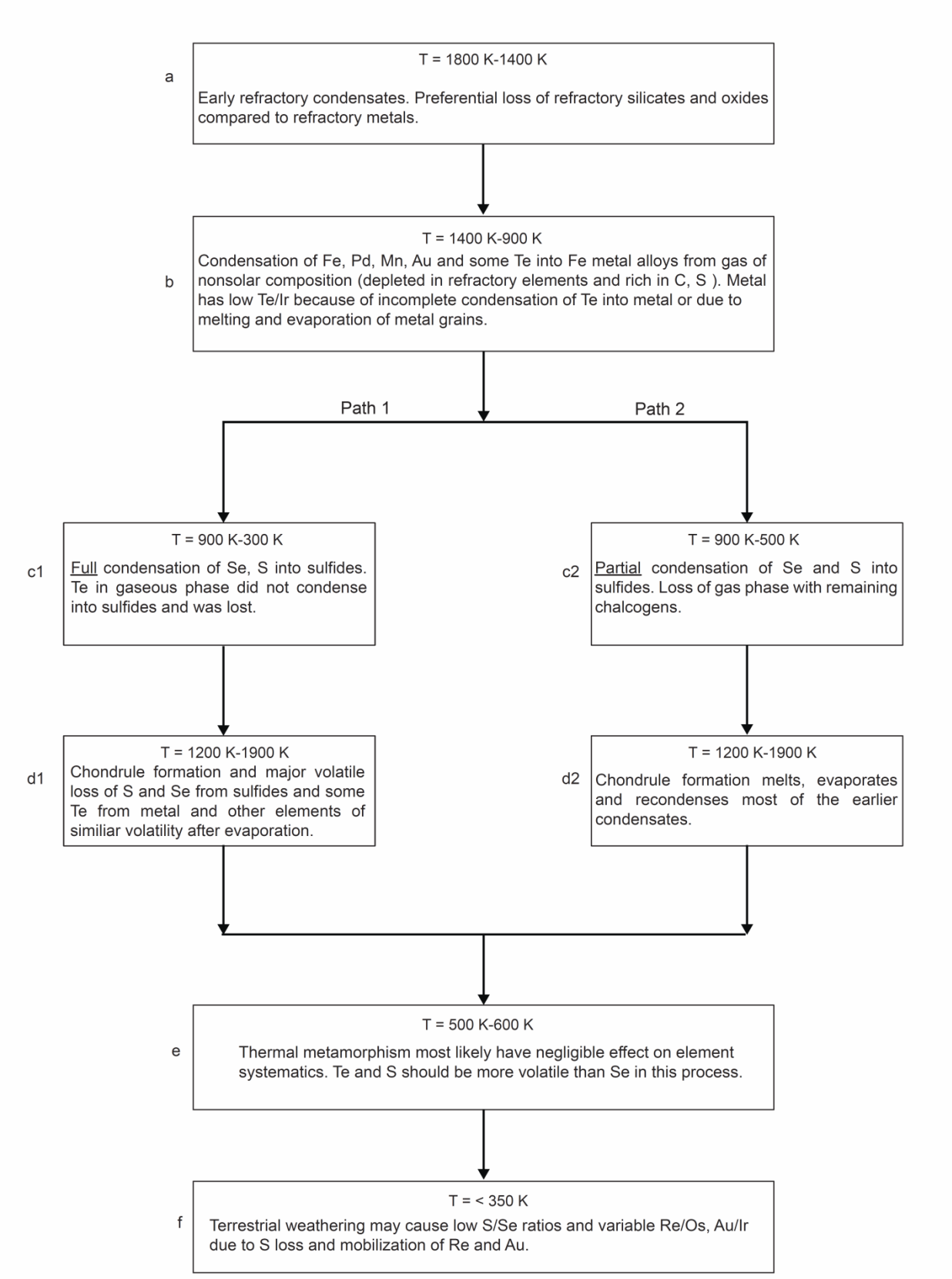

Fig.2.9. Nebular evolution of precursors of the main component in EH chondrites. Condensation sequence after the removal of early condensed phases and gas is shown at different stages. At lower temperatures two different evolutionary paths c1, d1 and c2, d2 are possible. See also Fig.2.10. Data from the present work and from Baedecker and Wasson (1975), Wai and Wasson (1977), Ebihara et al. (1982), Kallemeyn and Wasson (1986), Hewins and Radomsky (1990), Dreibus et al. (1995), Kong et al. (1997) and references therein were used in this figure.

The following scenario is proposed. (1) A fraction of refractory elements must have been lost from EH3 precursor material into high-temperature condensates (Fig.2.9a and block 1 of Fig.2.10). (2) The remaining fraction of refractory HSE condensed into Fe metal (Fig.2.9b and block 2 of Fig.2.10) below about 1400 K (Lodders, 2003). (3) Subsequent cooling of the grains in the gas may have condensed the remaining Pd as well as Au, As and Te into Fe-Ni metal and alkalies into silicates (Fig.2.9b and block 2 in Fig.2.10). From that point on, two different evolutionary paths are possible. (4) The chalcogens and highly volatile elements condensed only partially (i. e., another episode of fractional condensation, Fig.2.9c2 and block 3 of Fig.2.10) or partly evaporated during heating episodes (Fig.2.9c1). (5) As both meteorites are type 3 and well preserved Te-Ir correlations indicate the effect of metamorphic heating on the element loss is negligible. (6) Terrestrial weathering was the last process (Fig.2.9f) which may be responsible for the mobilization and loss of Re, Au, Te, Se and S (Dreibus et al., 1995; Walker et al., 2002b; Huber et al., 2006; Fischer-Gödde et al. 2010). Weathering processes should cause random

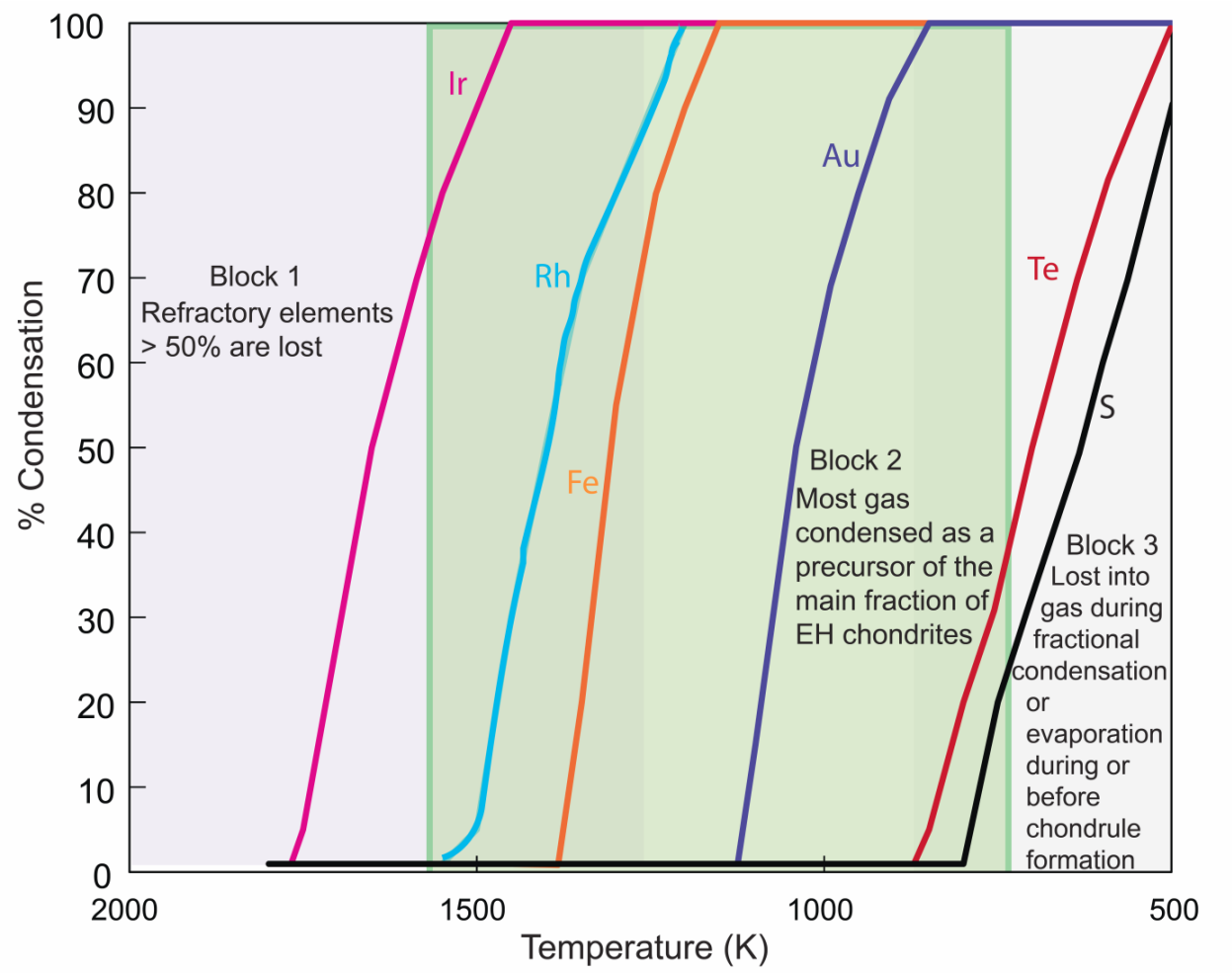

Fig.2.10. Pictorial representation of the condensation sequence of elements in the solar nebula. Initial and 50% condensation temperatures were from Lodders (2003). The y-axis shows % condensation of the elements. The condensation sequence is separated into three regions. EH chondrites are enriched in elements of Block 2. Almost 50% of the elements condensed before and after the temperature range of this block are lost because of fractional condensation or/and evaporation.

depletions or enrichments of elements that are easily mobilized. The scatter shown by the S-Se correlations of components of Sahara 97072 and Kota Kota might be explained this way.

The sequence of processes mentioned above (Fig.2.9 and 2.10), will yield the observed depletion of refractory and volatile elements (S, Se and Te) and enrichment of moderately volatile elements near Au. The main metal-silicate-sulfide component of EH3 chondrites is the product of selective sampling of condensates that formed in restricted temperature ranges from gas of non-solar composition, followed by evaporation of volatiles and recondensation in the course of chondrule formation. HSE carrier phases in the nonmagnetic and slightly magnetic fractions (predominantly metal-poor chondrule material) have not lost Te by evaporation (step 5), presumably because they were protected by silicate melt during chondrule formation, or, alternatively, because they condensed and were accreted only subsequently.

2.6 Conclusions

Two types of HSE bearing phase assemblages with different histories were identified in physically separated components of the EH3 chondrites Sahara 97072 and Kota Kota. The HSE host phase/s in slightly to non-magnetic components, WMPs fractions and in a dark clast in Sahara 97072 appear to have undergone less processing than the main metal + sulfide assemblages in magnetic components of EH chondrites. The main host of the HSE in enstatite chondrites is the metal in magnetic components, which shows nearly unfractionated, CI chondrite like refractory HSE ratios, and is enriched in the moderately volatile elements Pd and in particular Au and slightly enhanced Re/Os and $^{187}Os/^{188}Os$. Because of the decoupling of Pd and the chalcogens from Au, solid metal-liquid metal partitioning or low temperature redistribution processes are difficult to reconcile with the observed HSE variations. Because components with complementary HSE compositions and Au depletion do not occur in these meteorites, an in situ magmatic origin of these fractionations, for instance by impact heating, is unlikely. Thus we conclude that the siderophile element patterns in this assemblages were inherited from the nebular setting prior to their accretion into the EH chondrite parent body. The enrichment of Au with respect to all other HSE likely resulted from fractional condensation and the variability of Au concentrations may have resulted from the high mobility of Au.

The chalcogens in magnetic components are substantially more depleted compared to the HSE, which requires a decoupled three-stage fractionation history of refractory elements, moderately volatile elements (e. g., Au, Na, K) and chalcogen elements (Fig.2.9, 2.10). Tellurium in these meteorites mainly behaves as a siderophile element and likely condensed with metal, as Te/Ir is nearly CI chondritic in many components. The stronger depletion of Te compared to S and Se may have occurred during melting of metal grains and concurrent evaporation, whereas metamorphism may have been responsible for the non-systematic scatter of the correlations between Te, HSE, Se and S. The moderate S depletion compared to Se is most likely the result of

volatilization of S in the later stage of the evolution of EH3 chondrites. The extremely variable S/Se of a few components, Au variability and the redistribution of Re among the components may have been caused by terrestrial weathering.

Acknowledgements: We are grateful to the Natural History Museum, London for providing a piece of Kota Kota and the U.S. Natural History Museum in Washington D.C. for an aliquot of the Smithsonian Allende standard powder. We thank K. Hammerschmidt for technical help in the TIMS lab, M. Feth and S. Kommescher, T. Gawronski, Z. Wang, C. Meyer, S. Hohl and M. Weynell for their support in the clean lab, C. Behr, R. Milke and F. Mangels for guidance and assistance during sample preparation and analysis on the electron microprobe. We thank M. Horstmann, M. Horan and an anonymous reviewer for their thoughtful and constructive reviews which were helpful to improve the manuscript. We also thank associate editor, M. Humayun for his comments and suggestions. This project was funded by DFG-SPP 1385 “The first ten million years of solar system – a planetary materials approach” (Be1820/10-1).

2.7 Tables Chapter 2

Table 2.1. HSE, chalcogen element abundances and Re-Os isotopic data of components of EH3 chondrites

Component	Weight (mg)	Re (ng/g)	Re* (ng/g)	Os (ng/g)	Ir (ng/g)	Ru (ng/g)	Pt (ng/g)	Rh (ng/g)	Pd (ng/g)	Au (ng/g)	Te (µg/g)	Se (µg/g)	S (µg/g)	$^{187}Os/^{188}Os$	$^{187}Re/^{188}Os$	Δ_{Os} [a]
Sahara 97072																
Sah-M < 80	7.1	85	86	981	909	1471	2008	314	1383	667	3.21	24.9	36506	0.1292 ± 0.0003	0.427 ± 0.004	3
Sah-M 80-150	22.0	175	80	903	811	1234	1697	301	1303	804	2.30	25.3	45604	0.1289 ± 0.0001	0.934 ± 0.001	-400
Sah-M 150-200	12.4	83	82	948	863	1303	1793	314	1323	1006	2.38	103.8	49141	0.1280 ± 0.0001	0.421 ± 0.002	-4
Sah-M 200-250	28.4	72	72	810	729	1095	1531	235	1109	774	2.24	25.7	51541	0.1290 ± 0.0001	0.428 ± 0.001	0.1
Sah-M > 250	20.5	51	51	580	522	815	1099	188	869	454	1.88	24.1	44965	0.1286 ± 0.0001	0.421 ± 0.002	2
Sah-SM < 80	2.5	25	32	382	354	534	701	114	490	121	1.99	23.9	33409	0.1273 ± 0.0009	0.316 ± 0.029	71
Sah-SM 80-150	11.5	24	31	375	350	520	719	133	532	311	1.60	19.5	27303	0.1266 ± 0.0002	0.305 ± 0.007	73
Sah-SM 150-200	12.1	36	42	467	431	649	888	146	641	468	1.79	21.3	33615	0.1296 ± 0.0001	0.375 ± 0.005	47
Sah-SM 200-250	12.5	27	32	367	343	518	703	117	517	372	1.54	19.2	30432	0.1283 ± 0.0002	0.350 ± 0.006	54
Sah-SM > 250	29.6	20	33	376	406	616	813	143	625	270	1.49	18.2	21267	0.1285 ± 0.0001	0.257 ± 0.003	130
Sah-WMPs	1.3	3.2	9	109	104	180	234	33	123	60	0.55	8.63	10590	0.127 ± 0.005	0.143 ± 0.103	22
Sah-MSN	8.7	139	148	1601	1410	2156	3072	505	2241	916	2.28	37.2	48584	0.1304 ± 0.0001	0.418 ± 0.002	206
Sah-DC	6.2	12	17	201	179	253	355	51	248	116	0.99	9.28	13517	0.1273 ± 0.0006	0.294 ± 0.022	89
Sah-NM	7.0	1	2	33	31	46	56	8	32	16	0.21	9.91	17302	0.125 ± 0.003	0.200 ± 0.042	139
Sah-cal bulk	900	49	n.d.	556	505	781	1059	179	821	436	1.79	23.6	40224	0.1284 ± 0.0002	0.403 ± 0.007	14
Sahara-bulk [b]		58.2	53	607	532	867	1219	179	948	348	1.89	22.9	44220	0.12783	0.4531	-32
Kota Kota																
KK-M < 80	21.3	70	78	855	755	1181	1642	244	1122	663	2.88	25.1	43451	0.1297 ± 0.0001	0.393 ± 0.002	35
KK-M 80-150	24.5	76	80	902	800	1250	1729	278	1252	1064	2.60	24.5	44711	0.1291 ± 0.0001	0.405 ± 0.001	19
KK-M 150-200	18.7	72	77	866	757	1158	1651	244	1210	614	2.47	25.0	46555	0.1289 ± 0.0001	0.400 ± 0.002	21
KK-M 200-250	21.8	78	81	921	818	1222	1725	235	1075	973	2.37	24.8	47222	0.1290 ± 0.0001	0.411 ± 0.001	14
KK-M > 250	29.3	72	73	838	727	1066	1508	222	1112	654	2.22	25.4	44916	0.1284 ± 0.0001	0.413 ± 0.001	6
KK-SM < 80	19.8	14	14	194	173	248	326	57	394	135	0.94	25.6	55644	0.1240 ± 0.0006	0.353 ± 0.007	9
KK-SM 80-150	23.4	18	20	245	214	316	433	79	348	250	1.08	21.5	45103	0.1266 ± 0.0001	0.344 ± 0.005	42
KK-SM 150-200	19.7	16	24	293	255	387	528	81	366	223	1.26	19.7	40884	0.1271 ± 0.0001	0.261 ± 0.005	113
KK-SM 200-250	17.8	13	16	181	159	232	327	50	204	192	0.74	14.4	31175	0.1285 ± 0.0002	0.353 ± 0.009	54
KK-SM > 250	21.2	14	18	208	180	268	365	56	263	160	0.84	14.0	28797	0.1275 ± 0.0002	0.314 ± 0.006	75
KK-WMPs	0.9	27	34	411	370	501	740	131	410	507	0.26	18.0	34239	0.1271 ± 0.0019	0.316 ± 0.073	-142
KK-chondrules	23.4	19	13	157	139	206	285	46	248	151	0.59	14.0	30435	0.1278 ± 0.0006	0.593 ± 0.008	69
KK-NM	7.2	4	n.d.	82	27	41	48	5	95	43	0.13	12.5	24650	n.d.	n.d.	n.d.
KK-NM2	5.0	5	2	27	26	29	47	8	52	29	0.16	11.2	24881	0.121± 0.004	0.82 ± 0.09	-384
KK-cal bulk	950	56	n.d.	657	574	859	1207	179	873	569	1.88	22.6	42315	0.1281 ± 0.0002	0.422 ± 0.004	-4.0
Kota Kota-bulk [c]		53	n.d.	604	555	848	1131	179	897	304	1.60	22.3	34500	0.1285	0.43069	-7.1
CI-bulk [d]		36.6	37	450	418	627	871	130	567	149	2.31	21.3	54100	0.12641	0.4007	-4.35

The deviation of the Os isotopic composition (Δ_{Os}) from the IIIA iron meteorite isochron is calculated by the following relation.

[a] $\Delta_{Os} = (^{187}Os/^{188}Os_{chondrite} - (0.09524+0.07887 \times {}^{187}Re/^{188}Os_{chondrite})) \times 104$, 0.09524 is the $^{187}Os/^{188}Os$ at 4.558 Ga and 0.07887 is the slope of the IIIA iron meteorite reference isochron (Smoliar et al., 1996).

[b] HSE bulk rock values are from Fischer-Gödde et al. (2010). Bulk rock values of chalcogens for Sahara 97072 are average values of the published data for EH3 chondrites (Binz et al., 1974; Bhandari et al., 1980; Easton, 1985; Kallemeyn and Wasson, 1986; Kaczaral et al., 1988; Yanai et al., 1995; Zhang et al., 1995; Kong et al., 1997).

[c] Bulk rock data from Easton (1985), Kallemeyn and Wasson (1986), Walker et al. (2002b) and Horan et al. (2003).

[d] CI chondrite data from Dreibus et al. (1995), Walker et al. (2002b), Fischer-Gödde et al. (2010) and Wang et al. (2013).

Table 2.2. Concentrations of major and minor elements in the separated components of Sahara 97072 and Kota Kota.

Component	Mg (%)	Ca (%)	Mn (%)	Fe (%)	Co (%)	Ni (%)
Sahara 97072						
Sah-M < 80	5.5	0.4	0.151	30.7	0.128	2.45
Sah-M 80-150	9.9	0.4	0.243	52.1	0.165	3.10
Sah-M 150-200	8.4	0.6	0.206	46.5	0.135	2.66
Sah-M 200-250	9.2	0.7	0.201	38.3	0.110	2.20
Sah-M > 250	11.7	0.3	0.236	33.7	0.090	1.77
Sah-SM < 80	12.8	0.9	0.217	20.8	0.042	0.91
Sah-SM 80-150	16.4	1.0	0.202	22.8	0.048	1.02
Sah-SM 150-200	11.9	0.7	0.183	23.4	0.056	1.13
Sah-SM 200-250	15.5	0.9	0.211	20.9	0.053	1.08
Sah-SM > 250	11.5	0.4	0.138	23.6	0.046	0.96
Sah-WMPs	19.2	0.9	0.168	6.7	0.014	0.32
Sah-MSN	2.1	0.5	0.148	33.7	0.228	4.62
Sah-DC	14.6	0.8	0.115	10.6	0.024	0.51
Sah-NM	25.1	1.5	0.190	6.1	0.004	0.08
Sah-cal bulk	12.0	0.45	0.215	31.0	0.084	1.65
Kota Kota						
KK-M < 80	7.4	0.5	0.191	42.8	0.129	2.31
KK-M 80-150	7.2	0.8	0.176	46.0	0.140	2.50
KK-M 150-200	8.1	0.6	0.192	45.9	0.135	2.61
KK-M 200-250	7.9	0.7	0.184	46.2	0.138	2.52
KK-M > 250	9.5	0.2	0.220	46.2	0.129	2.56
KK-SM < 80	13.4	0.8	0.220	14.6	0.022	0.75
KK-SM 80-150	13.8	0.6	0.204	14.7	0.028	0.66
KK-SM 150-200	14.5	1.0	0.224	17.4	0.038	0.78
KK-SM 200-250	15.5	0.6	0.214	10.5	0.021	0.39
KK-SM > 250	16.7	0.6	0.175	12.2	0.027	0.53
KK-WMPs	17.3	1.1	0.184	24.5	0.069	0.92
KK-Chondrules	14.7	0.4	0.197	12.0	0.026	0.52
KK-NM	16.4	0.9	0.210	4.8	0.004	0.116
KK-cal bulk.	10.4	0.48	0.202	35.7	0.100	1.93
Kota Kota-bulk[a]	12.7	0.7	0.30	29.6	0.08	1.54
CI Bulk[b]	9.6	0.9	0.19	18.3	0.05	1.06

[a] Bulk rock data for Kota Kota from Easton and Elliott (1977).

[b] Data for CI chondrites from Lodders (2003).

Table 2.3. Proportions of metal, sulfides and silicates in the separated components of Sahara 97072 and Kota Kota.

Component	Metal (%)	Sulfide (%)	Silicate (%)
Sahara 97072			
Sah-M < 80	27	10	63
Sah-M 80-150	47	13	40
Sah-M 150-200	41	13	46
Sah-M 200-250	32	14	54
Sah-M > 250	28	12	60
Sah-SM < 80	16	9	75
Sah-SM 80-150	19	7	73
Sah-SM 150-200	19	9	72
Sah-SM 200-250	17	8	75
Sah-SM > 250	21	6	73
Sah-WMPs	5	3	92
Sah-MSN	30	13	57
Sah-DC	9	4	88
Sah-NM	3	5	92
Sah-cal bulk	25	12	63
Kota Kota			
KK-M < 80	38	12	50
KK-M 80-150	41	12	47
KK-M 150-200	41	13	47
KK-M 200-250	41	13	46
KK-M > 250	41	12	47
KK-SM < 80	6	15	79
KK-SM 80-150	8	12	80
KK-SM 150-200	11	11	78
KK-SM 200-250	5	9	86
KK-SM > 250	8	8	84
KK-WMPs	20	9	71
KK-chondrules	7	8	84
KK-NM	1	7	93
KK-cal bulk	32	9	59

Proportions of metal, sulfides and silicates in each fraction is calculated by considering total sum of the metal, sulfides and silicates is 100%. Percentage of sulfides were determined by assuming all measured S is hosted by sulfides. Metal content calculated from the concentrations of Fe, Ni and Co by subtracting the Fe present in sulfides. Metal content may have been underestimated by 1-2% because of the assumption that FeS is the major sulfide phase in all fractions. Silicates were determined by subtracting the metal and sulfides from 100%.

2.8 Appendix Chapter 2

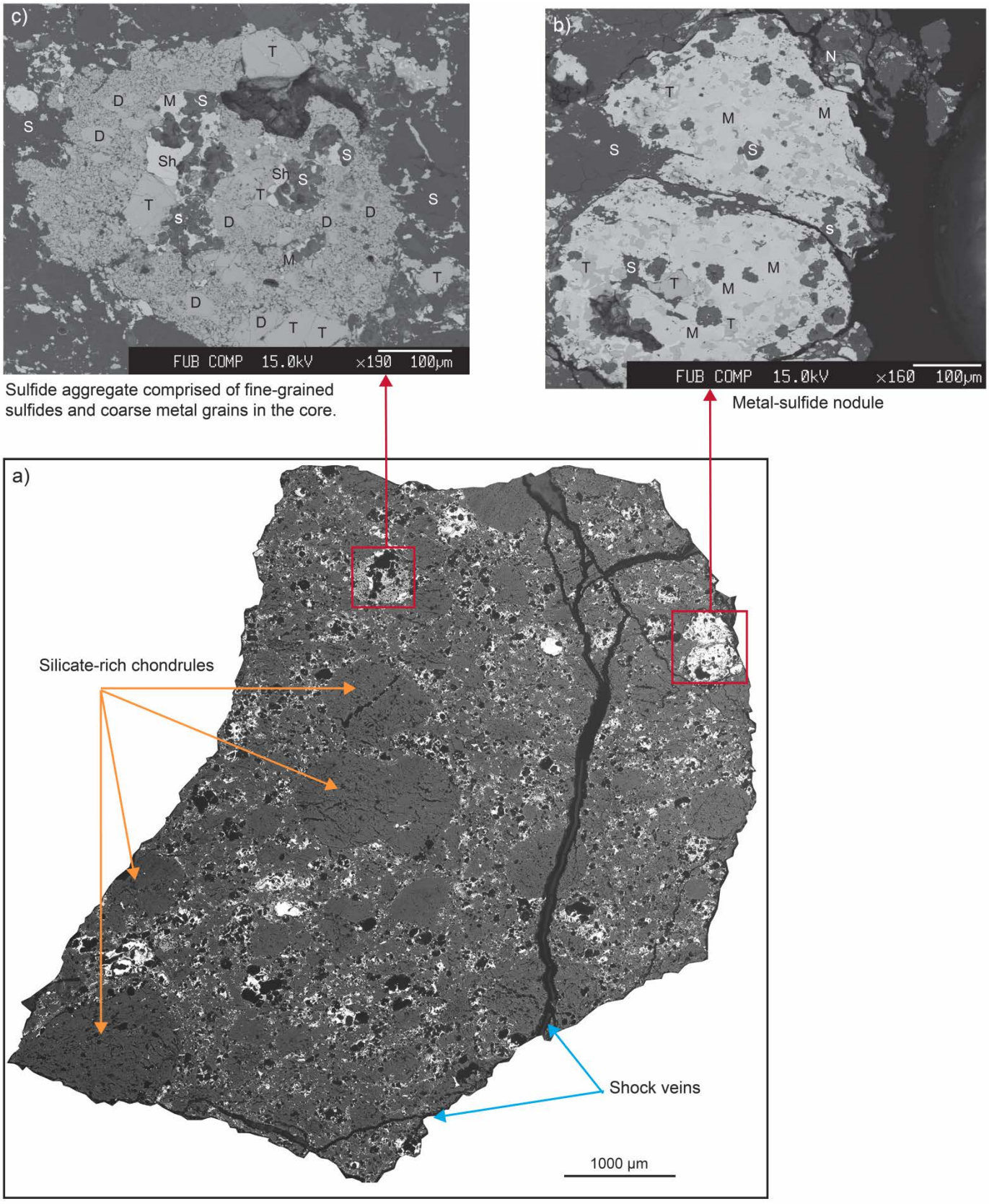

Fig.2.A1. a) Reflectance microscope image of a thick section of Sahara 97072. Enlarged images are backscattered electron images of highlighted areas which show b) a metal-sulfide nodule and c) a fine grained sulfide aggregate which also contains small amounts of fine and coarse grained metal. White phases are metal, light gray colored phases are sulfides, silicates are dark gray and black color shows holes, cracks and shock veins. S = silicate, Sh = schreibersite, T= troilite, D = djerfisherite, M = metal, P = perryite and N = niningerite. Bulk rock modal composition estimated from the color variation due to differences in reflectivity is approximately 19% metal + sulfides and 81% silicates in this piece of the rock.

Silicate rich chondrules and metal-sulfide nodules (diameter ranging from 1.5 mm to < 0.2 mm) are embedded in matrix. Matrix is mainly comprised of fine grained silicates, sulfides and metal (of varying sizes). Irrespectively of the variation in size, silicate-rich chondrules of Sahara 97072 are mostly devoid of large metal grains or at most contain only traces of very tiny metal grains. In contrast, in metal-sulfide nodules, silicate grains are small or absent. The melting process that formed the metal- and sulfide rich objects must have occurred before accretion of this meteorite and not on the EH3 parent body (e. g., Lehner et al., 2010; Horstmann et al., 2014). Most of the metal occurs in the form of metal-sulfide nodules and abundant fine and as some coarse metal grains dispersed within the matrix. Black veins reflect the effect of brief shock during later impacts. Chondrules and metal grains broken by the veins are fresh and show unaltered textures. All these observations either indicate that chondrule precursors were heated for longer duration of time or different melting episodes occurred before accretion which efficiently separate immiscible silicates, metal and sulfide rich material from each other. These metal-sulfide and sulfide rich objects may have formed by impact dispersal of differentiated portions of earlier planetesimals, planetary embryos or even planets such as Mercury, which is known to have metal-, sulfide and silicate rich reservoirs (e. g., Weider et al., 2012).

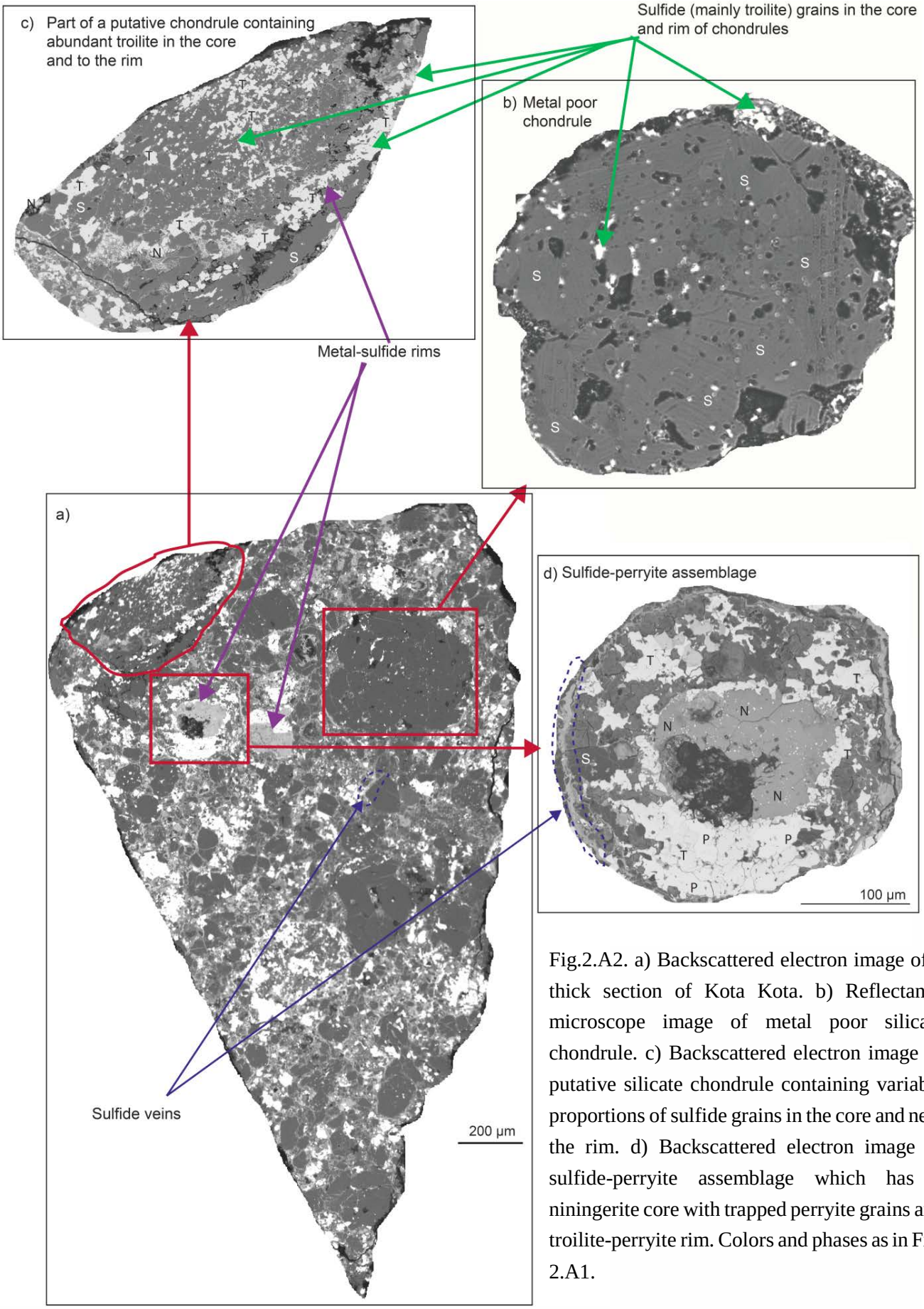

Fig.2.A2. a) Backscattered electron image of a thick section of Kota Kota. b) Reflectance microscope image of metal poor silicate chondrule. c) Backscattered electron image of putative silicate chondrule containing variable proportions of sulfide grains in the core and near the rim. d) Backscattered electron image of sulfide-perryite assemblage which has a niningerite core with trapped perryite grains and troilite-perryite rim. Colors and phases as in Fig. 2.A1.

Chondrules are varying in sizes. Matrix is comprised of silicates, sulfides and metal grains of varying size. Bulk rock modal composition calculated from the reflectance variation is 25% metal + sulfides and 75% silicates in this piece of the rock. Kota Kota chondrules contain a higher proportion of metal compared to chondrules in Sahara 97072. Metal + sulfide grains in chondrules and matrix of Kota Kota tend to have larger grain sizes compared to Sahara 97072.

Elongate aggregates of metal and sulfides (e. g., blue dashed line in a)) in the matrix and near chondrule rims suggest that in contrast to Sahara 97072, some of the matrix material of Kota Kota may have been warm and soft during accretion into the parent body. Accretion of warm material or impacts could be the source of the heating. Absence of shock veins in Kota Kota renders impact heating a less likely explanation. We also note that the matrix contains a broad range of grain sizes, which display a very heterogeneous spatial distribution. This observation does not favor post-accretional re-equilibration by impact or internal heat sources. The alternative would be accretion of warm and cold metal and sulfide grains, and subsequently local deformation and annealing of warm grains. The different textures of Sahara 97072 and Kota Kota indicate that their components, especially those in the matrix, have undergone a different thermal evolution before and after accretion.

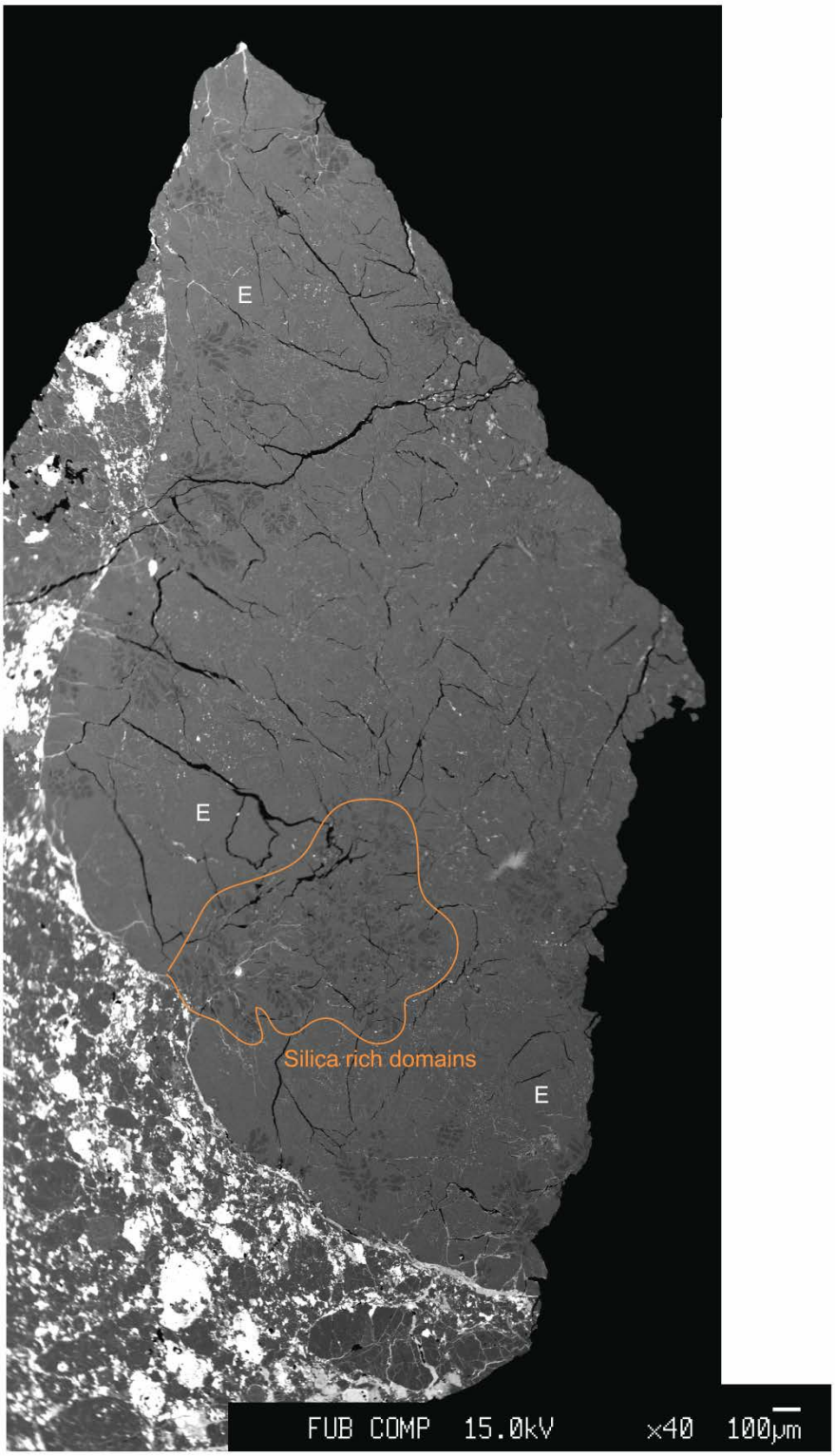

Fig.2.A3. Backscattered electron image of part of a dark clast (DC) of Sahara 97072. Mainly composed of E = Mg-rich enstatite (light gray) and silica (SiO2, dark gray color). Silica rich domains are present mostly near the rim of the clast. A silica rich area is highlighted by the line. A clast contains irregular sized sulfide veins at the boundary to the matrix. Some enstatite grains contain very small (<1µm) sulfide grains whereas other enstatite domains are completely devoid of sulfide grains.

Chapter 3

Highly siderophile and chalcogen element constraints on the origin of components of the Allende and Murchison meteorites

3.1 Abstract

^{187}Re-^{187}Os systematics and the abundances of highly siderophile elements (HSE: Re, platinum group elements and Au), chalcogen elements (Te, Se and S) and of some major and minor elements (Mg, Ca, Mn, Cr, Fe, Ni and Co) were determined in physically and magnetically separated components of the Allende and Murchison. Substantial differences exist in the absolute and relative abundances of elements in the components, but the similarity of calculated and literature bulk rock abundances of HSE and chalcogens indicate that chemical complementarity exists among the components, with CI chondrite like ratios for many elements in the bulk rocks.

The ^{187}Re-^{187}Os systematics and element variations of Allende are less disturbed compared to Murchison, which reflects different degrees of oxidation and alteration of the meteorites. Coupled Ru/Pt, Pd/Ir and Re/Os variations indicate the influence of fractional condensation and volatility during the evolution of the meteorite components. The HSE systematics (with the exception of Au) is controlled by two types of materials; Pd depleted condensates and CI chondrite like material. Magnetic components show the strongest enrichment of Au, which is heterogeneously distributed among the components, likely as a result of hydrothermal alteration. Chalcogen elements are depleted compared to HSE in all components, presumably due to their higher volatility. Te/Se and Se/S are close to CI chondrite values. Small systematic variations of these ratios in components bear the signature of fractional condensation or partial evaporation and metal-sulfide-silicate partitioning.

3.2 Introduction

CM and CV chondrites are composed of variable proportions of different types of chondrules, fine grained matrix, Ca-Al-rich inclusions (CAIs) and amoeboid olivine aggregates (AOAs) (Scott and Krot, 2003). These components formed in different environments and record information regarding the physical and chemical conditions in the early solar nebula as well as later secondary processes on meteorite parent bodies (Scott and Krot, 2003; Brearley, 2003 and references therein). CAIs are the most refractory components in chondrites and may represent the earliest condensed solids in the solar nebula from gas of solar composition (Grossman, 1972, 1980; Bouvier and Wadhwa, 2010). AOAs, chondrules and matrix mineral phases, which include magnetite, troilite, Fe-Ni sulfide, olivine and pyroxenes, are less refractory than CAIs (Lodders, 2003; Macpherson et al., 1985).

Different condensation temperatures of elements at conditions that are different from the canonical solar gas (like variations in fO_2, total pressure and gas composition) and later secondary processes such as metamorphism and aqueous alteration make it difficult to distinguish primary from secondary processes and associated chemical fractionations. Primary processes refer to processes in the solar nebula before accretion of the chondrite components, whereas secondary processes occur on the meteorite parent body or on the Earth's surface in case of meteorite 'finds'. Comprehensive study of abundances of refractory and volatile siderophile elements having similar geochemical properties in different chondritic components allows tracing back the history of nebular and secondary alteration processes (Dreibus et al., 1995; Becker et al., 2001; Brandon et al. 2005a, b; Fischer-Gödde et al. 2010; Archer et al., 2014; Palme et al., 2014).

Rhenium and Os are the most refractory HSE which condensed at high temperatures (50% condensation temperatures are 1812 K and 1821 K respectively, Lodders, 2003) in the solar nebula. These elements have condensation temperatures overlapping with refractory oxides in CAIs. Walker et al. (2002b) have shown that significant Re-Os fractionation occurs between matrix, magnetite bearing sulfide fractions, and chondrule material in the Allende CV chondrite. Iridium, Ru, Pt and Rh condense at slightly lower temperatures (the range of 50% condensations temperature is ~1600 K to1400 K) from a gas of solar composition. All these elements were condensed into refractory metal alloy phases before significant Fe-Ni metal condensation occurred and were later incorporated into Fe-Ni alloys when the full inventory of Fe and Ni condensed (Lodders, 2003, Campbell et al., 2005).

Every chondrite class has a distinct HSE abundance pattern. Systematic differences exist between carbonaceous chondrites and the other chondrite classes in terms of Re/Os (or $^{187}Os/^{188}Os$), Rh/Ir, Pd/Ir, Au/Ir and to a lesser extent Os/Ir, Ru/Ir and Pt/Ir (Jochum, 1996; Horan et al., 2003; Brandon et al., 2005a; Fischer-Gödde et al., 2010 and references therein). These chemical differences add to already established differences between carbonaceous and

other chondrites, such as in oxygen isotopes (Clayton, 1993), Cr isotopes (Trinquier et al., 2007) and lithophile refractory element ratios such as Y/Ho (Pack et al., 2007).

The chemical variations in refractory elements in chondrite components might be explained by different processes like fractional condensation (Mason and Taylor, 1982; Ireland et al., 1988; Campbell et al., 2003), inhomogeneous sampling of different phases and element loss or remobilization on the parent body or by terrestrial weathering at more oxidizing conditions (Becker et al., 2001; Walker et al., 2002b; Archer et al., 2014). Volatile elements are also fractionated by the above mentioned processes and by some additional processes including evaporation in the early solar nebula and by aqueous alteration (Dreibus et al., 1995; Kong et al., 1997). If terrestrial weathering processes can be excluded, abundances of the moderately volatile elements Pd, Au, Se, Te and S (50% condensation temperatures in the range of 1326-664 K, Lodders, 2003) can help to understand the role of volatility-controlled processes prior to accretion or in the parent body environment (Ebihara et al., 1982; Dreibus et al., 1995; Fischer-Gödde et al., 2010).

Previous work on HSE abundances in refractory metal alloy phases in CAIs from CV3 chondrites show depletions of volatile siderophile elements such as Pd and Au in these assemblages and support an origin by fractional condensation (Palme and Wlotzka, 1976; Blander et al., 1980; Blum et al., 1989; Sylvester et al., 1990; Palme et al., 1994; Campbell et al., 2003). Some of these data also indicate the later introduction of volatile elements by nebular or parent body processes. Archer et al., (2014) have studied HSE abundances in CAIs, chondrules and matrix from the Allende meteorite and concluded that the HSE variation in CAIs is mainly inherited from fractional condensation in the early solar nebula. These authors also assume that volatile depletion during the chondrule forming event may be responsible for the depletion of Pd in chondrules of carbonaceous chondrites. Recent work by Berg et al., (2009) has identified volatile element depleted submicron sized refractory metal nuggets in the acid resistant residue of Murchison meteorite which they interpreted as a direct nebular condensate.

All previous studies (Becker et al., 2001; Berg et al., 2009; Archer et al., 2014; Palme et al., 2014) were carried out on components from random sample aliquots. A detailed study of the mass balance of HSE and chalcogen elements (here, the latter denote S, Se and Te, but not O) within CM and CV chondrite components is not available. In the present work we study the variation of ^{187}Re-^{187}Os systematics, HSE (Re, Os, Ir, Ru, Pt, Rh, Pd and Au) and chalcogen elements in components of Allende and Murchison.

We have performed a complete analysis that will look at the mass balance of HSE distributions between matrix, magnetic components (magnetite-sulfide-metal intergrowths), chondrules and CAIs. This approach will be useful to better understand which components control the composition of the HSE and chalcogens in the bulk rocks. The composition of the components will be useful in constraining the effect of secondary processes such as magnetite

formation on the distribution of the HSE. We also present major element data for the components, which assists in the assessment of their mineralogical composition.

3.3 Sample preparation

Gram-sized pieces of Allende (No. ME. 2632, Spec. No. 17) and Murchison (No. ME. 2684, Spec. No. 23) were provided by Field Museum, Chicago have been broken into fragments. Components which can be distinguished under a binocular microscope (Kruss optronic MSZ 5600) like whole Ca-Al-rich inclusions (CAIs), large chondrules and their fragments were separated from broken pieces in an agate mortar using plastic tweezers. A detailed description of the procedure is discussed in Kadlag and Becker a (submitted).

The remaining material was separated into six different grain size fractions using nylon sieves (< 20 µm, 20-80 µm, 80-150 µm, 150-200 µm, 200-250 µm and > 250 µm). Each size fraction (except < 20: because of the small grain sizes, the fine material is sticking to each other as well as to the magnet and impose limit on good separation) was further divided into magnetic (M), slightly magnetic (SM) and nonmagnetic (NM) component by using a hand magnet. CAIs were very rare in our Murchison aliquot. Only a very small (655 x 588 µm) blue inclusion was identified. Because of its small size, it was not digested. The CAI data presented in this study are from Allende.

3.4 Analytical Techniques

We have used the isotope dilution method to obtain precise concentration data for most HSE (Re, Os, Ir, Ru, Pt and Pd) and chalcogen (Te, Se and S) in the components of Allende and Murchison. Abundances of Au and Rh were analyzed by a combination of external and internal standardization methods (Fischer-Gödde et al., 2010).

Samples were mixed with four different spikes (a ^{185}Re-^{190}Os mixed spike, a ^{191}Ir-^{99}Ru-^{194}Pt-^{105}Pd mixed spike, a ^{77}Se-^{125}Te mixed spike and a ^{34}S spike) and digested in reverse aqua regia (1ml HCl: 2 ml HNO_3) for 16 hrs at 100 Bar and 320 ºC in sealed quartz vessels using a Anton Paar^{TM} high pressure asher system (HPAS). After dissolution, Os was separated from other HSE and matrix by solvent extraction in CCl_4 and back extraction into HBr (Cohen and Waters, 1996; Fischer-Gödde et al., 2010) followed by purification step which involves micro distillation into HBr (Roy-Barman, 1993).

All other HSE and chalcogens were converted into chloride form and then separated from matrix by using ion exchange chromatography. Detailed procedures for chemical separation of HSE and chalcogen elements and preparation of samples and standards for major and minor element (Mg, Ca, Mn, Fe, Co and Ni) analysis were described in detail by Fischer-Gödde et al.

(2010); Wang et al. (2013) and Kadlag and Becker a, (submitted). Chromium concentrations in this study were obtained by using Allende standard powder dissolved in HF: HNO_3 as an external calibration standard. Except Os, Te and Se isotopic ratios of all other elements were measured on an Element XR ICPMS using a Scott-type glass spray chamber. Se and Te were measured by using hydride generation and a modified cyclonic double pass Scott-type spray chamber on Element XR ICPMS. Osmium isotopic measurements were determined by N-TIMS on a Triton instrument at Freie Universität Berlin. Details of measurement protocols and data reduction were given in Fischer-Gödde et al. (2010); Wang et al. (2013) and Kadlag and Becker a, (submitted).

3.4.1 Analytical blanks

Total procedure blanks were determined with each set of digested samples. Average total procedure blanks (n=15) for the duration of the project were: Re = 8 ± 3 pg, Os = 2 ± 2 pg, Ir = 0.9 ± 0.8 pg, Ru = 1 ± 1 pg, Pt = 9 ± 4 pg, Rh = 3 ± 1pg, Pd = 41 ± 19 pg, Au = 5 ± 3 pg, Te = 50 ± 20 pg, Se = 2.4 ± 0.5 ng and S = 9 ± 1 μg. Total procedure blanks contribute < 5% to analysed element budgets for most of the components. The NM << 80 component from Murchison, Murchison chondrules and Allende CAIs have somewhat higher blank contributions for some elements (Re, Pd) but not more than 10% in any case.

3.4.2 Precision and accuracy of measurements

Precision of isotopic ratios of HSE and chalcogen and major element ratios of in-house standards for ICPMS measurements at the Freie University Berlin over the period of analysis was < 4% (2σ). The repeatability of the $^{187}Os/^{188}Os$ ratio of the University of Maryland Os standard measured on the FU Berlin Triton by N-TIMS was 0.11381 ± 0.00004 (n = 8, 2σ) for Faraday cup measurements and 0.1139 ± 0.0004 (n = 11, 2σ) for electron multiplier measurements over the period of analysis.

3.5 Results

3.5.1 Major element concentrations

Major and minor element abundances in the components, bulk rock data from the literature and bulk rock values calculated from the mass balance of all components analyzed in this study are given in Table 3.1. We note that large differences between literature bulk rock values and calculated bulk rock values of Ca (up to 40%) and Ni (up to 33%) exist.

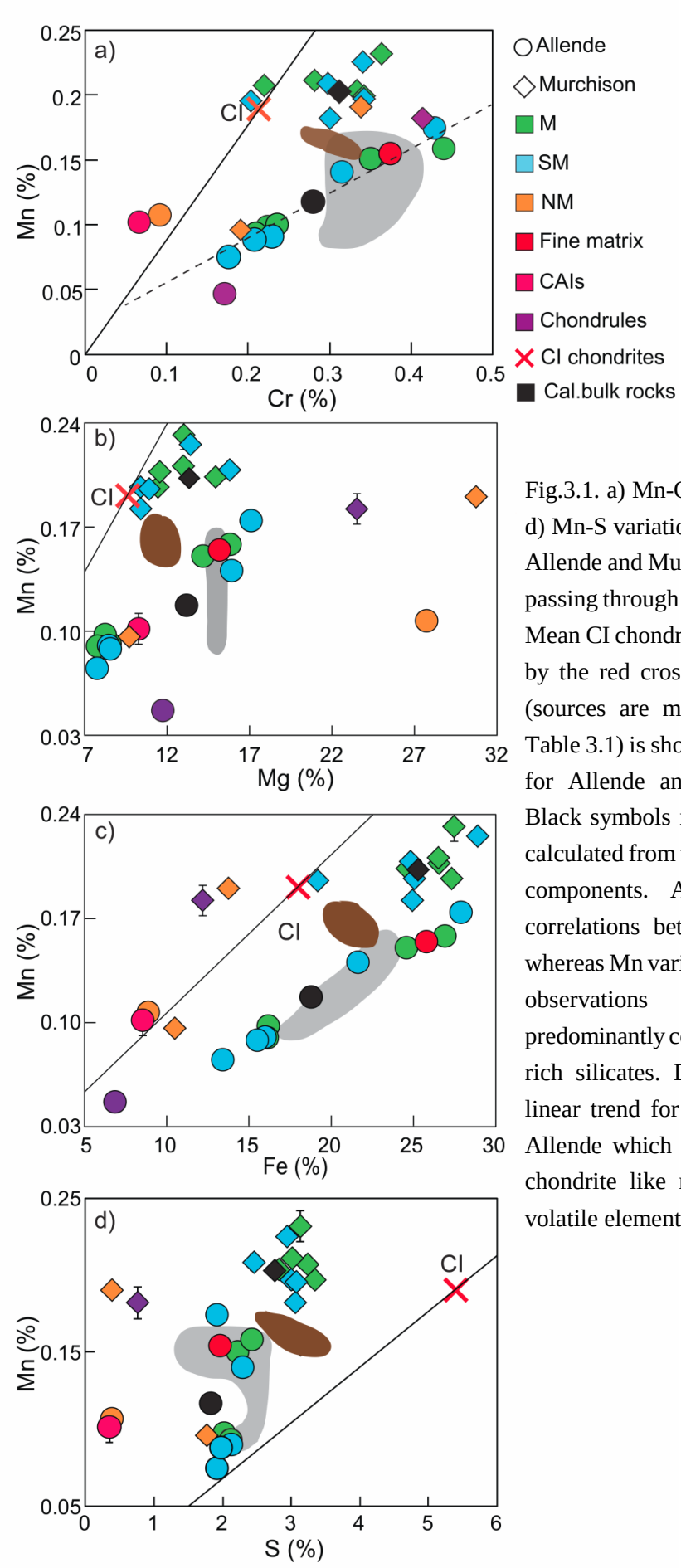

Fig.3.1. a) Mn-Cr b) Mn-Mg, c) Mn-Fe, and d) Mn-S variation among the components of Allende and Murchison. Black reference line passing through CI chondrites and the origin. Mean CI chondrite (Lodders, 2003) is shown by the red cross. Literature bulk rock data (sources are mentioned in the caption of Table 3.1) is shown by gray and brown fields for Allende and Murchison, respectively. Black symbols represent the bulk rock data calculated from the mass balance of analyzed components. Allende components show correlations between Mn, Mg Fe and Cr whereas Mn varies independently of S. These observations indicate that Mn is predominantly controlled by magnetite and Fe rich silicates. Dashed line in a) indicates linear trend for M and SM components of Allende which reflects mixing between CI chondrite like material and a fractionated volatile element depleted component.

The variation of major elements Mg, Cr, Mn, Fe and S is shown in Fig.3.1and Fig.3.A1 and 3.A2 of the appendix. Allende components show large variations in element abundances with linear relationships between Mn, Cr and Fe in most components of Allende (Figs.3.1a, b, c and 3.A2). The Allende components show linear mixing between a CI like and a Cr enriched end member (Fig.3.1 and 3.A2).

In contrast, Murchison M and SM components show limited, random variation in Cr, Mn and Fe abundances which mostly scatter around CI chondritic ratios (Fig.3.1 and 3.A2). Manganese and Cr concentrations display large variations in the components of both meteorites. These elements do not correlate with S concentrations; indicating that they are controlled by silicate phases, rather than sulfides (Fig.3.1c and 3.A2).

CAIs, Allende NM fraction and Murchison M 150-200 and SM 200-250 show Mn/Cr higher than in CI chondrites, whereas other components from both meteorites have $Mn/Cr < Mn/Cr_{CI}$. Higher Mn/Cr in CAIs and the NM fraction of Allende are mainly because of higher proportions of silicate phases in these fractions. The CAI fraction is strongly enriched in Ca (Ca = 6.2 vol. %), slightly enriched in Mg (Mg = 10 wt. %) and depleted in Fe, Cr and Mn compared to CI chondrites (Table 3.2). Differences in the Mn/Cr and Fe/Cr (Figs.3.1a and 3.A2) in the NM fractions of Allende and Murchison indicate a different mineralogy of these fractions.

3.5.2 ^{187}Re-^{187}Os systematics

Data of $^{187}Re/^{188}Os$ and $^{187}Os/^{188}Os$ and Δ_{Os} (the deviation of $^{187}Os/^{188}Os$ of a sample from the Re-Os isochron of the solar system calculated from parameters derived from IIIA iron meteorite isochron from Smoliar et al. (1996), for definition see caption of Table 3.2) of components are given in Table 3.2. A ^{187}Re-^{187}Os isochron diagram is shown in Fig.3.2a and Δ_{Os} - $^{187}Re/^{188}Os$ variations are shown in Fig.3.2b.

M components (except M 20-80 fraction of Murchison) show low $^{187}Os/^{188}Os$ compared to other components in both chondrites. The $^{187}Os/^{188}Os$ of M components of Allende are ~4% higher than $^{187}Os/^{188}Os$ of M components of Murchison.

The NM fraction of Murchison is depleted in the refractory elements (Fig.3.3) and shows a deviation from the isochron towards low $^{187}Re/^{188}Os$ (Fig.3.2). The Allende NM fraction plots on the isochron and shows the highest $^{187}Re/^{188}Os$ of all components of Allende (Fig.3.2).

With the exception of the CAI fraction, most components of Allende show only minor deviations from the IIIA iron meteorite isochron (Smoliar et al., 1996), whereas most of the Murchison components display deviations from the isochron, with negative Δ_{Os} (Fig.3.2). Another important observation to note here is that components with large deviation from the isochron have small sample weights (Table 3.2).

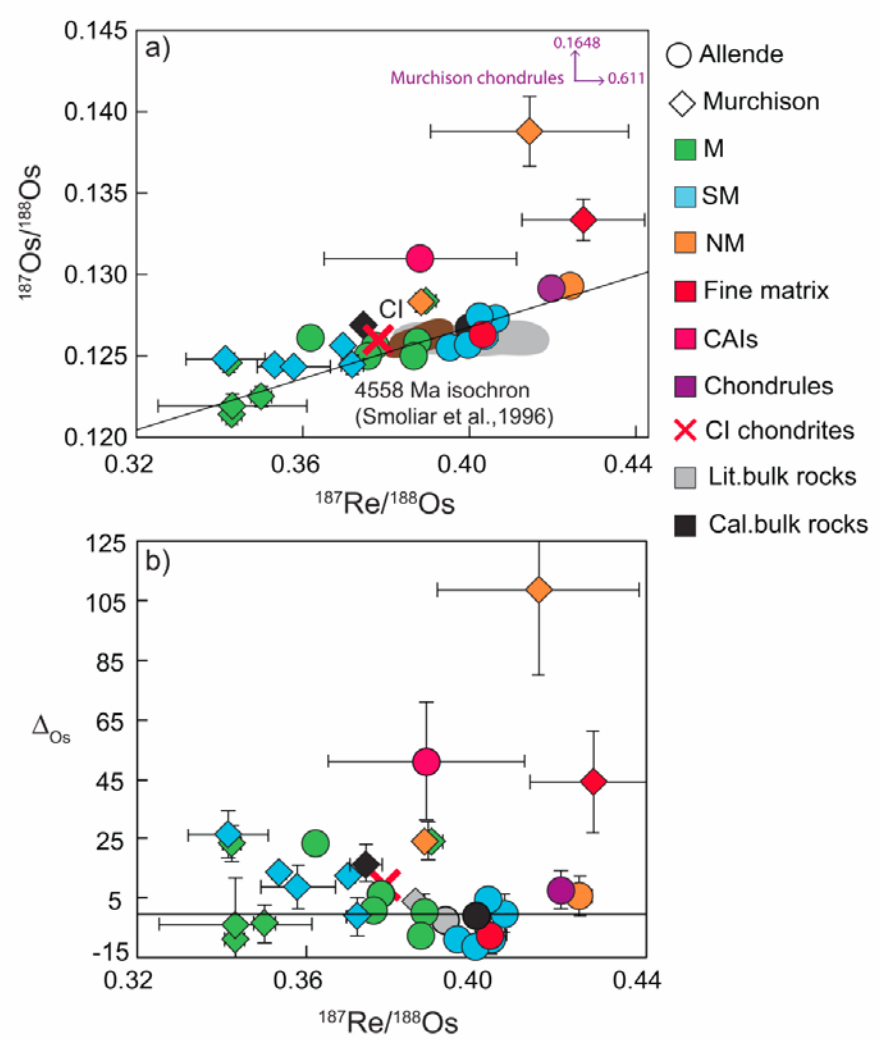

Fig.3.2. a) ^{187}Re-^{187}Os isochron diagram of components of Allende and Murchison. b) ΔOs versus $^{187}Re/^{188}Os$ diagram. Reference line is the IIIA iron meteorite isochron reflecting an age of 4558 Ma (Smoliar et al., 1996). CI chondrite data (Walker et al., 2002b; Fischer-Gödde et al., 2010) are shown by the red cross. Bulk rock data of Allende and Murchison (Walker et al., 2002b; Horan et al., 2003; Brandon et al., 2005a; Fischer-Gödde et al., 2010) in a) are shown by the gray and brown fields respectively.

3.5.3 HSE abundances

HSE abundances of the components, calculated bulk rocks and bulk rock data from the literature (Paul and Lipschutz, 1990; Dreibus et al., 1995; Friedrich et al., 2002; Walker et al., 2002b; Fischer-Gödde et al., 2010) are given in Table 3.2. Calculated bulk rock values show at most 20% deviations from literature bulk rock values. The data on components show 3-25 times variation in absolute element abundances (Fig.3.3). The HSE abundances of the components of Allende and Murchison display no systematic relationship with grain size (Table 3.2, Fig.3.3). M components are modestly enriched in HSE compared to SM and NM components, except for the NM fraction of Allende (Fig.3.3). The most prominent feature of the abundance patterns are the high CI normalized abundances of Au in most of the M and SM components of both chondrites compared to all other analysed elements (Fig.3.3).

M fractions of Allende show $Ru/Ir < Ru/Ir_{CI}$ whereas SM components show complementary enrichment in Ru ($Ru/Ir > Ru/Ir_{CI}$) (Fig.3.3a). M and SM fractions of Murchison are relatively unfractionated in the refractory HSE Os, Ir, Ru, Pt and Rh (Fig.3.3b). NM fractions from both chondrites are highly depleted (0.06-0.3 x CI) in Pd and Au, compared to all other HSE, whereas substantial differences exist in abundances of refractory HSE in NM fractions of both chondrites

(Fig.3.3). The NM fraction of Allende shows enrichment (2xCI) in the refractory HSE and a fractionated abundance pattern (Fig.3.3a.) relative to CI chondrites. In contrast, the NM fraction of Murchison shows depleted (0.5xCI) abundances of refractory HSE and an almost unfractionated abundance pattern of most of the elements (Fig.3.3b).

The CAI fraction of Allende is depleted (~0.5xCI) in all HSE, but shows an unfractionated abundance pattern of refractory HSE, with a slight depletion of Pd and enrichment of Au (Fig.3.3a). Absolute abundances of refractory HSE in the CAI fraction is consistent with abundance patterns of type II CAIs (Becker et al., 2001; Archer et al., 2014).

A chondrule fraction from Allende shows nearly CI chondritic abundances, almost unfractionated abundance pattern of refractory HSE and Au and a depletion of Pd (Fig.3.3a). In contrast, the chondrule fraction from Murchison shows a complex abundance pattern with strong

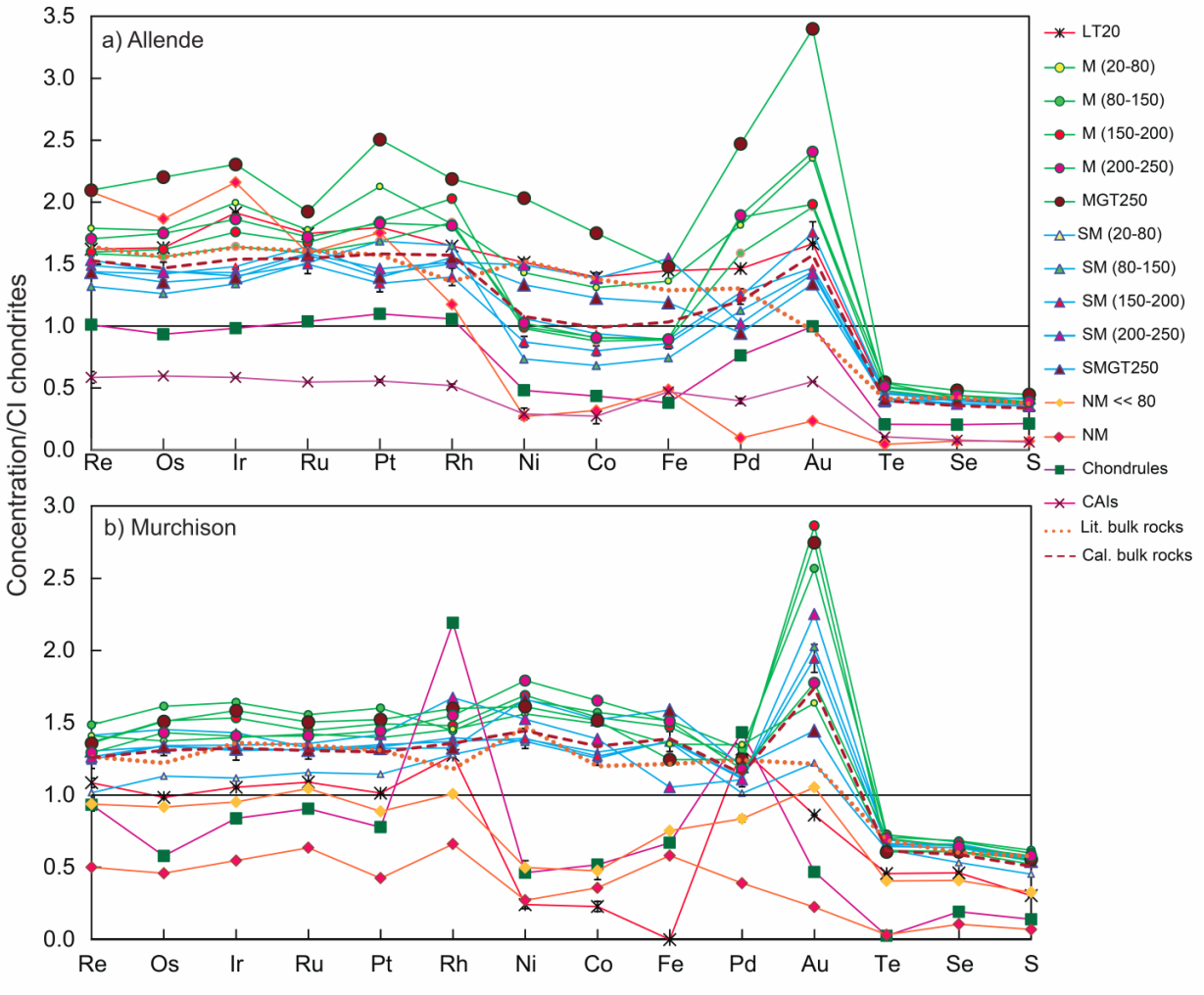

Fig.3.3. Element abundances normalized to CI chondrites. Elements are ordered from left to right based on increasing volatility under solar conditions (Lodders, 2003). CI and bulk chondrite values from the sources mentioned in Table 3.1 and 3.2.

enrichment in Rh, Re/Os > Re/Os_{CI} and depletion of Au compared to other HSE (Fig.3.3b). The fine grained fraction (< 20 µm) of Allende which is mainly comprised of matrix material shows

slightly higher abundances of Ir and Au and slightly lower Rh and Pd compared to CI normalized abundances of other HSE (Fig.3.3a). The < 20 µm fraction of Murchison shows nearly CI chondritic abundances of refractory HSE and slightly higher Rh and Pd (Fig.3.3b).

3.5.4 Chalcogen element abundances

Overall chalcogens are depleted in all components compared to CI chondrites and the HSE (Fig.3.3 and 3.4, Table 3.2). Calculated bulk rock concentrations are within 15% of literature bulk rock values (Table 3.2). The chalcogens are unfractionated relative to each other (Fig.3.3) in most of the components and show linear correlations with each other (Fig.3.4). Chalcogen elements are enriched in M and SM fractions compared to other components without any systematic relationship with grain size. CAIs, chondrules and NM fractions show the strongest depletion in chalcogen elements, consistent with a high temperature condensate origin of these components (Fig.3.3 and Fig.3.4). M components show Se/Te and S/Se slightly lower than in CI chondrites.

In other components these ratios are nearly CI chondritic or, as in Murchison chondrule fraction and NM fractions from both meteorites Se/Te is slightly higher than in CI chondrites (Fig.3.4a)

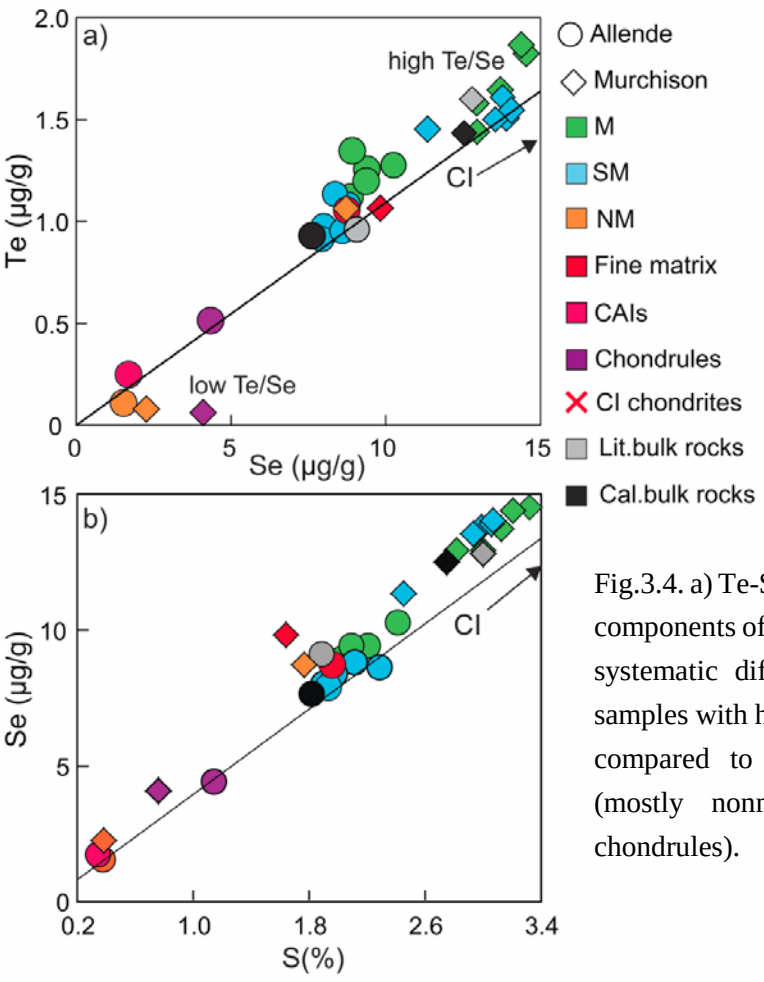

Fig.3.4. a) Te-Se and b) Se-S variation among the components of Allende and Murchison. Note the systematic differences of Te/Se and Se/S in samples with high abundances of these elements compared to samples with low abundances (mostly nonmagnetic fractions, CAIs and chondrules).

3.6 Discussion

3.6.1 Major and minor element variations in the components and the influence of mineralogy

Concentrations of major and minor elements were used to assess which minerals control the distribution of lithophile, siderophile and chalcophile elements in separated components. The major and minor elements reported in this study were analyzed by the same technique used previously for enstatite chondrites (Kadlag and Becker a, submitted). In this previous study, calculated bulk rock values were within 20% of literature data, which indicates that the dissolution technique is efficient. Therefore, substantial deviations observed in this study between calculated and literature bulk rock values for some elements (Ca, Cr and Ni) may reflect sample heterogeneity. Heterogeneity of elemental abundances in different splits of bulk carbonaceous chondrites is not uncommon, especially for lower petrologic types and for low sample weights (Morlok et al., 2006). Major element concentrations determined by various sources and techniques show variation in the abundances up to 30% in different splits of bulk rocks of Allende and Murchison (McCarthy and Ahrens, 1972; Fuchs et al., 1973; Fitzgerald, 1979a; Jarosewich et al., 1987; Johnson et al., 1990; Jarosewich, 1990; Dreibus et al., 1995).

High Fe, Ni and S abundances in the M components indicate that, these fractions are predominantly comprised of intergrown magnetite, sulfide and presumably minor metal, which are the main host phases of these elements in these meteorites. Components of Allende display systematic variations between certain major, minor and trace elements, whereas Murchison components show random variations of these elements (Figs.3.1, 3.A1 and 3.A2). We first discuss the systematic element variations observed for Allende. Manganese shows linear correlations with Fe (Fig.3.1b) and Cr (Fig.3.1a) in most Allende components and is decoupled from S (Fig.3.1c). According to the condensation sequence in the solar nebula (Lodders, 2003) most of the Cr and Fe condensed into the metal alloy phases, whereas Mn is a lithophile element and is mainly hosted by silicates. These correlations suggest that in case of the Allende meteorite most of the Fe and Cr condensed into the silicates (olivine or pyroxene) or condensed into original metal which was later oxidized and incorporated into magnetite and silicates. Nickel in most Allende components shows a correlation with the HSE (Fig.3.5), indicating predominantly siderophile behaviour of Ni. These observations are important as they suggest that, in spite of subsequent alteration and oxidation, the overall geochemical behaviour of moderately to highly siderophile elements during high-temperature processing has been preserved in components of Allende at the sampling scale of the present study.

Most components of both meteorites show CI chondritic Ni/Co (Fig.3.A1a), indicating that the phases which incorporate Co and Ni in these chondrites have preserved high temperature condensation signatures and were not redistributed during subsequent alteration. NM and some M

components show slight deviations from canonical CI chondrite values, such that they have complementary Ni/Co, Ni/Fe and Co/Fe (Fig.3.A1a). The Ni and Fe rich fractions (M) have higher Ni/Co than CI chondrites and Ni and Fe poor NM fractions show opposite behavior. These variations are likely due to differences in the metal-silicate partitioning of these elements during high-temperature fractionation processes, because Ni is more siderophile compared to Co (Schmitt et al., 1989).

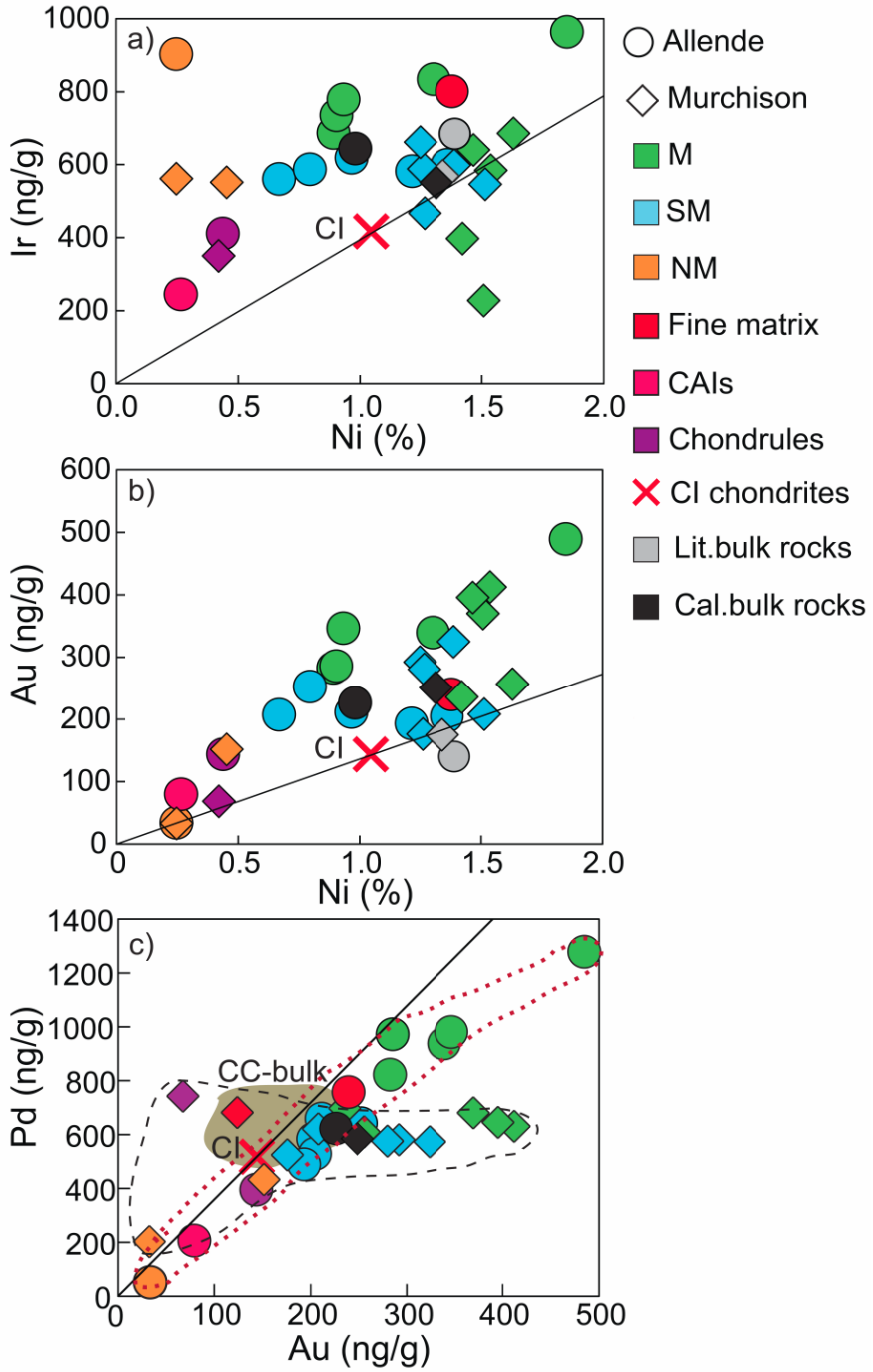

Fig.3.5. Variation of a) Ir-Ni, b) Au-Ni and c) Pd-Au in the components of Allende and Murchison. Combined bulk rock data of carbonaceous chondrites are shown by the green field in c). Symbols and literature data sources as mentioned before. In Murchison, Au is completely decoupled from Pd and other HSE, whereas in Allende components Au correlated well with Pd and Ni. With the exception of the NM fraction, the HSE in Allende components are well correlated with Ni. Ir is highly variable in silicate rich fractions indicating the presence of refractory metal phases in latter. The chondrule fraction from Murchison is depleted in Fe and in most volatile elements (e.g. Au) compared to Cr and Mg (see Figs. 3.1, 3. 3 and 3.A2).

The higher than CI chondritic Cr/Mn and in calculated bulk rocks (Fig.3.1) indicate that with the exception of the CAI and NM fraction, the chondrite components retain more Cr compared to Mn during condensation or evaporation processes. The random variations between Mg, Fe, Cr, Mn and S (Fig.3.1) among the components of Murchison can be attributed to aqueous alteration on the Murchison parent body.

Chemical complementarity observed for siderophile, chalcophile and lithophile trace elements between matrix and chondrule fractions from the carbonaceous chondrites (Bland et al., 2005; Hezel and Palme, 2008), is also evident from the complementary ratios of major elements such as Ni/Co, Mn/Mg and Mn/Fe, Mn/Cr (Figs.3.1, 3.A1 and 3.A2) in different components in this study. These complementarities suggest that all components, including CAIs, were formed from the same nebular reservoir. Thus, the slight differences in the ratios of some major elements (Cr/Fe, Cr/S, Mn/Cr, Mn/Mg, Mn/S, see Figs.3.1, 3.A1 and 3.A2) of bulk rocks of Allende and Murchison compared to CI chondrites may be an effect of inhomogeneous sampling of nebular condensates or high temperature processes (e. g., evaporation, chondrule formation) before accretion.

3.6.2 ^{187}Re-^{187}Os systematics

^{187}Re-^{187}Os systematics shows significant variation among the components (Fig.3.2). Most components plot on or close to the 4.558 Ga IIIA iron meteorite reference isochron (Smoliar et al., 1996) and show resolvable correlated variations in ^{187}Re/^{188}Os and ^{187}Os/^{188}Os (Fig.3.2).

M components in Allende and Murchison show lower Re/Os and ^{187}Os/^{188}Os compared to NM components (Fig.3.2). If the variation in Re/Os among the components is due to fractional condensation within gas in a closed system then the HSE bearing phases in M components of carbonaceous chondrites should be less refractory than the HSE carrier phases in NM components. M components of Allende have lower Os/Ir (Os/Ir ~ 0.994-1.070) and Re/Ir (Re/Ir ~ 0.079-0.085) than CI chondrites (Os/Ir_{CI} = 1.12, Re/Ir_{CI} = 0.088) suggesting that Re and Os behaved similarly in the fractionation processes that affected these components in Allende (Fig.3.A3). Higher Pd/Ir and lower Re*/Os (Re* is the calculated initial Re concentration from the measured Os isotopic composition) in M components of Allende and Murchison compared to SM and NM components (Fig.3.6b) also supports the fractional condensation scenario in solar gas. The behaviour of Re/Os (and ^{187}Os/^{188}Os) in M fractions of Allende and Murchison is opposite to that in M components of ordinary and enstatite chondrites where Re/Os is higher than in CI chondrites (Horan et al., 2009; Kadlag and Becker a, submitted). The different behaviour of Re and Os in ordinary and enstatite chondrite classes has been ascribed to fractional condensation and/or other partitioning processes.

Some components such as the CAI fraction from Allende and the NM, SM and < 20μm matrix rich fraction of Murchison show large deviations from the isochron towards

low $^{187}Re/^{188}Os$ (Fig.3.2a and b). Sample weights of these fractions are much smaller than those of components with isochronous behavior. Because Re and Os concentrations in these aliquots are low, the effects of late stage redistribution of Re might be more visible than in components with higher concentrations and sample weights. The CAI fraction from Allende is displaced from the isochron towards low $^{187}Re/^{188}Os$, consistent with similar observations for some CAIs with type II REE patterns by Becker et al. (2001) and Archer et al. (2014). Local alteration of the Allende parent body may have been responsible for the deviation, which may have been aided by, the low Re concentration and the porous nature of the CAI. It is notable that the CAI fraction shows higher $^{187}Os/^{188}Os$ than all other Allende components (Fig.3.2), an observation already made previously for CAIs with type II REE patterns (Becker et al., 2001).

3.6.3 HSE abundance variations in the components

The behaviour of the HSE in the components of Allende and Murchison is significantly different from each other. Therefore we will discuss HSE abundances in the components of these two meteorites separately in the next sections.

3.6.3.1 Allende

Previous work has indicated that the Allende meteorite is comprised of different components with different HSE abundances (Mason and Taylor, 1982; Sylvester et al., 1990; Palme et al., 1994; Becker et al., 2001; Walker et al., 2002b; Archer et al., 2014). Different types of CAIs from the Allende meteorite show substantial variations in HSE abundances (Becker et al., 2001; Archer et al., 2014), however, the bulk rock HSE abundances measured in different splits of Allende display limited variation of up to 16% (Becker et al., 2001; Walker et al., 2002b; Horan et al., 2003; Brandon et al., 2005a; Fischer-Gödde et al., 2010), and thus the influence of CAIs on the mass balance of the HSE must be limited. Bulk rock values of refractory HSE calculated from the mass balance of all analysed components in this study are within 8% of literature bulk rock values (Fischer-Gödde et al., 2010) that have used the same digestion technique and analytical methods as the present study. This observation indicates that the HSE abundances in different components are complementary.

Smooth correlations exist between Ru/Pt, Pd/Ir and Re*/Os in Allende components (Fig.3.6). M fractions show lower Re*/Os, $^{187}Os/^{188}Os$, Ru/Ir, Ru/Pt and higher Pd/Ir compared to SM and NM components (Figs.3.3 and 3.6). On the other hand, calculated bulk rock values show nearly CI chondritic ratios of refractory HSE, indicating that all components were formed from a reservoir with CI chondritic proportions of refractory HSE. If they formed in a closed system, earlier condensed refractory alloy phases, such as the HSE carrier phases in the NM and CAI fractions, may have slightly higher Re*/Os compared to condensates that formed later at somewhat lower temperatures (for instance M fractions, which contain most of the siderophile elements in the rock). This explanation is consistent with the variation of Ru/Pt and Pd/Ir among

the components (Figs.3.3 and 3.6). For this reason, the variation of HSE ratios in the components likely reflects the accumulation of fractionally condensed refractory metal phases in silicates and oxides of the NM fraction and CAIs. These metal phases did not equilibrate with precursor phases of the magnetite-sulfide-Fe-Ni metal assemblage.

Other explanations for the complementary variation in HSE ratios (Fig.3.3 and 3.6) in the M and SM components of Allende are possible. Changes in metal-silicate partitioning during high-temperature processing of the components or poorly constrained partitioning processes during parent body alteration (e. g., Brandon et al., 2005a and b) cannot be ruled out.

The NM fraction of Allende shows a fractionated abundance pattern of refractory HSE relative to CI chondrites (Fig.3.3). Pt/Os, Pd/Os, Pd/Ir and Ni/Ir in NM fraction are significantly lower than in CI chondrites (Table 3.1 and 3.2, Fig.3.3, 3.5 and 3.6), which is also a characteristic of most of the opaque inclusions from CAIs (Campbell et al., 2003).

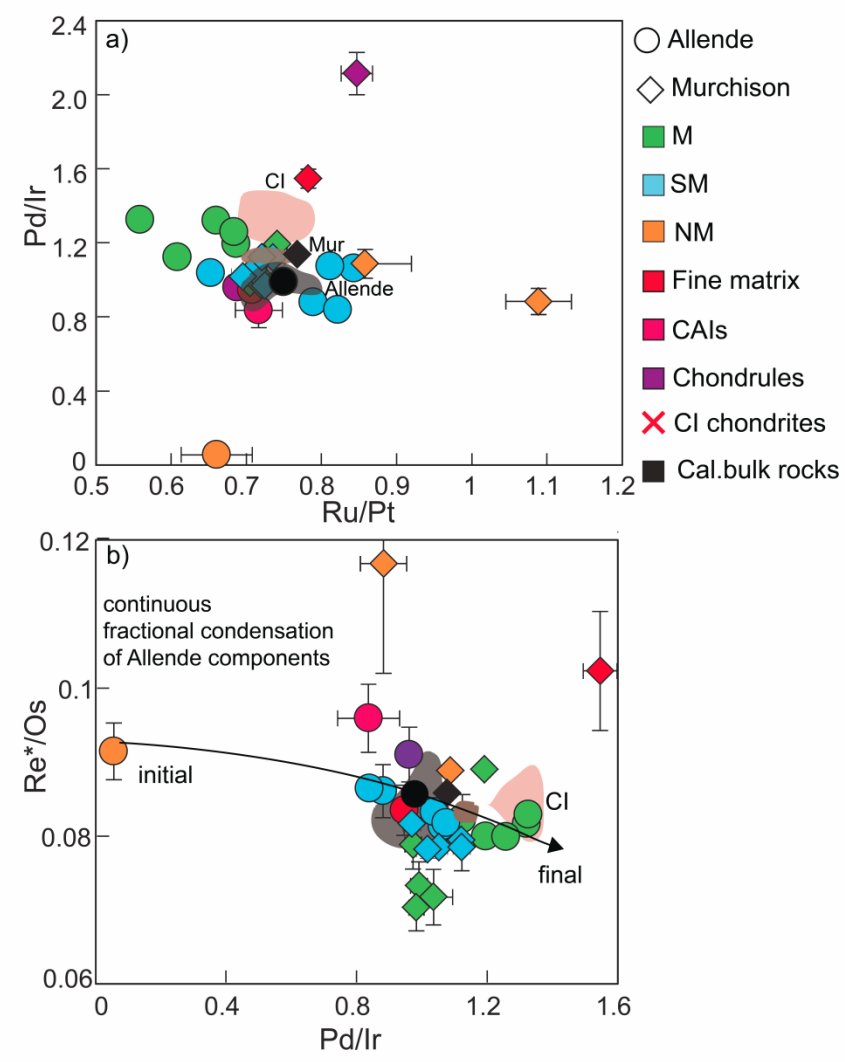

Fig.3.6. Ratios of highly siderophile elements a) Pd/Ir-Ru/Pt and b) Re*/Os-Pd/Ir of components of Allende and Murchison. Re/Os on the y-axis in b) was calculated from the measured osmium isotopic composition. Bulk rock data of Allende, Murchison and CI chondrites (Horan et al., 2003; Brandon et al., 2005a; Fischer-Gödde et al., 2010) are shown by the gray, brown and pink fields, respectively. The variation in Pd/Ir and Re/Os among the Allende components is likely the effect of continuous fractional condensation of a solar system composition in a closed system.

Because most CAIs (except CAIs with type II rare earth element patterns) are enriched in HSE and contain refractory metal nuggets (Palme and Wlotzka, 1976; Blander et al., 1980; Blum

et al., 1989; Sylvester et al., 1990; Palme et al., 1994; Becker et al., 2001; Campbell et al., 2003) and refractory metal phases also reside in the matrix of carbonaceous chondrites (Berg et al., 2009), it is unclear if these high temperature condensates in the NM fraction were derived from matrix silicates or from small CAIs.

The chondrule and the CAI fraction from Allende are depleted in Pd compared to CI chondrites and refractory HSE, likely reflecting high-temperature vapour-solid or vapour-liquid fractionation. CI chondrite normalized abundances of Fe, Ni and Co are lower compared to refractory HSE in these fractions (Figs.3.3 and 3.5). These depletions may reflect evaporation of Pd along with Fe-Ni metal during chondrule formation (Archer et al., 2014). Alternatively, CAIs and chondrule precursors were depleted in Pd, Fe and Ni due to fractional condensation.

The abundances of Re and the PGE in Allende components suggest that fractional condensation and isolation of condensed phases from remaining gas and melting and evaporation may be the primary nebular processes responsible for the HSE and Fe-Ni-Co abundance variations in components of Allende. The processes responsible for abundance variations of Au will be discussed separately in detail in 3.6.3.3.

3.6.3.2 Murchison

Compared to Allende, variations of the HSE are rather random in the components of Murchison (Figs.3.2, 3.3, 3.5 and 3.6). The HSE/Ni ratios in most Murchison components scatter around CI chondrite values (Fig.3.5). Slight differences in Ni/Co ratios in M and NM components (Fig.3.A1a) reflect metal-silicate partitioning that affected precursor material at high temperatures (Schmitt et al., 1989). Most of the M and SM components of Murchison show complementary variation in HSE (Figs.3.3b, 3.5c and 3.6), indicate the effect of redistribution or partitioning of initial CI chondrite like HSE ratios among these components. Chondrules, NM and fine grained, matrix rich fraction show significantly fractionated HSE abundance patterns (Fig.3.3). Solid metal-liquid metal partitioning at high temperatures may explain the elevated Re/Os and Pd/Ir ratio in the Murchison chondrule and matrix rich < 20 size fractions (Chabot et al., 2006). However, the significant enrichment of Rh and Cr (Fig.3.3) in chondrule fraction is inconsistent with this process.

Another observation to note here is that the ^{187}Re-^{187}Os systematics of Murchison is more disturbed than that of Allende (Fig.3.2). Some of these variations may reflect a combination of ancient and recent redistribution of Re on a small scale. Ancient aqueous alteration may also explain random variations of other HSE in the chondrule fraction, NM, some SM and the < 20μm matrix rich fraction, however, the behaviour of these elements in such processes are poorly understood (Ebihara et al., 1982, Fischer-Gödde et al., 2010) and need to be evaluated in further studies.

3.6.3.3 Origin of the non-systematic variation of Au abundances in components of Allende and Murchison

Compared to all other analysed elements calculated bulk rock Au abundances show substantial deviations from the literature bulk rock values of Murchison and Allende (Table 3.2). If these variations in different rock pieces of Allende and Murchison have a primary preaccretionary origin then similar variations should also be observed for Pd and Cr, because Cr and Pd are the closest elements to Au in terms of volatility behaviour. However Cr and Pd abundances in the calculated bulk rocks in this study are systematically lower and Au abundances are higher than most literature bulk rock values (Jarosewich et al., 1987; Fischer-Gödde et al., 2010). The large deviation of the Au abundances in the calculated bulk rocks of the present work from the literature bulk rock values (Table 3.2) is unlikely due to analytical artefacts because we have used the same techniques to obtain Au concentrations as in previous work on bulk rocks of chondrites (Fischer-Gödde et al., 2010). Correlations of Au with Pd and Ni for components of Allende (Fig.3.5b and c) are also difficult to preserve if Au is affected by analytical bias. Thus, we consider the enhancements of Au, compared to literature data to represent sample heterogeneity in different splits of bulk rocks of Allende and Murchison.

Gold correlates with Pd in Allende components (Fig.3.5c), however, such a correlation is not observed in case of Murchison. Chromium and Pd are more refractory and less mobile than Au, which is known to be susceptible to cm or even km scale transport during hydrothermal alteration (Ebihara et al., 1982). In case of Murchison it is clear that the large deviation of Au abundances from literature bulk rock values could be due to ancient hydrothermal alteration on the parent body. Gold is more enriched in the magnetite rich M fractions, which may also suggest that redistribution of Au is linked to fluid transport during the formation of magnetite-sulfide-metal assemblages. Similar processes may also be responsible for the differences of Au abundances in different bulk rocks splits of Allende (This study, Fischer-Gödde et al., 2010), although it is difficult to conceive that such random processes preserve the correlation between Pd, Ni and Au in most components (Fig.3.5b and c) of Allende. Heterogeneity in Au abundances during condensation of Fe-Ni metal may also be responsible for variations in Au abundances in different spits of bulk rocks. The nature of nebular processes, which may cause the heterogeneity in only Au abundances during condensation or the fluid induced parent body processes which would result in similar partitioning of Pd and Au are not clear.

3.6.4 Origin of chalcogen element variations

Most components of Allende and Murchison show nearly unfractionated, CI chondritic ratios of the chalcogens (Fig.3.4). The important observation to note is that despite of the extensive aqueous alteration of Murchison, the Te, Se and S systematics in the components of this meteorite are not significantly affected by these processes. Tellurium, Se and S display linear correlations with each other in most components (Fig.3.4). The nearly unfractionated, CI chondrite like ratios

of the calculated bulk rocks and of many components (Fig.3.4) indicate that the high volatility (Lodders, 2003) of these elements compared to HSE is the main cause of their depletion relative to CI chondrites. Volatility dependent processes like partial condensation or condensation followed by partial evaporation are most likely explanations for the depletion of the chalcogens compared to the HSE.

We note some minor systematic variations of Se/Te and S/Se in the components that bear on distribution processes. For instance, M components in both meteorites show systematically higher Te/Se and Se/S than CI chondrites. In contrast, NM and chondrules are either similar to CI chondrites (in case of Allende) or have low Te/Se and S/Se (Murchison, Fig.3.3 and 3.4). Other components lie on a mixing line defined by these end members (Fig.3.4). The differences in Se/Te between M and NM components (Fig.3.4) were likely caused by differences in metal-silicate partition coefficients of these elements. In sulfur bearing metal $D_{Te}^{met./silicate}$ is much higher compared to $D_{Se}^{met./silicate}$ and $D_{S}^{met./silicate}$ (Rose-Weston et al., 2009). The complementary behavior of Te and its enrichment relative to Se and S in M components may reflect metal-sulfide-silicate partitioning during the high-temperature processing of metal precursors that preceded accretion into the parent body. This explanation is supported by similar fractionation trends of Ni, Co and Fe in the components, notably higher Ni/Co in M components and lower Ni/Co in NM components, compared to CI chondrite values (Fig.3.A1).

Despite of the large variation in the abundances of refractory HSE, NM components from both meteorites have similar abundances of chalcogens (Fig.3.4). In contrast, M and SM components in Murchison have higher Se, Te and S abundances compared to the same components of Allende (Fig.3.4). The higher Te, Se and S in the bulk rock of Murchison compared to Allende are mainly caused by the difference in abundances of these elements in the M components. The higher abundances of Te, Se and S in M components of Murchison compared to those in Allende may have the following reasons:

i) Overall lower abundances of thermally processed components such as metal, CAIs and chondrules in Murchison compared to Allende, resulting in a higher proportion of volatile rich dust rims and matrix (Krot et al., 2003).

ii) Higher losses of S, Se and Te during metamorphic processes in Allende. The temperature experienced by the Allende meteorite during metamorphism is ~550-600°C (Huss and Lewis, 1994). Heating experiments on a homogenized Allende sample powder show almost no evaporative loss of Te and Se below 600 °C (Ikramuddin and Lipschutz, 1975; Ngo and Lipschutz, 1980). These results and the correlations of S, Se and Te in the components observed in this study suggest the metamorphic loss is a less likely cause for chalcogen depletion in Allende compared to Murchison.

iii) If the variation in Se/Te in the components of Murchison is due to metal-silicate partitioning and the conditions of partitioning process were similar for both meteorites then the enrichment of chalcogens in the M fraction of Murchison most likely occurred after the

partitioning process. In that case, chalcogens were added during the alteration stage of the metal in the M fraction of the Murchison as gases or the condensed gases in water ice grains (Lauretta et al, 1998; Palmer and Lauretta, 2011), or with the fine grained rim material which was accreted around coarse grained objects (Metzler et al., 1992).

We conclude that the calculated bulk rock abundances of chalcogens show nearly CI chondritic Se/Te, which suggests that all components contain material formed from a nebular reservoir with nearly CI chondritic ratios of these elements. The data on Murchison components suggest that the last thermal processing event prior to accretion, presumably chondrule formation, induced slight variations in chalcogen element ratios in components due to the slight differences in metal-silicate partition coefficients of these elements. Compared to Allende, a larger fraction of chalcogen elements were added before or during the accretion stage of Murchison components.

3.6.5 Main processes responsible for the element distribution in the components

The variation in Re*/Os, Pd/Ir, Ir/Ni and Au/Ni (Figs.3.5 and 3.6) clearly shows that at least two different carriers of refractory HSE are present in the components. The HSE carriers in NM fractions show Ir/Ni >> Ir/Ni_{CI} and Pd/Ir << Pd/Ir_{CI} (Fig.3.5a and 3.6b) which are the characteristics of high temperature fractional condensates (Campbell et al., 2003). The depletion of Pd relative to refractory HSE in most of the components and in the bulk rocks of Allende and Murchison reflects the presence of Pd depleted high temperature condensates (Fig.3.6). Another HSE carrier in both Allende and Murchison has Ir/Ni and Pd/Ir that scatter around CI chondrite values (Fig.3.5). This carrier mostly resides in the M components. The latter is comprised of an oxidized assemblage that may have formed by aqueous alteration of previous metal-sulfide-silicate assemblages. The latter formed by high-temperature condensation processes. Complementary Pd/Ir in different components of Allende may reflect continuous fractional condensation from the same reservoir at different temperatures. The scatter of HSE ratios around CI chondritic values in Murchison may have been caused by minor redistribution during the later oxidization of the metal phase. Despite of the variations in components, CI chondritic ratios of refractory HSE in the calculated bulk rocks strengthen the argument of the complementarity between different components (Bland et al., 2005; Hezel and Palme, 2008) and the precursors of the components were formed from the homogeneous reservoir having CI chondritic HSE ratios.

The chalcogens are depleted and decoupled from the HSE and the major elements (Figs.3.1c, 3.A2 and 3.A4) indicating that the late condensation or recondensation after evaporation of these elements occurred onto refractory siderophile and lithophile precursors before accretion of the components. Notably, the chalcogens were not significantly redistributed and fractionated among the components by aqueous alteration processes, in stark contrast to Au. The CAI fraction shows enrichment in Ca, Mg, Mn and depletion in HSE and chalcogens, mainly due to the sampling of lithophile phases (CAIs are mainly composed of high temperature silicates and oxides) and differences in volatility respectively. The depletion of chalcogens compared to HSE and

complementary Se/Te in some components indicate that volatility and metal-silicate partitioning are the most important processes for chalcogen fractionations in the components of Murchison and Allende.

3.7 Conclusions

Chemical complementarity exists in the HSE, chalcogen and major elements in different components of Allende and Murchison indicating that the components of each meteorite were derived from the same nebular reservoir. The element concentration systematics and CI chondritic Ni/Co in most components indicate that the precursors of these meteorites preserved their initial condensation characteristics for many elements. Lower Pd/Ir than in CI chondrites in most components and in the rocks indicate that the precursors of HSE carriers in both meteorites were formed by incomplete condensation or evaporation.

Abundance variations of Au and to some extent Re in components of Allende were affected by later oxidation processes. With the notable exception of geochemically similar groups of elements (e. g., the chalcogens, Ni, Co), many elements in Murchison are randomly distributed and most likely were redistributed by ancient aqueous alteration on the parent body. A disturbance in ^{187}Re-^{187}Os systematics is clear in samples with small sample weight and low HSE abundances. Surprisingly, these processes had almost no influence on the chalcogen element systematics of the components and bulk rocks, as no significant fractionation or S loss can be observed compared to Se and Te.

Due to their higher volatility, the chalcogens are depleted compared to HSE and elements such as Fe, Ni or Co; yet maintain ratios similar to CI chondrites in many components. Chalcogen depletion relative to CI chondrites might have occurred either during melting and evaporation during chondrule formation or from precursor gas due to incomplete condensation of volatiles, or may reflect both processes. Because the abundances of Te, Se and S are inversely proportional to the volume percent of refractory components (CAIs and chondrules) in these meteorites (Krot et al., 2003), the first explanation is more likely the cause.

Acknowledgements: We are grateful to The Field Museum, Chicago for providing Allende (No. ME. 2632, Spec. No. 17) and Murchison (No. ME. 2684, Spec. No. 23) sample chips and to the Natural History Museum in Washington D.C. for an aliquot of the Smithsonian Allende standard powder. We thank K. Hammerschmidt for technical help in the TIMS lab, M. Feth and S. Kommescher for support in clean lab. This work was funded by DFG-SPP 1385 “The first ten million years of solar system – a planetary materials approach” (BE1820/10-1/2).

3.8 Tables Chapter 3

Table 3.1. Concentrations of major and minor elements in the analyzed components of Allende and Murchison.

Component	Mg (%)	Ca (%)	Cr (%)	Mn (%)	Fe (%)	Co (%)	Ni (%)
Allende							
All < 20	15.2	1.4	0.375	0.154	25.8	0.070	1.38
All-M 20-80	14.2	1.0	0.351	0.150	24.6	0.066	1.30
All-M 80-150	8.6	0.5	0.225	0.091	16.0	0.044	0.89
All-M 150-200	8.3	0.8	0.237	0.098	16.2	0.045	0.90
All-M 200-250	7.8	0.4	0.214	0.090	16.1	0.045	0.93
All-M > 250	15.8	1.5	0.441	0.158	26.9	0.088	1.85
All-SM < 80	8.5	0.5	0.230	0.090	16.1	0.047	0.97
All-SM 80-150	7.8	0.4	0.177	0.075	13.4	0.034	0.67
All-SM 150-200	8.6	0.4	0.208	0.088	15.5	0.040	0.79
All-SM 200-250	17.1	1.6	0.429	0.174	27.9	0.069	1.36
All-SM > 250	15.9	1.6	0.316	0.141	21.6	0.061	1.21
All-CAIs	10.3	6.2	0.07	0.10	8.5	0.014	0.27
All-Chondrules	11.8	0.6	0.171	0.047	6.9	0.022	0.44
All-NM	27.7	3.2	0.092	0.107	8.9	0.016	0.25
All-cal bulk	13.2	1.1	0.280	0.117	18.8	0.049	0.98
All-bulk [a]	14.8	1.8	0.35	0.14	22.3	0.070	1.4
Murchison							
Mur < 20	4.2	n.d	0.09	0.044	3.7	0.011	0.22
Mur-M 20-80	14.9	0.9	0.333	0.204	24.6	0.075	1.42
Mur-M 80-150	11.5	1.0	0.342	0.197	27.3	0.079	1.51
Mur-M 150-200	11.6	1.0	0.220	0.207	26.6	0.077	1.54
Mur-M 200-250	13.0	0.8	0.36	0.232	27.5	0.083	1.63
Mur-M > 250	13.0	1.0	0.282	0.211	26.5	0.076	1.47
Mur-SM < 80	15.8	1.0	0.30	0.208	24.8	0.065	1.26
Mur-SM 80-150	10.4	0.8	0.342	0.197	25.1	0.063	1.25
Mur-SM 150-200	10.4	0.4	0.300	0.182	24.9	0.063	1.27
Mur-SM 200-250	10.9	1.0	0.20	0.196	19.2	0.069	1.39
Mur-SM > 250	13.4	0.9	0.341	0.225	28.9	0.076	1.51
Mur-Chondrules	23.5	1.2	0.41	0.181	12.2	0.026	0.42
Mur-NM << 80	30.7	2.0	0.339	0.191	13.8	0.018	0.25
Mur-NM	9.7	0.6	0.190	0.096	10.5	0.024	0.45
Mur-cal bulk	13.3	0.9	0.31	0.203	25.3	0.067	1.31
Mur-bulk [a]	11.7	1.3	0.301	0.16	21.3	0.061	1.37
CI chondrites [b]	9.6	0.91	0.259	0.191	18.2	0.050	1.06

Concentrations are given in w/w %.

[a] Bulk rock data of Allende and Murchison from Jarosewich et al. (1971, 1987), McCarthy and Ahrens (1972), Fuchs et al. (1973), Fitzgerald (1979a), Fulton and Rhodes (1984), Johnson et al. (1990), Jarosewich (1990), Dreibus et al. (1995).

[b] CI chondrite data from Lodders (2003).

Table 3.2. HSE and chalcogen element abundances and Re-Os isotopic data of components of Allende and Murchison

Component	Weight (mg)	Re (ng/g)	Os (ng/g)	Ir (ng/g)	Ru (ng/g)	Pt (ng/g)	Rh (ng/g)	Pd (ng/g)	Au (ng/g)	Te (µg/g)	Se (µg/g)	S (mg/g)	$^{187}Os/^{188}Os$	$^{187}Re/^{188}Os$	Δ_{Os}[a]
Allende															
All < 20	5.3	59.8	764	801	1095	1548	211	757	240	1.06	8.74	19.6	0.1263 ± 0.0006	0.403 ± 0.003	-7
All-M 20-80	19.0	66.0	830	834	1114	1831	233	938	339	1.26	9.40	22.2	0.1259 ± 0.0006	0.388 ± 0.001	1
All-M 80-150	50.0	58.5	729	687	997	1451	235	821	283	1.12	8.85	20.6	0.12499 ± 0.00008	0.387 ± 0.001	-7
All-M 150-200	13.7	59.0	758	735	1049	1588	260	971	286	1.35	8.93	20.3	0.1256 ± 0.0002	0.377 ± 0.003	6
All-M 200-250	27.8	62.9	818	778	1078	1576	232	979	347	1.20	9.39	20.1	0.1250 ± 0.0001	0.376 ± 0.001	1
All-M > 250	18.2	77.4	1031	963	1206	2158	280	1278	489	1.27	10.3	24.2	0.12610 ± 0.00006	0.362 ± 0.001	23
All-SM 20-80	23.3	53.1	665	619	1031	1222	193	657	212	1.08	8.80	21.2	0.1255 ± 0.0002	0.395 ± 0.001	-9
All-SM 80-150	61.9	48.7	591	561	948	1451	211	582	207	0.98	8.01	19.1	0.12622 ± 0.00008	0.404 ± 0.001	-9
All-SM 150-200	22.0	54.9	676	587	940	1158	179	631	253	1.13	8.37	19.8	0.1257 ± 0.0006	0.400 ± 0.002	-11
All-SM 200-250	18.3	56.6	671	599	994	1260	194	528	205	0.91	7.94	19.1	0.1273 ± 0.0006	0.406 ± 0.002	0
All-SM > 250	15.1	53.0	634	582	987	1201	199	489	193	0.95	8.61	22.9	0.12742 ± 0.00009	0.402 ± 0.003	4
All-CAIs	3.4	21.6	280	245	344	480	67	205	79	0.25	1.70	3.5	0.1310 ± 0.0008	0.388 ± 0.023	51
All-Chondrules	29.0	37.3	437	411	651	946	135	395	144	0.51	4.35	11.5	0.1291 ± 0.0006	0.420 ± 0.002	8
All-NM	11.3	76.9	873	903	998	1510	150	50	34	0.11	1.54	3.9	0.1293 ± 0.0006	0.424 ± 0.003	6
All-cal bulk	600	56.4	687	644	970	1364	201	622	226	0.93	7.63	18.2	0.1267 ± 0.0004	0.400 ± 0.002	-0.3
All-bulk[b]		60.5	729	684	1007	1357	174	674	139	0.96	9.08	20.3	0.12595	0.3926	-2.5
Murchison															
Mur < 20	4.1	40.1	461	441	683	873	163	681	124	1.06	9.83	16.5	0.1334 ± 0.0013	0.427 ± 0.015	44
Mur-M 20-80	18.1	52.0	643	585	892	1203	186	697	236	1.44	13.0	28.2	0.12838 ± 0.00008	0.390 ± 0.002	24
Mur-M 80-150	15.0	54.8	755	686	976	1379	185	680	370	1.82	14.6	33.5	0.1225 ± 0.0006	0.350 ± 0.002	-3
Mur-M 150-200	16.6	50.4	709	641	907	1285	189	630	412	1.87	14.4	32.4	0.1214 ± 0.0006	0.343 ± 0.002	-9
Mur-M 200-250	2.3	47.7	670	588	883	1243	198	609	256	1.63	13.7	31.3	0.1219 ± 0.0007	0.343 ± 0.018	-4
Mur-M > 250	19.8	50.1	706	662	944	1311	205	644	395	1.58	12.9	30.1	0.1246 ± 0.0006	0.342 ± 0.002	24
Mur-SM 20-80	5.6	37.5	530	467	725	986	164	524	176	1.45	11.4	24.5	0.1248 ± 0.0002	0.341 ± 0.009	26
Mur-SM 80-150	24.1	52.2	680	598	832	1148	179	580	292	1.61	13.8	29.9	0.12564 ± 0.00006	0.370 ± 0.002	12
Mur-SM 150-200	24.8	46.0	627	547	825	1161	175	575	280	1.52	13.9	30.6	0.12445 ± 0.00007	0.353 ± 0.002	13
Mur-SM 200-250	5.1	46.7	628	562	850	1222	214	572	324	1.55	14.1	30.7	0.1243 ± 0.0002	0.358 ± 0.009	9
Mur-SM > 250	17.0	48.2	625	552	822	1140	170	619	208	1.50	13.5	29.3	0.1245 ± 0.0006	0.372 ± 0.003	-1
Mur-Chondrules	2.2	34.4	271	351	568	670	281	741	67	0.06	4.11	7.6	0.1648 ± 0.0014	0.611 ± 0.047	214
Mur-NM << 80	41.8	34.6	429	398	655	764	129	432	152	1.06	8.72	17.7	0.1283 ± 0.0006	0.388 ± 0.002	24
Mur-NM	5.5	18.5	215	229	398	366	85	202	32	0.08	2.27	3.8	0.1388 ± 0.0021	0.414 ± 0.024	109
Mur-cal bulk	650	46.8	613	554	820	1118	174	592	251	1.44	12.5	27.6	0.127 ± 0.004	0.373 ± 0.004	16
CI chondrites[c]		36.6	450	418	627	871	130	567	149	2.31	21.3	54.1	0.12641	0.40073	-4.35

Reported uncertainties are 2σ. Deviation of the Os isotopic composition (ΔOs) from the IIIA iron meteorite isochron is calculated by the following relation.

[a] $\Delta Os = (^{187}Os/^{188}Os_{chondrite} - (0.09524+0.07887 \times {}^{187}Re/^{188}Os_{chondrite})) \times 10^4$, 0.09524 is the solar system $^{187}Os/^{188}Os$ at 4.558 Ga and 0.07887 is the slope of the IIIA iron meteorite isochron (Smoliar et al., 1996).

[b] Bulk rock values are from Paul and Lipschutz (1990), Jarosewich (1990), Burgess et al. (1991), Dreibus et al. (1995), Friedrich et al. (2002), Walker et al. (2002b), Fischer-Gödde et al. (2010).

[c] CI chondrite data from Dreibus et al. (1995), Walker et al. (2002b), Lodders (2003), Fischer-Gödde et al. (2010) and Wang et al. (2013).

3.9 Appendix Chapter 3

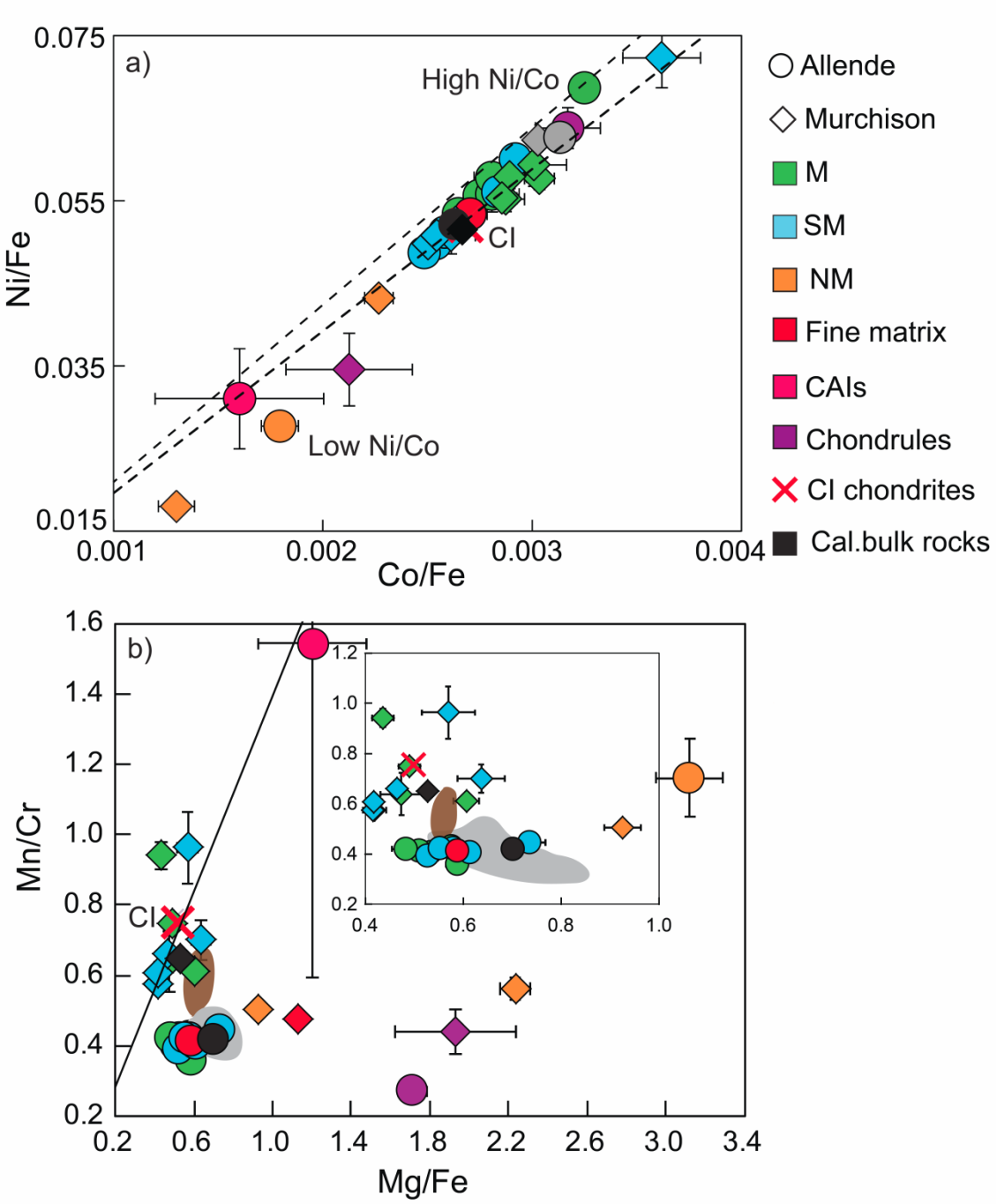

Fig.3.A1. a) Ni/Fe-Co/Fe and b) Mn/Cr-Mg/Fe variation among the components of Allende and Murchison. Variation of the ratios in CI chondrites is shown by dashed lines in a). Bulk rock Allende and Murchison data shown by gray and brown fields respectively (b). Bulk rock data calculated from the mass balance of all components analyzed in this study is shown by black symbols. Mn/Cr-Mg/Fe variation of magnetic and slightly magnetic components is shown in the enlarged image.

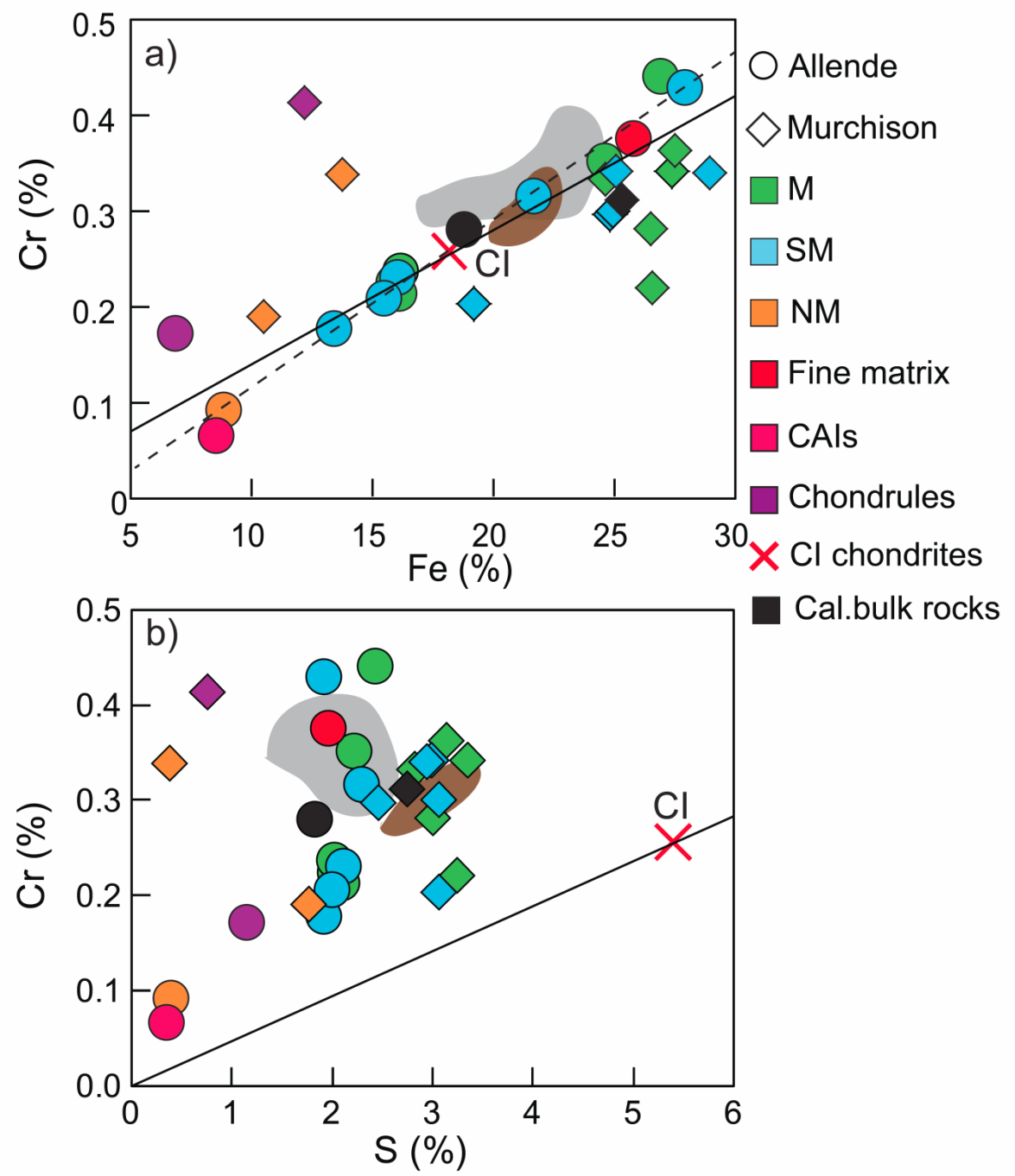

Fig.3.A2. a) Cr-Fe and b) Cr-S variation of the components of Allende and Murchison. Dashed line indicates linear trend for magnetic and slightly magnetic components of Allende which reflects mixing between CI chondrite like material (CAIs and NM fraction) and a fractionated volatile element depleted component.

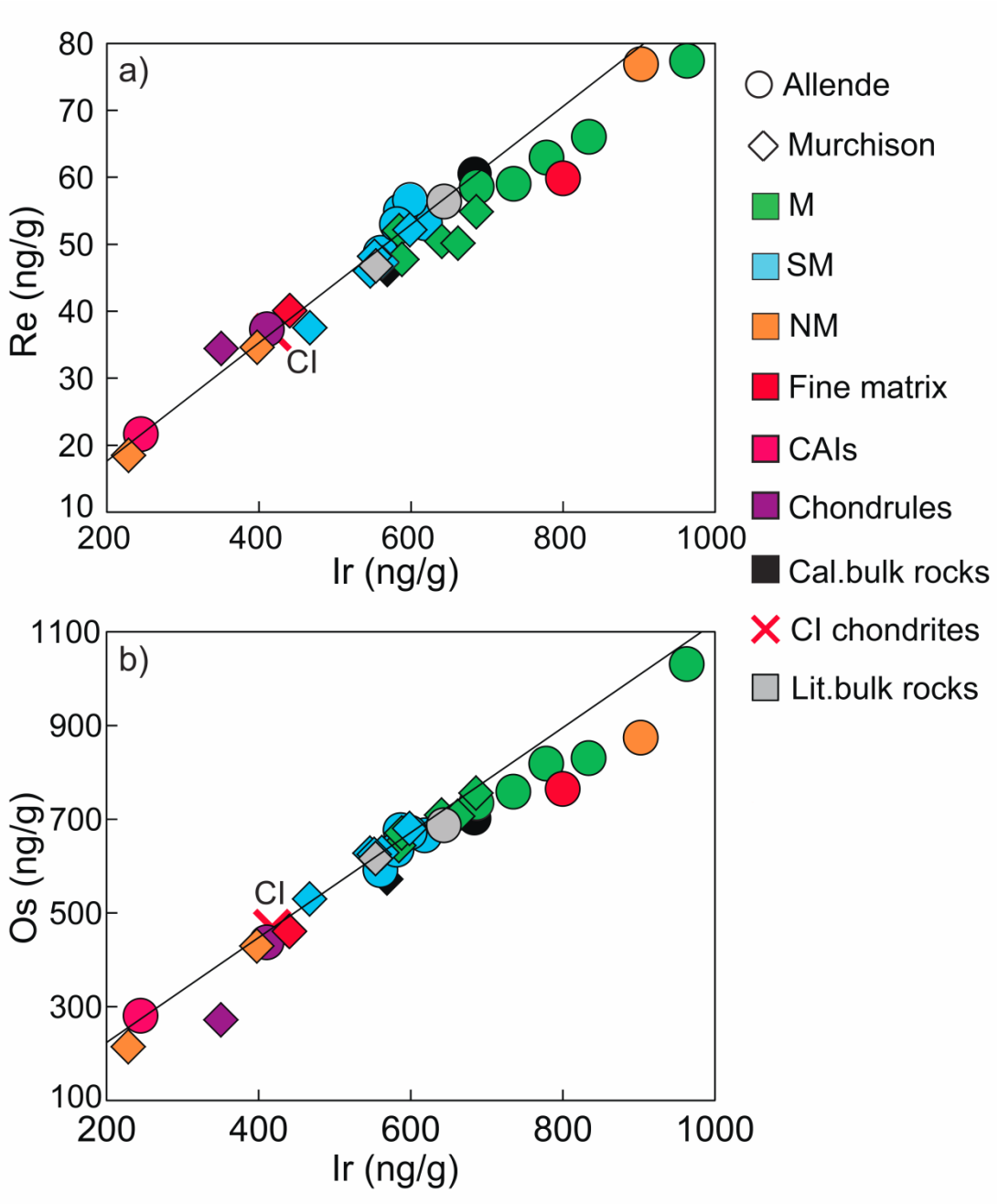

Fig.3.A3. a) Re-Ir and b) Os-Ir variation among the components of Allende and Murchison. Allende magnetic components show lower Re/Ir and Os/Ir than CI chondrite values. Murchison magnetic components show lower Re/Ir but CI chondritic Os/Ir, indicate that Re and Os are decoupled in the components of Murchison.

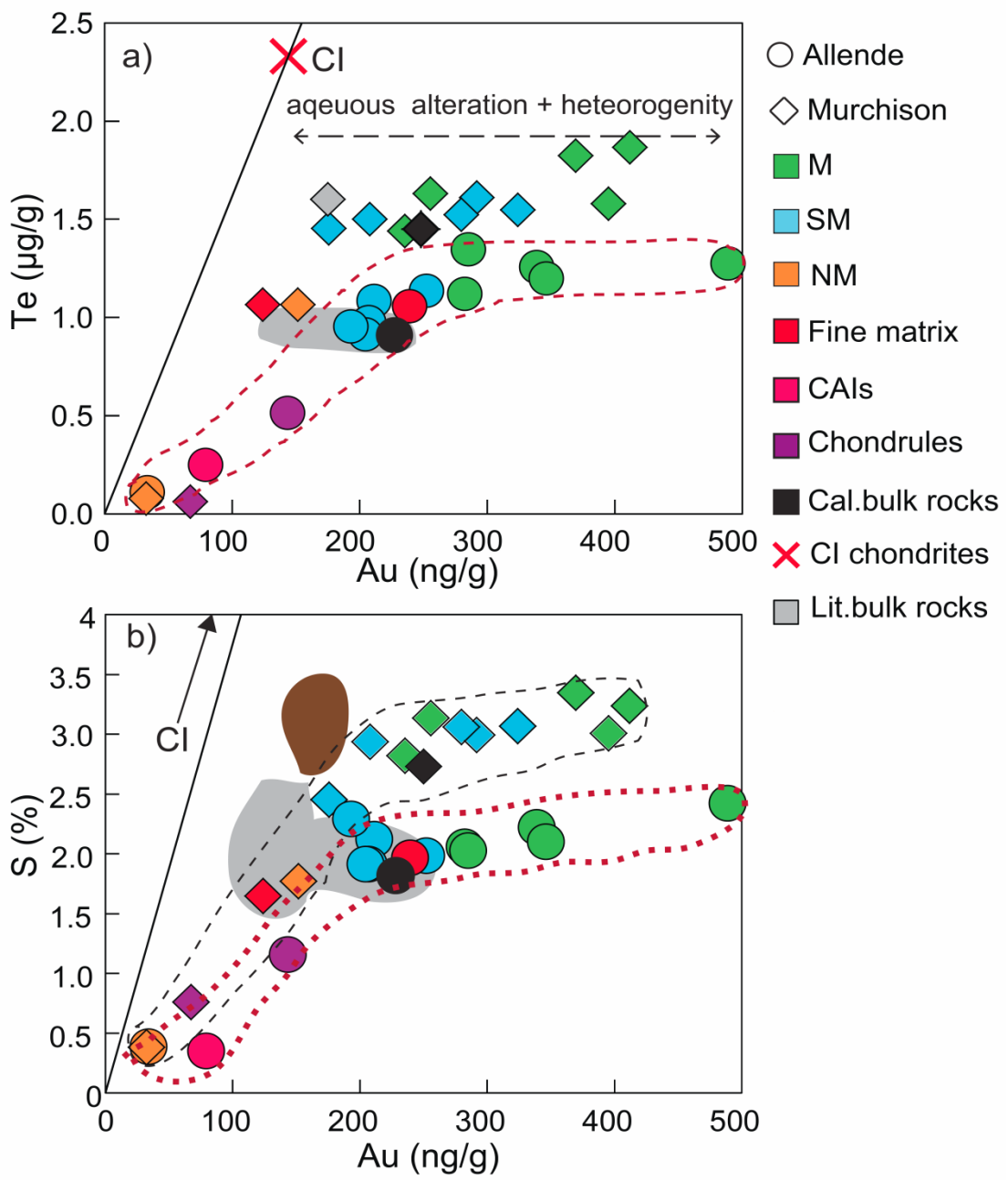

Fig.3.A4. a) Te-Au and b) S-Au variation in components of Allende and Murchison. Figures show the decoupling of Au from chalcogens mainly in magnetite rich (magnetic) aliquots.

Chapter 4

^{187}Re-^{187}Os systematics, highly siderophile and chalcogen element abundances in the components of unequilibrated L chondrites

4.1 Abstract

The ^{187}Re-^{187}Os systematics, abundances of highly siderophile elements (HSE: Re, platinum group elements and Au), chalcogens (Te, Se and S) and major and minor elements were determined in separated components of two unequilibrated L chondrites QUE 97008 (L3.05) and Ceniceros (L3.4). The ^{187}Re-^{187}Os systematics is disturbed in the components of both meteorites, most likely due to open system behaviour of Re during terrestrial weathering of QUE 97008 and alteration on the L chondrite parent body as indicated by an internal errorchron of components of Ceniceros. The HSE abundance patterns suggest that the bulk rock abundances are mainly controlled by two different end members. Nonmagnetic fractions display lower Re/Os and HSE/Ir than CI chondrites. Chondrules, metal-troilite spherules and fine magnetic fractions are depleted in refractory HSE and show higher Rh/Ir, Pd/Ir and Au/Ir than in CI chondrites. Most other components, however, lie in-between with HSE ratios close to CI chondrite values. The different HSE compositions indicate the presence of unequilibrated alloys and loss of refractory HSE rich carrier phase/s from the precursors of some L chondrite components. Gold is decoupled from other HSE in magnetic fractions and shows chalcophile affinities with a similar grain size dependent variation like S and Se, likely inherited from preaccretionary processes. Tellurium is depleted in all components compared to all other analysed elements, most likely was controlled by fractional condensation and different geochemical affinities. The volatility dependent depletion of Te requires different physical and chemical conditions than typical for the canonical condensation sequence as represented by carbonaceous chondrites. Tellurium also shows variable geochemical behaviour, siderophile in Ceniceros, predominantly chalcophile in QUE 97008. These differences may have been inherited from element partitioning during chondrule formation. Selenium and S on the other hand are almost unfractionated from each other and only show complementary S/Se in a few components, presumably due to the effects of volatility or metal-silicate partitioning during chondrule formation. Terrestrial weathering had negligible effects on the chalcogen element systematics.

4.2 Introduction

The unequilibrated ordinary chondrites (UOC) are some of the most primitive rocks in the solar system (Nagahara, 1984; Alexander et al., 1990). They are composed of components such as different sized chondrules, matrix, Fe-Ni metal and, more rarely, refractory inclusions (Scott and Krot, 2003). These components were formed in different chemical and physical environment in the solar nebula (Larimer and Anders, 1967, 1970; Huss et al., 2001). The components shows a diversity in elemental and isotopic compositions suggesting that they have underwent fractionation processes in the early solar system (Wasson, 1972; Gooding and Keil, 1980; McNaughton et al., 1981; King and King, 1981; McKinley et al., 1981; Scott et al., 1981; Hinton and Bischoff, 1984; Rambaldi and Wasson, 1984; Robert et al., 1987; Rosman and Laeter, 1988; Brearley et al., 1989; Alexander et al., 1990; Clayton et al., 1991; Fisenko et al., 1992; Brearley, 1993; Russell et al., 1997; McKeegan et al., 1998; Huss et al., 2001).

Osmium isotopic composition, highly siderophile (HSE: Re, Os, Ir, Ru, Pt, Rh, Pd and Au) and chalcogen (Te, Se and S) element abundances in the chondritic components are useful proxies to constrain the elemental fractionation processes under different physical and chemical conditions in the solar nebula, on the meteorite parent body or by terrestrial weathering (Walker et al., 2002b; Horan et al, 2003; Fischer-Gödde et al., 2010; Dreibus et al., 1995). These elements cover a wide range of condensation temperatures overlapping with major component elements and many refractory and volatile lithophile elements (Grossman, 1972; Lodders, 2003).

Previous studies of bulk chondrites show that all three ordinary chondrite groups have distinct abundance patterns of HSE and chalcogens (Case et al., 1973; Binz et al., 1976; Chen et al., 1998; Horan et al., 2003, Fischer-Gödde et al., 2010). Some previous studies on the separated components of ordinary chondrites (Chou et al., 1973; Rambaldi, 1976, 1977; Rambaldi et al., 1978; Grossman and Wasson, 1985; Kong and Ebihara, 1997; Humayun and Campbell, 2002; Horan et al., 2009) show that the differences in HSE ratios of the bulk rocks are caused by different compositions of the HSE carriers in the magnetic components of ordinary chondrites. The magnetic fractions are mainly comprised of kamacite, taenite and fine-grained plessitic inclusions, which formed due to the exsolution of Fe-Ni metal during cooling. Two different carriers with very different HSE patterns were observed in the nonmagnetic and magnetic fractions of the H chondrites Dhajala and Ochansk (Horan et al., 2009). Horan et al. (2009) proposed that these phases were formed separately in the solar nebula at different conditions and never equilibrated with each other.

Rambaldi et al. (1979) have shown that the H chondrites did not lose any refractory metal component before accretion, consistent with their CI chondrite like Fe/Mg (Wasson and Kallemeyn, 1988). In contrast, L and LL chondrites have lost a metal component, presumably in the solar nebula, because ratios of Fe and refractory siderophile elements relative to Mg are lower

than in CI chondrites (Rambaldi et al., 1979; Wasson and Kallemeyn, 1988). The content of metal and siderophile elements in these three groups shows a continuous range (metal content H > L > LL), therefore these groups may have been affected by common processes of metal loss. Different HSE carriers as observed in H chondrites may also occur in other types of ordinary chondrites. L chondrites are intermediate oxidized (Weisberg et al., 2006) and are important candidates to shed light on timing and the processes responsible for the origin of different HSE carrier phases in ordinary chondrites and to constrain HSE fractionation processes during the metal loss from metal poor ordinary chondrites (Rambaldi, 1976, 1977; Rambaldi et al., 1978; Kong and Ebihara, 1997).

Another important common feature of ordinary chondrites is the depletion of Te relative to Se and S (Larimer and Anders, 1967; Case et al., 1973; Wai and Wasson, 1977), the origin of which is highly controversial. Tellurium is less volatile compared to Se and S during condensation in the solar nebula (Lodders, 2003). Wai and Wasson (1977) explained the depletion of Te on the basis of different nebular conditions in the ordinary chondrite formation region compared to canonical solar nebula conditions. Heating experiments show that more Te than Se may be lost by diffusion-controlled processes during open-system heating of homogenized powder of ordinary chondrite (Ikramuddin et al., 1977a, b). However, the loss of Te relative to Se and S in ordinary chondrites is not showing any straightforward relationship with metamorphic grades (Ikramuddin et al., 1977a, b; Takahashi et al., 1978). The effect of terrestrial weathering on Te in chondrite finds is uncertain, because it has not been studied in a systematic way. Thus a combined study of the HSE and chalcogens in the components of L chondrite can be useful to understand how high and low temperature elemental fractionation processes have affected the composition of siderophile elements in the bulk rocks of L chondrites.

In this study we analyzed two unequilibrated L chondrites, QUE 97008 and Ceniceros. QUE 97008 is a meteorite find that has undergone minor weathering (weathering grade A and type L3.4, Grossman, 1999). It was classified into type L3.05 based on induced thermoluminescence (ITL) data (Benoit et al., 2002). Ceniceros on the other hand is a meteorite fall. It was initially classified as H3 (Graham, 1990), but reclassified later to type L3.7 (Rochette et al., 2003), based on magnetic susceptibility, detailed petrographic examination and abundances of HSE (Horan et al., 2003).

Here we present a study of the ^{187}Re-^{187}Os systematics, HSE and chalcogen element abundances and their mass balance in the components of QUE 97008 and Ceniceros. We have also analyzed the major and minor elements Mg, Ca, Cr, Mn, Fe, Ni and Co in the same aliquots to identify the mineralogy of separates and major HSE carrier phases present in the components. The main objectives of the study are to identify and constrain the timing and conditions of the siderophile element fractionation processes in the context of nebular, parent body or terrestrial alteration processes in case of unequilibrated ordinary chondrites.

4.3 Samples and their preparation

Approximately one gram piece of QUE 97008 (provided by Smithsonian National Museum of Natural History) and Ceniceros (off BM.1990, M6, provided by The Natural History Museum, London) were broken into fragments. Separation of chondrite components such as CAIs, chondrules, metal sulfide nodules and clasts were carried out on broken fragments by naked eye and under the optical microscope (Kruss optronic MSZ 5600) using plastic tweezers. The separation procedure was discussed in detail by Kadlag and Becker a, (submitted). Because of their rare occurrence in ordinary chondrites (Scott and Krot, 2003), CAIs were not observed in the rock pieces.

In case of QUE 97008, spherical objects were separated into two different samples, coarse silicate rich chondrules (C), having diameter >1.5 mm, and metal-troilite spherules (MTS), having diameters < 0.5 mm. A sulfide clast (SC), about 3 x 0.8 x 1 mm was found in Ceniceros, half of it was digested for this study.

The remaining material was separated into five different size fractions in case of QUE-97008: less than 80 µm (<80), 80-150 µm (80-150), 150-200 µm (150-200), 200-250 µm (200-250) and greater than 250 µm (>250). In case of Ceniceros remaining material was separated into three grain size fractions: less than 50 µm (<50), 50-200 µm (50-200) and greater than 200 µm (>200). All size fractions were further divided into magnetic (M), slightly magnetic (SM) and nonmagnetic (NM) components using a hand magnet. The slightly magnetic 80-150 fraction of QUE 97008 was divided into three fractions, a matrix rich fraction (QUE-SM 80-150_MTX) a fraction rich in chondrule fragments (QUE-SM 80-150_CHD) and a mixture of chondrule and matrix material (QUE-SM 80-150_MIX).

A small fragment of QUE 97008 was embedded in epoxy resin and polished for petrographic inspection. Because of the very unequilibrated nature and substantial heterogeneity of the distribution and textural position of troilite and metal, key petrographic details of this section are given in Fig.4.1. Chondrules of variable size (0.3 mm-2.5 mm) are present in the bulk rock section. Most chondrules have sulfide rims (similar to chondrules in some EH3 chondrites, Kadlag and Becker a, submitted). Metal grains of sizes ranging from < 1µm to 200 µm are dispersed in the matrix and more rarely occur as small grains in chondrules. Troilite is also present in the matrix and as a rim around some metal grains in matrix and as inclusions in chondrules. Silicates in chondrules and in matrix are mostly comprised of olivine and pyroxenes. Some chondrules contain a concentric zone of exsolved metal spheres near their rim, but no troilite inside the chondrule (Fig.4.1b, d). The absence of troilite in the chondrule and in its metal inclusions indicate that either all of S was evaporated during chondrule melting or it was not yet condensed during the crystallization of minerals in this chondrule (Fig.4.1b, d and e).

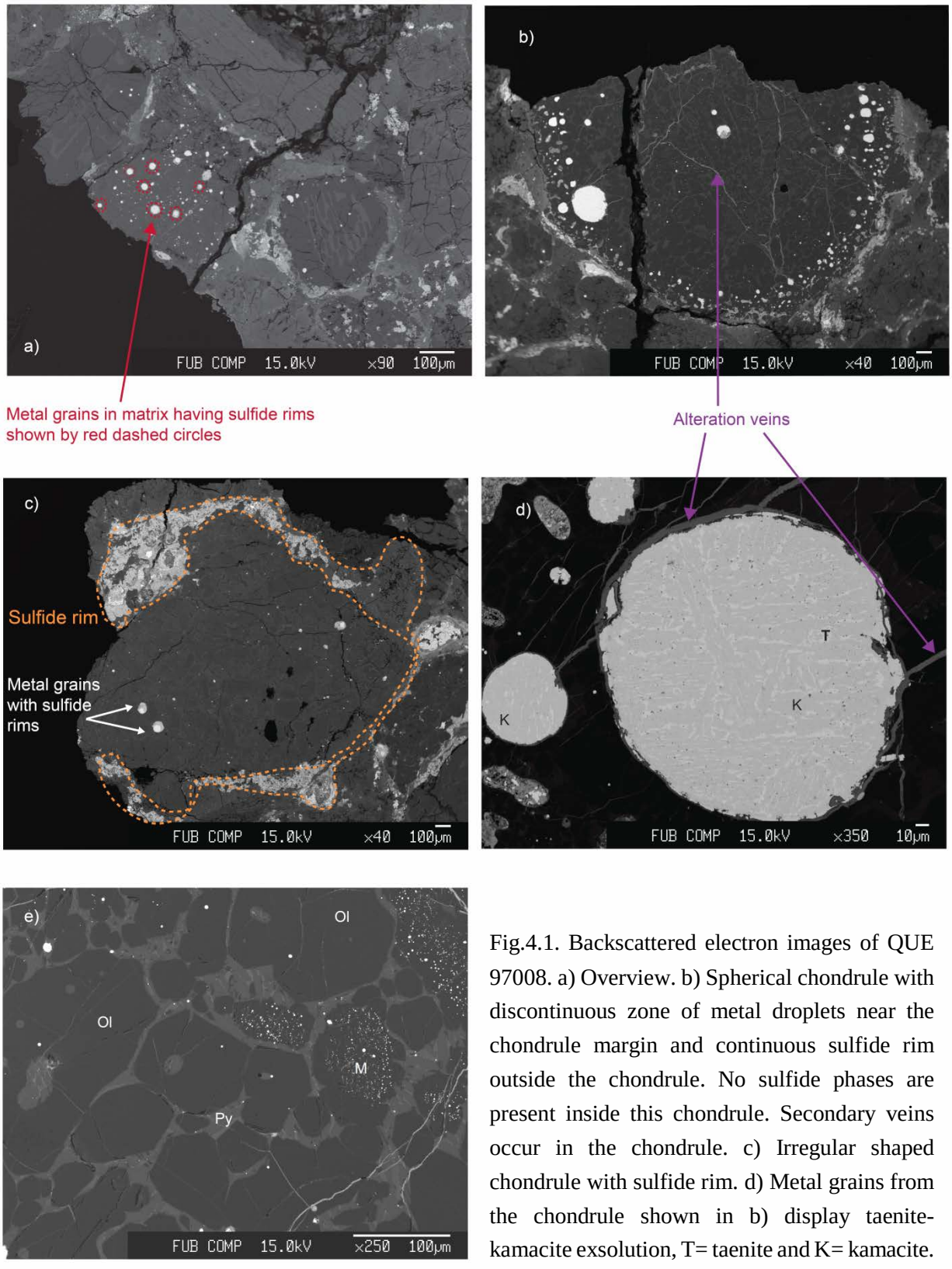

Fig.4.1. Backscattered electron images of QUE 97008. a) Overview. b) Spherical chondrule with discontinuous zone of metal droplets near the chondrule margin and continuous sulfide rim outside the chondrule. No sulfide phases are present inside this chondrule. Secondary veins occur in the chondrule. c) Irregular shaped chondrule with sulfide rim. d) Metal grains from the chondrule shown in b) display taenite-kamacite exsolution, T= taenite and K= kamacite. The taenite grains are smaller compared to kamacite, and may represent the Ni rich metal in the smallest size fractions. e) Enlarged image of a part of the chondrule from b), Ol = olivine, Py = pyroxene and M = metal. Pyroxene rims around sub- to euhedral olivine likely were formed from the interaction of olivine with remaining silicate melt and gas.

Some olivine crystals in the core of the chondrule contain abundant small (<1 µm) metal grains (Fig.4.1e). Such grains do not occur in all olivines and are very rare in pyroxenes surrounding olivines. Other chondrules contain metal inclusions which are rimmed by troilite (Fig.4.1c). The differences between the chondrules indicate variable degrees of oxidation or sulfur fugacity during the formation of different chondrules. These preserved differences between chondrules indicate the highly unequilibrated nature of this meteorite. The fine-grained nature and inhomogeneous distribution of sulfide rims around metal grains and chondrules indicate that most of these sulfide rims may represent a late product of the chondrule formation processes rather than of metamorphic origin. Sulfide rims around metal grains included in chondrules, may reflect coeval melting of silicates, metal and sulfides during chondrule formation and subsequent exsolution of troilite from metal during cooling. Oxidized rims and fractures around some metal grains in chondrules (Fig.4.1b, d) likely formed during late secondary process, such as terrestrial weathering.

4.4 Analytical Techniques

Separated samples were digested in reverse aqua regia in an Anton Paar^{TM} High Pressure Asher System (HPA-S). The isotope dilution method was used to obtain precise concentration and isotopic data of the HSE and chalcogens. Abundances of the monoisotopic elements Rh and Au were calculated by internal calibration relative to Ru and Ir, respectively. Procedures of sample digestion, chemical separation of the HSE and chalcogen elements and measurement protocols were described in detail by Fischer-Gödde et.al. (2010); Wang et al. (2013) and Kadlag and Becker a (submitted) and references therein.

For major element analysis aliquots of digestion solutions were diluted from $4*10^3$ to $2.6*10^5$. Mg, Ca, Cr, Mn, Fe, Co and Ni were analysed by the addition of Sc for drift correction of intensities and concentrations were determined by using the known concentrations of a matrix matched standard. Different dilutions of the Smithsonian Allende meteorite standard reference powder (USNM 3529, Split 18, position 1) were used as a calibration standard. Detailed analytical methods for major elements were described in Kadlag and Becker a (submitted). Concentrations of all elements were measured on the Element XR ICP-MS at Freie Universität Berlin, except for Os isotopic and concentration measurements, which were carried out on a Triton TIMS at Freie Universität Berlin.

4.4.1 Analytical blanks

Total procedure blanks were determined for all elements with each set of digested samples. Average values of blanks (n=12) over the duration of chemical procedure are Re = 1.9 ± 0.8 pg,

Os = 1 ± 1 pg, Ir = 2 ± 1 pg, Ru = 4 ± 7 pg, Pt = 40 ± 30 pg, Rh = 9 ± 7 pg, Pd = 40 ± 20 pg, Au = 2 ± 2 pg, Te = 30 ± 10 pg, Se = 2.8 ± 0.5 ng and S = 7.6 ± 0.8 µg. Total procedure blanks contribute less than 5% for most of the components. QUE-SM >250, QUE SM 80-150 CHD have a slightly higher blank correction up to 10% for Ru, Rh and Pd. Nonmagnetic coarse and fine (NMC and NMF) fractions of QUE 97008, Ce-chondrules and Ce-NM<50 have higher blank corrections of up to 30% for some elements (Re, Ru, Rh and Pd) because of the small sample weight and low abundances of these elements.

4.4.2 Reproducibility of Standards

The precision of isotopic ratios of HSE and chalcogen of an in-house standards for ICP-MS measurements at the Freie University Berlin over the period of analysis was $^{185}Re/^{187}Re = 0.607 \pm 0.004$ (n = 19), $^{191}Ir/^{193}Ir = 0.592 \pm 0.003$ (n = 25), $^{99}Ru/^{101}Ru = 0.735 \pm 0.004$ (n = 25), $^{106}Pd/^{105}Pd = 1.229 \pm 0.005$ (n=25), $^{194}Pt/^{195}Pt = 0.971 \pm 0.004$ (n = 25), $^{103}Rh/^{193}Ir = 0.42 \pm 0.03$ (n = 25), $^{197}Au/^{193}Ir = 0.31 \pm 0.07$ (n = 19), $^{77}Se/^{78}Se = 0.318 \pm 0.003$ (n = 15), $^{125}Te/^{126}Te = 0.375 \pm 0.005$ (n =15) and $^{32}S/^{34}S = 21.5 \pm 0.3$ (n=11). Reported uncertainties are 2σ. The precision (2σ) of major element ratios for different dilutions of the Allende Smithsonian standard was < 4% over the period of analysis. The repeatability of the $^{187}Os/^{188}Os$ ratio of the University of Maryland Johnson-Matthey Os standard measured on N-TIMS is 0.11382 ± 0.00003 (n=7, 2σ) for Faraday cup measurements and 0.11382 ± 0.00003 (n=12, 2σ) for electron multiplier measurements over the duration of a year.

4.5 Results

4.5.1 Major element abundances of the components

Abundances of the major elements are used to identify the dominant mineral phases in the components. Major and minor element data of the components, calculated bulk rock values from the mass balance of all analysed components and the average bulk rock composition of L3 chondrites from the literature are displayed in Fig.4.2 and in Table 4.1. The calculated bulk rock composition of QUE 97008 shows less than 20% difference compared to the average of L3 data from the literature (sources mentioned in the caption of Table 4.1), except for Ni, which differs by 29%. Calculated bulk rock values for Ceniceros show deviations of up to 40% from the literature average of L3 chondrites, except Ni, which shows a 55% difference. The large difference for Ceniceros is mainly the result of significant contributions from a sulfide clast which increases the Fe and S concentration and reduces the abundances of other elements in the piece of rock studied here.

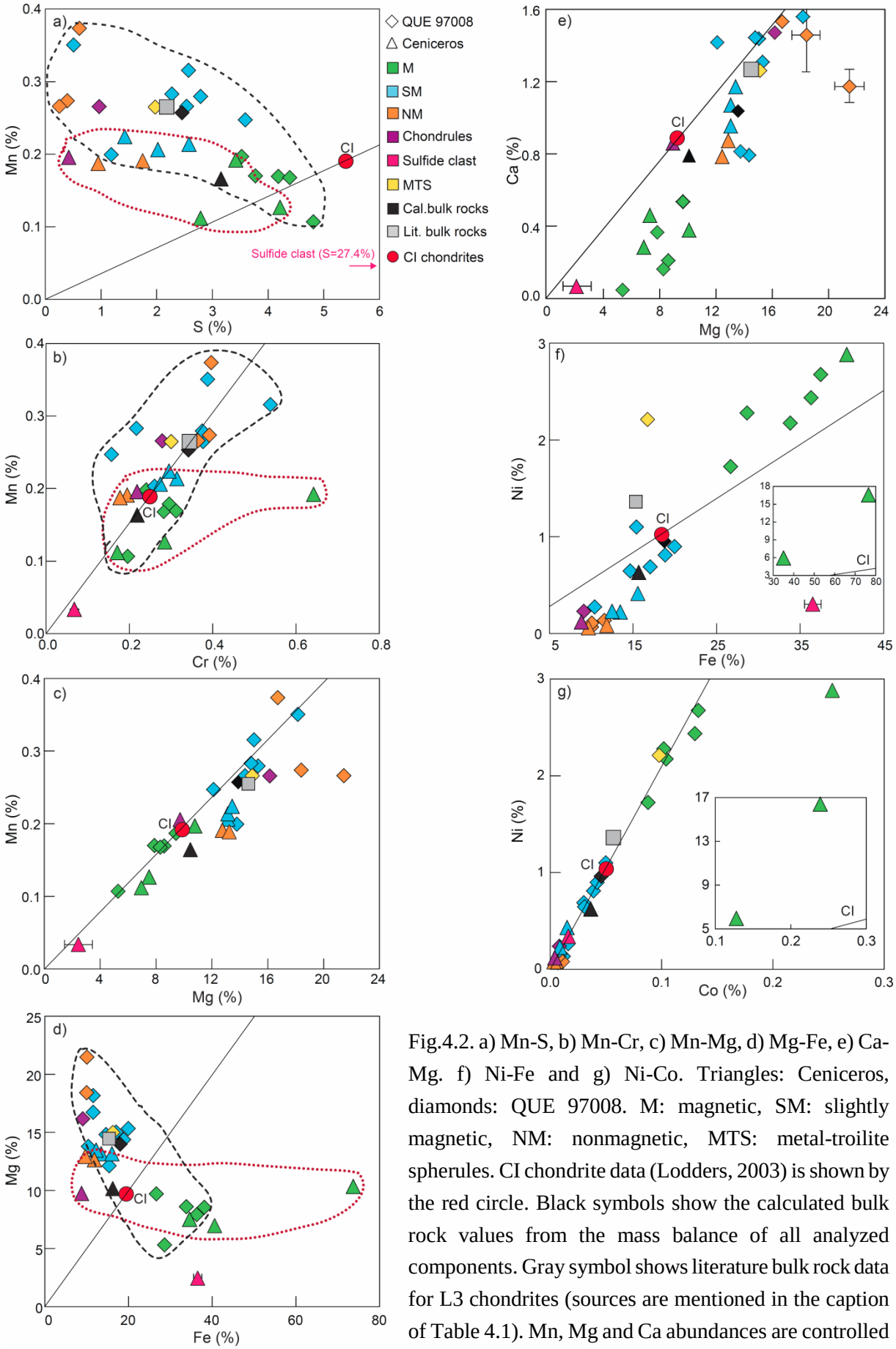

Fig.4.2. a) Mn-S, b) Mn-Cr, c) Mn-Mg, d) Mg-Fe, e) Ca-Mg. f) Ni-Fe and g) Ni-Co. Triangles: Ceniceros, diamonds: QUE 97008. M: magnetic, SM: slightly magnetic, NM: nonmagnetic, MTS: metal-troilite spherules. CI chondrite data (Lodders, 2003) is shown by the red circle. Black symbols show the calculated bulk rock values from the mass balance of all analyzed components. Gray symbol shows literature bulk rock data for L3 chondrites (sources are mentioned in the caption of Table 4.1). Mn, Mg and Ca abundances are controlled by silicate phases.

Lower than CI chondritic Ca/Mg in most components indicates the loss of refractory lithophile elements. Fe and S abundances are mainly controlled by variable proportions of sulfide and metal in the components. Most components have CI chondritic Ni/Co. Magnetic components of Ceniceros show large variations in Ni/Co ratio from CI chondrites. Higher Ni/Co in some magnetic fractions results from preferred sampling of exsolved taenite.

4.5.2 ^{187}Re-^{187}Os systematics

^{187}Re/^{188}Os and ^{187}Os/^{188}Os ratios and Δ_{Os} (the deviation of Os isotopic composition from the 4.56 Ga IIIA iron meteorite isochron from Smoliar et al., (1996), a precise definition is given in a caption of Table 4.2) of analyzed components are given in Table 4.2 and measured ^{187}Re/^{188}Os and ^{187}Os/^{188}Os are plotted in Fig.4.3. Most of the components show deviations from the IIIA iron meteorite isochron (Fig.4.3). Magnetic fractions of both meteorites show similar ^{187}Os/^{188}Os and ^{187}Re/^{188}Os and lie on or not far from the 4.56 Ga reference isochron, with higher ^{187}Os/^{188}Os compared to CI chondrites. The MTS fraction of QUE 97008 is characterized by an unusually high ^{187}Os/^{188}Os value compared to other components.

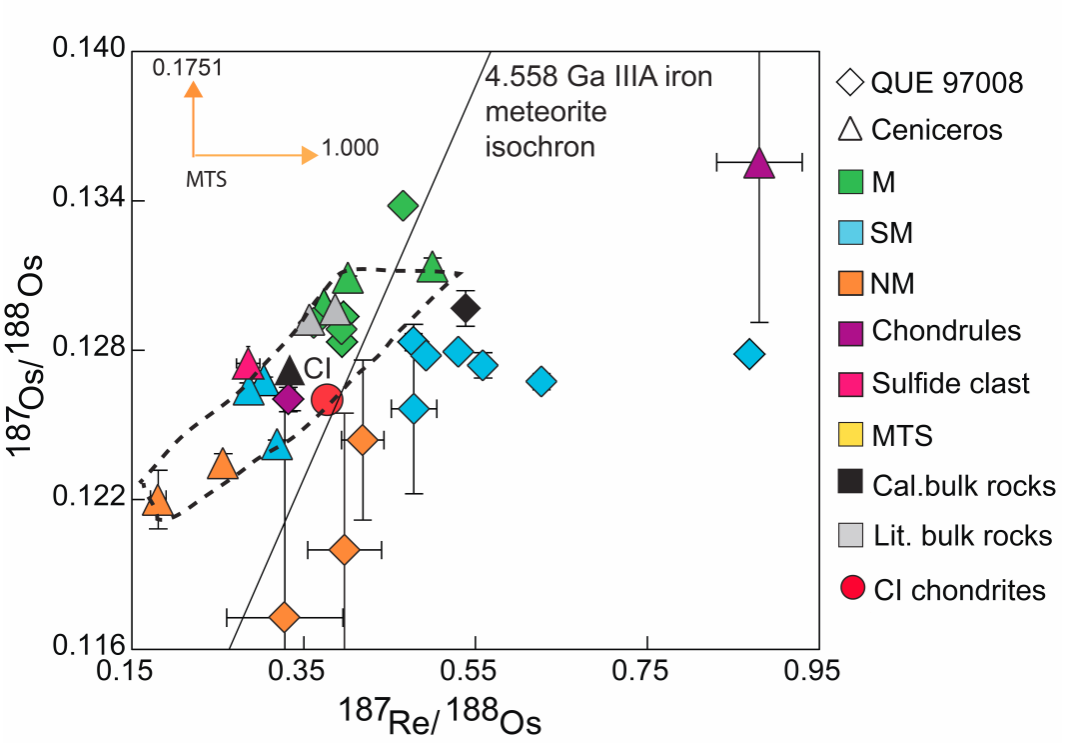

Fig.4.3. ^{187}Re-^{187}Os isochron diagram of analyzed components of QUE 97008 and Ceniceros. Reference line is the 4.56 Ga IIIA iron meteorite isochron (Smoliar et al., 1996). CI chondrite data and bulk rock data of Ceniceros from Fischer-Gödde et al. (2010) and Walker et al. (2002b). The components of Ceniceros show a linear trend (shown by the dashed field), whereas components of QUE 97008 show random variations, likely caused by redistribution of Re during terrestrial weathering.

The components of Ceniceros show an apparent linear trend in the Re-Os isochron diagram, with systematic deviations from the reference isochron (Fig.4.3). The chondrule fraction and magnetic components of Ceniceros have higher $^{187}Re/^{188}Os$ compared to the sulfide clast, slightly magnetic and nonmagnetic fractions (Fig.4.3). $^{187}Os/^{188}Os$ in the components of Ceniceros varies systematically: $^{187}Os/^{188}Os_{NM} < {}^{187}Os/^{188}Os_{SM} < {}^{187}Os/^{188}Os_{M}$. Significant differences exist between both meteorites in the behaviour of slightly magnetic and nonmagnetic fractions. Slightly magnetic components of QUE 97008 show higher $^{187}Re/^{188}Os$ and $^{187}Os/^{188}Os$ compared to SM components of Ceniceros and CI chondrites. In addition, $^{187}Re/^{188}Os$ in slightly magnetic components of QUE 97008 varies with the grain size. The smallest size fraction has higher $^{187}Re/^{188}Os$ and shows a larger deviation from the isochron. The NM fractions display the lowest $^{187}Os/^{188}Os$ compared to all other components. NM fractions of Ceniceros have lower $^{187}Re/^{188}Os$ compared to the NM fractions of QUE 97008 and CI chondrites, consistent with the variation in SM components.

The chondrule fractions of both meteorites also show deviations from the reference isochron. Chondrules from QUE 97008 show deviation from the isochron towards low $^{187}Re/^{188}Os$, whereas the chondrule fraction of Ceniceros lies at the high $^{187}Re/^{188}Os$ side of the isochron. The MTS fraction from QUE 97008 shows very high $^{187}Os/^{188}Os$ (0.1751 ± 0.0004) and $^{187}Re/^{188}Os$ (1.000 ± 0.003) and lies close to the isochron. The sulfide clast from Ceniceros also lies on the low $^{187}Re/^{188}Os$ side off the isochron (Fig.4.3). Calculated bulk rock values of both chondrites also deviate from the isochron, however, in different directions (Fig.4.3, Table 4.2). Calculated bulk rock values of Ceniceros show similar $^{187}Re/^{188}Os$ and slightly lower $^{187}Os/^{188}Os$ compared to literature bulk rock values of Ceniceros (Walker et al., 2002b).

4.5.3 HSE abundances

HSE abundances of the components, bulk rock values calculated from the mass balance of all analyzed components, L3 bulk rocks, bulk rock data of Ceniceros and CI chondrites from the literature (Ebihara, 1989; Kaczaral et al., 1989; Kallemeyn et al., 1989; Wasson et al., 1993; Ebihara and Ozaki, 1995; Kong and Ebihara, 1996; Bhandari et al., 2002; Horan et al., 2003 and Fischer-Gödde et al., 2010) are listed in the Table 4.2 and are shown in CI chondrite normalized diagrams in Fig.4.4. Calculated bulk rock values of the HSE in QUE 97008 are up to 25% lower than average literature bulk rock values of L3 chondrites, whereas for Ceniceros the calculated bulk rock composition is about 40% lower than literature data (Horan et al., 2003). This difference is mainly caused by the presence of a HSE poor sulfide clast in this piece of Ceniceros.

The HSE are enriched in magnetic fractions and in the MTS fraction of QUE 97008 (Fig.4.4). These components show 75-375 times higher HSE abundances compared to NM

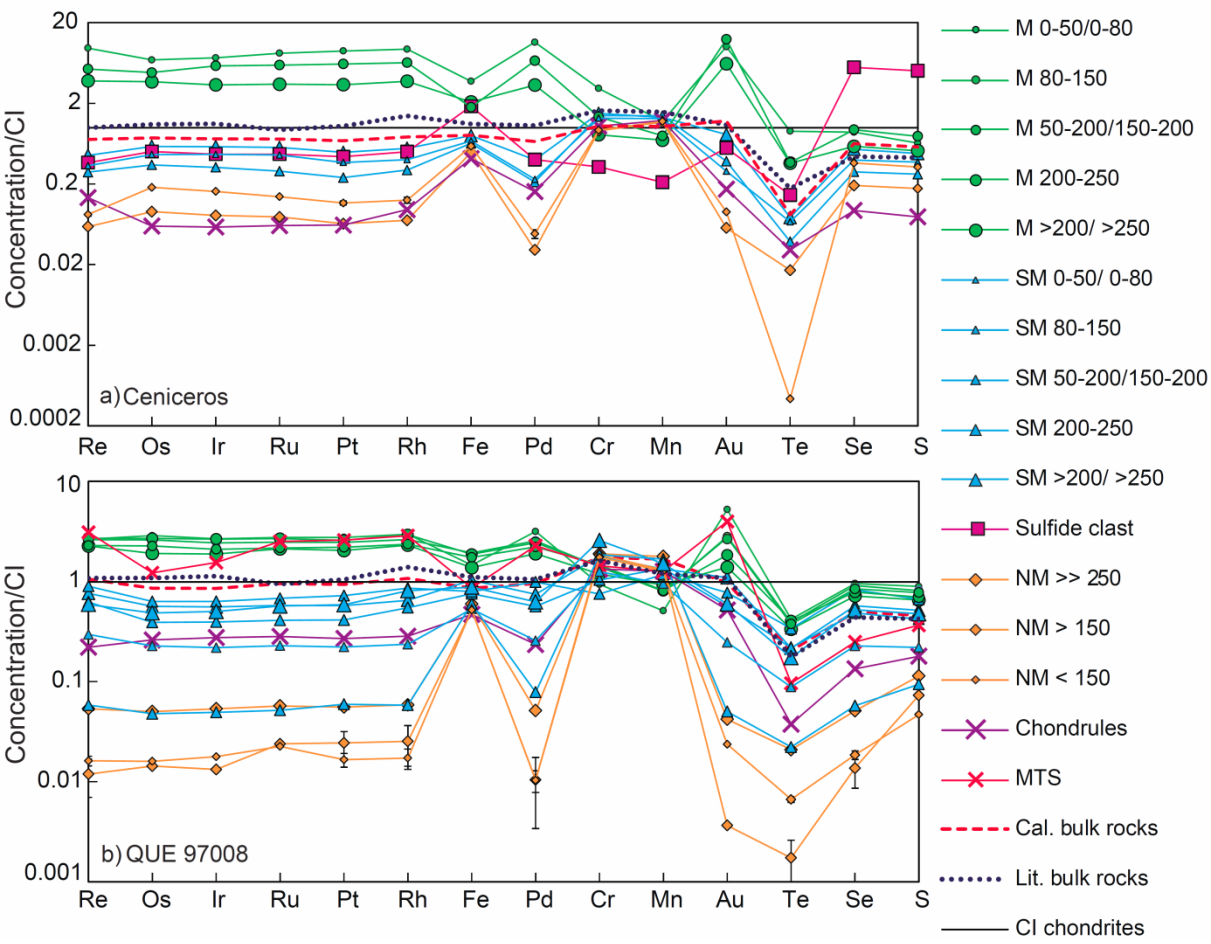

Fig.4.4. HSE, chalcogen and Fe, Cr, Mn concentrations in the components of the QUE 97008 and Ceniceros normalized to CI chondrites. Elements are ordered from left to right in increasing order of volatility, assuming the 50% condensation temperature in the solar nebula by Lodders (2003). Differences in the symbol size of some components indicate different grain size fractions (numbers given in the legend represent size fractions). CI chondrite values from Dreibus et al. (1995), Horan et al. (2003), Fischer-Gödde et al. (2010) and Wang et al. (2013, 2014). Bulk rock HSE data for Ceniceros from Horan et al. (2003). Bulk rock chalcogen element and Fe, Mn and Cr data for both meteorites are L3 chondrites average values (Yasinskaya and Osadchij, 1973; Kirova et al., 1975; Graham et al., 1976; Fitzgerald, 1979; Haramura et al., 1983; Jarosewich, 1984, 1990; Fulton and Rhodes, 1984; Jarosewich, 1984, 1990; Fredriksson et al., 1986; Hewins et al.,1988; Ebihara, 1989; Kaczaral et al., 1989; Kallemeyn et al., 1989; Graham, 1993; Wasson et al., 1993; Ebihara and Ozaki, 1995; Yanai et al., 1995; Kong and Ebihara, 1996; Bhandari et al., 2002; Horan et al., 2003).

components (Fig.4.4, Table 4.2). With the exception of Au, the HSE abundances in magnetic components of Ceniceros show an inverse relationship with the grain size similar as was observed in other unequilibrated ordinary chondrites (Rambaldi, 1976, 1977; Horan et al., 2009).

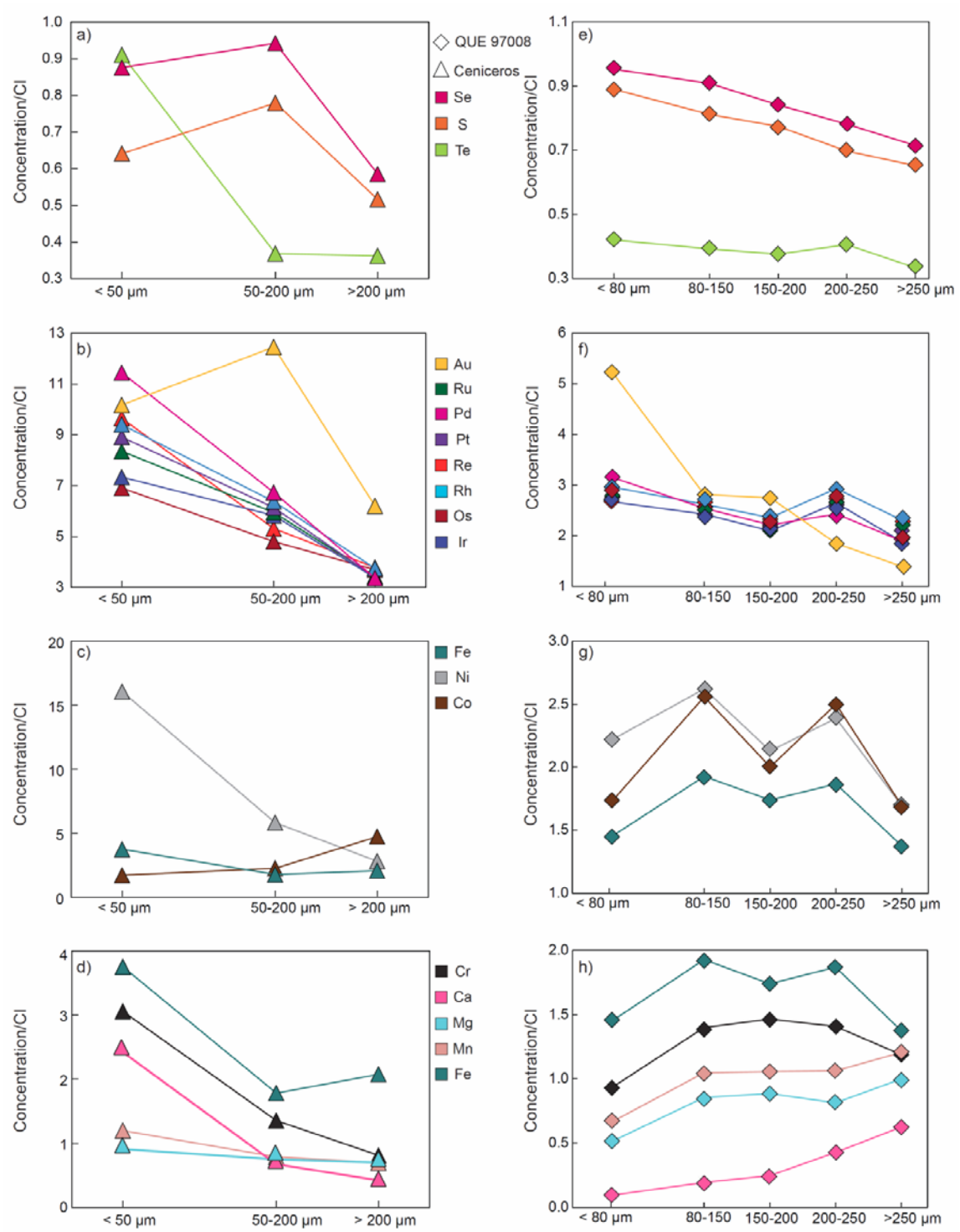

Fig.4.5. CI normalized abundances of a) S, Se and Te, b) HSE, c) Fe, Ni and Co, d) Cr, Ca, Mg, Mn and Fe of magnetic components of Ceniceros are shown as a function of grain size fraction. Au is decoupled from the HSE and show similar size dependent behavior like S and Se. All other HSE and Ni show similar size dependent behavior. Decoupled Fe, Co and Ni in magnetic fractions of Ceniceros are likely the result of kamacite-taenite exsolution. Abundance variations of e) S, Se and Te, f) HSE, g) Fe, Ni and Co, h) Cr, Ca, Mg, Mn and Fe of magnetic components of QUE 97008 with grain size fractions. All HSE but Au show similar size dependent behavior in magnetic components and are decoupled from Fe, Co and Ni (b and c). These variations indicate that either HSE carrier phases other than Fe-Ni metal alloys exist in magnetic components, or HSE carriers were not completely equilibrated with Fe-Ni metal.

On the other hand Au abundances in magnetic fractions of Ceniceros are higher in the intermediate size fraction and show a size dependent behavior that follows that of S and Se abundances (See Fig.4.5). HSE abundances in QUE 97008 are also enriched in the smallest (<80 µm) and intermediate sized (200-250 µm) magnetic fractions compared to magnetic fractions of other sizes (Fig.4.5). Gold behaves somewhat different from the other HSE, as it shows larger differences between the size fractions. Note that the size-dependent behavior of the HSE in magnetic fractions differs fundamentally from the size-dependent variations of Ni, Co and Fe (Fig.4.5c and g). It is clear from Fig.4.5 that Au abundances in the magnetic components of both meteorites are decoupled from other HSE and shows a similar behavior as S and Se.

Three different types of CI normalized HSE abundance patterns can be distinguished for the components (Fig.4.4, 4.6). Some components display nearly CI chondritic HSE ratios (QUE chond C, QUE slightly magnetic <80 and 80-150 CHD and >250 fractions, SC and slightly magnetic components of Ceniceros). Other components are depleted in the refractory HSE Os, Ir and Ru compared to the less refractory HSE such as Pt, Rh and Pd (most magnetic fractions, QUE chond S, slightly magnetic fractions of QUE 97008). A third type of pattern occurs in nonmagnetic fractions and shows depletions in Pd with respect to all other HSE.

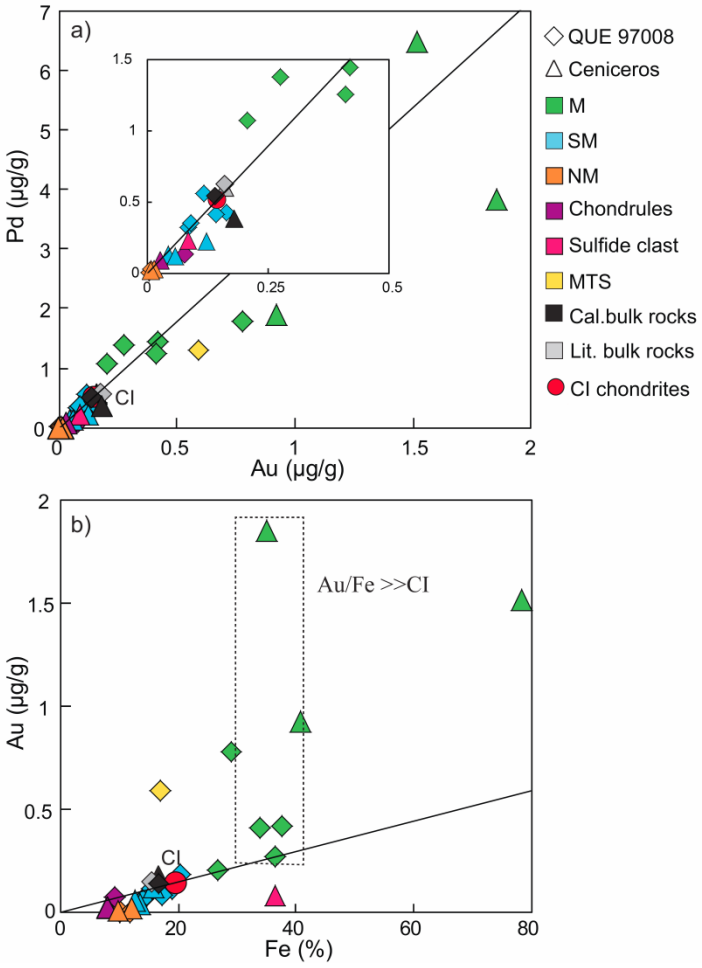

Fig.4.6. a) Pd-Au and b) Au-Fe variation among the components of QUE 97008 and Ceniceros. Au abundances in magnetic components are decoupled from Fe and Pd, indicating that the process that causes variation of Au in magnetic fractions is independent of fractionations of other highly siderophile elements.

4.5.4 Chalcogen element abundances

Concentrations of chalcogen elements in the components and calculated bulk rocks, literature average bulk L3 chondrites and CI chondrites are listed in Table 4.2 (Haramura et al., 1983; Jarosewich, 1984, 1990; Fredriksson et al., 1986; Hewins et al., 1988; Kaczaral et al., 1989; Kallemeyn et al., 1989; Graham, 1993; Wasson et al., 1993; Dreibus et al., 1995 ; Yanai et al., 1995; Kong and Ebihara, 1996; Bhandari et al., 2002 and Wang et al., 2013). The Chalcogen elements are depleted in all components compared to CI chondrites (Fig.4.4 and 4.7), except in the sulfide clast from Ceniceros (Fig.4.4 and 4.7). Chalcogen concentrations are higher in magnetic and slightly magnetic components compared to chondrules, MTS and nonmagnetic fractions.

In most components, Se and S are unfractionated and linearly correlated (Figs.4.4, 4.7a). CI normalized abundances in magnetic components are depleted in the order Se < S < Te. Systematic complementarity of S/Se ratios is observed between the components (Fig.4.7a). NM fractions, chondrules and some SM fractions have higher S/Se, whereas M and some SM fractions have lower S/Se than CI chondrites. Calculated bulk rocks have slightly lower S/Se than CI chondrites (the average S/Se of both chondrites is 2334 ± 49).

A characteristic feature in the CI normalized abundance pattern of L chondrites is the depletion of Te relative to neighbour elements and CI chondrites (Fig.4.4). With the exception of the <50 M fraction of Ceniceros, which has nearly CI chondritic ratios of Se and Te, the depletion of Te occurs in all components of the analysed chondrites. In case of QUE 97008, Te is more depleted than Se and S but shows a correlation with these elements (Fig.4.7a and b), indicating the chalcophile behavior of Te in all the components of this meteorite. Accordingly, the total variation of Se/Te (23 ± 3) in components of QUE 97008 is limited, whereas in case of Ceniceros Te is decoupled from Se and S (Fig.4.7b). Magnetic components of Ceniceros have CI chondrite like to moderately high Se/Te, whereas NM and SM fractions of Ceniceros have very high Se/Te. The decoupled behaviour requires that Te behaves as a siderophile element in magnetic fractions and as a chalcophile element in other fractions of Ceniceros.

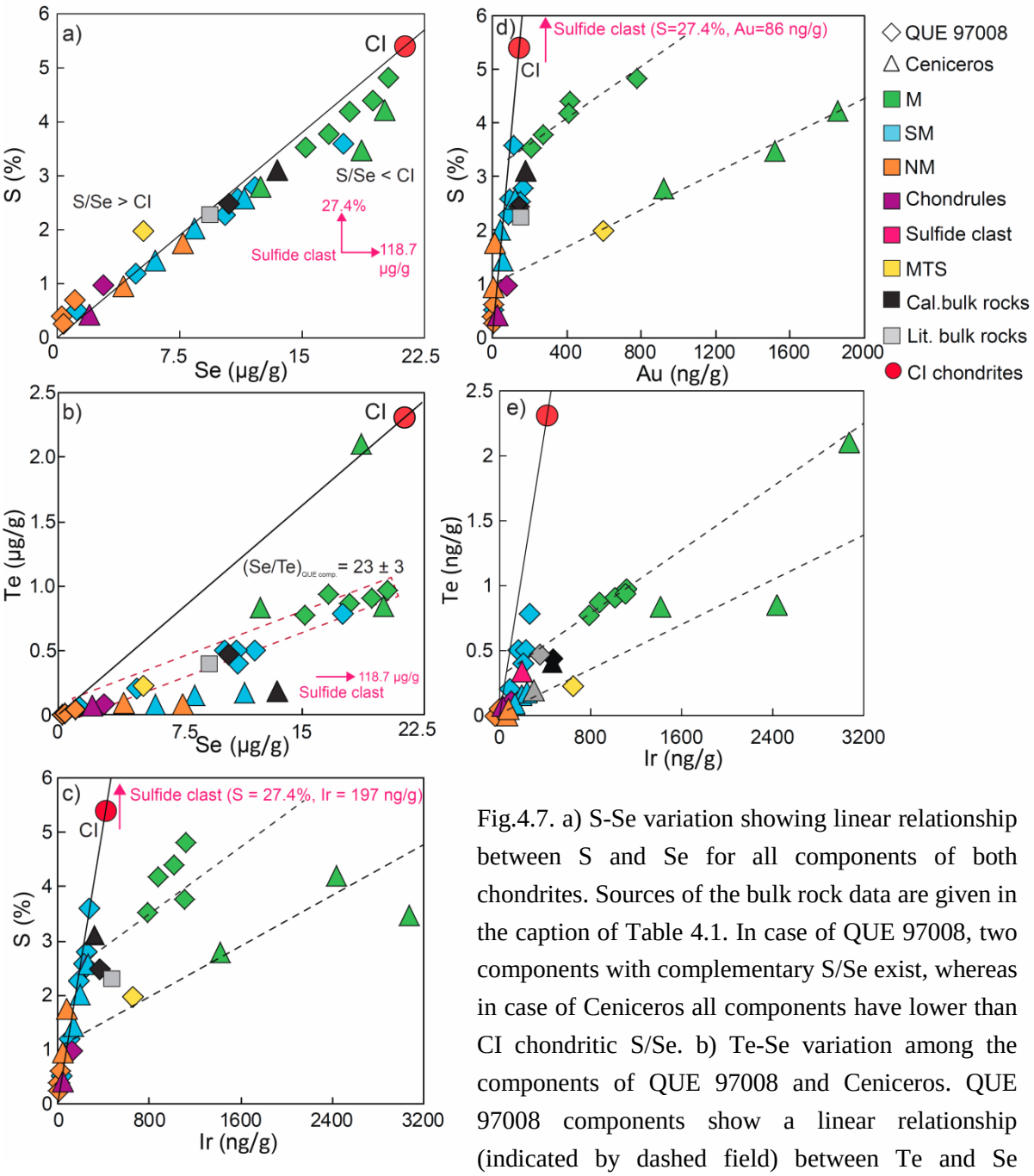

Fig.4.7. a) S-Se variation showing linear relationship between S and Se for all components of both chondrites. Sources of the bulk rock data are given in the caption of Table 4.1. In case of QUE 97008, two components with complementary S/Se exist, whereas in case of Ceniceros all components have lower than CI chondritic S/Se. b) Te-Se variation among the components of QUE 97008 and Ceniceros. QUE 97008 components show a linear relationship (indicated by dashed field) between Te and Se indicating the chalcophile nature of Te.

In contrast, $Te/Se_M >> Te/Se_{NM}$ in the components of Ceniceros suggest a predominantly siderophile behavior of Te in this meteorite. c) S-Ir, d) S-Au and e) Te-Ir variation among the components indicate that SM and NM components have nearly CI chondritic S/Au, S/Ir and Te/Ir ratios. S-HSE variations in the components indicate two-component mixing of CI chondritic material in NM and some SM components and volatile depleted material in M components. The S/Ir variation is more complex and involves mixing of at least two different carriers which have lower than CI chondritic S/Ir (shown by dashed lines) with CI chondritic S/Ir. The data also indicates that the S loss with respect to HSE may have occurred during the thermal processing of magnetic components.

4.6 Discussion

4.6.1 Mineral proportions and their influence on the composition of the components

The abundances of major elements were used to identify the role of silicate, sulfide and metal phases in separated components. Abundances of Mn and S show inverse correlations with each other (Fig.4.2a), indicating that Mn is mainly present in silicate phases (Lodders, 2003). This observation is consistent with the good positive correlation between Mn and Mg (Fig. 4.2c). The variation of Fe/Mg in magnetic and nonmagnetic components mainly stems from differences in metal, sulfide and silicate contents in these separates (Fig.4.2d). The outlier is magnetic <50 fraction of Ceniceros. This fraction is enriched in Fe-Ni metal (Fig.4.2f and g), which shows higher Cr and Fe content compared to all other magnetic components (Fig.4.2b and d). This difference is probably due to the presence of fine grained chromite ($FeCr_2O_4$). A predominance of silicates is indicated by higher abundances of Ca, Mn, Cr, Mg and lower S/Mn and Ni/Fe in the nonmagnetic components compared to magnetic components (Fig.4.2).

Magnetic components have higher Ni/Fe and Ni/Co (except for the M >200 fraction of Ceniceros) compared to the nonmagnetic components (Fig.4.2f and g). There are different possibilities to explain these variations. Iron is present in silicates, sulfides and metal phases, whereas Ni is mainly present in metal phases (Larimer and Anders, 1970). Higher Ni/Fe and Ni/Co than CI chondrites in the MTS fraction of QUE 97008 and in magnetic fractions indicate a predominance of metal phases over silicates and sulfides in these components. The higher $D^{metal/silicate}$ of Ni compared to Co and Fe at low pressures and moderate temperatures (Schmitt et al., 1989) provides the most likely explanation of the higher Ni/Co in magnetic fractions compared to nonmagnetic fractions. Thus the variation in Ni/Co in different mineral phases would be due to metal-silicate partitioning before the accretion of the components, probably during chondrule formation. Alternatively, large variations of Ni/Co in magnetic components of Ceniceros may also represent exsolution of Ni poor kamacite and Ni rich taenite during cooling of metal grains below 1080 K. The fine grained fraction is mostly enriched in taenite and shows higher Ni/Co ratio (Fig.4.2g). Note that not all magnetic fractions have higher Ni/Co compared to nonmagnetic fractions. Magnetic >200 fraction of Ceniceros have low Ni/Co compared to CI chondrites and all other components (Fig.4.2g).

The nonmagnetic fractions of both meteorites show almost 2 fold variations in the abundances of Ca, Mg, Mn, Cr and S without comparable variations in Fe, Ni and Co (Fig.4.2). Considering that troilite is the main sulfide phase in ordinary chondrites (Kong et al., 2000), differences in Fe and S behavior indicate that Fe abundances in silicate phases of the nonmagnetic fractions must be variable (Fig.4.4). The variation of Fe is mainly controlled by different proportions of pyroxene and olivine in nonmagnetic and chondrule fractions of the

meteorites (Fig.4.4). The presence of minor amounts of sulfides has negligible effect on the Fe abundances of these fractions. Higher Ca, Mn, Cr and Mg in the nonmagnetic components of QUE 97008 compared to the nonmagnetic components of Ceniceros (Fig.4.2) indicates that the nonmagnetic fraction in QUE 97008 contains more pyroxenes, whereas in the nonmagnetic fraction of Ceniceros, olivine and sulfides are more abundant (Fig.4.2a and e). The abundances of major elements in the calculated bulk rocks show a depletion in the order Mn ≈ Cr < Mg < Ca < Fe < S (Fig.4.2), indicating that refractory lithophile (Ca rich) and Fe rich phases were lost from the precursors of L chondrite components.

4.6.2 ^{187}Re-^{187}Os constraints on early and late fractionation processes

Significant variations in ^{187}Re/^{188}Os and ^{187}Os/^{188}Os are observed among the components (Fig.4.3). Only magnetic components lie close to the 4.56 Ga IIIA iron meteorite reference isochron (Smoliar et al., 1996), all other components show significant deviations from the reference isochron (Fig.4.3). Magnetic components have higher Re*/Os compared to slightly magnetic and nonmagnetic fractions (Fig.4.8). Re* is the initial Re concentration calculated from the measured Os isotopic composition, assuming that the Os isotopic composition was not disturbed by later processes. Re*/Os vary significantly among the components (0.06-0.213). Components of Ceniceros show a systematic increase in Re*/Os and Pd/Ir from nonmagnetic to magnetic components (Fig.4.8), indicating that either fractional condensation, evaporation or another partitioning processes occurred at 4.56 Ga (the details of the processes will be discussed further below).

In most components, variations in ^{187}Re/^{188}Os are not correlated with ^{187}Os/^{188}Os, indicating that the ^{187}Re-^{187}Os systematics was disturbed relatively recently. Although QUE 97008 was a meteorite find and Ceniceros a fall, the ^{187}Re-^{187}Os systematics was disturbed in the components of both meteorites. This observation implies that processes other than terrestrial weathering also may have played a role in the disturbance of the ^{187}Re-^{187}Os systematics of the components of L chondrites. If interpreted as an internal errorchron, the positive correlation of the Ceniceros components yields an age of 1388 ± 670 Ma (Fig.4.A2), suggesting a role of secondary processes on the L chondrite parent body (see also Becker et al., 2001 who reported an 1.6 Ga internal errorchron of a CAI from the Allende meteorite). The deviation of components from the isochron may have been caused by either mobilization of Re and/or Os, homogenization of Os isotopes among the components or nucleosynthetic effects.

^{187}Os/^{188}Os in most fractions of Ceniceros is higher than the ratio expected from the corresponding ^{187}Re/^{188}Os and hence likely it is independent of the ^{187}Re decay and might be related to the interaction of Re and Os with the cosmic rays. Large variations in neutron capture cross section of ^{187}Os, ^{188}Os and ^{187}Re (320, 4.7 and 76 barns respectively, Mughabghab, 2003) suggest that this process could produce 1ower ^{187}Os/^{188}Os and ^{187}Re/^{188}Os than the initial isotopic

composition at the time of the formation of Re-Os carriers. However, such a large deviation in $^{187}Os/^{188}Os$ isotopic composition due to neutron capture seems to be unlikely because similar effects have not been observed for other Os isotopes or $^{187}Os/^{188}Os$ even not in CAIs which are most prone to nucleosynthetic effects compared to other chondrite components (Archer et al., 2014; Brandon et al., 2005b).

Osmium isotopic homogenization during recent processes is also very unlikely, because then all components should have similar $^{187}Os/^{188}Os$ ratios, which is not the case (Fig.4.3, Table 4.2). If partial equilibration occurred then complementary deviations from the isochron should be observed in the components, but most components of Ceniceros lie on the low $^{187}Re/^{188}Os$ side and mass balance does not indicate a complementarity of Os isotopes in the components.

Rhenium is the most refractory element under solar conditions, but also the most volatile HSE under oxidizing conditions (Palme et al., 1998). The mobility of Re is higher than Os under oxidizing conditions (Palme et al., 1998), therefore redistribution of Re is the more likely reason for the resetting of the Re-Os systematics. A late exposure of the meteorite parent body to oxidizing conditions might be the reason for local Re mobilization and partial (or local?) resetting of the ^{187}Re-^{187}Os systematics, although it is difficult to assess what the causes of these changes may have been. Despite of the similar mineralogy of slightly magnetic fractions of both meteorites (Table 4.1 and 4.2), opposite trends are observed for the measured $^{187}Re/^{188}Os$ ratios. In QUE 97008, terrestrial weathering and aqueous alteration may be the likely causes of the partial disturbance of the Re-Os system (Dobrică and Brearley, 2011).

4.6.3 Origin of HSE variations in the components-volatility control or igneous processes?

Metal rich fractions (magnetic and MTS) show enrichment in HSE compared to CI chondrites and all other components (Fig.4.4), consistent with the high metal-silicate partition coefficients of these elements at low pressures (O'Neill et al., 1995). The important feature of the abundance pattern includes the variation in Re/Os among the components (Figs.4.3, 4.4 and 4.8) that were discussed in the previous chapter.

Abundances of Ir, Ru, Pt and Rh are correlated with each other in all components and show CI chondritic ratios in most of the components (See Fig.4.A1). On the other hand, components such as slightly magnetic fractions of QUE 97008 have lower CI normalized Ir, Ru and Pt abundances compared to Rh, Pd and Au (Fig.4.4), suggesting a slight loss of refractory HSE compared to moderately volatile HSE. This depletion may reflect a loss of early formed refractory condensates by fractional condensation before the condensation of Fe-Ni metal, a feature that is known from enstatite chondrites (e. g., Kadlag and Becker a, submitted).

Lower Ni/Ir, Pd/Ir, Ru/Ir, Re/Ir and Pt/Ir ratios in the sulfide clast, nonmagnetic and slightly magnetic fractions than in magnetic fractions and in CI chondrites (Fig.4.A1) indicate higher

partitioning of Ir into HSE host phases of nonmagnetic components. Previous studies of L chondrite components (Rambaldi, 1976, 1977a) show similar behaviour of Ir and Os in nonmagnetic fractions. Rambaldi (1976, 1977a) explained this behavior by the presence of Ir and Os enriched fine metal fractions in the nonmagnetic components. Fractionations between HSE in nonmagnetic and slightly magnetic fractions in the present study can be explained similarly. In contrast, the lower Os/Ir, Os/HSE, Ir/HSE, Ir/Ni than CI chondrites in the fine grained magnetic fractions (Fig.4.A1) and MTS fraction of QUE 97008 requires another explanation. Partitioning of trace elements during kamacite-taenite exsolution of the metal represents a feasible process. Nickel, Ru, Rh, Pd and Au have higher $D^{taenite/kamacite}$ compared to Os, Ir, Pt and Co (Rasmussen et al., 1988; Hsu et al., 1998; Campbell and Humayun, 2003; Ash et al., 2007). The depletion of Os and Ir compared to all other HSE (Fig.4.A1) in the fine grained magnetic component of Ceniceros can be explained by this process, if $D^{taenite/kamacite}$ of Pt < Os and Ir.

Solid metal-liquid metal partitioning processes can fractionate HSE as refractory HSE have higher $D^{solid\ metal/\ liquid\ metal}$ compared to Pd and Au (Chabot et al., 2003, 2011; Brenan and Bennett, 2010). Lower Pd/HSE in the nonmagnetic fractions can be explained on the basis of the Pd depleted solid metal composition, however Re, Os and Ir are unfractionated and behave similarly during solid metal- liquid metal partitioning processes (Chabot et al., 2003, 2011; Brenan and Bennett, 2010). The linear variation between Re*/Os and Pd/Ir in most components (Fig.4.8) is inconsistent with this fractionation process. It is more likely that the variation in HSE/Ir and HSE/Os ratios in different components is derived from the presence of Os-Ir rich alloys in nonmagnetic and slightly magnetic components.

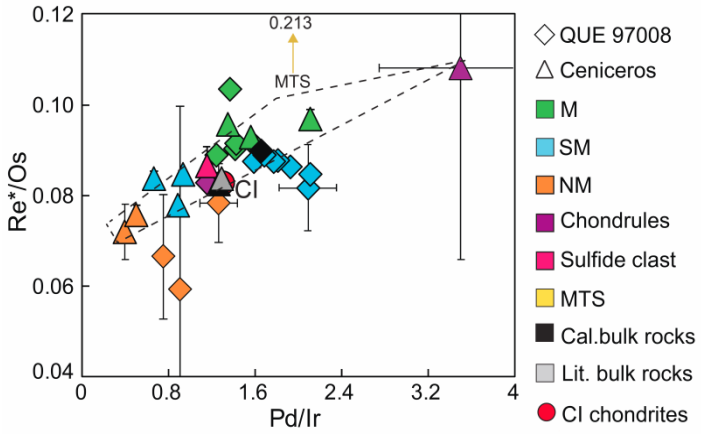

Fig.4.8. a) Re*/Os-Pd/Ir variation in the components of QUE 97008 and Ceniceros. Re* is the calculated Re concentration from the measured Os isotopic composition. Components of Ceniceros show a correlation of Re/Os and Pd/Ir. NM and SM components have lower Re*/Os and Pd/Ir compared to M components and the chondrule fraction of Ceniceros. No systematic variation is observed in case of QUE 97008.

Non-systematic variations in Au abundances with the HSE and Fe in magnetic components of both meteorites (Fig.4.6) may reflect secondary hydrothermal alteration on the parent body. Evidence of aqueous alteration on unequilibrated L chondrites has been noted in previous studies (Alexander et al., 1989; Wasson and Krot, 1994; Dobrică and Brearley, 2011). Similar size dependent behaviour of Au, S and Se (Fig.4.5) may have been caused by the high mobility of Au and S during the hydrothermal alteration (Ebihara et al., 1982; Dreibus et al., 1995). Sulfur is decoupled from refractory HSE (e.g. Ir, Fig.4.7c) and shows binary mixing relations with Au and Se abundances (Fig.4.7d and

4.8a). The correlation between S and Se (Fig.4.7a) and S/Se close to CI chondrites indicate that element systematics of these elements were not affected during alteration, therefore, high-temperature processes, mixing and dilution likely control the distribution of Au, S and Se abundances. Partitioning of Au in to sulfide phases could explain the correlations between S and Au (Fig.4.7d) and decoupling of Au from Fe and Pd (Fig.4.6).

4.6.4 Origin of chalcogen element variations

A first-order observation is that the calculated bulk rock abundances of Te, Se and S in L chondrites are depleted compared to other analyzed elements and CI chondrites (Figs.4.4 and 4.7). Because igneous processes involving sulfide-metal-silicate partitioning would strongly fractionate not only S and Se, but also the HSE (Helmy et al., 2010; Brenan, 2008; Mungall and Brenan, 2014), which is not observed at the bulk rock scale, the higher volatility of these elements (Lodders, 2003) compared to other analyzed elements is likely the main cause of this depletion. Therefore, volatility controlled processes like partial condensation or evaporation likely have played a key role in the overall depletion of the chalcogen elements. Almost all components display lower CI normalized Te abundances than normalized Se and S abundances (except Ceniceros magnetic <50 fraction), indicating that volatility dependent loss of these elements differs from canonical nebular conditions (where Te is more refractory than Se and S, Lodders, 2003). In detail, the variation of S/Se in the L chondrite components is much more simple and straightforward to explain, compared to S/Te and Se/Te (Fig.4.7a and b). Clearly, Te is the element with the complex behavior. Therefore in the next sections, we will discuss fractionation of S-Se and Te separately.

4.6.4.1 S-Se variations

Sulfur and Se in components of both chondrites show a linear correlation with S/Se close to CI chondrites (Fig.4.7a). Except for the sulfide clast in Ceniceros (27.4% S and 118.7 µg/g Se), concentrations of S and Se in the components are lower than in CI chondrites (Figs.4.4 and 4.7a), consistent with the volatile depletion in L chondrites compared to CI chondrites. QUE 97008 is an Antarctic find and Ceniceros is a fall meteorite, however, it is remarkable that no difference in the S-Se systematics in the components of both meteorites exists (Fig.4.7a). Slightly higher calculated bulk rock S and Se concentrations in Ceniceros compared to QUE 97008 is due to the presence of the large sulfide clast in this piece of rock, which contributes significantly to the bulk rock concentrations of S and Se. Therefore, we conclude that the effect of minor weathering (weathering grade A, Grossman, 1999) on S and Se concentrations of QUE 97008 components and on the bulk rock of the analyzed piece of rock is negligible. This behavior is in contrast to the Re-Os systematics, which suggests substantial internal redistribution of Re, notably in SM and chondrule fractions (Fig.4.3). The discrepancy with S and Se, suggests that most of the limited

alteration in QUE 97008 affected metal and not troilite (evidence for the late-stage alteration of metal along fractures and at metal-silicate grain boundaries is shown in Fig.4.1b, d).

Calculated bulk rock values have slightly lower S/Se compared to CI chondrites (Fig.4.7a). All components of Ceniceros show slightly lower than CI chondritic S/Se, whereas components of QUE 97008 show complementary S/Se variation of higher than CI chondritic S/Se in nonmagnetic material and slightly lower S/Se in magnetic fractions (Fig.4.7a). Two processes may be responsible for the S-Se fractionation between the components of L chondrites. The lower than CI chondritic S/Se in precursors of the components may reflect volatilization and S loss to the gas phase, which may be responsible for the slightly lower S/Se in the calculated bulk rocks compared to CI chondrites. However, MTS, chondrules and nonmagnetic fractions of QUE 97008 have higher S/Se and also higher S/HSE compared to metal rich magnetic fractions, suggesting more complicated processes. The differences of S/Se between nonmagnetic (S/Se $\geq$ CI chondrite) and magnetic (S/Se < CI chondrite) components, in QUE 97008, are suggestive of control by metal-silicate-sulfide partitioning, as such processes also control ratios of other moderately siderophile elements (e. g., Ni/Co, Ni/Fe, Fig.4.2). The complementary variations of S/Se and Se/Te in magnetic and nonmagnetic components (Fig.4.7a and b) are consistent with the large differences in partition coefficients of S, Se and Te during metal-sulfide-silicate partitioning (Rose-Weston et al., 2009). Sulfide rims around silicate rich chondrules indicate late condensation of sulfides around chondrules (Fig.4.1). Thus these partitioning processes likely have occurred during melting and segregation of metal, sulfide and silicates during chondrule formation.

The MTS fraction of QUE 97008 shows higher S/Se than CI chondrites and also has higher abundances of Ni, Co, HSE than CI chondrites (Figs.4.2, 4.4, 4.7a). Notably, this component also shows higher lithophile element abundances compared to magnetic fractions (Fig.4.2). This unusual combination of properties is consistent with a larger proportion of high temperature condensates in this component. Because of the relatively high concentration of volatile elements (e. g., Mn, Au, S), we suggest that MTS formed by late condensation of moderately siderophile volatile elements around refractory phase assemblages. The sulfide clast in Ceniceros has a very similar S/Se (2303) as other components and the bulk rocks of L chondrites. It may have formed by fragmentation of an earlier generation of genetically related differentiated objects. Collision with or impact on such differentiated planetesimals, might be responsible for melting and higher loss of S compared to Se.

In summary, the systematics of abundances S and Se and other siderophile elements in different components and textural evidence (Fig.4.1a-d) suggest that metal-sulfide-silicate partitioning was the main controlling factor on differences in abundances and in S/Se between different components. The distributions likely were established during chondrule formation and subsequent cooling. The data yields no evidence that terrestrial weathering had a significant influence on the bulk rock scale abundances of these elements as QUE 97008 (Antarctic find) and

Ceniceros (fall) display similar behavior of S and Se. The lower than CI chondritic concentrations and S/Se of both bulk rocks suggests preferred evaporative loss S. Considering the extreme heterogeneity of troilite distribution in chondrules, MTS and matrix in QUE 97008, a preaccretionary control of the S budget of the bulk rock is indicated. In the bulk rock of Ceniceros, the budget of S and Se is affected by the sulfide clast, which suggests that metamorphic heating had little influence on the abundances of these volatile elements in unequilibrated L chondrites.

4.6.4.2 Origin of the depletion of Te in L chondrites

One of the important features in the abundance patterns is the depletion of Te compared to all other elements (Fig.4.4). Only the magnetic <50 fraction of Ceniceros shows Se/Te similar to CI chondrites (Fig.4.4 and 4.7b). In all other components and calculated bulk rocks these ratios are substantially higher than in CI chondrites (Fig.4.4 and 4.7b). The behavior of Te in the two L chondrites is different. In QUE 97008 it correlates well with Se and S and shows predominantly chalcophile behavior in all components (Fig.4.7a and b). In contrast in Ceniceros, Te is decoupled from S and Se in magnetic components compared to other components. In the NM and SM components of Ceniceros, form a straight data array at high Se/Te (indicating that troilite in Ceniceros contains little Te), whereas Se/Te in the three metal fractions is lower and highly variable (Fig.4.7b). The variations in Se/Te among the components of Ceniceros indicate that Te preferably partitioned into metal (Fig.4.7b, 4.5a, b). Results from heating experiments at low pressures on homogenized powder of Krymka (L3) and chemical equilibrium calculations suggest that in the ordinary chondrite environment, Te should be highly mobile and volatile compared to Au, Se and S when temperature exceeds 600 °C (Ikramuddin et al., 1977a, b; Schaefer and Fegley, 2009). From these considerations, it follows that the depletion of Te compared to Se and S may be explained by volatilization during metamorphic heating. However these are unequilibrated meteorites, hence they never experienced high temperature metamorphism. In Ceniceros, Te shows a very similar size dependent behaviour like the HSE (Fig.4.5), which suggests that the predominantly siderophile behaviour of Te, acquired before accretion, has been preserved. Evaporation of Te would have resulted in random variations of Te in all components, not only in the magnetic fractions of Ceniceros. The linear correlation of Te and Se defined by components and different grain size fractions in QUE 97008 (Fig.4.7b) likely would not have survived substantial late element losses by evaporation. These observations and the S-Se systematics discussed in the previous chapter are difficult to reconcile with the notion that significant amounts of Te were lost during parent body metamorphism.

More significant evaporative loss of Te compared to Au, Se and S during metamorphic heating would also imply that ordinary chondrites of higher petrologic type should be more depleted in Te than highly unequilibrated chondrites. There is no evidence for larger Te depletions in the ordinary chondrites of higher metamorphic grades (Takahashi et al., 1978). In this study, the bulk rock of QUE 97008 (L3.05) shows 2.5 x higher Te abundances compared to

Ceniceros (L3.4), however, if we exclude the sulfide clast from Ceniceros then QUE 97008 has higher abundances of *all* volatile elements than Ceniceros. This difference may simply reflect sample heterogeneity or intrinsically higher abundances of volatile elements in components of the former. Similar Te-HSE systematics in the components also indicates that Te loss during terrestrial weathering is not a likely scenario (Fig.4.7e).

The element systematics suggests that the Te depletion in the components of both meteorites is independent of the different geochemical behavior in the rocks and that Te depletion must have occurred before accretion of the components. Several different models and processes may explain the depletion of Te, from the precursors of L chondrite components before accretion.

(1) Te depletion may simply reflect fractional condensation and the loss of a Te rich component from the region where L chondrite precursors were formed. This seems unlikely to be the case for all ordinary chondrites, because if Te was mostly siderophile, loss of Te must have occurred together with the loss of Fe metal from L and LL chondrite precursors. However, H chondrites also show Te depletion compared to S and Se (Case et al., 1973; Binz et al., 1976; Wai and Wasson, 1977) therefore; loss of Te by a simple fractional condensation process does not provide a universal explanation for Te loss from the ordinary chondrite formation region. The HSE carriers in the nonmagnetic fractions are depleted in Pd compared to other HSE. Formation of Pd, Te and Bi alloys and separation of these alloys due to fractional condensation could be envisioned as has been observed in R chondrites by Bischoff et al. (2011). However there is no evidence for the existence of telluride phases in UOC matrix yet, and it is unknown if such phases would have been stable in the relevant range of condensation temperatures.

(2) The depletion of Te relative to S and Se may indicate that the nebular conditions where the L chondrite precursors were formed were different from the canonical solar nebula. Tellurium may have been more volatile than S and Se and thus remained in the gas phase when most of the sulfide and metal condensed and may have been lost with remaining gas (Wai and Wasson, 1977). If Te was more volatile than Se and S, it should have condensed at lower temperature than Se and S and should be mainly hosted by sulfides (Schaefer and Fegley, 2009), which may be the case in QUE 97008, but not in Ceniceros (Fig.4.7b). In Ceniceros most Te is present in metal. The higher condensation temperature of Fe-Ni metal (Lodders, 2003) than FeS and the siderophile to partly siderophile behavior of Te are inconsistent with the notion that Te may be more volatile than S and Se. Changes in the volatility of Te can only be reconciled with its behavior in the L chondrites if the siderophility of Te was inherited from melting, evaporation and recondensation processes during chondrule formation. In any case, the data shows that the chemical affinity and condensation temperature of Te may be highly variable and may be affected by the composition of residual gas from condensation or evaporation processes.

4.7 Summary and conclusions

Inverse relationships between HSE abundances and grain size suggest that the HSE (also predominantly Te in Ceniceros) preferentially partitioned into Fe-Ni metal in magnetic components. Metal-sulfide-silicate partitioning likely occurred before accretion of the components. Solid metal-liquid metal partitioning is of limited importance as it cannot explain the observed HSE systematics among the components.

The variation of $^{187}Os/^{188}Os$ in the components of Ceniceros follows the order $^{187}Os/^{188}Os_{NM} < {}^{187}Os/^{188}Os_{SM} < {}^{187}Os/^{188}Os_{M}$ (also Pd/Ir show similar behavior). This systematic difference may reflect slight differences in the partitioning of Re, Pd, Os and Ir in different components or the volatility-controlled loss of Re and Pd compared to other HSE from the HSE carriers in nonmagnetic components. As in H chondrites (Horan et al., 2009), unequilibrated HSE carriers (Fe-Ni metal) with different HSE patterns are observed in L chondrite components. One carrier is characterized by CI chondritic ratios of refractory HSE and slightly higher Rh/Ir, Pd/Ir and Au/Ir. The smooth depletion of Pd, Au and Te with respect to Ir in the second HSE carrier phase is may have formed by fractional condensation. The latter carrier is more refractory and condensed before the full condensation of moderately volatile elements. The depletion of refractory elements ($T_{condensation} > 1400$ K) compared to moderately volatile elements such as Mn ($T_{condensation} < 1400$ K) is the effect of fractional condensation and loss of earlier formed refractory phases.

The loss of tellurium was inherited from precursor dust and may have occurred due to melting of the metal grains and subsequent changes in the volatility of Te relative to Se and S. Loss of Fe in the form of low temperature metal may also explain the Te depletion compared to HSE in magnetic components, but it is less likely, because H chondrites also show similar Te depletion (Case et al., 1973; Binz et al., 1976; Wai and Wasson, 1977). Tellurium and to some extent Se are more siderophile than sulfur (Rose-Weston et al., 2009), indicating incorporation of these elements into S bearing metal during high-temperature processing before accretion of the components.

The depletion of Se and S may have occurred either during melting and evaporation in the process of chondrule formation or from precursor gas due to incomplete condensation of volatiles or both. Tellurium is less volatile than Se and S under canonical solar nebula conditions (Lodders, 2003). The depletion of Te compared to S and Se by volatility-controlled processes requires that Te was more volatile than S and Se at some stage of the formation of L chondrites. The observed depletion suggests that condensation or evaporation of Te occurred significantly below 600 K and thus most Te should have condensed into FeS, which is not observed in Ceniceros. If Te is more refractory than S and Se (Lodders, 2003), then it must have been lost due to melting and evaporation of metal. Similar siderophility and the size dependent behaviour of Te and the HSE (Fig.4.5) support this scenario. Tellurium abundances in L3 bulk rocks vary by a factor of 7 or

more (Keays et al, 1971; Case et al., 1973, Binz et al., 1976; Kaczaral et al., 1989) indicate that heterogeneous recondensation of evaporated Te on metal grains might be the reason for Te depletion in the ordinary chondrites. The observed depletion requires that Te should be either significantly more refractory or more volatile than the conditions of troilite recondensation. The depletion of Te can be explained if re-condensation of Te on metal was inhibited by condensed troilite rims around metal and thereby the loss of remaining volatile siderophiles either in gas phase or dust alloys. The sulfide rims around the metal grains in matrix may represent such scenario.

The studied L chondrite aliquots show little evidence for an influence of terrestrial weathering on the S-Se-Te systematics of the components and bulk rocks. On the other hand, measured Re/Os show large random variations in QUE 97008, indicating that terrestrial weathering may partially reset the ^{187}Re-^{187}Os systematics of metal bearing components in chondrites. Rhenium is the element in this study that is most strongly affected element by terrestrial weathering of Fe-Ni metal.

The existence of components with distinct Re*/Os, Pd/Ir and Au/Ir in unequilibrated chondrites from different chondrite classes (this work, Horan et al., 2009; Kadlag and Becker a, submitted) indicates heterogeneous sampling of nebular material. These HSE carriers have undergone siderophile element fractionation processes before accretion and never equilibrated after accretion. The different origin of such components in unequilibrated chondrites should be considered in chronological studies using short-lived nuclides and in studies of isotopic variations of nucleosynthetic origin.

Acknowledgements: We are grateful to The Natural History Museum, London for providing Ceniceros (off BM.1990, M6) and Smithsonian National Museum of Natural History, Washington D.C. for providing the piece of QUE 97008 and an aliquot of the Smithsonian Allende standard powder (USNM 3529, Split 18, position 1). We thank M. Feth, T. Giebner, K. Hammerschmidt, S. Kommescher and F. Schubring for technical help in the lab. Thanks to F. Mangels and R. Milke for help in obtaining BSE images. This project was funded by DFG-SPP 1385 “The first ten million years of solar system – a planetary materials approach” (Be1820/10-1/2).

4.8 Tables Chapter 4

Table 4.1. Major, minor and trace element abundances of the analyzed components of QUE 97008 and Ceniceros.

Component	Mg (%)	Ca (%)	Cr (%)	Mn (%)	Fe (%)	Co (%)	Ni (%)
QUE 97008							
QUE-NMC	18.4	1.5	0.386	0.274	10.0	0.007	0.07
QUE-NMF	21.5	1.18	0.365	0.266	10.1	0.0069	0.078
QUE-NM > 250	16.7	1.53	0.397	0.373	11.6	0.009	0.13
QUE-M (0-80)	5.1	0.08	0.196	0.107	28	0.101	2.27
QUE-M (80-150)	8.3	0.2	0.294	0.168	37.5	0.133	2.67
QUE-M(150-200)	8.6	0.2	0.308	0.169	33.8	0.104	2.17
QUE-M(200-250)	7.9	0.37	0.296	0.170	38	0.137	2.49
QUE-M(>250)	9.7	0.54	0.249	0.193	27	0.088	1.72
QUE-SM_(0-80)	13.7	0.82	0.2627	0.1993	10.4	0.014	0.27
QUE-SM_MIX (80-150)	14.8	1.45	0.217	0.283	14.7	0.031	0.65
QUE-SM_CHD (80-150)	18.2	1.56	0.388	0.350	11.6	0.008	0.13
QUE-SM_MTX (80-150)	12.1	1.42	0.158	0.247	15	0.050	1.10
QUE-SM_(150-200)	15.3	1.3	0.375	0.279	20.0	0.042	0.90
QUE-SM(200-250)	14.4	0.79	0.369	0.266	18.9	0.039	0.81
QUE-SM(>250)	15.0	1.44	0.539	0.315	17.1	0.030	0.69
QUE-Chondrules-C	16.2	1.5	0.279	0.265	9.1	0.011	0.23
QUE-MTS	14.9	1.3	0.300	0.265	16.7	0.098	2.21
QUE-cal bulk	13.6	1.04	0.341	0.251	18.7	0.047	0.96
Ceniceros							
Ce-NM (0-50)	12.4	0.79	0.1952	0.1910	11.6	0.0047	0.072
Ce-NM (>50)	12.9	0.88	0.1912	0.1874	9.6	0.0041	0.057
Ce-M (0-50)	10.1	0.38	0.642	0.192	75	0.23	16.4
Ce-M (50-200)	7.4	0.46	0.285	0.1265	35	0.127	5.9
Ce-M (< 200)	6.9	0.29	0.1710	0.1118	40	0.25	2.9
Ce-SM (0-50)	13.0	0.96	0.2743	0.2061	13.3	0.0092	0.214
Ce-SM (50-200)	13.1	1.08	0.3145	0.2135	15.5	0.014	0.41
Ce-SM (<200)	13.4	1.17	0.2956	0.2241	12.4	0.0086	0.23
Ce-sulfide clast	2.1	0.07	0.068	0.0336	36	0.015	0.29
Ce-chondrules	9.4	0.87	0.219	0.1956	8.4	0.003	0.100
Ce-cal bulk	10.1	0.79	0.219	0.1655	15.7	0.035	0.61
L3-bulk[a]	15.1	1.3	0.34	0.25	21	0.05	1.1
CI-Bulk[b]	9.7	0.86	0.21	0.160	19.440	0.052	1.02

Values are given in w/w %.

[a] Bulk rock data of L3 chondrites from Yasinskaya and Osadchij (1973), Kirova et al. (1975), Graham et al. (1976), Fitzgerald (1979), Haramura et al. (1983), Jarosewich (1984, 1990), Fulton and Rhodes (1984), Fredriksson et al. (1986), Hewins et al. (1988), Graham (1993), Yanai et al. (1995).

[b] CI chondrite data from Lodders (2003).

Table 4.2. HSE, chalcogen element abundances and osmium isotopic composition of the analyzed components of QUE 97008 and Ceniceros.

Component	Weight (mg)	Re (ng/g)	Os (ng/g)	Ir (ng/g)	Ru (ng/g)	Pt (ng/g)	Rh (ng/g)	Pd (ng/g)	Au (ng/g)	Te (µg/g)	Se (µg/g)	S (mg/g)	$^{187}Os/^{188}Os$	$^{187}Re/^{188}Os$	Δ_{Os}
QUE 97008															
QUE-NMC	9	0.4	6.4	6.5	15.0	21.2	3.6	5.9	2.3	0.00	0.29	3.94	0.117 ± 0.017	0.33 ± 0.14	-38
QUE-NMF	27	0.6	7.2	7.8	14.1	14.4	2.3	5.9	4.1	0.02	0.39	2.53	0.120 ± 0.006	0.40 ± 0.04	-66
QUE-WMGT250	15	2.0	22.5	23.0	35.8	48.4	7.8	29.0	7.4	0.05	1.09	6.14	0.124 ± 0.003	0.42 ± 0.03	-39
QUE-M (0-80)	11	96.8	1288	1118	1720	2396	385	1790	779	0.97	20.3	48.2	0.12910 ± 0.00009	0.362 ± 0.001	53
QUE-M (80-150)	16	95.3	1165	1015	1546	2144	341	1443	419	0.91	19.3	43.9	0.12883 ± 0.00008	0.3942 ± 0.004	25
QUE-M(150-200)	11	83.6	1016	878	1353	1910	306	1255	409	0.87	17.9	41.9	0.1293 ± 0.0001	0.3968 ± 0.0007	28
QUE-M(200-250)	9	98.9	1208	1108	1682	2241	381	1380	275	0.94	16.6	37.7	0.1283 ± 0.0001	0.3948 ± 0.0008	20
QUE-M(>250)	15	82.7	856	787	1328	1776	300	1074	207	0.77	15.2	35.3	0.1338 ± 0.0001	0.4659 ± 0.0006	18
QUE-SM_(0-80)	53	10.8	102	91	143	193	31	145	37	0.20	4.83	11.9	0.1278 ± 0.0002	0.869 ± 0.002	-359
QUE-SM_MIX (80-150)	19	22.8	175	165	257	359	71	319	85	0.50	10.3	22.7	0.1267 ± 0.0003	0.627 ± 0.002	-179
QUE-SM_CHD (80-150)	15	2.1	21	21	32.4	52	8	44	9	0.05	1.22	5.08	0.126 ± 0.003	0.478 ± 0.026	-73
QUE-SM_MTX (80-150)	8	32.8	283	265	425	629	112	559	117	0.78	17.5	35.9	0.1274 ± 0.0005	0.559 ± 0.004	-119
QUE-SM_(150-200)	33	27.8	253	233	362	500	84	422	163	0.50	12.1	27.9	0.1279 ± 0.0001	0.530 ± 0.001	-91
QUE-SM(200-250)	43	26.6	260	233	365	503	79	413	143	0.50	11.0	25.4	0.1278 ± 0.0001	0.493 ± 0.001	-63
QUE-SM(>250)	15	21.6	218	210	356	510	105	354	90	0.40	11.1	25.7	0.1283 ± 0.0003	0.478 ± 0.003	-46
QUE-Chondrules-C	19	8.1	117	115	177	234	37	133	78	0.09	2.85	9.68	0.1260 ± 0.0005	0.332 ± 0.004	46
QUE-MTS	5	113.2	548	648	1573	2251	372	1290	593	0.22	5.30	19.7	0.1751 ± 0.0004	1.000 ± 0.003	10
QUE-cal bulk	1038	38.5	385	357	594	812	140	542	140	0.47	10.1	24.8	0.1297 ± 0.0007	0.539 ± 0.005	-80
Ceniceros															
Ce-NM (0-50)	11	3.1	81	68	87	101	17	27	15	0.00	7.72	18	0.122 ± 0.001	0.181 ± 0.009	125
Ce-NM (>50)	68	2.2	41	34	49	56	9	17	9	0.04	4.07	9	0.1235 ± 0.0004	0.256 ± 0.003	80
Ce-M (0-50)	1	353.3	3105	3073	5240	7769	1223	6496	1514	2.10	18.6	35	0.1314 ± 0.0003	0.500 ± 0.003	-33
Ce-M (50-200)	14	194.5	2161	2439	3732	5353	829	3821	1854	0.85	20.1	42	0.12985 ± 0.00007	0.3738 ± 0.0002	51
Ce-M (< 200)	21	138.5	1662	1415	2162	2965	488	1910	923	0.84	12.5	28	0.13091 ± 0.00007	0.4016 ± 0.0002	40
Ce-SM (0-50)	19	12.3	208	195	286	322	52	130	44	0.16	8.41	20	0.1264 ± 0.0003	0.286 ± 0.002	86
Ce-SM (50-200)	36	16.6	263	243	355	430	72	226	123	0.18	11.5	26	0.1268 ± 0.0001	0.304 ± 0.001	76
Ce-SM (<200)	40	10.3	155	135	181	209	39	119	57	0.09	6.01	14	0.1242 ± 0.0002	0.319 ± 0.001	38
Ce-sulfide clast	7	13.4	227	197	294	379	66	227	86	0.34	118.7	274	0.1275 ± 0.0007	0.285 ± 0.006	97
Ce-chondrules	6	4.9	27	26	38	54	13	91	28	0.07	2.00	4	0.136 ± 0.006	0.880 ± 0.05	-291
Ce-cal bulk	506	26.1	334	303	451	599	99	380	180	0.19	13.5	31.0	0.1261 ± 0.0005	0.336 ± 0.004	44
Ce-Bulk[a]		36.4	491.5	465	726	909		591					0.12922	0.35655	59
		43.9	546.9	506	779	1021		659					0.12964	0.38695	39
L3 bulk[b]		39.1	491	464	684	965		630	156	0.19	9.1	24.4			
CI chondrites[c]		36.6	449.5	418.4	627.2	871.4	130	567.4	148.8	2.31	21.30	54.1	0.12641	0.40073	-4.35

Reported uncertainties on isotopic ratios are 2σ. Deviation of the Os isotopic composition (Δ_{Os}) from the IIIA iron meteorite isochron is calculated by the following relation.

$\Delta_{Os} = (^{187}Os/^{188}Os_{chondrite} - (0.09524+0.07887 \times {}^{187}Re/^{188}Os_{chondrite})) \times 10^4$, where 0.09524 is the $^{187}Os/^{188}Os$ at 4.558 Ga and 0.07887 is the slope of the IIIA iron meteorite reference isochron (Smoliar et al., 1996).

[a] Ceniceros bulk values from Horan et al. (2003) and Walker et al. (2002b).

[b] L3 bulk rock values are from Haramura et al. (1983), Jarosewich (1984, 1990), Fulton and Rhodes (1984), Fredriksson et al. (1986), Hewins et al. (1988), Ebihara (1989), Kaczaral et al. (1989), Kallemeyn et al. (1989), Graham (1993), Wasson et al. (1993), Ebihara and Ozaki (1995), Yanai et al. (1995), Kong and Ebihara (1996), Bhandari et al. (2002) and Horan et al. (2003).

[c] CI chondrite data from Dreibus et al. (1995), Walker et al. (2002b), Lodders (2003), Fischer-Gödde et al. (2010) and Wang et al. (2013).

4.9 Appendix Chapter 4

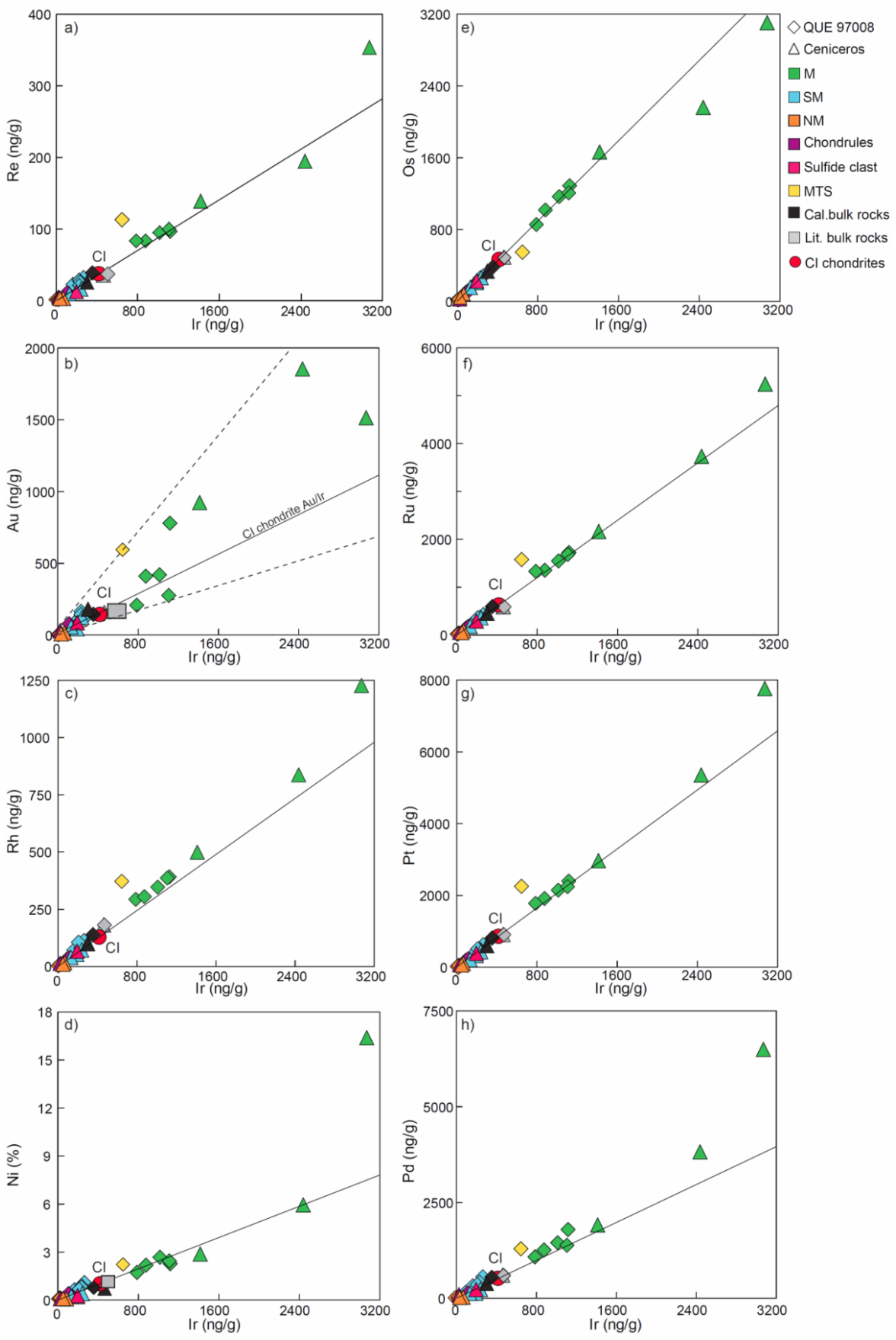

Fig.4.A1. a) Re-Ir, b) Au-Ir, c) Rh-Ir, d) Ni-Ir, e) Os-Ir, f) Ru-Ir, g) Pt-Ir and h) Pd-Ir variation in the components of QUE 97008 and Ceniceros. Components with higher Ni/Co (< 50 fraction of Ceniceros and MTS fraction of QUE 97008, see Fig.4.1 g) show higher HSE/Ir (except Os/Ir), likely due to their preferred partitioning into taenite compared to Ir (see text).

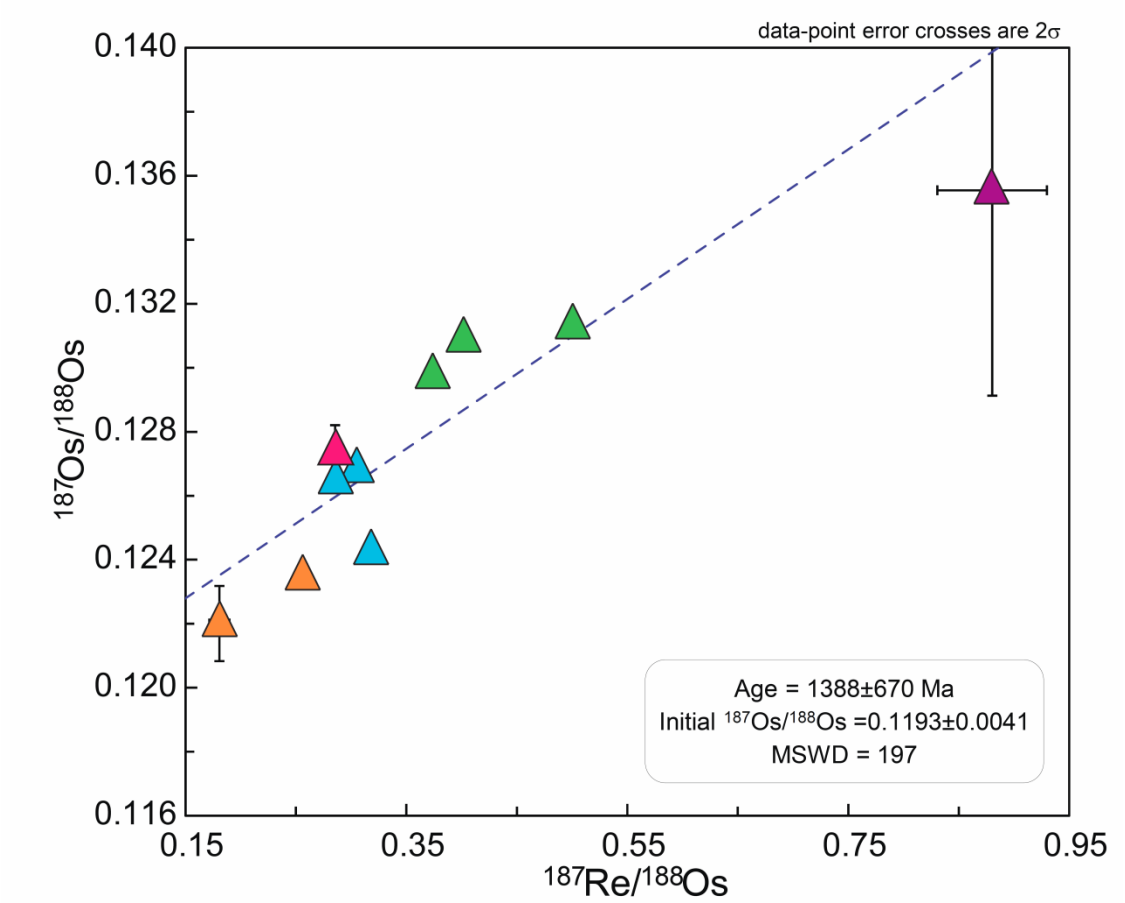

Fig.4.A2. An internal errorchron defined by components of Ceniceros, calculated by using Isoplot 4 (Ludwig, 2008), yields an age of 1388 ± 670 Ma, presumably indicating late alteration on the L chondrite parent body.

Chapter 5

Origin of highly siderophile and chalcogen element fractionations in the components of unequilibrated H and LL chondrites

5.1 Abstract

Osmium isotopic compositions, abundances of highly siderophile elements (HSE: platinum group elements, Re and Au), chalcogen elements (Te, Se and S), major and minor elements were analyzed in the mechanically and magnetically separated components of WSG 95300 (H3.3, find) and Parnallee (LL3.6, fall). Magnetic components are 160-20x enriched in HSE and chalcogen compared to the nonmagnetic fractions, mostly enriched in the smallest grain size fraction. Significant deviation of components of WSG 95300 from the 4.56 Ga ^{187}Re-^{187}Os isochron were caused by significant redistribution of Re in some components due weathering of metal and coupled behaviour of Au and S are more likely resulted from. HSE abundance patterns show that at least three different types of HSE carriers are present in the components of WSG 95300 and Parnallee, CI chondritic HSE ratios, lower than CI chondritic Pd/Ir and Au/Ir with unfractionated refractory HSE and higher HSE/Ir and HSE/Ru than in CI chondrites. These differences between components clearly indicate the loss of refractory HSE carrier phases before accretion of the components. Tellurium abundances correlate with Pd and are decoupled from S, suggesting that most Te partitioned into metal during the last high-temperature event. Tellurium is depleted in all components compared to CI chondrite normalized Se and S abundances, except for the fine magnetic fractions. The depletion of Te is likely associated with the high temperature history of the metal precursors of the H and LL chondrite components and is independent of the metal loss event that depleted LL chondrites in siderophile elements. S/Se is lower than in CI chondrites and the decoupling of these elements in magnetic components suggest the influence of volatility and metal-silicate partitioning on the abundances of the chalcogens. The influence of terrestrial weathering on chalcogen element systematics is negligible.

5.2 Introduction

Components of unequilibrated ordinary chondrites, such as chondrules of variable size, Fe-Ni metal grains and fine grained matrix may have formed at different physicochemical conditions, perhaps in different spatial environments of the solar nebula (Scott and Krot, 2003). The observed mineralogy of silicates, sulfides and metal phases in chondrite components mostly reflects secondary processing of nebular dust with remaining gas or processes on the meteorite parent bodies (Scott et al., 1981; Nagahara, 1984; Hutchison et al., 1987; Alexander et al., 1989; Krot et al., 1997; Lodders, 2003). One of the key questions in understanding the genesis of chondrites is concerned with possibility of whether or not the different components formed from common dust precursors and inherited their compositional differences from secondary processing in the nebula or, less likely, on the meteorite parent bodies. In carbonaceous chondrites, chemical complementarity of major and trace elements between the matrix and chondrules suggests that their precursors were derived from common reservoirs of similar material (Bland et al., 2005; Hezel and Palme, 2008, 2010). Similar REE and siderophile element patterns of metal and sulfide phases indicate that the chondrules and matrix from unequilibrated ordinary chondrites share the genetic relationship (Kong and Ebihara, 1997; Kong et al., 2000). What fraction of metal and sulfides from ordinary chondrites share similar or complementary trace element fractionations is not clear.

Previous work has shown that the distribution of the highly siderophile (HSE: Re, Os, Ir, Ru, Pt, Rh, Pd and Au) and chalcogen (Te, Se and S) elements between different components containing metal and sulfide phases is useful to understand the origin and evolution of the precursors of chondrite components (Rambaldi, 1976; Kong and Ebihara, 1997; Walker et al., 2002b; Archer et al., 2014). Metal in chondritic meteorites was interpreted to have formed either by direct condensation from nebular gas into refractory metal alloys or Fe-Ni metal alloys (Lodders, 2003, Campbell et al., 2005), desulfurization of Fe bearing sulfides (Hewins et al., 1997), or reduction of Fe^{2+} in silicates (Connolly et al., 2001). The siderophile and chalcophile element abundances in metal, sulfides and silicate phases reflect the origin of the metal and partitioning processes controlled by geochemical affinity of the elements and the state of chemical equilibrium between phases.

Carrier phases with different HSE compositions were observed in previous work on components of ordinary chondrites (Chou et al., 1973; Rambaldi, 1977b; Rambaldi et al., 1978; Grossman and Wasson, 1985; Kong et al., 1995; Kong and Ebihara, 1997; Humayun and Campbell, 2002; Campbell and Humayun, 2003; Horan et al., 2009; Kadlag and Becker c, submitted). Besides carrier phases with CI like HSE compositions, other phases that display depletions and enrichments of the slightly volatile HSE Pd and Au must be present in the components of ordinary, carbonaceous and enstatite chondrites (Horan et al., 2009; Archer et al.,

2014; Kadlag and Becker a, b and c, submitted). Because the Pd depleted component occurred in all classes of chondrites studied so far, the question arises whether this component was inherited from fractional condensation in the solar nebula or originated in secondary high temperature processes such as evaporation during chondrule formation or nebular loss of volatile element enriched metal?

In comparison to carbonaceous chondrites, ordinary and enstatite chondrites are characterized by systematically higher Re/Os ratios, also small differences in Re/Os between different groups of ordinary chondrites were observed (Walker et al., 2002b; Fischer-Gödde et al., 2010). In case of correlated $^{187}Os/^{188}Os$ and Re/Os, as in most chondrite bulk rocks and metal rich components, these differences were established either in the early solar nebula or during the early metamorphic and aqueous alteration processes on the meteorite parent body (Becker et al., 2001; Walker et al., 2002b; Brandon et al., 2005a; Rankenburg et al., 2007; Horan et al., 2009; Fischer-Gödde et al. 2010; Archer et al., 2014). Bulk rocks that are shifted from the 4.56 Ga reference isochron may have been affected by later open-system behavior (e.g., because of terrestrial weathering in case of meteorite finds), however, the causes of these shifts were not always clear (Becker et al., 2001; Kadlag and Becker c, submitted).

Different chondrite classes show systematic differences in their chalcogen element abundances (Case et al., 1973; Wai and Wasson, 1977; Dreibus et al., 1995; Lodders, 2003). Because of a significant depletion of Te, the ordinary and EH chondrites show lower Te/Se compared to CI chondrites (Kallemeyn and Wasson, 1986; Wai and Wasson, 1977; Kadlag and Becker a and c, submitted). The processes responsible for the depletion of Te in ordinary and enstatite chondrites may be similar or specific to local processes in the solar nebula or on the meteorite parent bodies, and the details remain to be evaluated (Wai and Wasson, 1977; Schaefer and Fegley, 2009).

In the quest to understand the influence of nebular and parent body processes on the origin of chondrite components, we have analyzed the ^{187}Re-^{187}Os systematics, HSE, chalcogen and major elements in the components of enstatite, carbonaceous and ordinary chondrites (Kadlag and Becker, a, b and c, submitted). In the present contribution we are reporting the results of a systematic mass balance study of the ^{187}Re-^{187}Os systematics, HSE, chalcogen, major and minor element abundances (Mg, Ca, Cr, Mn, Fe, Ni and Co) in mechanically and magnetically separated components of the unequilibrated ordinary chondrites WSG 95300 (H3.3, find, weathering grade A/B, Benoit et al., 2002) and Parnallee (LL3.6, fall, Dodd et al., 1967; Case et al., 1973; Chou and Cohen, 1973; Laul et al., 1973; Binz et al., 1976; Evensen et al., 1978; Afiattalab and Wasson, 1980). The objective of present study is to constrain the fractionation processes of HSE and chalcogen elements, which occur in the solar nebula and meteorite parent bodies in the components of the unequilibrated ordinary chondrites

5.3 Sample characterization and sample preparation

WSG 95300 is low-metamorphic-grade H chondrite contains organic matter, presolar grains and pristine chondrule textures which could not preserved at high temperatures indicates its highly unequilibrated nature (Lofgren and Le, 2002; Alexander et al., 2009). Parnallee is unequilibrated LL chondrite which extensively studied for its mineralogy and petrology, containing exceptionally large chondrule (~4 cm), and show low degree of aqueous alteration (Binns, 1967; Bridges et al., 1997; Lewis and Jones, 2014). Rock pieces of Parnallee (weight ~ 1g) and WSG 95300 (weight ~ 0.6 g) were broken into fragments to separate components. Chondrules of different size were separated from these fragments using plastic tweezers. An ~1 mm sized sulfide clast was found in Parnallee. A part was used for HSE and chalcogen element analysis and remaining material was embedded in epoxy resin and polished for petrological inspection. A description of the inclusion is given in Fig.5.A1 of the appendix.

The remaining material was separated into three different grain size fractions: less than 80 µm (<80), 80-200 µm (80-200) and a coarse fraction greater than 200 µm (>200). All size fractions were further divided into magnetic (M), slightly magnetic (SM) and nonmagnetic (NM) fractions depending on their magnetic strength using a hand magnet.

5.4 Analytical Techniques

All samples were digested in reverse aqua regia in a High Pressure Asher system (HPAS). Chemical separation of the HSE and chalcogen elements from other elements was carried out by chemical separation procedures established in the Geochemistry laboratories at Freie Universität Berlin (Fischer-Gödde et al., 2010; Wang et al., 2013; Kadlag and Becker a, submitted). The isotope dilution method was used to obtain precise concentrations of Re, Os, Ir, Ru, Pt, Pd, Te, Se and S. Concentrations of the monoisotopic elements Rh and Au were determined by internal calibration using intensities of ^{101}Ru and ^{193}Ir, respectively. Concentrations of the major and minor elements Mg, Ca, Cr, Mn, Fe, Co and Ni were determined by an external calibration method. Different dilutions of the digested Smithsonian Allende standard powder were used as a matrix-matched calibration standard, to correct the matrix effect.

Concentrations of all elements except Os were measured on the Element XR ICP-MS at Freie Universität Berlin. Precise isotopic compositions and concentration of Os was determined on the Triton TIMS at Freie Universität Berlin, using negative thermal ionization mass spectrometry. Detailed procedures of sample digestion, methods for chromatographic separation of elements and measurement protocols were described in Fischer-Gödde et.al. (2010); Wang et al. (2013) and Kadlag and Becker a, (submitted) and references therein.

5.4.1 Analytical blanks

Total procedure blanks were determined with each set of digested samples. Average values of total procedure blanks for 12 digestions over the duration of the study are: Re = 1.9 ± 0.8 pg, Os = 1 ± 1 pg, Ir = 2 ± 1 pg, Ru = 2 ± 2 pg, Pt = 40 ± 30 pg, Rh = 9 ± 7 pg, Pd = 40 ± 20 pg, Au = 2 ± 2 pg, Te = 30 ± 10 pg, Se = 2.8 ± 0.5 ng and S = 7.6 ± 0.8 μg. Total procedure blanks contribute less than 5% for most of the components. Ruthenium, Rh and Pd required higher blank corrections in case of chondrules, nonmagnetic fractions and the sulfide clast, but not more than 15%.

5.4.2 Repeatability of Standards

Repeatability of in-house HSE and chalcogen element standards during ICPMS measurements at the Freie University Berlin was within 3% (2σ) over the period of analysis. Repeatability of the oxygen and mass fractionation corrected $^{187}Os/^{188}Os$ ratio of the University of Maryland Os standard solution measured on the Triton N-TIMS is 0.11381 ± 0.00004 (n=8, 2σ) for Faraday cup measurements and 0.11392 ± 0.00038 (n=11, 2σ) for electron multiplier measurements over the duration of a year.

5.5 Results

5.5.1 Major element abundances

Major and minor element concentrations in the separated components of WSG 95300 and Parnallee and in the calculated bulk rocks are given in Table 5.1. Average bulk rock values of LL3 and H3 chondrites from the published literature are given for comparison (Wiik, 1966; Jarosewich, 1966, 1984, 1990; Kharitonova, 1969; Gopalan et al., 1976; Haramura et al., 1983; Fulton and Rhodes, 1984; MacPherson et al., 1993; Yanai et al., 1995). The distribution of element abundances in different grain size fractions of magnetic and slightly magnetic fractions are shown in Fig. 5.1 and 5.2. Substantial variations in the abundances and ratios of major elements are observed in the components. Mg shows linear correlations with Mn and Ca in most components (Fig.5.3a and b) and is enriched in slightly magnetic and nonmagnetic fractions compared to other components indicating the predominance of olivine and pyroxene in these components.

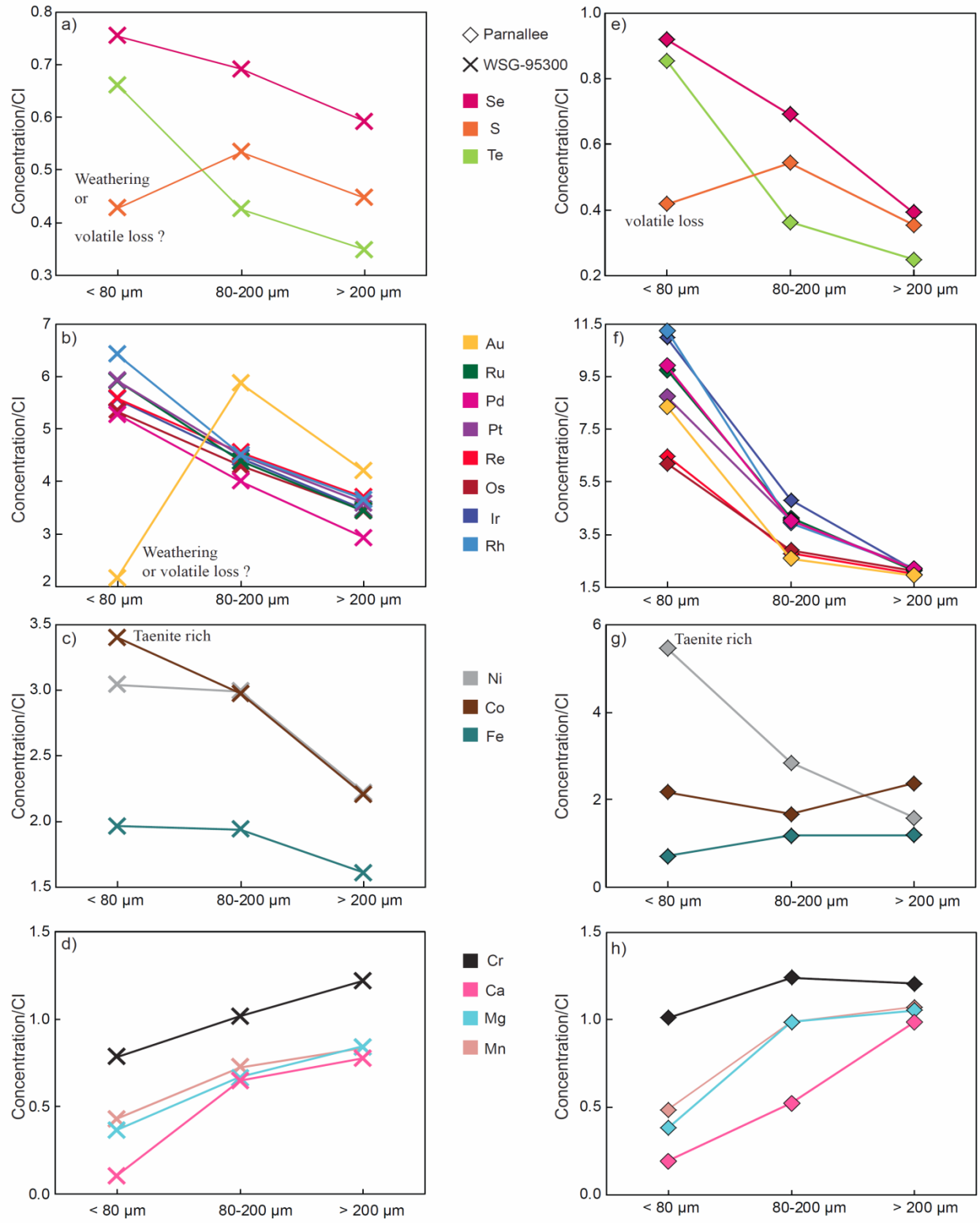

Fig.5.1. CI normalized abundances of a) S, Se and Te, b) HSE, c) Fe, Ni and Co, d) Cr, Ca, Mg, Mn and Fe of magnetic components of WSG 95300 are plotted against grain sizes. Abundance variation of e) S,Se and Te, f) HSE, g) Fe, Ni and Co, h) Cr, Ca, Mg, Mn and Fe in magnetic components of Parnallee with grain sizes. Au is decoupled from HSE in magnetic components of WSG 95300 and show similar size dependent behavior like S, more likely due to the terrestrial weathering. Differences in the HSE and Ni and Co variation are more likely resulted during kamacite-taenite exsolution of metal.

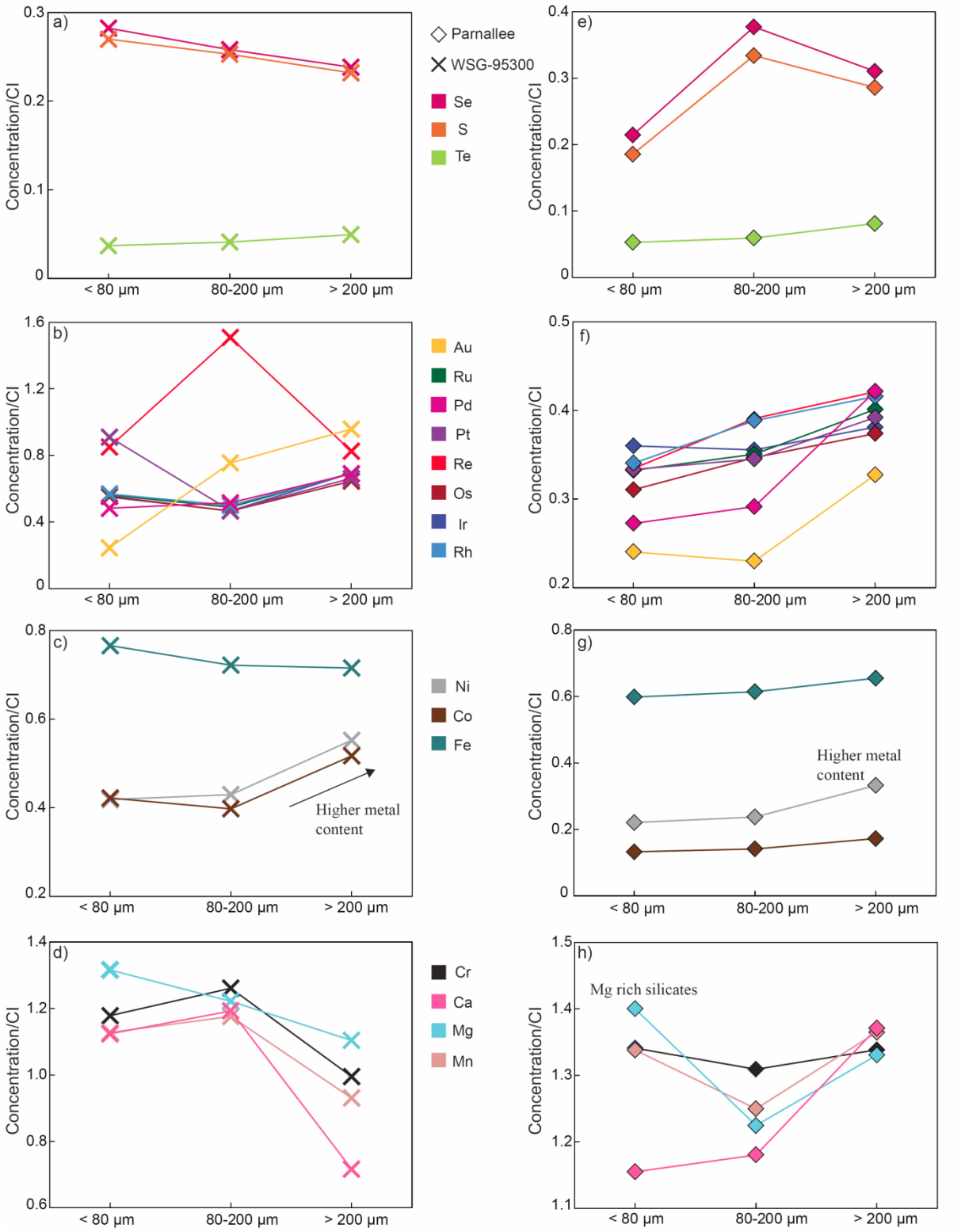

Fig.5.2. CI normalized abundances of a) S, Se and Te, b) HSE, c) Fe, Ni and Co, d) Cr, Ca, Mg, Mn and Fe of slightly magnetic components of WSG 95300 are plotted against grain sizes. Abundance variation of e) S,Se and Te, f) HSE, g) Fe, Ni and Co, h) Cr, Ca, Mg, Mn and Fe in slightly magnetic components of Parnallee with grain sizes. Rhenium and Au are decoupled from other HSE in components of WSG 95300, more likely due to the redistribution during terrestrial weathering.

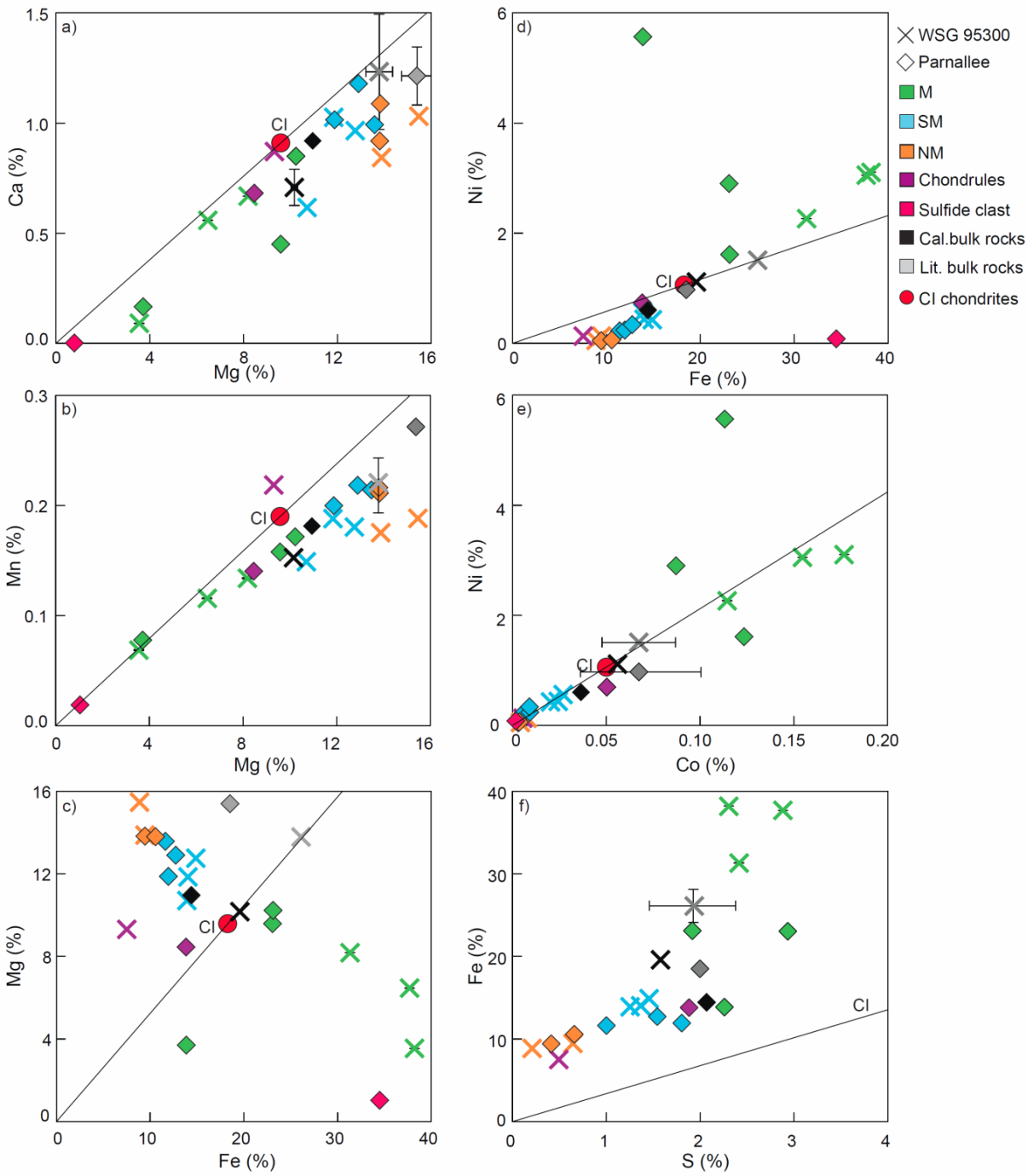

Fig.5.3. Variation of major elements a) Ca-Mg, b) Mn-Mg, c) Mg-Fe, d) Ni-Fe, e) Ni-Co and f) Fe-S in the components of WSG 95300 and Parnallee. Crosses: WSG 95300, Diamonds: Parnallee. M: magnetic, SM: slightly magnetic and NM: nonmagnetic. CI chondrite data is shown by the red circle. Black symbols show the calculated bulk rock values from the mass balance of all analyzed components. Gray symbols show the literature bulk rock data for Parnallee and H3 chondrites (sources are mentioned in the caption of Table 5.1 and 5.2). Significant variations in the abundances of major elements in the components are observed, which is mainly due to the different proportion of metal, silicate and sulfide phases in the components. Linear variation between Ca, Mn and Mg (a and b) indicate the dominance of single lithophile phase in the components. Variation in the abundances of siderophile elements Fe, Ni and Co (d and e) in the components is more likely resulted from metal-silicate-sulfide partitioning and kamacite-taenite exsolution. The Fe/S plot shows the dominance of metal over sulfide in magnetic components.

Magnesium abundances vary inversely with Fe (Fig.5.3c). Chondrules, slightly magnetic and nonmagnetic fractions show higher Mg/Fe than CI chondrites whereas magnetic fractions and the sulfide clast show Mg/Fe lower than CI chondrites (Fig.5.3c). With the exception of magnetic components and the sulfide clast in Parnallee, other components show linear relationships between Ni and Fe (Fig.5.3d). Magnetic components of both meteorites show Ni/Fe higher than in CI chondrites, whereas other components show Ni/Fe lower than in CI chondrites (Fig.5.3d). Ni/Co ratio is nearly CI chondritic in most components, except for the magnetic components of Parnallee, which show substantial scatter in Ni/Co and deviations from CI chondrites (Fig.5.3e). All components show Fe/S higher than in CI chondrites (Fig.5.3f). The Fe-S variations indicate mixing between two end members, a high-Fe/S end member (magnetic fractions) and other components with lower Fe/S. This difference in Fe/S is likely due to the presence of Fe and S in different phases with different Fe/S. Magnetic components show a higher metal/sulfide ratio compared to other components, which is reflected in higher Fe/S in the magnetic components (Fig.5.3f).

5.5.2 ^{187}Re-^{187}Os systematics

The concentrations of Re and Os, Re* (initial Re concentrations calculated from the measured Os isotopic compositions), $^{187}Re/^{188}Os$, $^{187}Os/^{188}Os$ and Δ_{Os} (the deviation of $^{187}Os/^{188}Os$ from solar system initial Os isotopic composition, a detailed definition is given in the caption of Table 5.2) values of analyzed components are listed in Table 5.2. The data are displayed in a ^{187}Re-^{187}Os isochron diagram in Fig.5.4. Components of Parnallee deviate less from the 4.56 Ga reference isochron (Smoliar et al., 1996) compared to components of WSG 95300. All components of WSG 95300 have systematically higher $^{187}Re/^{188}Os$ and $^{187}Os/^{188}Os$ compared to the similar components of Parnallee. Note that, the bulk rock data on H3 and LL3 chondrites (Walker et al., 2002b; Fischer-Gödde et al., 2010) shows that some H3 chondrites have higher $^{187}Os/^{188}Os$ and $^{187}Re/^{188}Os$ compared to the LL3 chondrites. The component data in Fig.5.4 mirrors this behaviour.

Magnetic components of both meteorites show the smallest deviations from the isochron compared to other components. However, magnetic components from Parnallee and WSG 95300 show substantial differences in their correlated $^{187}Os/^{188}Os$ and $^{187}Re/^{188}Os$, respectively. These differences between magnetic components of the meteorites are mainly responsible for the differences in $^{187}Os/^{188}Os$ and $^{187}Re/^{188}Os$ of the bulk rocks of Parnallee and WSG 95300 (Fig.5.4, Table 5.2). Chondrule fractions of both meteorites are plotted on the isochron, but show substantial differences in their Os isotopic composition. The chondrule fraction of WSG 95300 shows ~ 8% higher $^{187}Os/^{188}Os$ compared to the chondrule fraction of Parnallee. Slightly magnetic and nonmagnetic components of Parnallee are only slightly offset from the 4.56 Ga isochron but show resolvable differences in $^{187}Os/^{188}Os$. Slightly magnetic and nonmagnetic fractions of WSG 95300 and the sulfide clast of Parnallee show significant deviation from the

4.56 Ga isochron, which affects the calculated bulk rock values (Fig.5.4). Therefore the calculated bulk rock values of WSG 95300 display a greater deviation from the isochron compared to the bulk rock values of Parnallee.

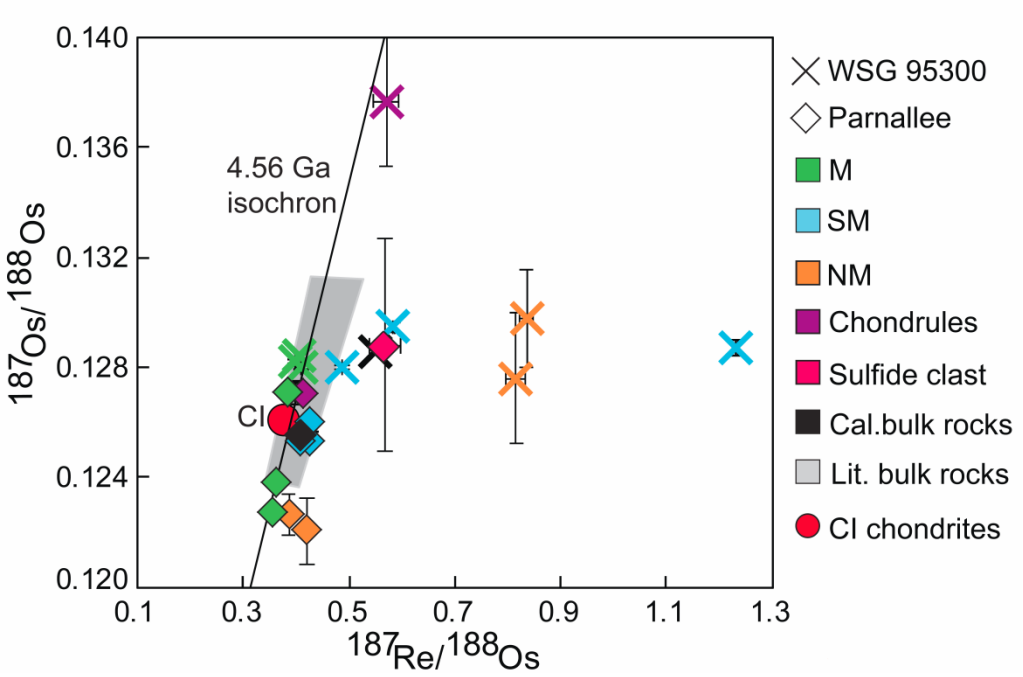

Fig.5.4. ^{187}Re-^{187}Os isochron diagram of components of WSG 95300 and Parnallee. 4.56 Ga isochron from Smoliar et al. (1996). Literature bulk rock data of H3 and LL3 chondrites (Walker et al., 2002b; Fischer-Gödde et al., 2010) is shown by the gray shaded area. Large deviation of slightly magnetic and nonmagnetic fractions of WSG 95300 from isochron is most likely effect of the Re mobilization during terrestrial weathering. Nonmagnetic, slightly magnetic and sulfide clast fractions of Parnallee show slight deviation from the isochron, more likely resulted from the oxidation on the meteorite parent body. Magnetic components of both chondrites show substantial variation in ^{187}Os/^{188}Os and ^{187}Re/^{188}Os more likely reflect the fractionation process in the solar nebula.

5.5.3 HSE abundances

HSE abundances of analyzed components and calculated bulk rock values calculated from the mass balance of all components are listed in Table 5.2. Also shown are average bulk rock data for Parnallee, and average bulk rock data for H3, LL3, and CI chondrites from the literature (Brearley et al., 1989; Ebihara, 1989; Ebihara and Ozaki, 1995; Smith et al., 1977; Hermann and Wichtl 1974; Rieder and Wänke 1969; Delisle et al., 1989; Wasson et al., 1993; Kimura et al., 2002; Chen et al., 1998; Kallemeyn et al., 1989; Case et al., 1973; Binz et al., 1976; Bischoff et al., 1993; Horan et al., 2003; Walker et al., 2002b; Dreibus et al., 1995 and Fischer-Gödde et al., 2010). The HSE abundances of calculated bulk rocks agree with literature bulk rock values within 20 %.

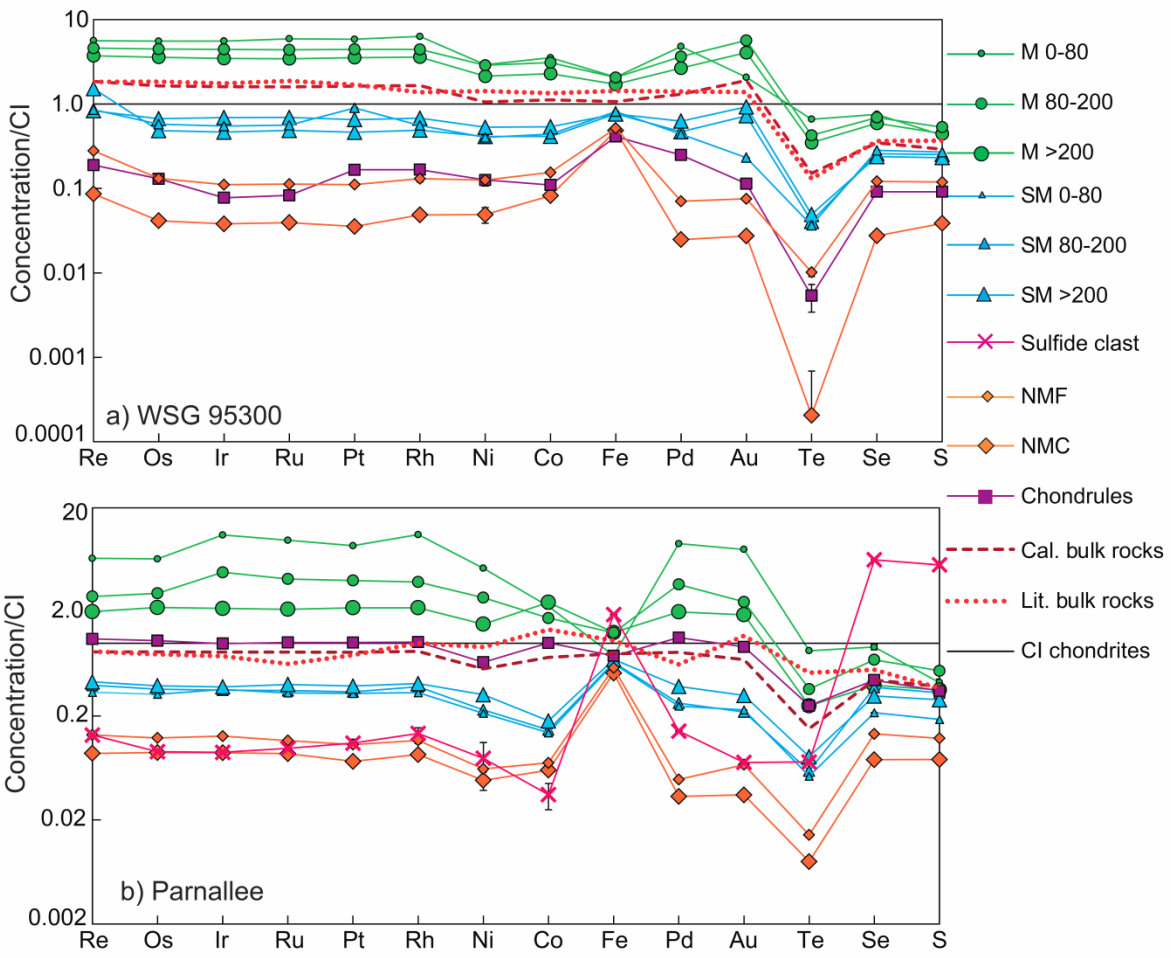

Fig.5.5. CI normalized abundances of HSE, chalcogen and Ni, Co and Fe in components of the WSG 95300 and Parnallee. Elements are ordered from left to right in increasing order of volatility, assuming the 50% condensation temperature in the solar nebula by Lodders (2003). Different symbol size of same components represents the different grain size fractions (numbers on the legend show the particular grain sizes). Sources of literature data are mentioned in captions of Table 5.1 and 5.2. HSE abundances in magnetic components show inverse size dependent variation. Magnetic components of Parnallee show higher HSE abundances compared to the magnetic components of WSG 95300.

Magnetic fractions of both meteorites are enriched in the HSE compared to other components as well as CI chondrites (Fig.5.5, Table 5.2). As in previous studies of ordinary chondrites (Rambaldi, 1977b; Rambaldi et al., 1978; Horan et al., 2009), HSE Abundances of magnetic components (except Au in WSG 95300, which is enriched in the intermediate size fraction) show inverse relationships with the grain size (Fig.5.1). In case of WSG 95300 magnetic components show unfractionated abundance patterns (Fig.5.5a) of the HSE (except Au in the smallest grain size fraction, which is depleted compared to refractory HSE). Magnetic fractions of Parnallee show slightly fractionated abundance patterns which are enriched in Ir and depleted in Re and Os compared to other HSE (Fig.5.5b). Other components of both meteorites display lower HSE abundances and higher measured Re/Os ratios compared to CI chondrites and magnetic components (Fig.5.4 and 5.5).

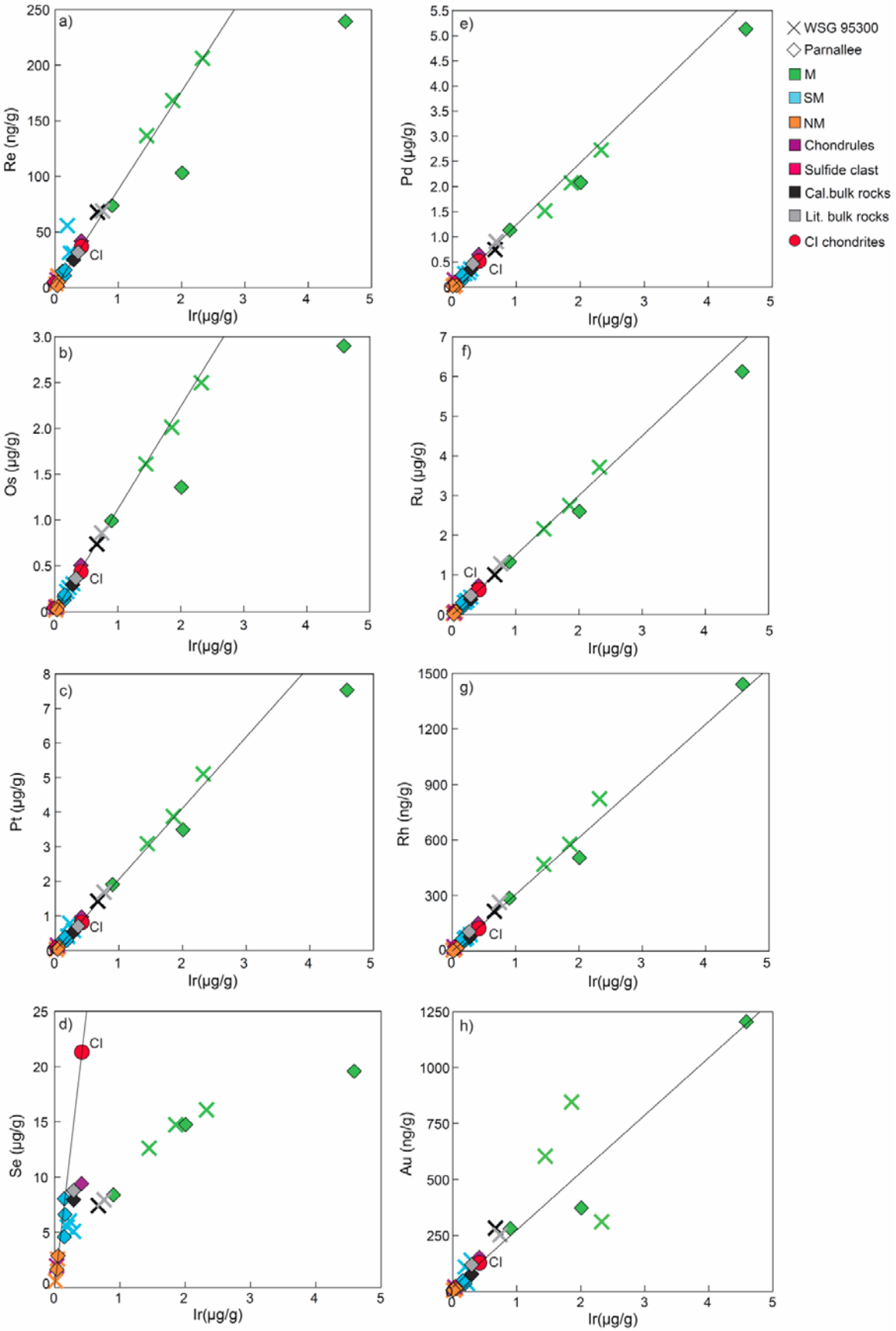

Fig.5.6. a) Re-Ir, b) Os-Ir, c) Pt-Ir, d) Se-Ir, e) Pd-Ir, f) Ru-Ir, g) Rh-Ir and h) Au-Ir variation in the components of WSG 95300 and Parnallee. All HSE (except Au) shows linear correlation with Ir and CI chondritic ratios of HSE/Ir in most components of WSG 95300, except scatter Re/Ir in some components of WSG 95300. Magnetic components of Parnallee shows lower than CI chondritic ratios of HSE/Ir.

Major and minor element variations (Fig.5.3) suggest that HSE abundance patterns of slightly magnetic components represent a mixture of the HSE abundance patterns of nonmagnetic and magnetic end members (Figs.5.5, 5.6). CI normalized abundances of Pd and Au in nonmagnetic fractions of both meteorites are depleted compared to other HSE (Fig.5.5). The chondrule fraction of WSG 95300 and the sulfide clast of Parnallee show depletions in Ru and Ir compared to other HSE whereas the chondrule fraction of Parnallee shows nearly CI chondritic ratios and abundances of the HSE.

5.5.4 Chalcogen abundances in components

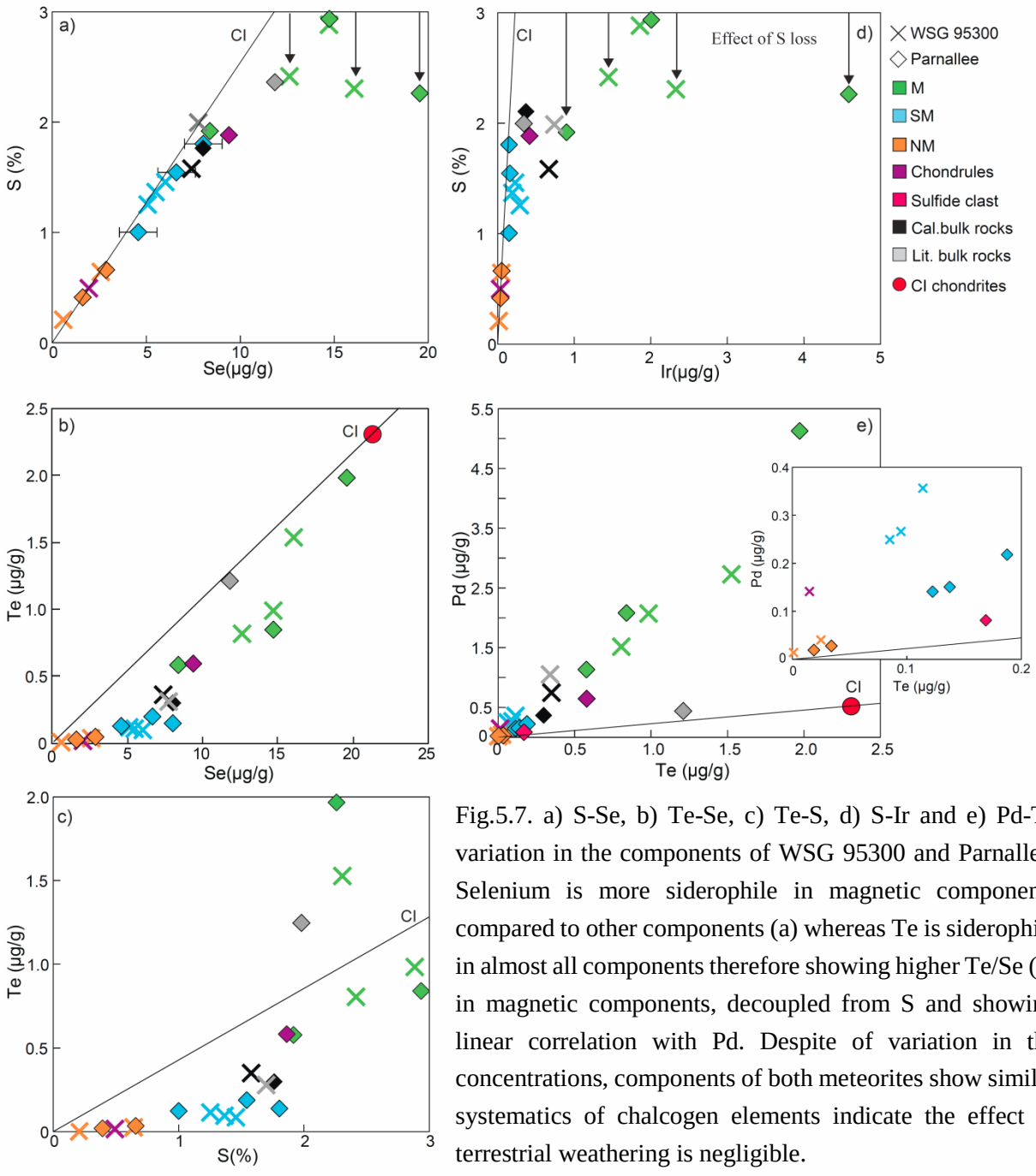

Fig.5.7. a) S-Se, b) Te-Se, c) Te-S, d) S-Ir and e) Pd-Te variation in the components of WSG 95300 and Parnallee. Selenium is more siderophile in magnetic components compared to other components (a) whereas Te is siderophile in almost all components therefore showing higher Te/Se (b) in magnetic components, decoupled from S and showing linear correlation with Pd. Despite of variation in the concentrations, components of both meteorites show similar systematics of chalcogen elements indicate the effect of terrestrial weathering is negligible.

Chalcogen element abundances in the components, calculated bulk rocks and average bulk rocks from the literature (Biswas et al., 1981; Kallemeyn et al., 1989; Bischoff et al., 1993; Brearley et al., 1989; Smith et al., 1977; Hermann and Wichtl 1974; Delisle et al., 1989; Dennison and Lipschutz 1987; Wasson et al., 1993; Kimura et al., 2002 and Wang et al., 2013) are listed in Table 5.2. The chalcogen elements are depleted in nearly all components (except for the sulfide clast in Parnallee) compared to CI chondrites and normalized HSE abundances (Fig.5.5 and 5.7). The sulfide clast of Parnallee mainly consists of fine-grained troilite (FeS) as the main phase (and minor olivine, orthopyroxene, plagioclase and chromite, Fig.5.A1), and thus shows strong enrichment of S and Se, compared to CI chondrites and other components (Fig.5.5). Most components and the calculated bulk rock values show a CI normalized abundances in the order Se > S > Te, which is inconsistent with the equilibrium nebular condensation sequence (Lodders, 2003).

With the exception of the magnetic components, all other components of both meteorites show a linear correlation between S and Se abundances and approximately CI chondritic S/Se (Fig.5.7a). Selenium and S are decoupled in magnetic components and show lower S/Se ratio than CI chondrites. All components show systematically lower Te/Se ratio than CI chondrites, with magnetic components having higher Te/Se compared to other components (Fig.5.7b). The systematics of Te/S is similar to Te/Se. Tellurium and S are decoupled in magnetic components and show a linear correlation in other components (Fig.5.7c). Tellurium correlates with Pd in the components (Fig.5.7e), although the data distribution indicates different mixing relations between nonmagnetic and magnetic components in the meteorites.

5.6 Discussion

5.6.1 The influence of mineral assemblages on element distribution between separated components

All separated components in this study are mixtures of variable proportions of silicates, sulfides and metal, which is reflected in the major element composition of the components (Table 5.1, Fig.5.3). Nonmagnetic components are dominated by silicates (< 2 wt. % troilite, Fig.5.3f), magnetic components are dominated by metal and contain minor proportions of sulfides (< 9 wt. % troilite, Fig.5.3f) and silicates. Slightly magnetic components are mixture of these two end members (Fig.5.3). The variation of Fe with S shows mixing of two components, nonmagnetic, slightly magnetic and chondrule fraction show a similar Fe/S ratio whereas magnetic components have a higher Fe/S ratio because of a higher proportion of metal. Calculated bulk rock values are a mixture of these two components (Fig.5.3f and 5.5b). Because S is exclusively present into sulfides, the variable in this case is the Fe. FeS is the major phase of sulfide clast of Parnallee (Fig.5.3 and 5.A1). Components of both meteorites show similar relationships for major and

minor elements (Fig.5.3) indicating that the influence of terrestrial weathering on these elements in WSG 95300 must be negligible.

Linear mixing relationships between Ca, Mn and Mg indicate the presence of variable proportions of pyroxenes, olivine and perhaps glass in all components (Fig.5.3a and b). The different geochemical behaviour of Fe reflect in the variation in the Mg/Fe in the components, $Mg/Fe_{silicate\ rich} > Mg/Fe_{sulfide\ rich} > Mg/Fe_{metal\ rich}$. The major element systematics indicates that the chondrule fraction of WSG 95300 contains a larger proportion of silicates compared to the chondrule fraction of Parnallee (Fig.5.3). Differences in the Ca/Mg and Mn/Mg of the nonmagnetic components of both meteorites indicate that nonmagnetic fractions of WSG 95300 have a higher other silicate minerals /olivine ratio compared to the nonmagnetic fraction of Parnallee (Fig.5.3a and b). Calculated bulk rock values of major and minor elements in Parnallee and WSG 95300 are 20-30% lower compared to average bulk rock compositions of H3 and LL3 chondrites from the literature (Wiik, 1966; Jarosewich, 1966, 1984, 1990; Kharitonova, 1969; Gopalan et al., 1976; Haramura et al., 1983; Fulton and Rhodes, 1984; MacPherson et al., 1993; Yanai et al., 1995). These differences may either result from mineralogical heterogeneities in different bulk rocks or from incomplete dissolution of phases in our study. In the latter case pyroxenes are the most likely candidates as they may not dissolve completely in aqua regia. However, previous work on enstatite chondrites that applied the same techniques did not observe systematic shifts in major elements compared to literature data (Kadlag and Becker a, submitted). In any case, because the main host phases of the HSE and chalcogen elements, metal and sulfides, dissolve completely in aqua regia, abundances of these elements should not be affected significantly by undissolved silicates.

In ordinary chondrites Fe-Ni metal is the main host phase of the siderophile elements Ni and Co (Larimer and Anders, 1970). Some magnetic components show large deviations of their Ni/Co from the CI chondritic value (Fig.5.3e). Differences in metal-silicate partitioning of Ni and Co (Schmitt et al., 1989) may explain the variable Ni/Co in the components, however, most other components show nearly CI chondritic Ni/Co (Fig.5.3e). Large deviations in Ni/Co and Ni/Fe occur in magnetic components of Parnallee (Fig.5.3e and 5.8). The differences in Co, Ni and Fe abundances and ratios of magnetic fractions may also have been caused by the exsolution of kamacite and taenite in the metal. Higher Ni/Co and Ni/Fe in fine grained magnetic fractions of Parnallee indicate a higher taenite/kamacite ratio compared to coarse grained fractions (Fig.5.3e, 5.1 and 5.8). Magnetic components of WSG 95300 are closer to CI chondrites in their Ni/Co ratio (Fig.5.3 e and 5.8). The different Ni/Co between magnetic components of the meteorites may be a reflection of the slightly different higher metamorphic grades.

5.6.2 ^{187}Re-^{187}Os systematics

Components of WSG 95300 have higher $^{187}Os/^{188}Os$ compared to similar components from the Parnallee (Fig.5.4), which likely represents the cause for the slightly higher $^{187}Os/^{188}Os$ of the bulk rocks of H3 chondrites compared to some LL3 chondrites (Walker et al., 2002b; Fischer-Gödde et al., 2010). The systematic differences in the bulk rocks suggest that the differences between the components were caused by processes that occurred before their accretion into chondrite parent bodies and not by parent body alteration processes. The lower $^{187}Os/^{188}Os$ in the magnetic components of Parnallee compared to the magnetic components of the WSG 95300 may reflect the loss of Re enriched phases from the precursors of the magnetic components of Parnallee due to fractional condensation in the solar nebula.

Some components of both chondrites show deviations from the 4.56 Ga isochron (Fig.5.4, Table 5.2), indicating that the ^{187}Re-^{187}Os systematics was disturbed more recently. The calculated bulk rock values deviated from the isochron indicate that the process involve in the disturbance of Re-Os systematics was more likely open system redistribution of Re or, less likely, Os. Slightly magnetic and nonmagnetic components of WSG 95300 show larger deviations from the isochron compared to the similar components of Parnallee (Fig.5.4). Because WSG 95300 represents a meteorite find, the different behaviour compared to Parnallee, a meteorite fall, must be attributed to a disturbance of the ^{187}Re-^{187}Os system during terrestrial weathering, which was also suggested in previous Re-Os studies of chondrites (Becker et al., 2001; Walker et al., 2002b; Brandon et al., 2005a; Rankenburg et al., 2007; Horan et al., 2009; Fischer-Gödde et al. 2010; Archer et al., 2014; Kadlag and Becker, a and c, submitted). Some slightly magnetic and nonmagnetic fractions and the sulfide clast in Parnallee also show a resolvable deviation from the isochron, suggesting that the process of disturbance of the ^{187}Re-^{187}Os system occurred on the parent body of LL3 chondrites. Processes such as aqueous alteration, metasomatism or heating of HSE carrier phases by impact events under more oxidized conditions on the chondrite parent body (Palme et al., 1998; Becker et al., 2001; Walker et al., 2002b; Lewis and Jones, 2014) might be responsible for the redistribution of Re in the components.

To conclude the major processes which are responsible for the variation in $^{187}Re/^{188}Os$ and $^{187}Os/^{188}Os$ in the components are the early loss of Re-Os alloys from the precursors of HSE carriers of LL3 chondrites, for instance due to fractional condensation followed by later small-scale redistribution of Re on the parent body. Components of WSG 95300, which have low Re and Os abundances were strongly affected the terrestrial weathering, which induced Re mobilization in these components.

5.6.3 HSE fractionation processes

Components of both meteorites display significant differences in the abundances of the HSE (Fig.5.5). Four principle types of HSE abundance patterns have been observed: 1) abundance patterns with nearly CI chondrite like HSE ratios 2) Abundance patterns with higher Re/Os ratio than in CI chondrites. In components where the higher Re/Os are correlated with $^{187}Os/^{188}Os$, these compositions reflect primordial fractionations, such as in the chondrule fraction of WSG 95300 and in magnetic components of WSG 95300 that show little deviation from the 4.56 Ga isochron (Fig.5.4). In other components of the high Re/Os reflect secondary redistribution process (e. g., terrestrial weathering). 3) Depleted CI normalized Pd and Au abundances compared to other HSE, e.g. in nonmagnetic fractions of both meteorites. iv) CI normalized Ir and Ru abundances are lower than other HSE, e.g. in the chondrule fraction of WSG 95300 and in the sulfide clast of Parnallee. In the following HSE fractionations in different components will be discussed.

5.6.3.1 HSE carriers in magnetic fractions

The abundance of Fe-Ni metal in Parnallee is lower compared to WSG 95300 (Fig.5.3, Table 5.1), however absolute abundances of HSE in the magnetic components of Parnallee are higher than in magnetic components of WSG 95300 (Fig.5.5, Table 5.2). The differences in the HSE abundances in the magnetic components of both chondrites reflect the differences in the metal component of the meteorites. These differences were inherited from local nebular heterogeneities in the formation region of the different classes of the ordinary chondrites.

Unfractionated abundance patterns of the magnetic fractions of WSG 95300 (Fig.5.5) indicate that the HSE were fully condensed from a gas of solar composition into Fe-Ni metal (Rambaldi et al., 1979; Lodders, 2003; Campbell et al., 2003). Small magnetic size fractions of Parnallee are depleted in Re and Os compared to other HSE, indicating that Re-Os enriched refractory alloys may have been lost from metal precursor phases in Parnallee. The process may have been fractional condensation before most of the Fe and Ni condensed. Other processes such as metal–silicate and solid metal-liquid metal partitioning may also fractionate Re/Os, however, it would be more difficult to fractionate Os and Ir from each other (O'Neill et al., 1995; Chabot and Jones, 2003; Chabot et al., 2006). Another process that should be evaluated is the partitioning of HSE during the exsolution of kamacite and taenite that may occur during cooling of metal. Fine grained (< 80 and 80-150 μm) size fractions of magnetic components from Parnallee show higher Ni/Co compared to CI chondrites (Figs.5.3e and 5.5), indicating that these fractions are taenite rich. Coarse grained magnetic fractions are enriched in kamacite as their Ni/Co is lower. However, the HSE abundance patterns of these fractions are not complementary to each other. Taenite rich, fine grained magnetic fractions show higher CI normalized Ir abundances compared to all other HSE (Fig.5.5 and 5.6), whereas coarse grained magnetic fractions are almost unfractionated compared to CI chondrites. Previous studies of ordinary chondrite metal suggest

that during Fe-Ni metal exsolution processes, Ir and Os will not be fractionated from each other, even in highly equilibrated chondrites (Rasmussen et al., 1988; Hsu et al., 1998; Campbell and Humayun, 2003; Ash et al., 2007). Therefore the component rich in Ir and depleted in Re and Os was more likely produced during earlier high-temperature processing (e. g., during nebular condensation).

5.6.3.2 HSE carriers in nonmagnetic fractions

Nonmagnetic components of both meteorites are depleted in Pd and Au compared to other HSE (Fig.5.5). Depletions of Pd were also observed in previous work on H chondrite components (Rambaldi et al., 1978; Horan et al., 2009). Several processes may account for the Pd depletion. In case of Parnallee, Ni and Co in nonmagnetic components show similar depletions like Pd and Au and compared to refractory HSE (Fig.5.5). The higher Fe abundances compared to Ni, Co and HSE in nonmagnetic fractions are mostly a mineralogical effect from the higher Fe contribution from sulfides and silicates in these fractions (Fig.5.3c, d and f). However, Pd and Au are highly siderophile. Therefore, the Pd depletion compared to refractory HSE may be because of incomplete condensation of Pd into Fe-Ni metal, or evaporation of Pd, Ni, Co and Fe from the HSE carriers of nonmagnetic fractions of WSG 95300 and Parnallee, scenario as discussed for the components of H chondrites by Horan et al. (2009). Although, it is still difficult to distinguish between fractional condensation and evaporation processes, it is worth pointing out that Pd-Au depleted HSE carrier phases have been identified in the nonmagnetic fractions of carbonaceous chondrites, EH chondrites and all ordinary chondrites groups (Archer et al., 2014; Horan et al., 2009; Kadlag and Becker a, b, and c, submitted).

5.6.3.3 HSE carriers in the chondrules and sulfide clast

The chondrule fraction of Parnallee have higher metal content compared to the chondrule fraction of WSG 95300 (Fig.5.3d and e), which is also reflected in the differences in the HSE abundances in these fractions. Unfractionated and nearly CI chondritic abundances of the HSE in the chondrule fraction of Parnallee indicates that no fractionation of the HSE occurred during the heating, and presumed evaporation of chondrule metal. The chondrule fraction of WSG 95300 and sulfide clast of Parnallee show very similar HSE abundance patterns (Fig.5.5). The HSE abundance pattern of the chondrule fraction of WSG 95300 is highly fractionated and complex (Fig.5.5a). The higher Re/Os compared to other components and depleted Ir and Ru are complementary to Ir and Ru enriched patterns observed in the fine grained magnetic fractions of Parnallee (Fig.5.5b). These patterns for refractory HSE most likely represent nebular processing before accretion.

5.6.4 Chalcogen element systematics

With the exception of the sulfide clast in Parnallee, abundances of chalcogen elements in all components are depleted compared to CI chondrites, (Fig.5.5 and 5.7). The higher volatility of these elements compared to other elements analyzed in the present work is the main cause of the depletion (Lodders, 2003). Calculated abundances of the HSE in bulk rocks of Parnallee and WSG 95300 differ by almost 50% (Figs.5.5, 5.6). In contrast, chalcogen elements show only slight differences in their abundances in calculated bulk rocks, which is mainly due to the differences in chalcogen element abundances in magnetic components and chondrule fractions (Fig.5.7). This behavior indicates that the components of H and LL chondrites would have acquired their inventory of volatile elements from a similar source and that any losses, for instance resulting from evaporation during chondrule formation were minor. Because of the similar volatility of these elements, the stronger depletion of Te compared to Se and S in most components is of particular interest, as it is also typical for bulk rocks of ordinary chondrites and also occurs in components and bulk rocks of enstatite chondrites (Binz et al., 1974; Wai and Wasson, 1977; Hertogen et al., 1983; Kallemeyn and Wasson 1986; Kaczaral et al., 1988; Kong et al., 1997).

5.6.4.1 Te loss during nebular or parent body processes?

One important property of the abundance patterns is the depletion of Te compared to Se in all components (Fig.5.5 and 5.7). This observation is not consistent with the simple nebular condensation sequence (Lodders, 2003) of elements where Te is more refractory compared to Se. Tellurium is depleted in the components of all H, L and LL chondrites (this study and Kadlag and Becker c, submitted). Here, we will evaluate the role of different processes which may be responsible for the depletion of Te.

We rule out terrestrial weathering as an important process for the depletion of Te on the basis of the preserved correlations between Te, Pd and Se (Fig.5.7b and e) and the insolubility of TeO_2 in water (Greenwood and Earnshaw, 1984). Results from all components in this study show that although Te is depleted, it shows a linear correlation with Pd (Fig.5.7e) and thus clearly behaves as a siderophile element, which is also suggested by the decoupling of Te from S in most components (Fig.5.7c). The Te depletion could be explained by fractional condensation of metal and loss of Te into the gas phase from the ordinary chondrite formation region. However, this scenario appears inadequate to explain the lower Te/Se than CI chondrite in magnetic components, because gas-solid separation should also remove volatile Se and S (Fig.5.7a). Fractionation of Te from Se and S by volatility-controlled processes may be viable if the volatility of the elements change because of changes in the physicochemical environment such as total pressure or gas composition (Wai and Wasson, 1977). The results obtained in this study show that CI normalized Te abundances are lower in calculated bulk rocks compared to S and Se (Fig.5.5 and 5.7), consistent with the calculated volatility sequence Te > S > Se at low pressure

conditions ($p=10^{-6}$ bar) as suggested by Wai and Wasson (1977). However, relative differences in the absolute abundances of these elements are inconsistent with the slight differences in their condensation temperature, e.g. abundances of the Se and S in calculated bulk rocks are nearly 62-65% and 67-70% less than CI chondritic Se and S abundances respectively (Table 5.2). Tellurium abundances in the calculated bulk rocks are 85-87% less than in CI chondrites (Table 5.2). The differences in the condensation temperature of Se, S and Te at lower total pressures are between 36 and 48 K, which is not very different (according to Wai and Wasson, 1977, 50% condensation temperatures at $p=10^{-6}$ bar are 684 K, 648 K and 600 K for Se, S and Te, respectively). Therefore, changes in volatility at lower pressure may not be the only reason for the Te depletion, as we also note changes in the geochemical properties of Te in different groups of chondrites. In the components of ordinary and enstatite chondrites Te behave as more siderophile element whereas in the components of carbonaceous chondrites it is predominantly chalcophile element (Kadlag and Becker a, b, and c, submitted). The combination of changing geochemical behavior and volatility may have played a role in the Te depletion processes.

Several previous studies suggested higher Te loss compared to Se during the thermal metamorphism in meteorite parent bodies (Ikramuddin et al., 1977; Takahashi et al., 1978; Schaefer and Fegley, 2009). The depletion of Te due to metamorphism is thought to occur by evaporative loss of Te and other highly volatile elements with increasing metamorphic temperature. The process requires the loss of a gas phase and sufficient porosity and permeability for the gas to escape to space. However, it is rather unlikely that the linear correlation between Pd and Te would be preserved after Te loss during metamorphism (Fig.5.7e), and thus, we discard this possibility.

Considering all observations, the likely processes that may account for the depletion of Te is the strongly siderophile nature of Te in the components of these two meteorites and a change in the volatility of Te compared to Se and S.

5.6.4.2 S and Se variation in the components

Sulfur and Se both are truly chalcophile elements and condensed into FeS or as FeSe in the solar nebula (Lodders, 2003). In the present study, S and Se are correlating with each other in all, except the magnetic components (Fig.5.7a). All magnetic components have S/Se ratios lower than CI chondrites and Se is decoupled from S in these components (Fig.5.7a). The S-Ir diagram shows similarities with the S-Se diagram (Fig.5.7d). Nonmagnetic and slightly magnetic components show nearly CI chondritic S/Se and S/Ir and a linear correlation between these elements whereas in magnetic components they are decoupled from each other (Fig.5.7d). The Se-Ir diagram (Fig.5.6d) shows that the rocks represent a mixture of two types of components, nearly CI chondritic Se/Ir ratio in nonmagnetic and slightly magnetic components and lower Se/Ir than CI chondrites in magnetic components. The decoupling of Se from S in magnetic components and the correlation of Se with Te and Ir in magnetic components indicate that Se

behaves as a siderophile element in the phases in magnetic components (Figs.5.7a, b and 5.6d). In the case of magnetic components of Parnallee (Fig.5.8a) this conclusion is supported by the correlation of Ni/Co with Se/S, whereas the variation of Se/S in the magnetic components of WSG 95300 is independent of Ni/Co, and thus losses of S due to evaporation or weathering may have a stronger influence on Se/S. Experimentally determined partition coefficients of S, Se and Te show that, the metal-silicate partition coefficients of Se and Te increases with increasing S concentration in metallic liquid (Rose-Weston et al., 2009), thus Te and Se should be more enriched in magnetic components due to higher S abundances compared to other components.

Calculated bulk rock S/Se values of both chondrites are lower than values of CI chondrites (Fig.5.7a, Table 5.2). This may be explained if more S was lost compared to Se during high temperature melting processes in the solar nebula, for instance during chondrule formation. However, the chondrule fraction of WSG 95300 does not show S depletion compared to Se (Fig.5.5 and 5.7a). Another possibility is the evaporative loss of S from sulfides during metamorphism. Parnallee underwent slightly higher grade metamorphic conditions (3.6) and has lower calculated S/Se in its bulk rock compared to WSG 95300 (3.3).

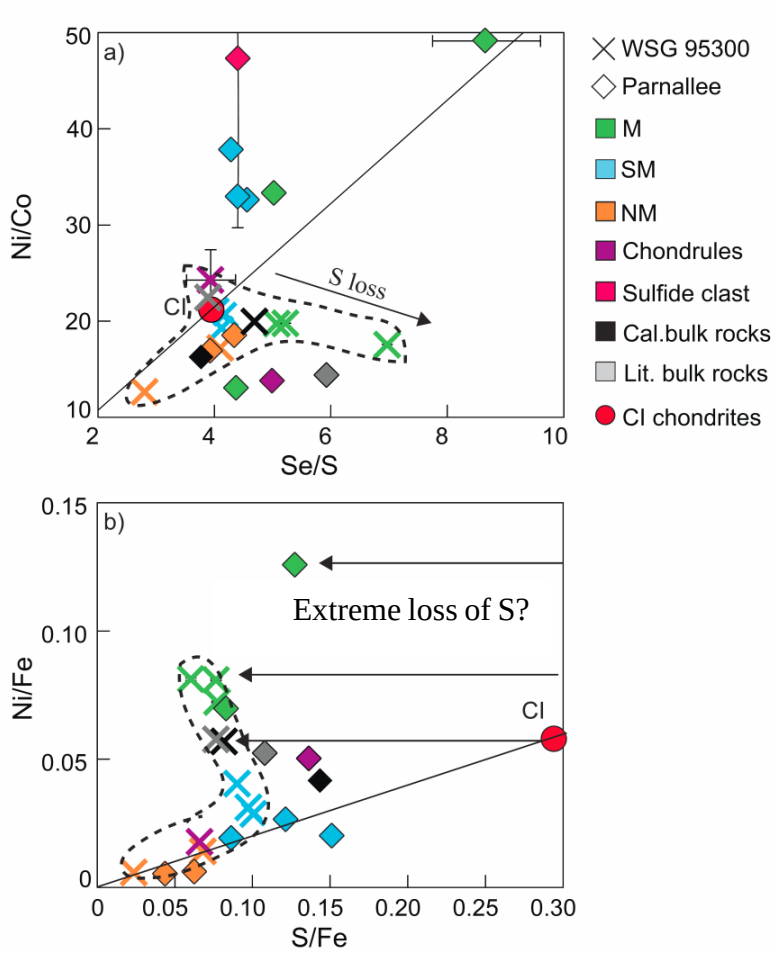

Fig.5.8. a) Ni/Co-Se/S and b) Ni/Fe-S/Fe variation in the components of WSG 95300 and Parnallee. Components of Parnallee show significant variation in the Ni/Co with nearly constant Se/S, more likely due to the exsolution and metal-silicate partitioning. Higher Se/S in the magnetic components of WSG 95300 more likely reflect either high metal-silicate partitioning of Se or loss of S during terrestrial weathering.

However, sulfides in nonmagnetic and slightly magnetic components should be affected equally by S loss during metamorphism, yet they are apparently not as their S/Se are close to the CI chondrite value. We thus favor that evaporation of S occurred preceding the accretion process, presumably during chondrule formation. The nonmagnetic and slightly magnetic components may

derive from dust that has escaped evaporation or may have shielded sulfide components from evaporative losses. Preserved correlations between S and Se in most components and similar systematics of the components in both meteorites (Fig.5.7a) indicates the effect of terrestrial weathering on the S-Se systematics is minor or negligible in case of WSG 95300.

5.7 Conclusions

Early stage loss of refractory HSE alloys from Parnallee is reflected in the depleted Re and Os abundances in magnetic components. The occurrence of HSE carrier phases which are depleted in Pd and Au compared to other HSE reflect the loss of a Pd-Au enriched Fe-Ni metal during high temperature processing, most likely in the nebula. Size dependent HSE abundances in magnetic fractions indicate that the HSE are concentrated in taenite compared to kamacite.

Rhenium is the most mobile element compared to all elements analyzed in this study and the only element which is strongly affected by terrestrial weathering. Components of meteorite falls also show resolvable disturbance of the Re-Os system, which must have occurred by late processes on the parent body. Therefore, ratios such as $^{187}Re/^{188}Os$ or Re/HSE may not be reliable to constrain early solar system processes.

The depletion of Te likely resulted from the highly siderophile nature of Te coupled with a change in the volatility compared to solar conditions. Parent body metamorphism or terrestrial weathering can be ruled out as causes for the Te depletion because under such circumstances correlations between Te and the HSE would not be preserved. The effect of terrestrial weathering on the chalcogen element systematics is negligible, even in the meteorite find. The decoupling of S and Se in magnetic components of the meteorites is either due to the evaporative loss of S or preferred partitioning of Se into the metal.

HSE and chalcogen abundances and ratios in different components of unequilibrated chondrites from different classes show resolvable differences (Kadlag and Becker, a, b and c submitted) indicating that the nebular material that accreted to chondrite parent bodies was composed of different components. The precursors of planetary bodies may have been influenced by these local differences in elemental abundances, thus the refractory and volatile element composition of the building materials of the terrestrial planets may not necessarily reflect the average solar system composition.

Acknowledgements: This project was funded by DFG-SPP 1385 “The first ten million years of solar system – a planetary materials approach” (Be1820/10-1). We are thankful to The Natural History Museum, London for providing specimen of Parnallee (off BM.34792) and Smithsonian National Museum of Natural History, Washington D.C. for providing the piece of WSG 95300 and an aliquot of the Smithsonian Allende standard powder (USNM 3529, Split 18, position 1). We thank K. Hammerschmidt for technical help in the TIMS lab, M. Feth and S. Kommescher for support in clean lab. We are also thankful to F. Mangels, C. Bahr and R. Milke for assistance and guidance in the preparation of thick section and electron microprobe analysis.

5.8 Tables Chapter 5

Table 5.1. Concentrations of major and minor elements in the separated components of WSG 95300 and Parnallee

Component	Mg (%)	Ca (%)	Cr (%)	Mn (%)	Fe (%)	Co (%)	Ni (%)
WSG-95300							
WSG-NMC	15.5	1.0	0.2501	0.1882	8.9	0.0041	0.052
WSG-NMF	13.9	0.8	0.232	0.1751	9.5	0.0077	0.133
WSG-M (0-80)	3.5	0.09	0.164	0.0687	38.2	0.177	3.10
WSG-M (80-200)	6.5	0.6	0.213	0.1157	37.7	0.155	3.05
WSG-M (> 200)	8.2	0.67	0.2558	0.1339	31.3	0.114	2.27
WSG-SM (0-80)	12.8	1.0	0.2474	0.1804	14.9	0.0219	0.43
WSG-SM (80-200)	11.8	1.0	0.2648	0.1881	14.0	0.0207	0.44
WSG-SM (> 200)	10.7	0.62	0.2090	0.1489	13.9	0.0269	0.563
WSG-chondrules	9.3	0.9	0.252	0.2185	7.5	0.0055	0.13
WSG-cal bulk	10.2	0.7	0.2328	0.1525	19.6	0.0559	1.116
H-Bulk[a]	13.7	1.17	0.29	0.22	26.0	0.07	1.47
Parnallee							
Parn-NMC	13.8	1.1	0.2716	0.2112	9.4	0.0030	0.051
Parn-NMF	13.8	0.92	0.2663	0.2123	10.6	0.0035	0.066
Parn-M (0-80)	3.7	0.2	0.212	0.078	14	0.113	5.56
Parn-M (80-200)	9.6	0.5	0.260	0.1579	23.1	0.087	2.90
Parn-M (> 200)	10.2	0.85	0.2532	0.1716	23.1	0.123	1.61
Parn-SM (0-80)	13.6	1.0	0.2816	0.2141	11.6	0.0069	0.225
Parn-SM (80-200)	11.9	1.0	0.2749	0.1999	11.9	0.0073	0.242
Parn-SM (> 200)	12.9	1.2	0.2810	0.2184	12.7	0.0090	0.339
Parn-chondrules	8.5	0.68	0.2185	0.1403	13.8	0.0502	0.69
Parn-sulfide clast	1.0	0.00	0.024	0.0189	41.3	0.0018	0.08
Parn-cal bulk	11.0	0.92	0.2513	0.1812	14.4	0.0364	0.6009
Parn -lit bulk[a]	15.4	1.21	0.38	0.2713	18.5	0.0674	0.97
CI Bulk[b]	9.59	0.91	0.26	0.19	18.28	0.050	1.06

[a] Bulk rock data for H3 chondrites and Parnallee from Wiik (1966), Jarosewich (1966, 1984, 1990), Kharitonova (1969), Gopalan et al. (1976), Haramura et al. (1983) Fulton and Rhodes (1984), MacPherson et al. (1993), Yanai et al. (1995).

[b] Data for CI chondrites from Lodders (2003).

Table 5.2. HSE, chalcogen abundances and osmium isotopic composition of separated components of WSG 95300 and Parnallee and Parnallee

Component	Weight (mg)	Re (ng/g)	Os (ng/g)	Ir (ng/g)	Ru (ng/g)	Pt (ng/g)	Rh (ng/g)	Pd (ng/g)	Au (ng/g)	Te (ng/g)	Se (ng/g)	S (µg/g)	$^{187}Os/^{188}Os$	$^{187}Re/^{188}Os$	Δ_{Os}
WSG-95300															
WSG-NMC	24.2	3	19	16	25	31	6	14	4	1	585	2089	0.128 ± 0.002	0.82 ± 0.02	-320 ±14
WSG-NMF	10.3	10	59	46	71	97	17	40	11	25	2585	6436	0.130 ± 0.002	0.84 ± 0.01	-313 ±10
WSG-M (0-80)	6.7	206	2496	2327	3710	5100	822	2725	308	1525	16065	23057	0.12820 ± 0.00009	0.3978 ± 0.0005	15.9 ± 0.5
WSG-M (80-200)	18.1	168	2010	1858	2748	3873	576	2070	845	983	14722	28836	0.12823 ± 0.00007	0.4031 ± 0.0002	12.0 ± 0.3
WSG-M (> 200)	21.5	136	1610	1447	2153	3089	468	1513	603	804	12611	24153	0.12801 ± 0.00007	0.4084 ± 0.0002	5.6 ± 0.3
WSG-SM (0-80)	22.7	31	259	229	352	783	73	249	34	85	6013	14576	0.1295 ± 0.0002	0.583 ± 0.001	-118 ± 1
WSG-SM (80-200)	19.6	56	218	194	306	403	64	266	108	94	5496	13659	0.12800 ± 0.00009	0.4864 ± 0.0005	-56.0 ± 0.5
WSG-SM (> 200)	51.0	30	302	289	435	570	88	356	138	114	5077	12525	0.1287 ± 0.0003	1.233 ± 0.002	-637 ± 2
WSG-chondrules	6.0	7	58	32	52	145	22	141	17	12	1945	4949	0.138 ± 0.002	0.57 ± 0.02	-25 ± 15
WSG-cal bulk	625	68	736	670	1003	1422	215	742	282	350	7400	15793	0.1286 ± 0.0004	0.551 ± 0.003	-101 ± 2
H3-Bulk[a]		66	805	716	1178	1475	179	785	223	301	7737	19963	0.128 ± 0.002	0.42 ± 0.02	-4 ± 13
Parnallee															
Parn-NMC	35.6	3	40	37	54	64	11	19	5	18	1618	4119	0.1227 ± 0.0007	0.385 ± 0.006	-30 ± 4
Parn-NMF	15.9	5	55	53	73	92	15	28	10	33	2863	6594	0.122 ± 0.001	0.420 ± 0.009	-63 ± 7
Parn-M (0-80)	0.9	239	2898	4578	6120	7514	1437	5128	1185	1955	19560	22609	0.1271 ± 0.0004	0.398 ± 0.003	5 ± 2
Parn-M (80-200)	12.8	103	1357	2009	2595	3490	503	2080	371	838	14741	29351	0.12388 ± 0.00008	0.3656 ± 0.0005	-1.9 ± 0.5
Parn-M (> 200)	39.9	74	990	902	1327	1908	284	1131	279	577	8383	19181	0.12284 ± 0.00006	0.3579 ± 0.0002	-6.2 ± 0.3
Parn-SM (0-80)	28.7	12	145	150	208	287	43	141	34	122	4571	10024	0.1254 ± 0.0003	0.409 ± 0.002	-22 ± 2
Parn-SM (80-200)	26.1	14	162	148	220	297	50	151	32	137	8033	18037	0.1254 ± 0.0003	0.429 ± 0.002	-36 ± 1
Parn-SM (> 200)	50.6	16	175	159	251	337	53	218	47	187	6611	15441	0.1261 ± 0.0001	0.4279 ± 0.0009	-29.3 ± 0.8
Parn-chondrules	9.4	40	475	415	638	883	133	641	137	580	9397	18827	0.1272 ± 0.0002	0.407 ± 0.002	-2 ± 1
Parn-sulfide clast	6.8	5	41	37	61	95	18	81	11	167	134896	306312	0.129 ± 0.004	0.57 ± 0.03	-112 ± 23
Parn-cal bulk	1087	26	315	292	438	607	92	395	88	297	8031	17629	0.1256 ± 0.0003	0.410 ± 0.002	-19 ± 2
LL3-lit bulk[a]		30	352	314	396	671	130	355	139	1200	9407	20000	0.1282 ± 0.0006	0.41 ± 0.01	2 ± 6
CI-Bulk[b]		36.6	449.5	418.4	627.2	871.4	130	567.4	148.8	2310	21300	54100	0.12641	0.40073	-4.35

Uncertainties on isotopic ratios are 2σ. Deviation of the Os isotopic composition (Δ_{Os}) from the IIIA iron meteorite isochron is calculated by the following relation. $\Delta_{Os} = (^{187}Os/^{188}Os_{chondrite} - (0.09524+0.07887 \times {}^{187}Re/^{188}Os_{chondrite})) \times 10^4$, where 0.09524 is the $^{187}Os/^{188}Os$ ratio at 4.558 Ga and 0.07887 is the slope of the IIIA iron meteorite reference isochron (Smoliar et al., 1996).

[a] Average LL3 and H3 bulk values from Rieder and Wänke (1969), Case et al. (1973), Hermann and Wichtl (1974), Binz et al. (1976), Smith et al. (1977), Biswas et al. (1981), Dennison and Lipschutz (1987), Brearley et al. (1989), Delisle et al. (1989), Ebihara (1989), Kallemeyn et al. (1989), Bischoff et al. (1993), Wasson et al. (1993), Ebihara and Ozaki (1995), Chen et al. (1998), Kimura et al. (2002), Walker et al. (2002b), Horan et al. (2003) and Fischer-Gödde et al. (2010).

[b] CI chondrite data from Dreibus et al. (1995), Walker et al. (2002b), Fischer-Gödde et al. (2010) and Wang et al. (2013).

5.9 Appendix Chapter 5

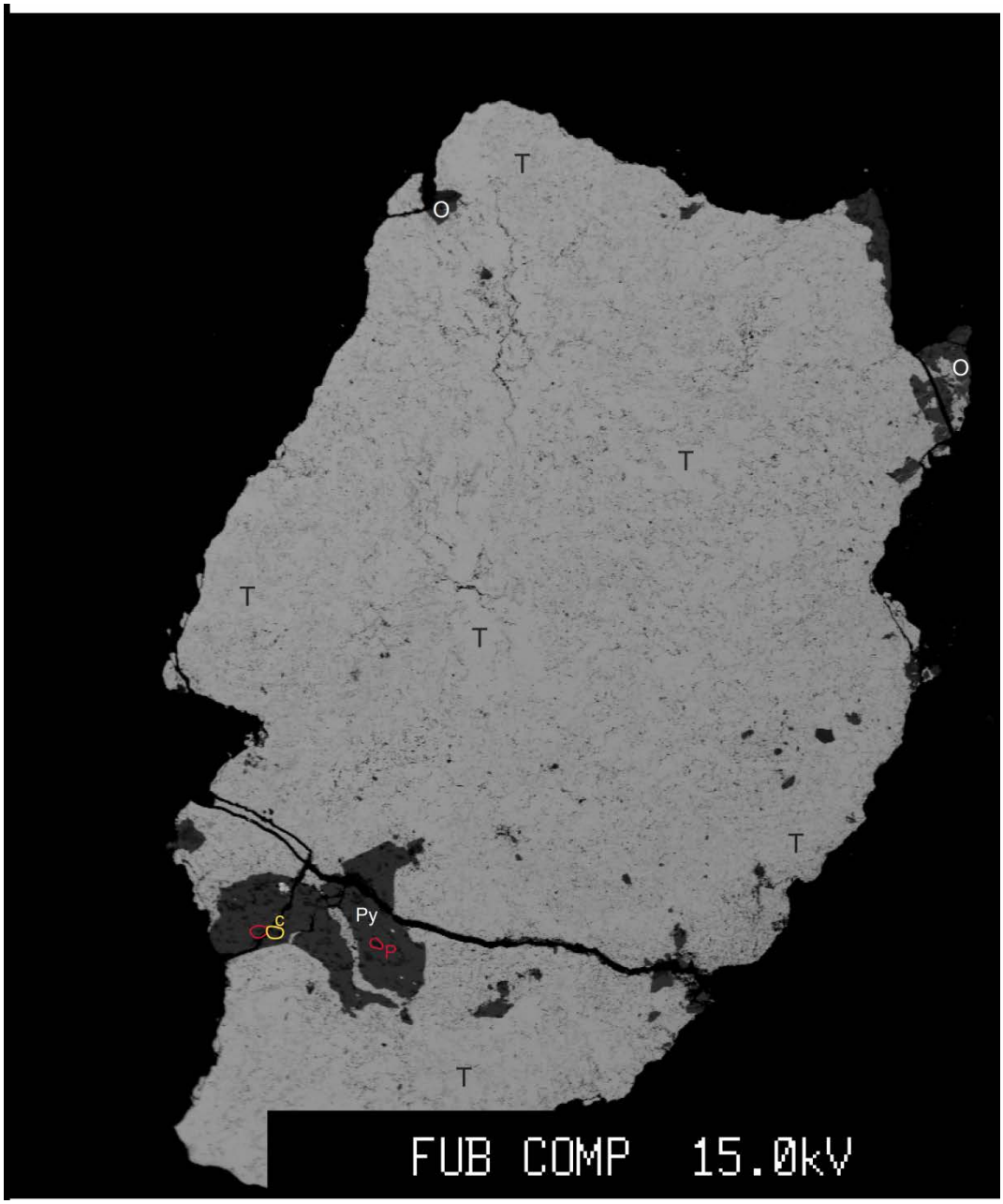

Fig. 5.A1 Small fragment of the sulfide clast of Parnallee. Dominant mineral phase is fine and coarse grained troilite which is light gray in color and shown by notation T in a figure, with minor amount of O = olivine, P = plagioclase, Py = pyroxene, C = chromite. Fe-Ni metal is almost absent in the clast.

Chapter 6

6. Conclusion and outlook

6.1 Conclusion

The main contribution of this dissertation is to constrain the processes that are responsible for the variation in the Os isotopic composition and for the fractionation of HSE and chalcogen elements in the components of unequilibrated chondrites. Method to analyze major elements was newly developed in our laboratory as a part of this work to constrain the dominance of different mineral phases in separated components. Combinations of methods which were developed in our laboratory were used to obtain precise concentrations of HSE (Fischer-Gödde et al., 2010), chalcogen (Wang et al., 2013) and major elements (this study) in the same sample aliquots.

6.1.1 ^{187}Re-^{187}Os and HSE fractionations

The abundances of HSE in enstatite, ordinary chondrites and in Murchison are enriched in metal rich components and proportional to the Ni and Co concentrations, which indicates that the Fe-Ni metal is the major HSE host phase in these chondrites, whereas in case of Allende significant fractions of HSE carrier phases occur in the form of trapped refractory metal alloys in silicate rich nonmagnetic fraction which were not completely equilibrated with the Fe-Ni metal. Variation of refractory HSE (Ir, Ru, Pt, Rh and Rh) in the components of enstatite and ordinary chondrites are likely inherited from the fractionation in the solar nebula before the accretion of the chondrite components. HSE fractionations in cooling processes such as in taenite-kamacite exsolution are also observed in case of magnetic components of unequilibrated L and LL chondrites. HSE fractionation due to exsolution effects is more prominent in the components of meteorites of higher metamorphic grades (>3.5).

Remarkable observation is the redistribution of the Ru in magnetic and slightly magnetic components of the Allende. It is likely occurred during the later oxidizing processes on Allende parent body, surprisingly which is not observed in more oxidized Murchison. Higher HSE abundances in magnetic components compared to slightly magnetic and nonmagnetic components is consistent with high metal-silicate partition coefficients of these elements. HSE ratios in the nonmagnetic components of Kota Kota (EH3) show a hint for the solid metal-liquid metal partitioning process, however the complementary HSE composition of solid metal is not observed. It likely indicates that the melting and crystallization processes of the metal are occurred before the accretion of the chondrite components. The role of this process is negligible for bulk rock HSE compositions of the enstatite chondrites.

Most magnetic components of all chondrites show negligible or minor disturbance in the ^{187}Re-^{187}Os systematics. Magnetic components of enstatite and ordinary chondrites have higher ^{187}Re/^{188}Os and ^{187}Os/^{188}Os compared to the magnetic components of carbonaceous chondrites. These differences in magnetic components are mainly responsible for the variation in the ^{187}Re/^{188}Os and ^{187}Os/^{188}Os in the bulk rocks of chondrites from different classes. Higher

initial Re/Os in magnetic components of the enstatite and ordinary chondrites compared to carbonaceous chondrites may be due to fractional condensation or slight variations in metal-silicate partitioning or ancient Re loss in oxidizing conditions at about 4.56 Ga from the components of carbonaceous chondrites. Rhenium loss process in the components of the carbonaceous chondrites might also linked with the process of formation of the magnetite-sulfide assemblages from earlier condensed metal, however the detailed evaluation of this possibility is out of scope of this study. Magnetic components of enstatite and ordinary chondrite which are close to/on the isochron show higher $^{187}Os/^{188}Os$ compared to nonmagnetic components, whereas magnetic components in carbonaceous chondrites show opposite variations. This difference indicates that in ordinary and enstatite chondrites most HSE reside in the metal fraction, whereas in carbonaceous chondrites significant amount of HSE are present in the form of trapped refractory alloys in nonmagnetic fraction. If this variation is due to continuous fractional condensation of the same reservoir material and isolation of earlier formed condensates then the Pd depleted HSE host phases present in nonmagnetic components of most chondrites analyzed in this study are more refractory and formed earlier compared to the HSE carriers of magnetic components. HSE abundance patterns depleted in Pd compared to other HSE exist in all chondrites classes, and are likely remnants of high temperature fractional condensation or evaporation processes in the solar nebula before the accretion of chondrite components.

The ^{187}Re-^{187}Os systematics is disturbed in most other components of the studied chondrites, regardless of class. The small disturbance in ^{187}Re-^{187}Os systematic in the components of some meteorite falls (Murchison, Allende, L and LL chondrites) is mostly due to the redistribution of Re in the chondrite components due to the mobility of Re during hydrothermal/aqueous alteration on the parent bodies. It indicates that these parent bodies experienced hydrothermal alteration. Because of the random scatter it is difficult to constrain the timing of this event in other chondrites, whereas in case of Ceniceros an internal errorchron of the components is poorly constrained to 1.4 ± 0.7 Ga.

Components from all find meteorites analyzed in this study also show significant disturbance in the ^{187}Re-^{187}Os systematics, likely due to terrestrial weathering. Therefore the use of ^{187}Re-^{187}Os systematics to evaluate the influence of early solar system processes is not reliable in case of the meteorites from both, cold and hot dessert finds and also oxidized fall meteorites and components with relatively small (<10 mg) sample weight, where the effect of Re mobilization is most obvious.

After Re, the most mobile element is Au. Abundances of Au are highly influenced by later alteration processes in all components of Murchison and possibly in some components of other chondrites. The heterogeneity of Au abundances in the bulk rocks of Allende may have been inherited from the complex processing during or prior to the formation of the magnetite-sulfide assemblages in carbonaceous chondrites. The strong enrichment of Au in enstatite chondrites is

likely a product of fractional condensation and probably partly initial condensation of Au in sulfides which recondensed with metal during melting and evaporation in reduced environments.

6.1.2 Chalcogen element systematics

Sulfur, Se and Te abundances and S/Se, Se/Te and S/Te in the components of all chondrite classes analyzed in this study are significantly different from each other. These differences can be used to constrain the chondrite classes along with other established differences used for the classification of these rocks. In most components of carbonaceous chondrites, Te, Se and S are depleted but unfractionated relative to CI chondrites and correlate with each other, indicating similar (chalcophile) behavior and the volatility controlled depletion of chalcogens relative to the HSE. Complementary S/Se and S/Te in some components of carbonaceous chondrites can be explained by differences in the metal-silicate partition coefficients of these elements.

Strong depletion of Te from S and Se in most enstatite and ordinary chondrite components may have been caused by several processes, which presented below by the less likely to more likely order: i) If greater Te loss compared to S and Se occurred during thermal metamorphism, then Te should be more mobile/volatile in ordinary and enstatite chondrite material compared to carbonaceous chondrites. However, this possibility seems unlikely, because Te is more mobile and volatile compared Se at temperatures > 600 °C (Ikramuddin et al., 1977a, b; Schaefer and Fegley, 2009). All chondrites analyzed in this study are of type 3.0-3.6, thus metamorphic temperatures experienced by these meteorites are less than temperature required for Te loss (Huss et al., 2006). ii) Te loss during terrestrial weathering is also unlikely, because at Earth's surface in oxidizing conditions Te forms the solid compound TeO_2 due to oxidation which is highly insoluble in water (Greenwood and Earnshaw, 1984). iii) Lower total pressures in the solar nebula would cause Te to be more volatile than Se and S at the location of the formation of all ordinary and enstatite chondrite classes. iv) The incorporation of Te into Fe-Ni metal and S and Se into sulfides takes place before accretion and greater Te loss occurred during melting and evaporation of volatile siderophile elements from metal grains, e.g. during chondrule formation. This loss is independent of the total metal content of the chondrites (it is nearly same in H, L, LL and EH chondrites), and therefore, Te condensation and loss must have occurred after the metal loss that resulted in the low concentrations of siderophile elements in L and LL chondrites.

6.2 Outlook

The variation of HSE and chalcogen elements in the components of unequilibrated chondrites suggests the major influence of nebular, parent body and weathering processes for meteorite finds on the element fractionation in the components of unequilibrated chondrites. Limited small scale redistribution of Re, Os, Ru, Rh and Au in the components of carbonaceous

chondrites may have occurred by the interaction with the oxidizing fluid/fluids on the parent bodies, however the nature of the oxidized fluid and mobility sequence of all HSE under those conditions is not well understood. Future experimental studies need to constrain the interaction of HSE carrier phases with oxidizing fluids in closed/open system environment and at variable oxygen fugacities and temperatures.

HSE and chalcogen element fractionation processes should also have affected other elements of similar volatility and geochemical properties like HSE and chalcogen. Further studies of siderophile element abundances having volatility between Au and Te (such as As, Cu, Ag, Sb, Ge, Bi and Pb) in the components need to be done to test and confirm the role of the processes discussed here. Processes affecting the elements in this temperature regime can be further tested by extending it to the elements having different geochemical behavior and similar volatility.

Similar to the unequilibrated chondrites, the precursors of planetary bodies likely were also influenced by differences in elemental and isotopic abundances of nebular domains, thus the starting composition of refractory and volatile elements of some solar system objects (including terrestrial planets) may not reflect the average composition of the solar system. Therefore, to better constrain the initial chemical and isotopic composition of elements incorporated into planetary bodies, the mass balance of different components having nonsolar composition, which were accreted into planetesimals in different nebular regions should be identified and evaluated in more detail in future work.

References

Afiattalab F. and Wasson J. T. (1980) Composition of the metal phases in ordinary chondrites: implications regarding classification and metamorphism. *Geochim. Cosmochim. Acta* **44**, 431-446.

Alexander C. M. O'D., Barber D.J. and Hutchison R. (1989) The microstructure of Semarkona and Bishunpur. *Geochim. Cosmochim. Acta* **53**, 3045-3057.

Alexander C. M. O'D., Arden J.W., Ash R. D. and Pillinger C.T. (1990) Presolar components in the ordinary chondrites. *Earth and Planet. Sci. Lett.* **99**, 220-229.

Alexander C. M. O'D., Newsome S. N., Fogel M. L. and Cody G. D. (2009) Deuterium enrichments-parent body products or a question of preservation? (abstract #2546) 40th Lunar and Planetary Science Conference.

Archer G. J., Ash R. D., Bullock E. S. and Walker R. J. (2014) Highly siderophile elements and ^{187}Re-^{187}Os isotopic systematics of the Allende meteorite: Evidence for primary nebular processes and late stage alteration. *Geochim. Cosmochim. Acta* **131,** 402-414.

Ash R. D., Luong R. J., McDonough W. F. and McCoy T. J. (2007) Trace element fractionation in kamacite and taenite in IV A irons. (abstract #2383) XXXVIIIth Lunar and Planetary Science Conference.

Baedecker P. A. and Wasson J. T. (1975) Elemental fractionations among enstatite chondrites. *Geochim. Cosmochim. Acta* **39**, 735-765.

Barrat J. A., Zanda B., Jambon A. and Bollinger C. (2014) The lithophile trace elements in enstatite chondrites. *Geochim. Cosmochim. Acta* **128**, 71-94.

Becker H., Morgan J. W., Walker R. J., MacPherson G. J. and Grossman J. N. (2001) Rhenium–osmium systematics of calcium–aluminium-rich inclusions in carbonaceous chondrites. *Geochim. Cosmochim. Acta* **65**, 3379-3390.

Benoit P. H., Akridge G. A., Ninagawa K. and Sears D. W. G. (2002) Thermoluminescence sensitivity and thermal history of type 3 ordinary chondrites: Eleven new type 3.0-3.1 chondrites and possible explanations for differences among H, L, and LL chondrites. *Meteoritics & Planet. Sci.* **37**, 793-805.

Berg T., Marosits J., Maul J., Schoenhense G., Hoppe P., Ott U. and Palme H. (2009) Evidence for nebular condensation of submicron refractory metal alloys. (abstract #1585) 40th Lunar and Planetary Science Conference.

Bhandari N., Shah V. B. and Wasson J. T. (1980) The Parsa enstatite chondrite. *Meteoritics* **15**, 225-233.

Bhandari N., Murty S. V. S., Shukla P. N., Shukla A. D., Mahajan R. R., Sarin M. M., Srinivasan G., Suthar K. M., Sisodia M. S., Jha S. and Bischoff A. (2002) Itawa Bhopji (L3-5)

chondrite regolith breccia: Fall, classification, and cosmogenic records. *Meteoritics & Planet. Sci.* **37**, 549-563.

Binz C. M., Kurimoto R. K. and Lipschutz M. E. (1974) Trace elements in primitive meteorites-V. Abundance patterns of thirteen trace elements and interelement relationships in enstatite chondrites. *Geochim. Cosmochim. Acta* **38**, 1579-1606.

Binz C.M., Ikramuddin M., Rey P., Lipschutz M.E. (1976) Trace elements in primitive meteorites- VI. Abundance patterns of thirteen trace elements and interelement relationships in unequilibrated ordinary chondrites. *Geochim. Cosmochim. Acta* **40**, 59-71.

Bischoff A., Geiger T., Palme H., Spettel B., Schultz L., Scherer P., Schlüter J. and Lkhamsuren J. (1993) Mineralogy, chemistry, and noble gas contents of Adzhi-Bogdo - an LL3-6 chondritic breccia with L-chondritic and granitoidal clasts. *Meteoritics* **28**, 570-578.

Bischoff A., Vogel N. and Roszjar J. (2011) The Rumuruti chondrite group. *Chemie der Erde* **71**, 101-133.

Biswas S., Walsh T., Bart G. and Lipschutz M.E. (1980) Thermal metamorphism of primitive meteorites-XI. The enstatite meteorites: origin and evolution of a parent body. *Geochim. Cosmochim. Acta* **44**, 2097-2110.

Biswas S., Walsh T. M., Ngo H. T. and Lipschutz M. E. (1981) Trace element contents of selected Antarctic meteorites-II: Comparison with non-Antarctic specimens. *Mem. Natl. Inst. Polar Res. (Tokyo)*, **20**, 221-228.

Bland P. A., Smith T. B., Jull A. T., Berry F. J., Bevan A., Cloudt S. and Pillinger C.T. (1996) The flux of meteorites to the Earth over the last 50 000 years. *Monthly Notices of the Royal Astronomical Society*, **283 (2)**, 551-565.

Bland P. A., Alard O., Benedix G. K., Kearsley A. T., Menzies O. N., Watt L. E. and Rogers N. W. (2005) Volatile fractionation in the early solar system and chondrule/matrix complementarity. *Proceedings of the National Academy of Sciences of the United States of America* **102**, 13755-13760.

Blander M. (1971) The constrained equilibrium theory: Sulphide phases in meteorites. *Geochim. Cosmochim. Acta* **35**, 61-76.

Blander M., Fuchs L. H., Horowitz C. and Land R. (1980) Primordial refractory metal particles in the Allende meteorite. *Geochim. Cosmochim. Acta* **44**, 217-219, 221-223.

Blander M., Pelton A. D. and Jung I. (2009) A condensation model for the formation of chondrules in enstatite chondrites. *Meteoritics & Planet. Sci*. **44**, 531–543.

Blitz L. (1993) Giant molecular clouds. Editors Levy E.H. and Lunine J.I. *Protostars and Planets III*. Univ. Arizona Press, Tucson, Arizona, 125-161.

Blum J. D., Wasserburg G. J., Hutcheon I. D., Beckett J. R. and Stolper E. M. (1989) Origin of opaque assemblages in C3V meteorites: Implications for nebular and planetary processes. *Geochim. Cosmochim. Acta* **53**, 543-556.

Bouvier A. and Wadhwa M. (2010) The age of the Solar System redefined by the oldest Pb-Pb age of a meteoritic inclusion. *Nature geoscience* **3**, 637-641.

Brandon A. D., Humayun M., Puchtel I. S. and Zolensky M. E. (2005a) Re–Os isotopic systematics and platinum group element composition of the Tagish Lake carbonaceous chondrite. *Geochim. Cosmochim. Acta* **69,** 1619-1631.

Brandon A. D., Humayun M., Puchtel I. S., Leya I. and Zolensky M. (2005b) Osmium isotope evidence for an s-process carrier in primitive chondrites. *Science* **309**, 1233-1236.

Brearley A. J. (1993) Matrix and fine-grained rims in the unequilibrated CO3 chondrite, ALHA77307: Origins and evidence for diverse, primitive nebular dust components. *Geochim. Cosmochim. Acta* **57**, 1521-1550.

Brearley A. J. (2003) Nebular versus Parent-body Processing. Treatise on Geochemistry. Editors Davis A. M., Holland H. D. and Turekian K.K. Vol.**1**, 247-268.

Brearley A. J., Scott E. R. D., Keil K., Clayton R. N., Mayeda T. K., Boynton W. V. and Hill D. H. (1989) Chemical, isotopic and mineralogical evidence for the origin of matrix in ordinary chondrites. *Geochim. Cosmochim. Acta* **53**, 2081-2093.

Brenan J. M. and Bennett N. (2010) Soret separation of highly siderophile elements in Fe-Ni-S melts: Implications for solid metal-liquid metal partitioning. *Earth and Planet. Sci. Lett.* **298**, 299-305.

Bridges J. C., Alexander C. M. O'D, Hutchison R., Franchi I. A. and Pillinger C. T. (1997) Sodium-, chlorine-rich mesostases in Chainpur (LL3) and Parnallee (LL3) chondrules. *Meteoritics & Planet. Sci.* **32**, 555-565.

Cameron A. G. W. (1993) Nucleosynthesis and star formation. Editors Levy E. H. and Lunine J. I. *Protostars and Planets III*. Univ. Arizona Press, Tucson, Arizona, 47-73.

Cameron A. G. W. (1995) The first ten million years in the solar nebula. *Meteoritics* **30**, 133-161.

Campbell A. J. and Humayun M. (2003) Formation of Metal in Grosvenor Mountains 95551 and comparison to ordinary chondrites. *Geochim. Cosmochim. Acta* **67**, 2481-2495.

Campbell, A. J., Humayun, M., and Weisberg, M. K. (2002) Siderophile element constraints on the formation of metal in the metal-rich chondrites Bencubbin, Weatherford, and Gujba. *Geochim. Cosmochim. Acta* **66**, 647-660.

Campbell A. J., Simon S. B., Humayun M. and Grossman L. (2003) Chemical evolution of metal in refractory inclusions in CV3 chondrites. *Geochim. Cosmochim. Acta* **67**, 3119-3134.

Campbell A. J., Zanda B., Perron C., Meibom A. and Petaev M. I. (2005) Origin and Thermal History of Fe-Ni Metal in Primitive Chondrites. Chondrites and protoplanetary Disk, Edited by A.N. Krot, E.R.D. Scott and B. Reipurth. ASP conf. series Vol. **341**, 407-431.

Case D. R., Laul J. C., Pelly I. Z., Wechter M. A., Schmidt-Bleek F. and Lipschutz M. E. (1973) Abundance patterns of thirteen trace elements in primitive carbonaceous and unequilibrated ordinary chondrites. *Geochim. Cosmochim. Acta* **37**, 19-33.

Chabot N. L. and Jones J. H. (2003) The parameterization of solid metal–liquid metal partitioning of siderophile elements. *Meteoritics & Planet. Sci.* **38**, 1425-1436.

Chabot N. L., Campbell A. J., Jones J. H., Humayun M. and Agee C. B. (2003) An experimental test of Henry's Law in solid metal–liquid metal systems with implications for iron meteorites. *Meteoritics & Planet. Sci.* **38**, 181-196.

Chabot N. L., Campbell A. J., Jones J. H., Humayun M. and Lauer J. H. V. (2006) The influence of carbon on trace element partitioning behavior. *Geochim. Cosmochim. Acta* **70**, 1322-1335.

Chabot N. L., McDonough W. F., Jones J. H., Saslow S. A., Ash R. D., Draper D. S. and Agee C. B. (2011) Partitioning behavior at 9 GPa in the Fe-S system and implications for planetary evolution. *Earth and Planet. Sci. Lett.* **305**, 425-434.

Chen J. H., Papanastassiou D. A. and Wasserburg G. J. (1998) Re–Os systematics in chondrites and the fractionation of the platinum group elements in the early solar system. *Geochim. Cosmochim. Acta* **62**, 3379-3392.

Chou C.-L. and Cohen A. J. (1973) Gallium and germanium in the metal and silicates of L- and LL-chondrites. *Geochim. Cosmochim. Acta* **37**, 315-327.

Chou C.-L., Baedecker P. A. and Wasson J. T. (1973) Distribution of Ni, Ga, Ge and Ir between metal and silicate portions of H group chondrites. *Geochim. Cosmochim. Acta* **37**, 2159-2171.

Clayton R. N. (1993) Oxygen isotopes in meteorites. *Ann. Rev. Earth Planet. Sci.* **21**, 115-149.

Clayton R. N., Mayeda T. K. and Rubin A. E. (1984) Oxygen isotopic compositions of enstatite chondrites and aubrites. *J. Geophys. Res.* **89**, C245-C249.

Clayton R. N., Mayeda T. K., Goswami J. N. and Olsen E. J. (1991) Oxygen isotope studies of ordinary chondrites. *Geochim. Cosmochim. Acta* **55**, 2317-2337.

Cohen A. S. and Waters F. G. (1996) Separation of osmium from geological materials by solvent extraction for analysis by thermal ionisation mass spectrometry. *Anal. Chim. Acta* **332**, 269-275.

Connolly H. C. Jr., Huss G. R. and Wasserburg G. J. (2001) On the formation of Fe-Ni metal in Renazzo-like carbonaceous chondrites. *Geochim. Cosmochim. Acta* **65**, 4567-4588.

Crabb J. and Anders E. (1981) Noble gases in E-chondrites. *Geochim. Cosmochim. Acta* **45**, 2443-2464.

Crabb J. and Anders E. (1982) On the siting of noble gases in E- chondrites. *Geochim. Cosmochim. Acta* **46**, 2351-2361.

Davis A. M. and Richter F. M. (2003) Condensation and evaporation of solar system materials. *Treatise on Geochemistry*. Editors Davis A.M., Holland H.D. and Turekian K.K. **1**, 407-430.

Delisle G., Schultz L., Spetter B., Weber H. W., Wlotzka F., Höfle H.-C., Thierbach R., Vogt S., Herpers U., Bonani G., Suter M. and Woelfli W. (1989) Meteorite Finds in the Frontier Mountain Range in Northern Victoria Land, Antarctica. Geol. Jahrb. **E38**, 253-283.

Dennison J. E. and Lipschutz M. E. (1987) Chemical studies of H chondrites. II: Weathering effects in the Victoria Land, Antarctic population and comparison of two Antarctic populations with non-Antarctic falls. *Geochim. Cosmochim. Acta* **51**, 741-754.

Dobrică E. and Brearley A. J. (2011) Earliest stages of metamorphism and aqueous alteration observed in the fine-grained materials of two unequilibrated ordinary chondrites. (abstract #2092) 42th Lunar and Planetary Science Conference.

Dodd Jr. R. T., Van Schmus W. R. and Koffman D. M. (1967) A survey of the unequilibrated ordinary chondrites. *Geochim. Cosmochim. Acta* **31**, 921-951.

Dreibus G., Palme H., Spettel B., Zipfel J. and Wänke H. (1995) Sulfur and selenium in chondritic meteorites. *Meteoritics* **30**, 439-445.

Easton A. J. (1985) E-chondrites: Significance of the Partition of elements between 'silicate' and 'sulphide'. *Meteoritics* **20**, 89-101.

Easton A. J. and Elliott C. J. (1977) Analyses of some meteorites from the British Museum (Natural History) Collection. *Meteoritics* **12,** 409-416.

Ebata S., Nagashima K., Itoh S., Kobayashi S., Sakamoto N., FaganT. J. and Yurimoto H. (2006) Presolar silicate grains in enstatite chondrites. (abstract #1619) 37th Lunar and Planetary Science Conference.

Ebata S., Fagan T. J. and Yurimoto H. (2008) Identification of silicate and carbonaceous presolar grains by SIMS in the type-3 enstatite chondrite ALHA81189. *Applied Surface Scienc*e **255**, 1468-1471.

Ebihara M. (1989) Rare earth and some other elements in acid-residues of unequilibrated ordinary chondrites. *Proc. NIPR Symp. Antarct. Meteorites* **2**, 279-287.

Ebihara M. and Ozaki H. (1995) Re, Os, and Ir in Antarctic unequilibrated ordinary chondrites and implications for the solar abundance of Re. *Geophys. Res. Lett.* **22**, 2167-2170.

Ebihara M., Wolf R. and Anders E. (1982) Are C1 chondrites chemically fractionated? A trace element study. *Geochim. Cosmochim. Acta* **46**, 1849-1861.

El Goresy A., Lin Y., Feng L., Boyet M., Hao J., Zhang J. and Dubrovinsky L. (2012) Almahata Sitta EL-3 chondrites: sinoite, graphite, and oldhamite (CaS) assemblages C- and N-isotopic compositions and REE patterns (abstract #5108). *Meteoritics & Planet. Sci.***47**, A125.

Evensen N. M., Hamilton P. J. and O'Nions R. K. (1978) Rare-earth abundances in chondritic meteorites. *Geochim. Cosmochim. Acta* **42**, 1199-1212.

Fischer-Gödde M., Becker H. and Wombacher F. (2010) Rhodium, gold and other highly siderophile element abundances in chondritic meteorites. *Geochim. Cosmochim. Acta* **74**, 356-379.

Fisenko A. V., Russell S. S., Ash R. D., Semjenova L. F., Verchovsky A. B. and Pillinger C. T. (1992) Isotopic composition of carbon and nitrogen in the diamonds from the unequilibrated ordinary chondrite Krymka LL3.0. (abstract #365) XXIIIth Lunar and Planetary Science Conference.

Fitzgerald M. J. (1979a) The chemical composition and classification of the Karoonda meteorite. *Meteoritics* **14**, 109-115.

Fitzgerald M. J. (1979b) The Chemistry and Mineralogy of the Meteorites of South Australia and Adjacent Regions. Ph. D. Thesis, Univ. of Adelaide, 323 pp.

Fredriksson K., Fredriksson B. J. and Kraut F. (1986) The Hedjaz meteorite. *Meteoritics* **21**, 159-168.

Friedrich J. M., Wang M.-S. and Lipschutz M. E. (2002) Comparison of the trace element composition of Tagish Lake with other primitive carbonaceous chondrites. *Meteoritics & Planet. Sci.***37**, 677-686.

Fuchs L. H., Olsen E. and Jensen K. J. (1973) Mineralogy, mineral-chemistry, and composition of the Murchison (C2) meteorite. *Smiths. Contrib. Earth Sci., no*. 10, 39.

Fulton C. R. and Rhodes J. M. (1984) The chemistry and origin of the ordinary chondrites: Implications from refractory-lithophile and siderophile elements. *J. Geophys. Res.* **89**, B543-558.

Gooding J. L. and Keil K. (1980) Elemental abundances in chondrules from unequilibrated chondrites: evidence for chondrule origin by melting of pre-existing materials. *Earth and Planet. Sci. Lett.* **50**, 171-180.

Gopalan K., Rao M. N., Suthar K. M. and Venkatesan T. R. (1976) Rare Gases in the Dhajala Stone Meteorite. *Meteoritics* **11**, 290-291.

Graham A. L. (1990) The Meteoritical Bulletin, No.68, 1990 March. *Meteoritics* **25**, 59-70.

Graham A. L. (1993) The Julesburg (L3) chondrite. *Meteoritics* **28**, 122-125.

Graham A. L., Easton A. J., Hutchison R. and Jérome D. Y. (1976) The Bovedy meteorite: mineral chemistry and origin of Ca-rich glass inclusions. *Geochim. Cosmochim. Acta* **40**, 529-535.

Greenwood N. N. and Earnshaw A. (1984) Chemistry of the elements. Pergamon Press, Oxford, first edition: 911.

Grossman L. (1972) Condensation in the primitive solar nebula. *Geochim. Cosmochim. Acta* **36**, 597-619.

Grossman L. (1980) Refractory inclusions in the Allende meteorite. *Ann. Rev. Earth Planet. Sci.* **8**, 559-608.

Grossman J. N. (1998). The meteoritical bulletin, No.82, 1998 July. *Meteoritics & Planet. Sci.* **33**, 221-239.

Grossman J. N. (1999) The Meteoritical Bulletin, No.83, 1999 July. *Meteoritics & Planet. Sci.***34**, A169-A186.

Grossman J. N. and Wasson J. T. (1985) The origin and history of the metal and sulfide components of chondrules. *Geochim. Cosmochim. Acta* **49**, 925-939.

Haramura H., Kushiro I. and Yanai K. (1983) Chemical Compositions of Antarctic Meteorites I. Mem. Natl. Inst. Polar Res. (Tokyo), Spec. Issue **30**, 109-121.

Helmy H. M., Ballhaus C., Wohlgemuth-Ueberwasser C., Fonseca R. O. C. and Laurenz V. (2010) Partitioning of Se, As, Sb, Te and Bi between monosulfide solid solution and sulfide melt-application to magmatic sulfide deposites. *Geochim.Cosmochim.Acta* **47,** 2241-2255.

Hermann F. and Wichtl M. (1974) Neutronenaktivierungsanalytische Bestimmung von Spurenelementen in Meteoriten der Vatikanischen Sammlung. In: Analyse extraterrestrischen Material. (Editors W. Kiesl and H. Malissa Jun.), pp. 163-172. Springer-Verlag, Wien.

Hertogen J., Janssens M., Takahashi H., Morgan J. W. and Anders E. (1983) Enstatite chondrites: Trace element clues to their origin. *Geochim. Cosmochim. Acta* **47**, 2241-2255.

Hewins R. H. and Radomsky P. M. (1990) Temperature conditions for chondrule formation. *Meteoritics* **25,** 309-318.

Hewins R. H., Radomsky P. M., Lu Jie, Hasan F. A., Sears D. W. G. and Jarosewich E. (1988) Villa Natamoros, an L3.7 chondrite from the Allende strewn field. *Meteoritics* **23**, 273-274 (abs.).

Hewins R. H., Yu. Y., Zanda B. and Bourot-Denise M. (1997) Do nebular fractionations, evaporative losses, or both, influence chondrule compositions? *Antarct. Meteorite Res.* **10**, 275-298.

Hezel D. C. and Palme H. (2008) Constraints for chondrule formation from Ca-Al distribution in carbonaceous chondrites. *Earth and Planet. Sci. Lett.* **265**, 716-725.

Hezel D. C. and Palme H. (2010) The chemical relationship between chondrules and matrix and the chondrule matrix complementarity. *Earth and Planet. Sci. Lett.* **294**, 85-93.

Hinton R. W. and Bischoff A. (1984) Ion microprobe magnesium isotope analysis of plagioclase and Hibonite from ordinary chondrites. *Nature* **308**, 169-172.

Horan M. F., Walker R. J., Morgan J. W., Grossman J. N. and Rubin A. E. (2003) Highly siderophile elements in chondrites. *Chem. Geol.* **196**, 5-20.

Horan M. F., Alexander C. M. O'D. and Walker R. J. (2009) Highly siderophile element evidence for early solar system processes in components from ordinary chondrites. *Geochim. Cosmochim. Acta* **73**, 6984-6997.

Horstmann M., Humayun M. and Bischoff A. (2014) Clues to the origin of metal in Almahata Sitta EL and EH chondrites and implications for primitive E chondrite thermal histories. *Geochim. Cosmochim. Acta* **140**, 720-744.

Hsu W., Huss G. R. and Wasserburg G. J. (1998) Ion probe analyses of PGEs in metallic phases of chondrites: implications for the origin of chondritic metals. (abstract #1939) XXIXth Lunar and Planetary Science Conference.

Huber H., Rubin A. E., Kallemeyn G. W. and Wasson J. T. (2006) Siderophile-element anomalies in CK carbonaceous chondrites: Implications for parent-body aqueous alteration and terrestrial weathering of sulfides. *Geochim. Cosmochim. Acta* **70**, 4019-4037.

Humayun M. and Campbell A. J. (2002) The duration of ordinary chondrite metamorphism inferred from tungsten micro distribution in metal. *Earth and Planet. Sci. Lett*. **198**, 225-243.

Huss G. R. and Lewis R. S. (1994) Noble gases in presolar diamonds II: Component abundances reflect thermal processing. *Meteoritics* **29**, 811-829.

Huss G. R., MacPherson G. J., Wasserburg G. J., Russell S. S. and Srinivasan G. (2001) Aluminum-26 in calcium-aluminum-rich inclusions and chondrules from unequilibrated ordinary chondrites. *Meteoritics & Planet. Sci.* **36**, 975-997.

Hutchison R., Alexander C.M.O'D. and Barber D. J. (1987) The Semarkona meteorite: First recorded occurrence of smectite in an ordinary chondrites, and its implications. *Geochim. Cosmochim. Acta* **51**, 1875-1882.

Ikramuddin M. and Lipschutz M. E. (1975) Thermal metamorphism of primitive meteorites-I. Variation of six trace elements in Allende carbonaceous chondrite heated at 400-1000°C. *Geochim. Cosmochim. Acta* **39**, 363-375.

Ikramuddin M., Binz C. M. and Lipschutz M. E. (1976) Thermal metamorphism of primitive meteorites-II. Ten trace elements in Abee enstatite chondrite heated at 400-1000 °C. *Geochim. Cosmochim. Acta* **40**, 133-142.

Ikramuddin M., Binz C. M. and Lipschutz M. E. (1977a) Thermal metamorphism of primitive meteorites-III. Ten trace elements in Krymka L3 chondrite heated at 400-1000 °C. *Geochim. Cosmochim. Acta* **41**, 393-401.

Ikramuddin M., Matza S., Lipschutz M. E. (1977b) Thermal metamorphism of primitive meteorites. V. Ten trace elements in Tieschitz H3 chondrite heated at 400–1000 °C. *Geochim. Cosmochim. Acta* **41**, 1247-1256.

Ireland T. R., Fahey A. J., and Zinner E. K. (1988) Trace element abundances in hibonites from the Murchison carbonaceous chondrite: constraints on high-temperature processes in the solar nebula. *Geochim. Cosmochim. Acta* **52**, 2841-2854.

Jarosewich E. (1966) Chemical analyses of ten stony meteorites. *Geochim. Cosmochim. Acta* **30**, 1261-1265.

Jarosewich E. (1971) Chemical analysis of the Murchison meteorite. *Meteoritics* **6**, 49-52.

Jarosewich E. (1984) Bulk chemical analyses of Antarctic meteorites, with notes on weathering effects on FeO, Fe-metal, FeS, H2O, and C. *Smithson. Contrib. Earth Sci.* **26**, 111-114.

Jarosewich E. (1990) Chemical analyses of meteorites: A compilation of stony and iron meteorite analyses. *Meteoritics* **25**, 323-337.

Jarosewich E., Clarke R. S. and Barrows J. N. (1987) The Allende meteorite reference sample. *Smithson Contrib. Earth Sci.* **27**, 1-49.

Jochum K. P. (1996). Rhodium and other platinum-group elements in carbonaceous chondrites. *Geochim. Cosmochim. Acta* **60**, 3353-3357.

Johnson C. A., Prinz M., Weisberg M. K., Clayton R. N. and Mayeda T. K. (1990) Dark inclusions in Allende, Leoville, and Vigarano: Evidence for nebular oxidation of CV3 constituents. *Geochim. Cosmochim. Acta* **54**, 819-830.

Kaczaral P. W., Dennison J. E., Verkouteren R. M. and Lipschutz M. E. (1988) On volatile/mobile trace element trends in E3 chondrites. *Proc. NIPR Symp. Antarct. Meteorites* **1**, 113-121.

Kaczaral P. W., Dodd R. T. and Lipschutz M. E. (1989) Chemical studies of L chondrites: IV. Antarctic/non-Antarctic comparisons. *Geochim. Cosmochim. Acta* **53**, 491-501.

Kadlag Y. and Becker H. (2014) Highly Siderophile and Chalcogen Element Constraints on the Origin of Components of Unequilibrated L Chondrites. (abstract #1771) 45th Lunar and Planetary Science Conference.

Kadlag Y. and Becker H. (2015a) Fractionation of highly siderophile and chalcogen elements in components of EH3 chondrites. *Geochim. Cosmochim. Acta (submitted).*

Kadlag Y. and Becker H. (2015b) Highly siderophile and chalcogen element constraints on the origin of components of the Allende and Murchison meteorites. *Meteoritics & Planet. Sci. (submitted).*

Kadlag Y. and Becker H. (2015c) ^{187}Re-^{187}Os systematics, highly siderophile and chalcogen element abundances in the components of unequilibrated L chondrites. *Geochim. Cosmochim. Acta (submitted).*

Kallemeyn G. W. and Wasson J. T. (1981) The compositional classification of chondrites: I. The carbonaceous chondrite groups. *Geochim. Cosmochim. Acta* **45**, 1217-1230.

Kallemeyn G. W. and Wasson J. T. (1982) The compositional classification of chondrites: III. Ungrouped carbonaceous chondrites. *Geochim. Cosmochim. Acta* **46**, 2217-2228.

Kallemeyn G. W. and Wasson J. T. (1985) The compositional classification of chondrites: IV. Ungrouped chondritic meteorites and clasts. *Geochim. Cosmochim. Acta* **49**, 261-270.

Kallemeyn G. W. and Wasson J. T. (1986) Compositions of enstatite (EH3, EH4, 5 and EL6) chondrites: implications regarding their formation. *Geochim. Cosmochim. Acta* **50**, 2153-2164.

Kallemeyn G. W., Rubin A. E., Wang D. and Wasson J. T. (1989) Ordinary chondrites: Bulk compositions, classification, lithophile-element fractionations, and composition-petrographic type relationships. *Geochim. Cosmochim. Acta* **53**, 2747-2767.

Kallemeyn G. W., Rubin A. E. and Wasson J. T. (1996) The compositional classification of chondrites: VII. The R chondrite group. *Geochim. Cosmochim. Acta* **60**, 2243-2256.

Keays R. R., Ganapathy R. and Anders E. (1971) Chemical fractionations in meteorites-IV. Abundances of fourteen trace elements in L chondrites: Implications for cosmothermometry. *Geochim. Cosmochim. Acta* **35**, 337-363.

Kharitonova V. Y. (1969) Chemical compositions of the Oesel, Kargapole, Dimmitt, Chico, and New Almelo chondrites from the collection of the Committee on meteorites of the USSR Academy of Sciences. *Meteoritika* **29**, 91-100.

Kimura M., Hiyagon H., Palme H., Spettel B., Wolf D., Clayton R. N., Mayeda T. K., Sato T., Suzuki A. and Kojima H. (2002) Yamato 792947, 793408 and 82038: The most primitive H chondrites, with abundant refractory inclusions. *Meteoritics & Planet. Sci.* **37**, 1417-1434.

King T. V. V. and King E. A. (1981) Accretionary dark rims in unequilibrated chondrites. *ICARUS* **48**, 460-472.

Kirova O. A., Dyakonova M. I. and Kharitonova V. Y. (1975) Petrographical and chemical study of the Polujamki and Rakity meteorites and their comparison with the Markovka meteorite. *Meteoritika* **34**, 57-64.

Kong P. and Ebihara M. (1996) Metal phases of L chondrites: their formation and evolution in the nebular and in the parent body. *Geochim. Cosmochim. Acta* **60,** 2667-2680.

Kong P. and Ebihara M. (1997) The origin and nebular history of the metal phase of ordinary chondrites. *Geochim. Cosmochim. Acta* **61,** 2317-2329.

Kong P., Ebihara M., Nakahara H. and Endo K. (1995) Chemical characteristics of metal phases of the Richardton H5 chondrite. *Earth and Planet.Sci.Lett.***136**, 407-419.

Kong P., Mori T. and Ebihara M. (1997) Compositional continuity of enstatite chondrites and implications for heterogeneous accretion of enstatite chondrite parent body. *Geochim. Cosmochim. Acta* **61,** 4895-4914.

Kong P., Deloule E. and Palme H. (2000) REE-bearing sulfide in Bishunpur (LL3.1), a highly unequilibrated ordinary chondrite. *Earth and Planet. Sci. Lett.* **177**, 1-7.

Krot A. N., Zolensky M. E., Wasson J. T., Scott E. R. D., Keil K. and Ohsumi K. (1997) Carbide-magnetite assemblages in type-3 ordinary chondrites. *Geochim. Cosmochim. Acta* **61**, 219-237.

Krot A. N., Keil K., Goodrich C. A., Scott E. R. D. and Weisberg M. K. (2003) Classification of Meteorites. *Treatise on Geochemistry*. Editors Davis A.M., Holland H.D. and Turekian K.K. Vol.**1**, 83-128.

Krot A. N., MacPherson G. J., Ulyanov A. A., and Petaev M. I. (2004) Fine-grained, spinel-rich inclusions from the reduced CV chondrites Efremovka and Leoville: I. Mineralogy, petrology, and bulk chemistry. *Meteoritics & Planet. Sci.* **39**, 1517-1553.

Larimer J. W. and Anders E. (1967) Chemical fractionations in meteorites-II. Abundance patterns and their interpretation. *Geochim. Cosmochim. Acta* **31**, 1239-1270.

Larimer J. W. and Anders E. (1970) Chemical fractionations in meteorites-III. Major element fractionations in chondrites. *Geochim. Cosmochim. Acta* **34**, 367-387.

Laul J. C., Ganapathy R., Anders E. and Morgan J. W. (1973) Chemical fractionations in meteorites-VI. Accretion temperatures of H-, LL-, and E-chondrites, from abundance of volatile trace elements. *Geochim. Cosmochim. Acta* **37**, 329-357.

Lauretta D. S., Lodders K., and Fegley B. Jr. (1998) Kamacite sulfurization in the solar nebula. *Meteoritics & Planet. Sci.* **33**, 821-834.

Lehner S.W. and Buseck P.R. (2009) The highly unequilibrated EH chondrite, Sahara 97072, may be a primitive breccia. (abstract #2154) 40th Lunar and Planetary Science Conference.

Lehner S.W. and Buseck P. R. (2011) Trace element distribution among matrix, chondrules, metal and sulfides in Sahara 97072 EH3. (abstract #1430) 42th Lunar and Planetary Science Conference.

Lehner S. W., Buseck P. R. and McDonough W. F. (2010) Origin of kamacite, schreibersite, and perryite in metal-sulfide nodules of the enstatite chondrite Sahara 97072 (EH3). *Meteoritics & Planet. Sci.* **45**, 289-303.

Lehner S. W., Petaev M. I., Zolotov M. Yu. and Buseck P. R. (2013) Formation of niningerite by silicate sulfidation in EH3 enstatite chondrites. *Geochim. Cosmochim. Acta* **101**, 34-56.

Leitch C. A. and Smith J. V. (1981) Mechanical aggregation of enstatite chondrites from an inhomogeneous debris cloud. *Nature* **290,** 228-230.

Lewis J. A. and Jones R. H. (2014) Nephelinization and metasomatism in the ordinary chondrite Parnallee (LL3.6). (abstract #1661) 45th Lunar and Planetary Science Conference.

Libourel G. and Krot A. N. (2007) Evidence for the presence of planetesimals material among the precursors of magnesian chondrules of nebular origin. *Earth and Planet. Sci. Lett.* **254**, 1-8.

Lin Y. and El Goresy A. (2002) A comparative study of opaque phases in Qingzhen (EH3) and MacAlpine Hills 88136 (EL3): Representatives of EH and EL parent bodies. *Meteoritics & Planet. Sci*. **37**, 577-599.

Lissauer J. J. and Stewart G. R. (1993) Growth of planets from planetesimals. Editors Levy E.H. and Lunine J.I. *Protostars and Planets III*. Univ. Arizona Press, Tucson, Arizona, 1061-1088.

Lodders K. (2003) Solar system abundances and condensation temperatures of the elements. *Astrophys. J.* **591**, 1220-1247.

Lofgren G. E. and Le L. (2002) Experimental reproduction of type-1B chondrules. (abstract #1746) XXXIIIth Lunar and Planetary Science Conference.

Lorand J.-P. (1990) Are spinel lherzolites xenoliths representative of abundance of sulfur in the upper mantle? *Geochim. Cosmochim. Acta* **54**, 1487-1492.

Luck J. M. and Allégre C. J. (1983) ^{187}Re-^{187}Os systematics in meteorites and cosmochemical consequences. *Nature* **302**, 130-132.

Ludwig K. R. (2008) Isoplot 4.1 program (Berkeley Geochronology Center http://www.bgc.org/isoplot_etc/isoplot.html).

MacPherson G. J. (2003) Calcium-Aluminum-rich inclusions in chondritic meteorites. *Treatise on Geochemistry*. Editors Davis A.M., Holland H.D. and Turekian K.K. **1**, 201-246.

MacPherson G. J., Hashimoto A. and Grossman L. (1985) Accretionary rims on inclusions in the Allende meteorite. *Geochim. Cosmochim. Acta* **49**, 2267-2279.

MacPherson G. J., Jarosewich E. and Lowenstein P. (1993) Magombedze: A new H-chondrite with light-dark structure. *Meteoritics* **28**, 138-142.

Mason B. and Taylor S. R. (1982) Inclusions in the Allende meteorite. *Smithson Contrib. Earth Sci.* **25**, 10-30.

McCarthy T. S. and Ahrens L. H. (1972) Chemical sub-groups amongst HL chondrites. *Earth and Planet. Sci. Lett.* **14**, 97-102.

McKeegan K. D., Leshin L. A., Russell S. S., and MacPherson G. J. (1998) Oxygen Isotopic Abundances in Calcium-Aluminum–Rich Inclusions from Ordinary Chondrites: Implications for Nebular Heterogeneity. *Science* **280**, 414-418.

McKinley S. G., Scott E. R. D., Taylor J. G. and Keil K. (1981) A unique type 3 ordinary chondrite containing graphite-magnetite aggregates-Allan Hills A77011. Proc. Lunar and Planetary Science Conference. **12B**, 1039-1048.

McNaughton N. J., Borthwick J., Fallick A. E. and Pillinger C. T. (1981) Deuterium/hydrogen ratios in unequilibrated ordinary chondrites. *Nature* **294**, 639-641.

McSween H. (1999) Meteorites and Their Parent Planets. *Cambridge University Press*.

Metzler K., Bischoff A. and Stöffler D. (1992) Accretionary dust mantles in CM chondrites: Evidence for solar nebula processes. *Geochim. Cosmochim. Acta* **56**, 2873-2897.

Morlok A., Bischoff A., Stephan T., Floss C., Zinner E. and Jessberger E. K. (2006) Brecciation and chemical heterogeneities of CI chondrites. *Geochim. Cosmochim. Acta* **70**, 5371-5394.

Moskovitz N. and Gaidos E. (2011) Differentiation of planetesimals and the thermal consequences of melt migration. *Meteoritics & Planet. Sci.* **46**, 903-918.

Mughabghab S. F. (2003) Thermal neutron capture cross sections resonance integrals and G-factors. INDC(NDS)-440.

Mungall J. E. and Brenan J. M. (2014) Partitioning of platinum-group elements and Au between sulfide liquid and basalt and the origins of mantle-crust fractionation of the chalcophile elements. *Geochim. Cosmochim. Acta* **125**, 265-289.

Nagahara H. (1984) Matrices of type 3 ordinary chondrites-primitive nebular records. *Geochim. Cosmochim. Acta* **48**, 2581-2595.

Ngo H. T. and Lipschutz M. E. (1980) Thermal metamorphism of primitive meteorites-X. Additional trace elements in Allende (C3V) heated to 1400°C. *Geochim. Cosmochim. Acta* **44**, 731-739.

Nuth, J. A. (2001) How were the comets made? *American Scientist* **89**, 230-237.

O'Neill H. S. C., Dingwell D. B., Borisov A., Spettel B. and Palme H. (1995) Experimental petrochemistry of some highly siderophile elements at high temperatures, and some implications for core formation and the mantle's early history. *Chem. Geol.* **120**, 255-273.

Pack A., Russell S. S., Shelley J. M. G., and van Zuilen M. (2007) Geo- and cosmochemistry of the twin elements yttrium and holmium. *Geochim. Cosmochim. Acta* **71**, 4592-4608.

Palme H. and Wlotzka F. (1976) A metal particle from a Ca, Al-rich inclusion from the meteorite Allende, and the condensation of refractory siderophile elements. *Earth and Planet. Sci. Lett.* **33**, 45-60.

Palme H. and Boynton W. V. (1993) Meteoritic constraints on conditions in the solar nebula. Editors Levy E.H. and Lunine J.I. *Protostars and Planets III*. Univ. Arizona Press, Tucson, Arizona, 979-1004.

Palme H., Hutcheon I. D., and Spettel B. (1994) Composition and origin of refractory-metal-rich assemblages in a Ca, Al-rich Allende inclusion. *Geochim. Cosmochim. Acta* **58**, 495-513.

Palme H., Borisov A. and Wulf A.V. (1998) Experimental determination of the oxidation sequence of refractory metals. (abstract #1611) XXIXth Lunar and Planetary Science Conference.

Palme H., Spettel B. and Hezel D. (2014) Siderophile elements in chondrules of CV chondrites. *Chemie der Erde* **74**, 507-516.

Palmer E. E. and Lauretta D. S. (2011) Aqueous alteration of kamacite in CM chondrites. *Meteoritics & Planet. Sci.* **46**, 1587-1607.

Paul R. L. and Lipschutz M. E. (1990) Consortium study of labile trace elements in some Antarctic carbonaceous chondrites: Antarctic and non-Antarctic meteorite comparisons. *Proc. NIPR Symp. Antarct. Meteorites* **3**, 80-95.

Piani L., Libourel G., Marrocchi Y. and Tissandier L. (2013) Sulfur and volatile element behavior in enstatite chondrite chondrules. *Met. Soc*. **76,** 5178.

Rankenburg K., Brandon A. D. and Humayun M. (2007) Osmium isotope systematics of ureilites. *Geochim. Cosmochim. Acta* **71**, 2402-2413.

Rambaldi E. (1976) Trace element content of metals from L-group chondrites. *Earth and Planet. Sci. Lett.* **31**, 224-238.

Rambaldi E. R. (1977a) The content of Sb, Ge and refractory siderophile elements in metals of L-group chondrites. *Earth and Planet. Sci. Lett.* **33**, 407-419.

Rambaldi E. R. (1977b) Trace element content of metals from H and LL-group chondrites. *Earth and Planet. Sci. Lett.* **36**, 347-358.

Rambaldi E. R., Cendales M. and Thacker R. (1978) Trace element distribution between magnetic and non-magnetic portions of ordinary chondrites. *Earth and Planet. Sci. Lett.* **40**, 175-186.

Rambaldi E. R. and Cendales M. (1980) Siderophile element fractionation in enstatite chondrites. *Earth and Planet. Sci. Lett.* **48**, 325-334.

Rambaldi E. R., Wänke H. and Larimer J. W. (1979) Interelement refractory siderophile fractionation in ordinary chondrites. 10^{th} Proc. Lunar and Planetary Science Conference. 997-1010.

Rambaldi E. R. and Wasson J. T. (1984) Metal and associated phases in Krymka and Chainpur: Nebular formational processes. *Geochim. Cosmochim. Acta* **48**, 1885-1897.

Rasmussen K. L., Malvin D. J. and Wasson J. T. (1988) Trace element partitioning between taenite and kamacite; relationship to the cooling rates of iron meteorites. *Meteoritics* **23**, 107-112.

Rieder R. and Wänke H. (1969) Study of trace element abundances in meteorites by neutron activation. In: Meteorite Research (ed. P. M. Millman), 75-86.

Robert F., Javoy M., Halbout J., Dimon B. and Merlivat L. (1987) Hydrogen isotope abundances in the solar system. Part I: Unequilibrated chondrites. *Geochim. Cosmochim. Acta* **51**, 1787-1805.

Rochette P., Sagnotti L., Bourot-Denise M., Consolmagno G., Folco L., Gattacceca J., Osete M.L. and Pesonen L. (2003) Magnetic classification of stony meteorites: 1. Ordinary chondrites. *Meteoritics & Planet. Sci.* **38**, 251-268.

Rose-Weston L., Brenan J. M., Yingwei F., Secco R. A. and Frost D. J. (2009) Effect of pressure, temperature, and oxygen fugacity on the metal-silicate partitioning of Te, Se and S: Implications for earth differentiation. *Geochim. Cosmochim. Acta* **73**, 4598-4615.

Rosman K. J. R. and Laeter J. R. (1988) Cadmium mass fractionation in unequilibrated ordinary chondrites. *Earth and Planet. Sci. Lett.* **89**, 163-169.

Roy-Barman M. (1993) Mesure du rapport $^{187}Os/^{186}Os$ dans les basalts et les pe´ridotites: contribution a` la syste´matique$^{187}Re–^{187}Os$ dans le manteau. Ph. D. thesis, Paris Univ.

Rubin A. E. and Wasson J. T. (2011) Shock effects in “EH6” enstatite chondrites and implications for collisional heating of the EH and EL parent asteroids. *Geochim. Cosmochim. Acta* **75**, 3757-3780.

Rubin A. E., Scott E. R. D. and Keil K. (1997) Shock metamorphism of enstatite chondrites. *Geochim. Cosmochim. Acta* **61**, 847-858.

Russell S. S., Huss G. R., MacPherson G. J. and Wasserburg G. J. (1997) Early and late chondrule formation: new constraints for solar nebula chronology from $^{26}Al/^{27}Al$ in

unequilibrated ordinary chondrites. (abstract #1468) XXVIIIth Lunar and Planetary Science Conference.

Schaefer L. and Fegley B. Jr. (2009) Volatile element chemistry during metamorphism of ordinary chondritic material and some of its implications for the composition of asteroids. *Icarus* 205, 483-496.

Schmitt W., Palme H., and Wänke H. (1989) Experimental determination of metal/silicate partition coefficients for P, Co, Ni, Cu, Ga, Ge, MO, and W and some implications for the early evolution of the Earth. *Geochim. Cosmochim. Acta* **53**, 173-185.

Scott E. R. D. (1972) Chemical fractionation in iron meteorites and its interpretation. *Geochim. Cosmochim. Acta* **36**, 1205-1236.

Scott E. R. D. and Jones R. H. (1990) Disentangling nebular and asteroidal features of CO3 carbonaceous chondrites. *Geochim. Cosmochim. Acta* **54**, 2485-2502.

Scott E. R. D. and Krot A. N. (2003) Chondrites and their components. *Treatise on Geochemistry*. Editors Davis A.M., Holland H.D. and Turekian K.K. **1**, 143-200.

Scott E. R. D., Taylor G. J., Rubin A. E., Okada A. and Keil K. (1981) Graphite-magnetite aggregates in ordinary chondrite meteorites. *Nature* **291**, 544-546.

Sears D. W. G., Grossman J. N., Melcher C. L., Ross L. M. and Mills A. A. (1980) Measuring the metamorphic history of unequilibrated ordinary chondrites. *Nature* **287**, 791-795.

Sears D. W. G., Hasan F. A., Batchelor J. D., and Lu J. (1991) Chemical and physical studies of type 3 chondrites: XI. Metamorphism, pairing, and brecciation of ordinary chondrites. 21st Proc. Lunar and Planetary Science Conference, 493-512.

Shirey S. B. and Walker R. J. (1998) The Re–Os isotope system in cosmochemistry and high-temperature geochemistry. *Ann. Rev. Earth Planet. Sci.* **26**, 423-500.

Shu F., Najita J., Galli D., Ostriker E. and Lizano S. (1993) The collapse of cloud and the formation and evolution of stars and disks. Editors Levy E.H. and Lunine J.I. *Protostars and Planets III*. Univ. Arizona Press, Tucson, Arizona, 3-45.

Shu F. H., Shang H., Glassgold A. E. and Lee T. (1997) X-rays and fluctuating X-winds from Protostars. *Science* **277**, 1475-1479.

Shukolyukov A. and Lugmair G. W. (2000) On the ^{53}Mn heterogeneity in the early solar system. *Space Sci. Rev.*, **92**, 225-236.

Smith C. L., Laeter de J. R. and Rosman K. J. R. (1977) Mass spectrometric isotope dilution analyses of tellurium in meteorites and standard rocks. *Geochim. Cosmochim. Acta* **41**, 676-681.

Smoliar M. I., Walker R. J. and Morgan J. W. (1996) Re–Os ages of group IIA, IIIA, IVA, and IVB iron meteorites. *Science* **271**, 1099-1102.

Strom S. E., Edwards S. and Skrutskie M. F. (1993) Evolutionary time scales for circumstellar disks associated with intermediate- and solar-type stars. Editors Levy E.H. and Lunine J.I. *Protostars and Planets III*. Univ. Arizona Press, Tucson, Arizona, 837-866.

Swindle T. D. (1993) Extinct radionuclides and evolutionary time scales. Editors Levy E.H. and Lunine J.I. *Protostars and Planets III*. Univ. Arizona Press, Tucson, Arizona, 867-881.

Sylvester P. J., Ward B. J., Grossman L., and Hutcheon I. D. (1990) Chemical compositions of siderophile element-rich opaque assemblages in an Allende inclusion. *Geochim. Cosmochim. Acta* **54**, 3491-3508.

Takahashi H., Gros J., Higuchi H., Morgan J. W. and Anders E. (1978) Volatile elements in chondrites: metamorphism or nebular fractionation? *Geochim. Cosmochim. Acta* **42**, 1859-1869.

Trinquier A., Birck J. L., and Allégre C. J. (2007) Widespread ^{54}Cr heterogeneity in the inner solar system. *The Astrophysical Journal* **655**, 1179-1185.

Tscharnuter W. M. and Boss A. P. (1993) Formation of the Protosolar nebula. Editors Levy E.H. and Lunine J.I. *Protostars and Planets III*. Univ. Arizona Press, Tucson, Arizona, 921-938.

van Niekerk D. and Keil K. (2011) Metal/sulfide-silicate intergrowth textures in EL3 meteorites: origin by impact melting on the EL parent body. *Meteoritics & Planet. Sci.* **46**, 1484-1497.

van Niekerk D., Humayun M. and Keil K. (2009) In situ determination of siderophile trace elements in EL3 meteorites. (abstract #2049) 40th Lunar and Planetary Science Conference.

Van Schmus W. R. and Wood J. A. (1967) A chemical-petrologic classification for the chondritic meteorites. *Geochim. Cosmochim. Acta* **31**, 747-765.

Wai C. M. and Wasson J. T. (1977) Nebular condensation of moderately volatile elements and their abundances in ordinary chondrites. *Earth and Planet. Sci. Lett.* **36**, 1-13.

Walker R. J., Prichard H. M., Ishiwatari A., and Pimental M. (2002a) The osmium isotopic composition of convecting upper mantle deduced from ophiolite chromitites. *Geochim. Cosmochim. Acta* **66**, 325-349.

Walker R. J., Horan M. F., Morgan J. W., Becker H., Grossman J. N. and Rubin A. E. (2002b) Comparative ^{187}Re–^{187}Os systematics of chondrites: implications regarding early solar system processes. *Geochim. Cosmochim. Acta* **66**, 4187-4201.

Wang Z., Becker H. and Gawronski T. (2013) Partial re-equilibration of highly siderophile elements and the chalcogens in the mantle: A case study on the Baldissero and Balmuccia peridotites massifs (Ivrea Zone, Italian Alps). *Geochim. Cosmochim. Acta* **108**, 21-44.

Wang Z., Becker H. and Wombacher F. (2014) Mass fractions of S, Cu, Se, Mo, Ag, Cd, In, Te, Ba, Sm, W, Tl and Bi in geological reference materials and selected carbonaceous chondrite

determined by isotope dilution ICP-MS. *Geostand. Geoana. Res*. Doi: 10.1111/j.1751-908X.2014.00312.x.

Wasson J. T. (1972) Formation of ordinary chondrites. Rev. Geophys. Space Phys. **10**, 71l-759.

Wasson J. T. (1988) The building stones of the planets. In *Mercury* (ed. F. Vilas et al.), 622-650, Univ. Arizona.

Wasson J. T. and Kallemeyn G. W. (1988) Composition of chondrites. *Philos. Trans. R. Soc. Lond. Ser. A.* **325**, 535-544.

Wasson J. T. and Krot A. N. (1994) Fayalite-silica association in unequilibrated ordinary chondrites: Evidence for aqueous alteration on a parent body. *Earth and Planet. Sci. Lett.* **122**, 403-416.

Wasson J. T. and Hoppe P. (2012) Co/Ni ratios at taenite/kamacite interfaces and relative cooling rates in iron meteorites. *Geochim. Cosmochim. Acta* **84**, 508-524.

Wasson J. T., Rubin A. E. and Kallemeyn G. W. (1993) Reduction during metamorphism of four ordinary chondrites. *Geochim. Cosmochim. Acta* **57**, 1867-1878.

Weider S. Z., Nittler L. R., Starr R. D., McCoy T. J., Stockstill-Cahill K. R., Byrne P. K., Denevi B. W., Head J. W. and Solomon S. C. (2012) Chemical heterogeneity on Mercury's surface revealed by the MESSENGER X-ray spectrometer. *J. Geophy. Res.* **117**, (E00L05), doi:10.1029/2012JE004153.

Weisberg M. K. and Prinz M. (1998) Sahara 97096: A highly primitive EH3 chondrite with layered sulfide-metal-rich chondrules. (abstract #1741) XXIXth Lunar and Planetary Science Conference.

Weisberg M. K., Fogel R. A. and Prinz M. (1997) Kamacite enstatite intergrowths in enstatite chondrites. (abstract #1768) 28th Lunar and Planetary Science Conference.

Weisberg M. K., McCoy T. J. and Krot A. N. (2006). Systematics and evaluation of meteorite classification. Meteorites and early solar system II (D. S. Lauretta and H. Y. McSween Jr., eds.), 19-52.

Weisberg M. K., Ebel D. S. and Connolly Jr. H. C. (2013) EL3 chondrites: primitive nebular materials, not products of asteroidal processing. (abstract #2871) 44th Lunar and Planetary Science Conference.

Weisberg M. K., Zolensky M. E., Kimura M. and Ebel D. S. (2014) Primitive fine-grained matrix in the unequilibrated enstatite chondrites. (abstract # 1551) 45th Lunar and Planetary Science Conference.

Wiik H. B. (1966) On the genetic relationship between meteorites. Arizona State University Spec. Contrib. 18.

Xiong Y. and Wood S. A. (2002) Experimental determination of the hydrothermal solubility of ReS_2 and the Re-ReO_2 buffer assemblage and transport of rhenium under supercritical conditions. *Geochem. Trans*. **3(1),** 1-10.

Yanai K., Kojima H. and Haramura H. (1995) Catalog of the Antarctic Meteorites collected from December 1969 to December 1994, with special reference to those represented in the collections of the National Institute of Polar Research. National Institut of Polar Research, Tokyo, 44-76.

Yasinskaya A. A. and Osadchij E. G. (1973) New meteorite Andreevka. *Meteoritika* **32**, 100-102.

Zhang Y., Benoit P. H. and Sears D. W. G. (1995) The classification and complex thermal history of the enstatite chondrites. *J. Geophys. Res.* **100**, (E5), 9417-9438.

Curriculum Vitae

For reasons of data protection,

the curriculum vitae is not included in the online version

For reasons of data protection,

the curriculum vitae is not included in the online version

For reasons of data protection,

the curriculum vitae is not included in the online version

For reasons of data protection,

the curriculum vitae is not included in the online version

For reasons of data protection,

the curriculum vitae is not included in the online version

For reasons of data protection,

the curriculum vitae is not included in the online version

For reasons of data protection,

the curriculum vitae is not included in the online version

Acknowledgements

First of all I would like to thank the energy which creates the Universe and the big solar system laboratory which made and provides the samples for this study.

This project was a part of the special priority program SPP 1385 “The first ten million years of solar system – a planetary materials approach” (Be1820/10-1/2). I am very thankful to the DFG (Deutsche Forschungsgemeinschaft) for providing financial support to this work.

I would like to express my special thanks to one of the great human beings I have met and my supervisor Prof. Dr. Harry Becker for offering me this Ph.D. project. He is a great mentor for me. I would like to thank him for constant encouragement and support throughout my Ph.D. tenure. His advices on research as well as on my career are priceless and are gratefully acknowledged. Without his guidance and support this dissertation would not have been possible.

I am very thankful to Prof. Dr. Maria Schoenbaechler for being the second referee of this thesis.

Dr. Konrad Hammerschmidt is acknowledged for his help and support in the TIMS laboratory and for his great overview concerning any questions regarding to the mass spectrometry and data interpretation.

I would like to express my gratitude to Ms. Monica Feth for her help and support in the clean laboratory.

I am thankful to Ms. Michaela Schreiber for helping in all administrative matters.

I am thankful to Ms. Christiane Behr for helping in the preparation of thick sections used for electron microprobe analysis. Thanks goes to Dr. Ralf Milke for support and guidance during analysis on the electron microprobe.

Mr. Bernd Treczka and Mr. Michael Golinski are thanked for troubleshooting of the problems with softwares and computer issues.

Mr. Sebastian Kommescher and Ms. Franziska Shubring are acknowledged for assistance during different stages of laboratory work. Thanks go to Franziska for writing the German version of the summary of this thesis. Special thanks to Mr. Marc Weynell and Dr. Elis Hoffmann for constructive discussions and suggestions during the preparation of this work.

I would particularly like to thank to my project students Ms. Franziska Schubring, Ms. Tanja Giebner, Ms. Franziska Mangels and Andreas Harbott. I was greatly benefited from the discussions with them.

Mr. Timo Gawronski, Mr. Christian Meyer and Dr. Zaicong Wang are specially thanked for their support during my first steps in laboratory work.

Mr. Marc Weynell, Mr. Simon Hohl, Mr. Chunhui Lee, Dr. Philipp Gliessner, Dr. Uwe Wiechert and Dr. Elis Hoffmann are gratefully acknowledged for inspiring discussions in related topics which help in broadening my view in my research field.

Special thanks go to the recent and former members of the geochemistry department of the Freie Universität Berlin for providing an encouraging and friendly atmosphere. I want to thank Ms. Feth, Ms. Schreiber, Harry, Uwe, Mr. Hammerschmidt, Christian, Timo, Marc, Simon, Zaicong, Chunhui, Philipp, Elis, Frederike, Sebastian, Mathias, Marie, Tanja, Elfrun, Franziska Schubring and Franziska Mangels, it has always been a pleasure working with you.

My siblings Manoj, Shital and Sagar, my sister-in-law Sonali, my brother-in-law Sandip and long list of my friends in Germany as well as in India are gratefully acknowledged for their kind help, support and understanding in the academic as well as in personal life. Finally I am forever indebted to my parents Mr. Uttam Kadlag and Mrs. Sunanda Kadlag for encouragement throughout my whole student life and for making me the person who I am.